Université de Lille

Doctoral school: Science of Matter, Radiation and Environment

Discipline: Theoretical, Physical and Analytical Chemistry

Dissertation

Role of the organic waste products reactivity in secondary organic aerosol formation

by

Kawssar Mujtaba HAIDER

Thesis submitted in partial fulfillment of the requirements for the degree of

Doctor of Philosophy of the University of Lille

Defended on December 9th, 2022 in front of the defense committee composed of:

Jury president	Sabine Houot	INRAE, AgroParisTech, University of Paris-Saclay
Reviewer	John Wenger	University College Cork, Ireland
Reviewer	Estelle Roth	University of Reims, France
Examiner	Karine Sartelet	CEREA, Ecole des Ponts ParisTech
Examiner	Valérie Gros	CNRS LSCE Gif-sur-Yvette
Thesis director	Cristian Focsa	University of Lille
Thesis co-director	Raluca Ciuraru	INRAE, AgroParisTech, University of Paris-Saclay
Thesis co-director	Denis Petitprez	University of Lille

PhLAM Physique des Lasers Atomes et Molécules

INRAE

EcoSys

PC2A

Ecole Doctorale: Sciences de la Matière, du Rayonnement et de l'Environnement

Discipline: Chimie Théorique, Physique et Analytique

Thèse de doctorat

Rôle de la réactivité des déchets organiques dans la formation d'aérosols organiques secondaires

présentée par

Kawssar Mujtaba HAIDER

pour obtenir le grade de docteur de l'Université de Lille

soutenue le 09 décembre 2022

Présidente du jury	Sabine Houot	INRAE, AgroParisTech, Université Paris-Saclay
Rapporteur	John Wenger	University College Cork, Irlande
Rapporteure	Estelle Roth	Université de Reims
Examinatrice	Karine Sartelet	CEREA, Ecole des Ponts ParisTech
Examinatrice	Valérie Gros	CNRS LSCE Gif-sur-Yvette
Directeur de thèse	Cristian Focsa	Université de Lille
Co- encadrante de thèse	Raluca Ciuraru	INRAE, AgroParisTech, Université Paris-Saclay
Co-directeur de thèse	Denis Petitprez	Université de Lille

Rôle de la réactivité des déchets organiques dans la formation d'aérosols organiques secondaires

Résumé

Le recyclage des produits résiduaires organiques (PRO) en tant qu'engrais agricoles se développe aujourd'hui comme une approche plus durable et plus écologique par rapport aux méthodes traditionnelles d'élimination des déchets. Cependant, l'épandage des déchets organiques pourrait libérer divers polluants tels que des composés organiques volatils (COV). Ces derniers présentent des effets néfastes sur l'écosystème et la santé humaine liés à la production d'ozone et peuvent servir comme précurseurs critiques d'aérosols organiques secondaires (AOS) dans l'atmosphère. La mesure des COV émis par les PRO est donc indispensable pour évaluer leur impact sur l'environnement et la santé humaine, ainsi que pour comprendre les mécanismes de formation des AOS associés, qui sont jusqu'à ce jour peu documentés.

Nous avons étudié les émissions de COV de divers échantillons : des boues d'épuration, du fumier animal (vache, cheval, mouton et chèvre), des digestats de biodéchets ainsi que leurs produits d'oxydation en phase gazeuse dus aux réactions d'ozonolyse. Cette étude a été faite grâce au développement d'un dispositif expérimental, composé de chambres de simulation atmosphérique combinées à des techniques de spectrométrie de masse telles que : la spectrométrie de masse à temps de vol par réaction de transfert de protons (PTR-QiTOF-MS) et de désorption thermique - chromatographie en phase gazeuse - spectrométrie de masse (TD-GC-MS) pour identifier et quantifier les émissions de COV de chaque échantillon. L'étude de la composition chimique des AOS a été effectuée en utilisant la spectrométrie de masse laser à deux étapes (L2MS).

Nos résultats ont montré que les échantillons de boues d'épuration, de fumier animal et de biodéchets digérés émettent une large gamme de COV, avec plusieurs centaines de composés détectés et quantifiés. Les COV identifiés ont été classés en différentes familles chimiques : hydrocarbures, composés oxygénés, soufrés, azotés et "autres" (contenant des hétéroatomes distincts dans la formule moléculaire). Les échantillons de boues d'épuration ont émis un flux élevé d'hydrocarbures tels que les composés aromatiques (phénol, indoles et skatole), et les terpènes (isoprène, D-limonène, sesquiterpènes, etc.). Les composés oxygénés (par exemple, l'éthanol, la butanone, le crésol, l'acide acétique, le phénol) ont été fortement émis par les digestats de biodéchets et les échantillons de fumier. Des composés azotés (ammoniac, triméthylamine, scatole, etc.) et des composés soufrés (méthanethiol, DMS, DMDS, etc.) ont également été trouvés dans ce travail.

Des émissions significatives de scatole ont été estimées à partir des boues d'épuration et de digestat. Le mécanisme de formation de nouvelles particules a été démontré. Nos résultats impliquent que pendant l'épandage des PRO, le scatole est un important contributeur potentiel à la formation de nouvelles particules dans des conditions atmosphériques pertinentes. Les résultats de ce travail contribuent à faire progresser nos connaissances sur les COV et leur rôle dans la formation des AOS. Ils pourraient également être utiles pour mieux comprendre les caractéristiques des émissions des PRO, concevoir des stratégies de contrôle de ces émissions.

Mots clés: émissions agricoles, produits résiduels organiques, composés organiques volatils, aérosols organiques secondaires, ozonolyse, précurseurs d'aérosols, spectrométrie de masse.

Role of the organic waste products reactivity in secondary organic aerosol formation

Abstract

Recycling of organic waste products (OWP) as agricultural fertilizers is nowadays expanding as a more sustainable and eco-friendly approach compared to the traditional methods of waste disposal. However, OWP spreading may release various pollutants such as volatile organic compounds (VOC), which adversely affect the ecosystem and human health through ozone production and may serve as critical precursors of atmospheric secondary organic aerosols (SOA). The measurement of VOCs emitted by OWPs is therefore essential to assess their environmental and human health impact and, furthermore, to fundamentally understand the associated SOA formation mechanisms, which remain to date poorly documented.

With this aim, we studied the VOC emissions from various sewage sludge (SS) samples, animal manure (cow, horse, sheep and goat) and digestate biowastes, along with their gas-phase oxidation products due to ozonolysis reactions. With the development of an experimental set-up consisting of atmospheric simulation chambers combined with mass spectrometric techniques, it has become possible to characterize the VOC emissions and follow the process of new particle formation (NPF) upon ozonolysis. We used proton transfer reaction quadrupole-ion-guide time-of-flight mass spectrometry (PTR-QiTOF-MS) and thermal desorption - gas chromatography - mass spectrometry (TD-GC-MS) techniques to identify and quantify the VOC emissions from each sample. In addition, we studied the chemical composition of SOA using two-step laser mass spectrometry (L2MS).

Our results showed that sewage sludge, animal manure and digestate biowaste samples emitted a large spectrum of VOCs where 380, 385 and 221 compounds were detected and quantified, respectively. The assigned VOCs were classified into different chemical families: hydrocarbons, oxygenated, sulphuric, nitrogenated, and “other” compounds (containing distinct heteroatoms in the molecular formula). Sewage sludge samples were characterized by high emission flux of hydrocarbons such as aromatic compounds (phenol, indoles and skatole), terpenes (isoprene, D-limonene, sesquiterpenes, etc.). Oxygenated compounds (e.g., ethanol, butanone, cresol, acetic acid, phenol) were highly emitted from digestate biowastes and manure samples. Nitrogenated compounds (ammonia, trimethylamine, skatole, etc.) and sulphur compounds (methanethiol, DMS, DMDS, etc.) were also found in this work.

Significant skatole emissions were estimated from undigested SS and digestate biowastes. The ozonolysis of skatole resulted in the formation of 2-acetyl phenyl formamide identified as the main skatole ozonolysis product. The NPF mechanism was demonstrated. Our findings imply that during OWPs spreading, skatole is an important potential contributor to the formation of new particles under atmospherically relevant conditions. The results of this work would advance our knowledge of VOCs and their impact on SOA formation and would be helpful in understanding the OWP emission characteristics and designing effective emission control strategies.

Keywords: agricultural emissions, organic waste products, volatile organic compounds, secondary organic aerosols, ozonolysis, aerosol precursors, mass spectrometry.

Acknowledgements

I would like to start with a lovely quote I have memorized since childhood *"Every container becomes tightly packed with what is put in it, except for the container of Knowledge, for surely it expands"*. It would not have been possible to write this doctoral thesis without the help and support of the kind people around me, to only some of whom it is possible to give a particular mention here.

Above all, I would like to thank my parents, **Mujtaba** and **Zeinab**. During this thesis, we may not always see eye to eye, but I know we see heart to heart. In my heart, I love you and thank you for being someone who did the best to share wisdom, life lessons, love and prayers so I could be the person I am today. Thank you for always supporting my hopes, goals, and dreams. You are always sitting here thinking… caring… praying for me.

It all started on April 2018 when I received a scholarship for my second year of Master studies, which allowed me to enrol in the International Master's degree program in "Atmospheric Environment" "Atmospheric Environment" program at University of Lille. During that year, I had the opportunity to perform my MSc research internship in the ANATRAC group at the PhLAM laboratory. This first contact with research activities at the University of Lille determined me to continue my studies with a Ph.D thesis. This thesis was carried out as a collaboration between research groups from three research labs: ECOSYS at University of Paris-Saclay, & INRAE, PhLAM (ANATRAC group) and PC2A laboratories at University of Lille. This work would not have been possible without the financial support I received from the University of Lille and INRAE, and for that I would like to express my special thanks to all their members.

First and foremost, I am extremely grateful to my supervisor and PhLAM Director, **Prof. Cristian Focsa** for his invaluable advice, continuous support, and patience during my Ph.D study. His immense knowledge and plentiful experience have raised the quality of this thesis and given me enthusiasm for science. He has always encouraged me to think outside the box and given innovative ideas to address the challenges that I faced in my Ph.D and during Covid-lockdown period. Every moment I have met him and he asked *"how are things Kawssar?"* I have the feeling that everything is easy because of him so I answered *"very good!"* I would like also to thank my esteemed supervisor – **Prof. Denis Petitprez** for his invaluable supervision, support and tutelage during the course of my Ph.D degree. I am thankful for their assistance at every stage of the research project, their insightful comments and suggestions, and their unwavering support and belief in me.

I have been extremely lucky to have **Dr. Raluca Ciuraru** as my supervisor. She spent valuable time to teach me the methodology to carry out experimental research, to carefully analyze and interpret the collected data and to present the results in a clear and sound manner. I am grateful for her offering advice and encouragement with a perfect blend of insight and humour. She is not only a knowledgeable scientist but a humble leader, a passionate chemist, a motivational speaker and a great friend. She gave me a complete freedom to define my thesis and helped me identify research priorities. I never forget her warm smile every morning at ECOSYS, her support and motivating words, and the deep trust and confidence she gave me, with her lovely words *"let's move in baby steps"*. I am also grateful for all the time she spent revising my manuscript.

I would like to express my sincere gratitude to PhLAM laboratory members, especially technical and administrative staff, its precedent Director **Prof. Marc Douay**, and to all ANATRAC research group members, especially **Dr. Yvain Carpentier** and **Dr. Claire Pirim**. I would also like to thank all ECOSYS members I met in Grignon, for the excellent work environment they provided and their kind

help and support that have made my study and life in the Grignon a wonderful time. I really had unforgettable memories with those people and their humorous reactions to each experiment I performed on the *"shitty"* samples. Sorry for spreading *"alarming smells"* in the Institute, but it is *"Science"*. Special thanks to the researchers **Benjamin Loubet, Henri Wortham** and **Sabine Houot.** Thanks for engineer **Florence Lafouge** for helping me to use the PTR-MS instruments and treat the data. Great thanks to the engineer **Céline Decuq** and the technician **Baptiste Esnault** for performing the GC-MS analysis and treating the data. Thanks all for their treasured support which was really influential in shaping my experiment methods and critiquing my results of PTR-MS and GC-MS.

I am deeply honored and would like to express my gratitude to all the members of the defense committee for accepting to evaluate this Ph.D work: **Prof. John Wenger**, **Dr. Estelle Roth**, **Dr. Karine Sartelet**, **Dr. Valérie Gros** and **Dr. Sabine Houot**. Special thanks to **Prof. John Wenger** and **Dr. Estelle Roth** for serving on my committee and reviewing my thesis.

Every result in this thesis was accomplished with the help and support of my lab mates. Special thanks go to **Dr. Dumitru Duca** for long discussions on statistical data treatment methods. I very much appreciate the support I received from **Dr. Siveen Thlaijeh** and **Dr. Tirthankar Mitra** for their help with instrumentation and data analysis along with their continuous encouragements that significantly facilitated my work and contributed to an unforgettable Ph.D. Special thanks for my colleagues, **Joelle Al Aseel** and **Vikas Madhur**, who are dedicated to lift spirit, spread positivity, jokes and drink coffee. Happiness during these years is doubled because you never let me feel blue.

There is no one with whom I can share my tears and fears, if you were not here; my soulmate, **Zeinab Srour**, and my sensitive whales **Doha Kdouh** and **Nour Beyrouti**. Thanks for being by my side and always giving me reasons to laugh. Special thanks go to **Zahraa Khatib** for her wonderful caring, lovely words, and unconditional support, for sharing me laughs and tears, good and bad moments. She is the mirror which hides my weaknesses and makes my strengths more visible. To **ALL** my **Friends**, I would say, you are a home of warmth… soldiers… shields… and angels of mercy…

To my beautiful **BIG** family, **Father** and **Mother**, my SIX SISTERS (**Zahraa**, **Hawraa**, **Mariam**, **Rokaya**, **Batoul**, **Fatima**), my ONE BOTHER **Abbas**, and my brothers-in-law (**Ibrahim**, **Ali**^{3} and **Abdo**), whenever I am alone, you sneak in lovely and brilliantly. You are my pillar of strength and the wall which shields me from every sorrow. You are my home where I live in peace and warmth. Thanksgiving to my adorable **Nieces**, for giving me endless happiness and hope. Thank you for making my life complete! Now, at 02:35 am of October 19th, 2022 I miss you so much, so I can't write more …

Kawssar M. Haider

Table of Contents

List of acronyms

ANOVA	Analysis of variance
BVOC	Biogenic volatile organic compound
CCN	Cloud condensation nuclei
CPC	Condensation particle counter
DBE	Double bond equivalent
DMA	Differential mobility analyzer
DMDS	Dimethyl disulphide
DMS	Dimethyl sulphide
DS	Dry solid
DSS	Digested sewage sludge
FWHM	Full width at half maximum
GC	Gas chromatography
GC-MS	Gas chromatography mass spectrometry
GHG	Greenhouse gas
HC	Hydrocarbon
HR-PT-QiTOF-MS	High resolution - proton transfer reaction quadrupole ion-guide time-of-flight mass spectrometry
HR-L2M	High resolution two step laser mass spectrometry
MS	Mass spectrometry
NMVOC	Non-methane volatile organic compound
NO_3	Nitrate radicals
NPF	New particle formation
OC	Organic carbon
OH	Hydroxyl radicals
OM	Organic matter
OVOC	Oxygenated volatile organic compounds
OWP	Organic waste product
PA	Proton affinity
PAH	Polycyclic aromatic hydrocarbons
PC	Principal component
PCA	Principal component analysis
PM	Particulate matter

PMMA	Poly(methyl methacrylate)
ppb	parts per billion
ppm	part per million
ppt	part per trillion
QFF	Quartz fiber filter
RH	Relative humidity
SMPS	Scanning mobility particle sizer
SOA	Secondary organic aerosol
SS	Sewage sludge
SS 30%	Sewage sludge with 30% dryness
SS 60%	Sewage sludge with 60% dryness
SVOC	Semi-volatile organic compound
TD-GC-MS	Thermal desorption gas chromatography mass spectrometry
TIC	Total ion count
TMA	Trimethyl amine
TOF	Time of flight
TOF-SIMS	Time of flight secondary ion mass spectrometry
UDSS	Undigested sewage sludge
UHPLC-HRMS	Ultra-high performance liquid chromatography coupled to high resolution mass spectrometry
UV	Ultraviolet
VOC	Volatile organic compound
VOSC	Volatile organosulphur compound
WHO	World Health Organisation
WWTP	Wastewater treatment plant

List of Figures

List of Tables

Chapter 1

Introduction

1.1. Context of the study

The studies performed during this PhD thesis were carried out as a collaboration between research groups from three research labs:

-ECOSYS : Ecologie fonctionnelle et écotoxicologie des agroécosystèmes, Thiverval-Grignon, UMR 1402, AgroParisTech, University of Paris-Saclay, & INRAE – the French national research institute for agriculture, food and the environment;

-PhLAM : Physique des Lasers, Atomes et Molécules, Villeneuve d'Ascq, UMR 8523, Université de Lille & CNRS;

-PC2A : Physico-Chimie des Processus de Combustion et de l'Atmosphère, Villeneuve d'Ascq, UMR 8522, Université de Lille & CNRS;

This PhD thesis is a part of the ANR project SOFORA (Secondary Organic aerosol Formation by Organic waste Recycling in Agriculture), which aims to investigate secondary organic aerosol formation and fate in real atmospheric and in controlled simulation chamber conditions by two different organic waste products: urban waste application (sewage sludge or green waste composts) and livestock manure.

The volatile organic compound emissions from agricultural activities appear to be at the center of current scientific research and agricultural challenges that are in direct contact with the global changes (climate and environmental pollution) and the ecological transition initiated in agricultural areas. Accurate and precise information on volatile organic compound emissions is crucial for their control. In addition, their emission inventory is considered as a significant input parameter for the air quality models to simulate their variations and relative impacts on the secondary pollutants. In addition, emission inventories provide critical information for understanding the emission characteristics and designing effective emission control strategies.

This introductory Chapter presents a scientific overview on the volatile organic compounds, atmospheric aerosols and organic waste products and the state of the art on the subject of the thesis. Finally, the main scientific objectives of the thesis and the structure of this dissertation are outlined.

1.2. Volatile organic compounds (VOCs)

1.2.1. VOCs definition, sources and impacts

Organic compounds include at least one carbon and one hydrogen atoms in the molecular structure. They can be classified into various categories, which include volatile organic compounds (VOCs), semi-volatile organic compounds (SVOCs) and non-volatile organic compounds (NVOCs). The term VOC in the United States is defined in the Code of Federal Regulations 40 CFR 51.100(s): ‘‘(VOC) means any compound of carbon, excluding carbon monoxide, carbon dioxide, carbonic acid, metallic carbides or carbonates and ammonium carbonate, which participates in atmospheric photochemical reactions’’. VOCs are a mixture of gaseous species that have high vapour pressures in the atmosphere (Anand et al., 2014; Ciganek & Neca, 2008). VOCs are molecules containing atoms of carbon and hydrogen, often bonded with halogens, oxygen, sulphur, phosphorous and nitrogen. VOCs without methane are termed as non-methane VOCs (NMVOCs). VOCs include a large number of families such as ketones, aldehydes, alcohols, esters, ethers, nitriles, aliphatic hydrocarbons, aromatic hydrocarbons, diols, etc. (Anand et al., 2014).

Atmospheric VOC emissions originate from natural biogenic and anthropogenic sources. Natural sources of VOCs include soil, oceans, vegetation, forest fires, etc. (Liu et al., 2018). Anthropogenic emissions such as those from vehicles (Gentner et al., 2013), industries (Zheng et al., 2017), secondary formation due to oxidation (Spaulding et al., 2003), combustion sources, fuel storage and transport, etc. (Placet et al., 2000). About 90% of the total VOC emissions result from terrestrial vegetation (Guenther et al., 1995). Throughout the European Union EU-28 area, VOCs are emitted by various sources (**Figure 1.1**). About two third of the total EU-28 emissions result from industrial and commercial (50%), institutional and household fuel consumption (16%), while the contribution of agriculture to VOC emissions is 11%, according to Air Quality in Europe – EEA Report, (2017).

Biogenic VOC (BVOC) emissions represent the largest VOC source with an estimated annual emission amount of 760 Tg (carbon) yr^{-1} (Sindelarova et al., 2014). BVOCs contribute up to 5-10% of the total net carbon exchange between the biosphere and the atmosphere (Sindelarova et al., 2014). The contribution of forest is 55% of the total BVOC emissions while that of crops is around 27% in Europe (Karl et al., 2009).

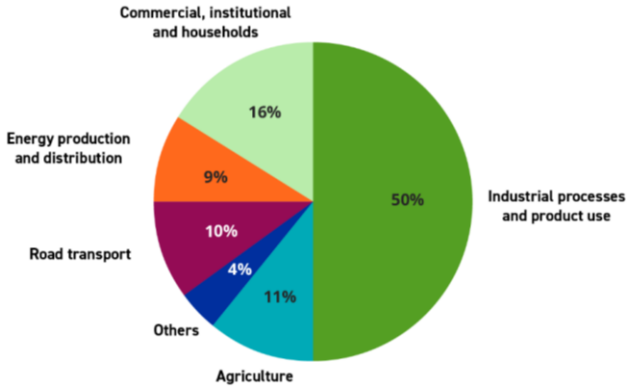

Figure 1.1 *VOC emission sources in the EU-28 area (Air Quality in Europe – EEA Report, 2017).*

VOCs include a wide range of common atmospheric organic chemicals and can cause acute or chronic health effects. Moreover, VOCs can have different toxicity due to their difference in the physical and chemical properties (Cicolella, 2008). These properties in addition to the smaller molecular size and lack of charge enable the inhalation of VOCs and their absorption across the lungs, gastrointestinal tract and skin. VOCs affect health at concentrations above thresholds as other aerial pollutants. Several symptoms are associated with exposure to some VOCs that have adverse effects for humans and animals such as conjunctive irritation, nose and throat discomfort, headache, allergic skin reaction, nausea, epistaxis, fatigue and dizziness (Jones, 1999). Exposure to VOCs during normal indoor activities has been linked to lifetime cancer risks (Guo et al., 2004). Little is known about the health risks that could be associated with some volatile compounds detected in indoor and outdoor samples from the animal farms (Ciganek & Neca, 2008).

1.2.2. VOCs measurement

The wide range of molecules with different functional groups makes the ensemble of VOCs difficult to be fully detected and identified (Harrison et al., 2006). Indeed, a large number of VOCs have not been identified yet. In addition, the large number of different compounds is associated with a number of problems such as the sampling and analysis techniques, understanding the biological metabolisms, the biological emission and deposition regulations, the exchange description and modelling as well as the atmospheric chemistry of all compounds. Thus, a better knowledge concerning the exchange processes on local and regional scales is needed to address the production and fate of VOCs. Moreover, a better understanding of the factors influencing the VOC emissions from different biogenic and anthropogenic sources is necessary to implement suitable strategies for air pollution abatement as VOCs are responsible

for malodor and environmental hazards. There are large uncertainties associated with the VOC emissions, chemical processing and sinks of atmospheric VOCs (Chen et al., 2019).

The measurements of VOCs in the atmosphere have been widely performed by using gas chromatographic (GC) analysis. The air can be sampled either by using canisters or adsorbents. Such measurements are characterized by high sensitivity and giving a high degree of chemical detail, where tens of VOCs with a detection limit of 0.1 pptv can be determined in the sample. However, those methods have several disadvantages such as the sampling time of several minutes needed to get enough sample material on the adsorbent. This limits the GC measurements which is not able to follow the changes in the atmospheric conditions with the necessary response time, as for, e.g., the sampling close to emission source. The use of canister samples that can be filled within few seconds could be a solution to this disadvantage while the acquisition and analysis of canister samples is time consuming and labor intensive. Thus the amount of data acquired is limited. Therefore, GC measurements allow the detailed snapshots of the atmospheric VOCs, but are too slow to suit the rapid changes in air mass composition (de Gouw & Warneke, 2007). Proton-transfer-reaction mass spectrometry (PTR-MS) has been widely applied for the measurements of atmospheric VOCs since 1998. A detailed description of this technique and its application is given in **Chapter 2** of the manuscript.

1.2.3. Atmospheric interactions of VOCs

Emissions of nitrogen oxides, VOCs and sulphur compounds (including SO_2) can lead to a complex series of chemical and physical transformation. Such transformations can contribute to ozone formation, acid deposition and secondary particulate matter formation through gas/particle partitioning of both emitted chemical compounds and the atmospheric reaction products of VOCs, NO_x, SO_2 and organosulphur compounds (Atkinson, 2000). VOCs are considered as major air pollutants due to their hazardous, malodorous and reactivity in atmosphere (Chen et al., 2019). Recently, VOCs gained much attention due to their pivotal role in climate changes. The aim of this paragraph is to describe the different cycles and atmospheric transformations that involve VOCs and contribute to harmful air pollutants such as ozone.

1.2.3.1. Oxidation reactions of VOCs

In the atmosphere, VOCs are removed or transformed by various physical and chemical processes. Physical removal of VOCs may occur by deposition at the Earth's surface either directly (dry deposition) or by uptake in rain droplets (wet deposition). Such phenomena have been widely described elsewhere (Wesely & Hicks, 2000). In this paragraph, we will focus on

the chemical processes (i.e. photo-oxidation) that leads to the atmospheric degradation of VOCs resulting in two important byproducts in the atmosphere: ozone and organic aerosol, both having significant impacts on air quality and climate (de Gouw & Warneke, 2007).

The photochemical processes vary from minutes to months (Atkinson & Arey, 2003). VOCs such as isoprene, terpenes, alkanes, alkenes, alcohols, esters, carbonyls and acids play a significant role in both atmospheric photochemistry and pollution and contribute indirectly to global warming. They can interact with other atmospheric trace compounds, thus affecting the distributions of secondary air pollutants such as ozone and particles. VOCs are transformed by the chemical process of photolysis, various oxidation reactions with ozone, hydroxyl radicals (during the daylight hours) or with nitrate radicals (during the nighttime) or reaction with Cl atoms in coastal and marine regions (at dawn) (Atkinson & Arey, 2003, 2007). The atmospheric transformation of VOCs in the troposphere occurs at a level ranging from part per trillion (ppt, 10^{-12}) to several part per billion (ppb, 10^{-9}) (Kesselmeier & Staudt, 1999). **Table 1.1** reports the lifetime of the some VOCs in the atmosphere due to the reaction with OH, NO_3 and O_3 and as a result of photolysis. Isoprene, monoterpenes and some other VOCs can be reactive under atmospheric conditions due to their short chemical lifetimes that range between minutes and hours. Acetone and methanol are quite stable with regards to reaction with OH, NO_3 and O_3 (Guenther et al., 2006; Sindelarova et al., 2014).

Table 1.1 *Lifetime of some VOCs in the atmosphere reacting with OH radical, NO_3 radical and O_3 and due to photolysis. NA = not available, sd = standard deviation (Atkinson, 2000; Guenther et al., 2006; Sindelarova et al., 2014).*

		Life time of some biogenic VOCs			
VOCs	**Biogenic emissions Tg C yr^{-1} ± sd**	**OH[1]**	**NO_3[2]**	**O_3[3]**	**Photolysis[4]**
Isoprene	594 ± 34	1.4h	50 min	1.3 day	-
Monoterpenes	95 ± 3	2.7h	5 min	1.9h	-
Acetone	37 ± 1	53 days	>11 years	NA	~ 60 days
Acetaldehyde	19 ± 1	8.8h	17 days	>4.5 years	6 days
Methanol	130 ± 4	12 days	1 year	-	-

[1] *For a 12-h daytime average OH radical concentration of 2 * 10^6 molecule cm^{-3}*

[2] *For a 12-h daytime average NO_3 radical concentration of 5 * 10^8 molecule cm^{-3}*

[3] *For a 12-h daytime average O_3 concentration of 7 * 10^{11} molecule cm^{-3}*

[4] *For overhead sun*

Where no lifetime is given, this is because the process is too slow to be measured and is not expected to be significant.

Biogenic VOCs and their reaction products interfere in the tropospheric chemistry and affect directly or indirectly the production of air pollutants and GHG as well as the formation of atmospheric aerosols (Andreae & Crutzen, 1997). A study was performed to determine the reactivity of VOCs emitted from six concentrated animal feeding operation sites (Yuan et al., 2017). The reactivity was studied toward photo-oxidants (OH and NO_3 radicals) (**Figure 1.2**). The results of this work showed that alcohols and carboxylic acids were highly reactive toward OH radicals among the detected VOCs, while phenolic compounds followed by sulphur compounds showed the highest reactivity toward NO_3 radicals.

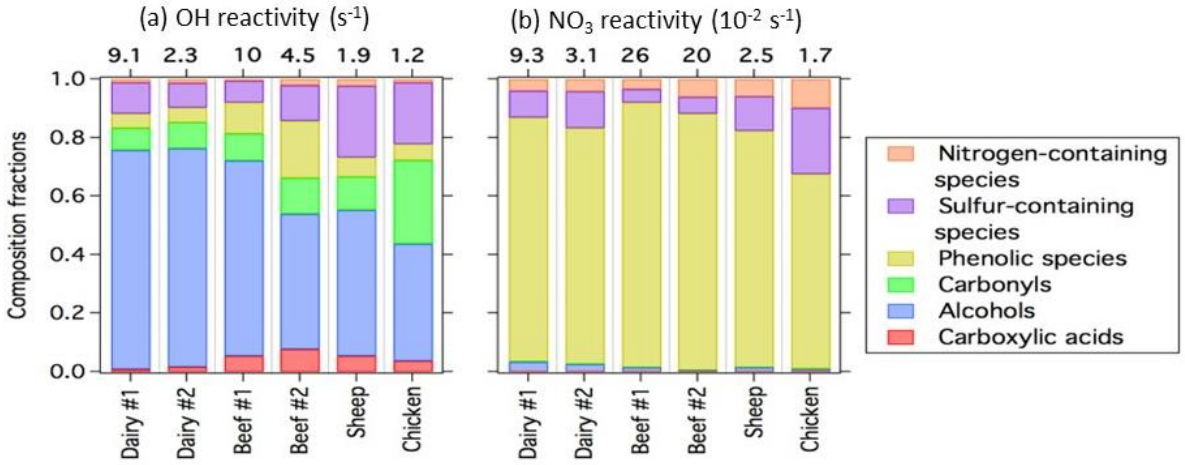

Figure 1.2 *(a) OH reactivity and (b) NO_3 reactivity for the six investigated concentrated animal feeding operation sites (Yuan et al., 2017).*

1.2.3.2. Role of VOCs in O_3 formation

Hydroxyl radical (OH) is the key reactive and the primary oxidizing species in the troposphere. The OH radical is involved in the formation of O_3 by reacting with VOCs. O_3 is formed by two possible pathways: the NO_x reactions with O_x and the NO_x reaction with O_x in the presence of VOCs. **Figure 1.3** shows both pathways that lead to O_3 formation. The degradation reactions of VOCs start with the oxidation of VOCs by OH radical, leading to the formation of RO_2 and HO_2 radicals as intermediate products (**Figure 1.3, B**). The intermediate products RO_2 and HO_2 convert NO in NO_2 and result in the net formation of O_3 as represented in **Figure 1.3**, **A** (Atkinson, 2000).

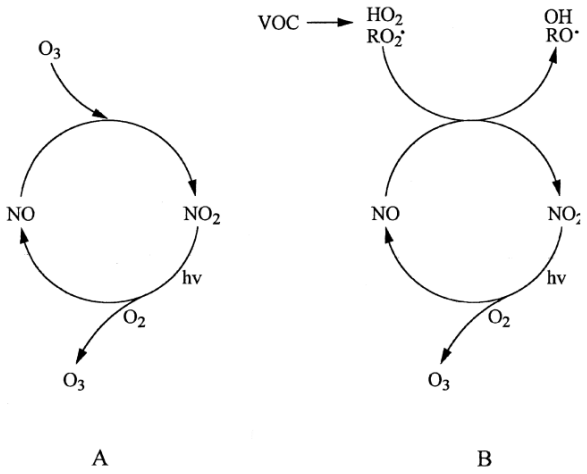

Figure 1.3 *Schematic representation of the reactions involved in NO-to-NO_2 conversions and ozone formation in (A) NO-NO_2-O_3 systems in the absence of VOCs, and (B) NO-NO_2-O_3 systems in the presence of VOCs (Atkinson, 2000).*

In the following sub-Chapter, we briefly review the fundamental concepts of atmospheric aerosols, their formation pathways, chemical composition and sources, and their multiple roles in climate and impacts on human health. The current understanding on the new particle formation, in particular secondary organic aerosol (SOA) from precursor gases (i.e. VOCs), is discussed.

1.3. Atmospheric aerosols

1.3.1. Formation pathways, sources and chemical composition

Atmospheric aerosols are an important component of the climate system. They are defined as liquid or solid particles (particulate matter – PM) suspended in the atmosphere and have profound impacts on the Earth-atmosphere system. The particle size may span from a few nanometers to a few micrometers and the bulk / surface chemical composition exhibit a huge variety, reflecting diverse origins and atmospheric processing (Wang, 2016). Understanding the sources, properties and evolution of these particles in the atmosphere is one of the major challenges in environmental research today. Significant progress has been made over the past two decades in understanding atmospheric aerosol chemistry and its connections to climate. Advances in technology for characterizing aerosol chemical composition and physical properties have enabled rapid discovery in this area. McNeill, (2017) has reviewed the fundamental concepts and recent developments on ambient aerosols, their chemical

composition and sources, light-absorbing aerosols, aerosols and cloud formation, and aerosol-based solar radiation management (also known as solar geoengineering).

Atmospheric aerosols are classified in two categories according to their formation pathways: primary or secondary (McNeill, 2017). Primary aerosols are emitted directly into the atmosphere in solid or liquid forms by processes such as bulk-to-particle conversion (e.g., wind-blown dust from arid regions), liquid-to-particle conversion (e.g., sea-salt aerosols), emissions of pollen and spores by vegetation, combustion processes (e.g., carbon particles emitted during wild fires) and volcanic eruptions (e.g., volcanic ash). Inorganic primary aerosols have short atmospheric lifetimes, typically only a few days. Secondary aerosols are formed by the chemical and physical processing of gas-phase precursors in the atmosphere (McNeill, 2017). Secondary aerosols are small; they range from a few nanometers up to 1 μm and have lifetimes of days to weeks. They consist of mixtures of compounds; the main components are sulphate, nitrate and organic carbon (McNeill, 2017). Sulphate aerosols are formed by the oxidation of SO_2 gas that may be neutralized by the uptake of NH_3 (Silvern et al., 2016).

According to their size, particles are classified into three categories: ultrafine particles (with aerodynamic diameter less than 0.1 μm), fine particles in the fine more or those with in the PM2.5 fraction. Coarse particles: fraction of the measured particle mass concentration determined from PM10 minus PM2.5 (*Particulate Matter in the United Kingdom*).

The chemical composition of aerosols varies widely based on their diverse sources, natural or anthropogenic (**Table 1.2**). Some aerosols have mainly natural origins (e.g., dust, sea salt, volcanic ash and volcanic sulphates), while other result from human activities (e.g., carbonaceous particles, ammonium sulphate and ammonium nitrate). Natural aerosols account for the largest aerosol mass in the atmosphere since they have relatively large dimensions (e.g., mineral dust and sea salt) and are considered in the coarse size range (> 2.5 μm in diameter). The concentration of anthropogenic aerosols in the atmosphere significantly increased from the start of the industrial revolution (Hinds, 1999). They exhibit on average a smaller size and thus show a lower global mass emission rate compared to natural aerosols (**Table 1.2**) (McNeill, 2017).

Table 1.2 *Sources of atmospheric aerosols with an estimation of their magnitudes (with ranges, where available)(reviewed by (McNeill, 2017)).*

Source	Magnitude (Tg yr^{-1})
Secondary inorganic (anthropogenic sulphates, nitrates)	69.9
Mineral dust (natural)	1000
Sea salt	1-3 x 10^4
Black carbon	7.5 (2-29)
Primary organic aerosol	33.9 (17-77)
Secondary organic aerosol	140 (50-380)

1.3.2. New particle formation: secondary organic aerosol

New particle formation (NPF) represents the first step in the complex processes leading to formation of cloud condensation nuclei in the atmosphere. NPF is characterized by a sudden burst of high concentrations of subnanometer-sized particles (1-3 nm) in the atmosphere followed by their growth. This represents the major source of the tropospheric aerosol population. Several NPF events have been observed under several environmental conditions such as urban locations, marine/coastal regions and forested areas (Lee et al., 2019). NPF has been shown to produce a large number of nanoparticles that go into submicron-sized particles (e.g., cloud condensation nuclei "CCN" size) even under polluted environments (Guo et al., 2014).

Secondary organic aerosols (SOA) are one of the main sources of uncertainty in the current understanding of the Earth's climate. SOA form by two major pathways: condensational and aqueous phase. Condensational SOA formation involves the thermodynamically driven partitioning of organic gases (for instance lower volatile species formed by the oxidation of VOCs) onto existing aerosol particles (Donahue et al., 2011). The VOCs emitted into the atmosphere from various anthropogenic and biogenic sources or formed in situ as products of atmospheric transformations of other VOCs are of great interest as they contribute significantly to atmospheric photochemical reactions mentioned in Section 1.2.3. The aqueous SOA formation involves the uptake of water-soluble VOCs by aqueous aerosols, cloud droplets or fog water that is followed by aqueous chemistry to form the lower-volatile SOA (McNeill, 2015).

The atmospheric formation of SOA is illustrated in **Figure 1.4**. The tropospheric oxidation of VOCs by photo-oxidants (such as O_3, NO_x and OH radicals) leads to the formation of lower volatility organic products (Atkinson, 2000; McNeill, 2017). The addition of oxygen and nitrogen to organic compounds reduces their volatility to several orders of magnitude (Atkinson, 2000; Lee et al., 2006). These SVOCs can efficiently initiate particle formation (Lee

et al., 2006) (**Figure 1.4**). The ability of a VOC to form SOA depends on its concentration in the atmosphere, its chemical structure, chemical reactivity and on the volatility of its oxidation products (Williams, 1995).

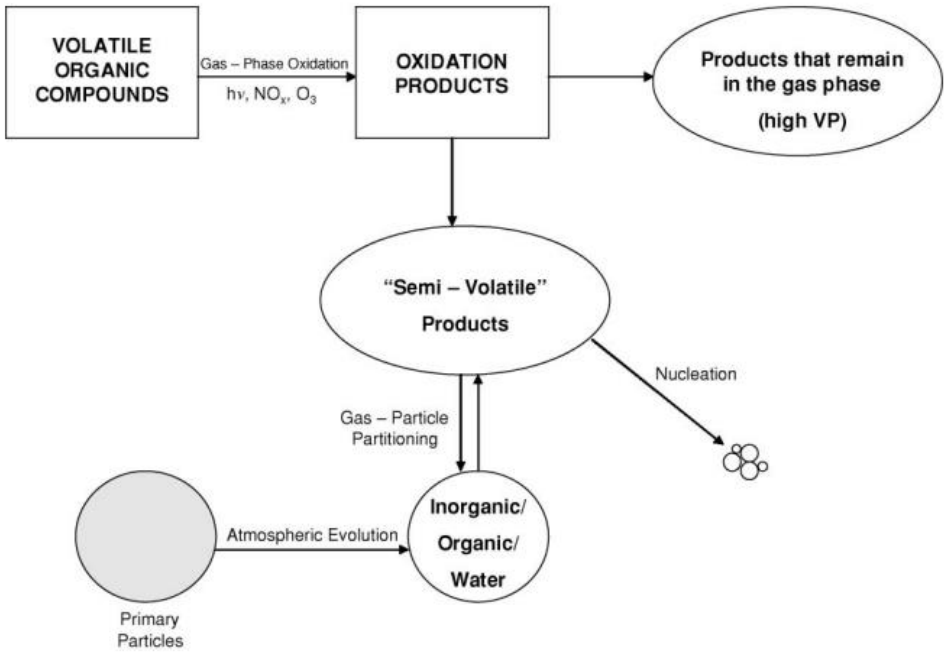

Figure 1.4 *Formation of secondary organic aerosols (Seinfeld & Pankow, 2003).*

The mechanism of the nucleation leading to the NPF remains not well understood (Bianchini et al., 2016). The oxidation products of VOCs are important for SOA formation and growth. However, their role in the particle nucleation or growth has remained unclear. It was thought that sulphuric acid is essential to initiate most of particle formation in the atmosphere and that ions have a relatively minor role. Some laboratory studies have reported the formation of organic particle from oxidized organic molecules, highly oxidized biogenic vapours or ion-induced nucleation of pure organic particles (Cappa, 2016; Kirkby et al., 2016). The latest studies together report that the highly oxidized multifunctional organic compounds represent the key players in SOA formation. Measurement studies have quantified the formation of these compounds from ozonolysis of monoterpenes in measurement chambers (Ehn et al., 2014) and modelling studies have quantified the formation of these compounds in the atmosphere and their role in air quality (Chrit et al., 2017). Furthermore, all these processes receive an increased attention since field observations revealed that aerosol properties can be significantly modified during atmospheric fate. In spite of significant instrumentation progress, our understanding of the processes of formation and aging of organic aerosol is still limited but entirely necessary to improve the robustness of these models.

1.3.3. Atmospheric aerosol impact on climate and health

Due to their small size, atmospheric particles have little inertia, and thus they may stay airborne for several days after their emission or formation in the atmosphere (McNeill, 2017). Accordingly, during their atmospheric lifetime, aerosols may be transported long distances and participate in atmospheric chemical reactions that impact human health, environmental quality and climate (McNeill, 2017). Even though atmospheric aerosols have relatively short atmospheric lifetime, ranging from a few days to a few weeks in contrast to greenhouse gases (GHG) with lifetimes up to a century or more, they can still contribute significantly to the radiative forcing, and thus influence the weather and climate (McNeill, 2017). As a direct effect, aerosols scatter and/or absorb solar radiation, referred to as direct radiative forcing. This effect, commonly referred to aerosol-radiation interaction, can contribute significantly to cooling (by scattering) or warming (by absorption) in the atmosphere (McNeill, 2017). A large concentration of inorganic aerosols will tend to scatter sunlight back into space (e.g., sulphate and nitrate aerosols), hereby preventing the direct radiation from reaching the surface, which induces cooling of the Earth-atmosphere system. Such an increase in the reflected solar radiation at the top of the atmosphere is nearly identical to the reduction in the solar radiation at the surface. While the direct radiation is prevented from reaching the surface, more scattered light is available which can affect the photosynthesis process, and thus improve plant productivity (Hinds, 1999).

As an indirect effect, aerosols in the lower atmosphere can modify the size of cloud particles, changing how clouds reflect and absorb solar radiation, and thus modify the Earth's energy budget (indirect radiative forcing). Cloud formation would not be possible without aerosols serving as CCN thus cloud droplets require an initial "seed" to start the concentration of water which is provided by aerosols (McNeill, 2017). Changes in aerosol characteristics can therefore lead to changes in cloud properties. The increase in aerosol concentrations due to human activities lead to an increase in cloud droplet numbers and smaller cloud droplets, which makes the clouds more reflective (McNeill, 2017). In addition, it is also believed that such clouds have a longer atmospheric lifetime (Rotstayn, 1999). For instance, sulphate aerosols can cause the augmentation in the number of cloud droplets while also reducing their size. The resulting clouds reflect more sunlight than they would have reflected without the presence of these aerosols (Rotstayn, 1999).

Besides their effects on climate, aerosols have also an impact on human health. Every year, about 7 million people die from air pollution-related illness, such as heart diseases,

respiratory illness and cancer according to a recent World Health Organization (WHO) report (World Health Organization, 2014). The size of the PM determines how the human body is affected by the pollutant. For instance, particles > 100 µm are usually too large to be inhaled. Aerosols with a diameter ranging from 10 to 100 µm usually get processed by the mucus membranes in the respiratory system - defence mechanisms of the body. Particles with size between 2.5 and 10 µm (coarse mode) are frequently deposited in the nose, pharynx and larynx. Fine aerosols (i.e. PM smaller than 2.5 µm or $PM_{2.5}$) are singled out as being the most hazardous portion of the aerosol population as they have a high chance of penetrating deep into the lungs, reaching bronchioles and alveoli (Carvalho et al., 2011; Sankhe et al., 2019). More than 3 million premature deaths worldwide have been estimated due to exposure to $PM_{2.5}$, thus representing one of the public health concerns (Lim et al., 2012).

1.4. Organic waste products (OWPs)

1.4.1. Types of OWPs

The wide increase in global population accompanied with urbanization and industrial progress has increased the generation of complex solid waste (Singh et al., 2011). Around 55% of all world population lives in urban areas. According to the estimated world population of 7.7 billion in 2019, the world population is estimated to increase to 8.51 billion in 2030 to 9.69 billion in 2050 and 10.36 billion in 2100 (World Bank, 2019). This leads to increasing demand for food production and thus yielding a proportional increase in agricultural wastes (Gontard et al., 2018). Agroecosystems are sources of pollution through their gaseous (e.g., ammonia, VOCs and GHG) and PM (Aneja et al., 2009) emissions. Air quality in agricultural areas is usually endangered by local emissions related to different activities like harvesting, soil cultivation, pesticides usage, livestock sector, soil dust particle emissions or organic waste products spreading.

Organic waste products (OWPs) are defined as the exogenous organic matter applied to the soil as substituent to mineral fertilizers. OWPs are classified according to their source: animal-based organic wastes (e.g., manure), plant wastes (e.g., green waste and garden wastes), urban wastes (e.g., sewage sludge and municipal solid wastes) and agricultural wastes which are defined as plant or animal residues that are not further processed into food. OWPs are classified as solid organic wastes compromising of organic biodegradable fraction with a moisture content below 85-90%. In Europe, about 1.6 million tons of OWPs are generated every year, where 61% comes from animal wastes, 25% comes from crop residues, 7% comes from municipal wastes and finally 7% comes from industrial wastes (ADEME, 2011). In

France, animal manure is considered the major source of OWPs annual production and 50% of this production is returned to soil (ADEME, 2011). France produces about 32 Mt of municipal and industrial OWPs where 40% of this are recycled as OWPs amendments to soil (ADEME, 2011). In the following, we give a brief description of sewage sludge, food biowaste and animal manure which are the main subjects of study throughout this thesis.

1.4.1.1. Urban waste products

The overall global waste generation is expected to become 3.4 billion tons by 2050 compared to 2.01 billion tons in 2016 (World Bank, 2019). Urban wastes include liquid waste (e.g., wastewater), solid waste (e.g., municipal solid waste), plastic waste, paper waste, metals, ceramics, organic household wastes (e.g., sewage sludge, food and kitchen biowastes, etc.), radioactive waste, recyclable waste, sanitary waste, hazardous and non-hazardous wastes, etc.

1.4.1.1.1. Sewage sludge

In developing countries, the generation of wastewater increases significantly. Around 90% of wastewater is left untreated into lakes, rivers and oceans (Khan et al., 2019). Wastewater treatment plants (WWTPs) collect a large amount of domestic waste, industrial waste, agricultural waste and waste from commercial spaces and provide treatment. This involves primary, secondary and tertiary treatment of wastewater that uses physical, biological and chemical means to purify the wastewater. Sewage sludge (SS) refers to the residual, solid, semisolid or liquid material that is generated at WWTPs as treatment by-products of wastewaters released from various sources (e.g., homes, industries, medical facilities, street runoff, etc.) (Christodoulou & Stamatelatou, 2016; Harrison et al., 2006). SS has potential fertilizer properties due to high nitrogen, phosphorous and organic matter content (Annabi et al., 2011; Diacono & Montemurro, 2010). It is composed of organic and inorganic materials, heavy metals and other hazardous materials. Therefore, it is extremely important to properly process SS in order to minimize its environmental repercussions (Iticescu et al., 2018). The amount of SS produced in European and developing countries is growing due to the increased demand for wastewater treatment. The average SS production in the top 13 European producing countries between 2010 and 2017 ranged between 181 and 1850 Gg DS $year^{-1}$, resulting in an average specific production of 21 ± 4 kg DS $person^{-1}$ $year^{-1}$ (DS = dry solid, see **Table 1.3**). The increasing production of SS results in higher costs for pre-treatment, transportation and disposal. Nowadays, SS treatment and management have become practical issues due to the massive increase of population in urban areas and to the constant changes in living standards.

SS production increased by 50% annually in European countries from 1992 to 2005 and further increase of the total sludge production being expected in the coming years (Bianchini et al., 2016). The main disposal routes of SS are landfilling, recycling as building materials, elimination through thermal processing or use in agriculture (**Table 1.3**).

Table 1.3 *SS production and disposal methods in European countries between 2010 and 2017. DS: Dry Solid (Eurostat. SS Production and Disposal, 2020).*

	SS production (Gg DS year^{-1})	Specific SS production (kg DS person^{-1} year^{-1})	SS disposal method (%)			
			Agricultural use	*Composting*	*Incineration*	*Landfill + other*
Germany	1850	22.8	27.1	14.5	58.3	0.1
United Kingdom	1278	19.9	79.5	n.a.	19.8	0.7
Spain	1144	24.6	76.5	n.a.	4.4	19.1
Italy	1103	18.4	33.1	n.a.	3.8	63.1
France	1060	16.1	44.3	30.4	19.2	6.1
Poland	550	14.5	20.1	6.3	12.8	60.8
The Netherlands	348	20.7	0	0.2	99.4	0.4
Austria	252	29.5	16.8	18.7	48.7	15.8
Czech Republic	227	21.6	41.0	42.6	5.0	11.4
Sweden	203	21.1	28.5	32.7	1.4	37.4
Switzerland	195	24	0	0	96.8	3.2
Hungary	186	18.7	9.8	46.1	22.0	22.1
Portugal	181	17.3	43.6	n.a.	0	56.4

n.a. = not available.

The traditional disposal methods of sludge have been incineration, dumping in rivers or oceans or depositing in landfills. However, these methods are costly and cause environmental pollution (Jamil Khan et al., 2006). For instance, sea dumping is banned in many countries due to its pollution to sea incurred by heavy metals, oil and microorganisms (Tay et al., 2001). Since SS is a good source of organic matter and plant nutrients, the most feasible ways to reduce the sludge quantities is their recycling and use as fertilizer (Iticescu et al., 2018). Thus the agricultural application of biosolid can represent an interesting strategy to improve crops productivity by increasing soil organic matter content, nutrients (e.g., N, P, K, Cu, Fe, Mn, etc) and soil fertility (Christodoulou & Stamatelatou, 2016). Moreover, the use of sludge on land, compared to incineration or sanitary landfill, has lower costs. The agricultural reuse of SS should be prioritized as recommended by the European Commission in the Circular Economy Action Plan (Collivignarelli et al., 2019). This use of SS has been preferred in France where nearly 44% of SS is applied to soil as organic fertilizer (**Table 1.3**). In addition, SS should be treated prior its agricultural application such as by anaerobic digestion, composting or chemical treatment to reduce its fermentability and the health hazards (Christodoulou & Stamatelatou, 2016; Collivignarelli et al., 2019).

1.4.1.1.2. Food biowaste

Food processing waste is derived from the processing of biological materials and it is biodegradable. Biowaste is defined in the landfill directive as "waste capable of anaerobic or aerobic decomposition such as food and garden waste, paper and cardboard" (Waldron, 2007). In addition, biowastes include organic food wastes originated from restaurants, supermarkets, commercial facilities, institutions and source separated organic waste collected form residences (Waldron, 2007). Food waste contains carbohydrates (starch, cellulose, etc.), proteins, lignin, fat and a high amount of moisture (Chojnacka et al., 2020). Fertilizers can be produced from food waste by anaerobic digestion, aerobic composting and chemical hydrolysis (Chojnacka et al., 2020). In the European Union, between 118 and 138 Mt of biowaste are produced annually. Around 40% of biowaste are effectively recycled into high-quality compost and digestate. Germany is considered the leading country in the biowaste management as it has the highest population in Europe. It collects more than 14 Mt of biowaste every year, followed by the UK with 8.9 Mt, Italy with 6.5 Mt and France 4.6 Mt of biowaste. Composting is a main treatment process of biowaste in Denmark and Sweden, while in Italy, anaerobic digestion is usually combined with a post-composting step (Siebert et al., 2019).

1.4.1.2. Animal manure

Animal products can be divided into two types: (1) valuable products, which are the conversion of feeds into meat, milk, eggs and wool; (ii) unavoidable products i.e. animal wastes (Mackie et al., 1998). Animal wastes (feces, urine and respiration and fermentation gases) are excreted in solid, liquid and gaseous forms. After excretion, solid and liquid animal wastes are subjected to microbial conversion (mainly anaerobic and aerobic), that converts organic substrates into microbial biomass and soluble and gaseous products (Williams, 1995). Animal manure is a complex mixture of undigested dietary residues, endogenous secretions and bacterial cells and their metabolic end points. It can have considerable values in agriculture if properly utilized (Mackie et al., 1998). Common forms of animal manure include farmyard manure (FYM) or farm slurry (liquid manure). FYM contains plant material (often straw), which has been used as bedding for animals and has absorbed the feces and urine (Dittmar et al., 2009). Agricultural manure in liquid form, known as slurry, is produced by more intensive livestock rearing systems where concrete or slats are used, instead of straw bedding (Liu et al., 2018).

Historically, manure has been valued based on the macronutrients N, P, K, S and organic matter (OM) content. The nutrients vary considerably in the excreted manure due to the feed composition, feed intake, animal type and production levels (Safley et al., 1986). The

concentrations of nutrients in manure are affected by the type of housing, manure management system, bedding and timing of manure removal, storage conditions and storage duration (Higgins et al., 2004). The carbon content of manure helps increase microbial biomass and soil respiration rates by acting as a feed source for native soil microorganisms (Dittmar et al., 2009). Manure from different animals has different qualities and requires different application rate when used as agricultural fertilizer. For instance, sheep manure contains high amounts of nitrogen and phosphorous, while pig manure is relatively low in both. Cattle manure is a good source of nitrogen and organic carbon (Bernal et al., 2009; Dittmar et al., 2009). Thus the nutrient composition of different manures varies greatly with the type of animal (omnivores, ruminant, etc), sex, age and diet fed to the animal, as well as geographical and climate conditions (Liu et al., 2013). High amounts of manure residue are produced in regions devoted to animal breeding. This results in intensive odours and bacteria contamination, high greenhouse gas emissions and high organic matter and nutrient loads (Gontard et al., 2018).

1.4.2. Organic waste management

The production of solid waste is characterized by poor handling and management and lack of proper disposal facilities (Ngoc & Schnitzer, 2009). The inadequate organic waste management like open burning and open dumping creates various problems such as environmental pollution, eutrophication, GHG emissions and effects on human health. Open waste dumps increase the risk of soil pollution in dumping areas as a result of leaching of heavy metals and other contaminants (Ngoc & Schnitzer, 2009). Other disposal methods such as burning or incineration of solid waste like municipal solid waste releases polychlorinated dibenzo-p-dioxins, dibenzofurans and toxic gases in addition to GHG emissions (e.g., CH_4 and CO_2) that cause air pollution and global warming (Vaish et al., 2019). The traditional disposal methods of wastes not only poses a grave threat to environmental quality and public health but also results in loss of nutrients presents in the waste and therefore of the economic value of wastes. In addition, development of technologies that convert the waste into fuel has been enhanced to reduce the emissions result from organic waste disposal (Pagliano et al., 2017).

Recently, agricultural recycling of OWPs becomes a more sustainable and eco-friendly approach than the traditional methods of waste disposal (Sharma et al., 2017). Through OWP recycling methods, organic wastes are decomposed and stabilized in terms of their volume, mass, pathogenic content and malodorous compound emissions (Diacono & Montemurro, 2010). OWPs recycling constitutes an alternative method to waste management via landfilling or incineration. The conversion (such as by composting and vermicomposting) and the use of

organic waste for agricultural purposes have several advantages on soil, such as it increases the soil organic matter (Peltre et al., 2012) by improving the soil chemical fertility, simulating microbial activity and increasing water retention (Diacono & Montemurro, 2010).

In the following two Sections, we briefly describe composting and vermicomposting, while focusing more on the anaerobic digestion processes applied on wastes for agricultural purposes, as anaerobically digested samples are analyzed during this PhD thesis (anaerobically digested SS and digestate biowastes).

1.4.2.1. Composting

Composting techniques for different organic solid wastes has become an environmentally friendly and efficient alternative for landfilling and other disposal methods. Composting is a natural process of biochemical conversion of heterogeneous solid organic waste (e.g., SS, crop residue, food and kitchen waste, garden waste, wood, paper, etc.) into humus-like substances. The decomposition of organic matter to a nutrient-rich end-product by microorganisms like bacteria and fungi occurs under controlled conditions of moisture, temperature, aeration and other controlling factors (Atalia et al., 2015).

Despite the advantage of composting as a proper waste and digestate management, it is considered a potential source of air and odor pollution (Zhu et al., 2016a). Composting is known to emit considerable amounts of gases such as CO_2, N_2O and CH_4. The gas emissions such as NH_3, sulphur compounds, most VOCs and semi-VOCs associated with composting process commonly contribute to considerable odor nuisance and to adverse health and environmental impacts (Scaglia et al., 2011). The VOCs emitted from composting plants are mostly biodegradable due to their biological origin and are released due to the aerobic, anaerobic and anoxic metabolic reactions of organic matter (Zhu et al., 2016a). Moreover, VOCs have properties of water solubility and adsorption potential. Based on the raw material and the operational conditions, a wide range of VOCs are being emitted. Yard waste composting is characterized by terpene emissions as well as alcohols, ketones and benzene as a result of biological breakdown. Composting of municipal solid waste is characterized by the emissions of organic acids, alcohols and sulphides (Büyüksönmez & Evans, 2007; Eitzer, 1995). Thus, the chemical composition of the gas emissions from composting depends on the substrate nature and operational conditions used as reported in Rincón et al., (2019).

Vermicomposting is another biological process using earthworms and microbial activity under controlled environmental conditions to convert organic waste materials into

vermicompost. Vermicompost is considered as an excellent, nutrient-rich organic fertilizer and soil conditioner (Yadav & Garg, 2011).

The recycling of organic waste as compost or vermicompost have several advantages, such as (a) reducing the size and mass of organic solid waste and resulting in a compost/vermicompost efficient for agricultural purposes (Dhamodharan et al., 2019), (b) reducing the air and water pollution and being very efficient in terms of economy compared to other treatment technologies if operated under suitable parameters, (c) reducing the GHG emissions, and (d) improving the soil nutrient profile and structure and reducing soil erosion (Colón et al., 2012). Apart from the listed advantages, the recycling of organic waste is also associated with some risk such as food contamination due to the presence of toxic heavy metals (Cr, Cd, Pb, Hg, Zn, Ni, etc.) (Sharma et al., 2019) and other hazardous organic contaminants such as polycyclic aromatic hydrocarbons, polychlorinated biphenyl, etc. Such contaminants can cause diseases like skin allergies, cancer, disorders in central nervous system, etc. (Clarke & Smith, 2011). Therefore, the compost/vermicompost should be properly tested before their agricultural application to avoid soil and food contamination. In addition, the over application of organic waste can pose several problems such as nutrient loss which necessitates to take the nutrient and soil demands into account before the application (Schulz & Römheld, 1997).

1.4.2.2. Anaerobic digestion

Anaerobic digestion is well adopted as an effective mean of organic waste treatment. It is a promising management technique involving simultaneous stabilization of organic waste and energy recovery due to several advantages in being able to handle large amounts of raw materials, simple process, high efficiency and production of renewable energy. Anaerobic digestion is a widely used biological process in which the organic matter is converted by microbial degradation into energy-rich biogas (~70% CH_4 and 30% CO_2) and a nutrient-rich residue called digestate (Appels et al., 2011). The resulting biogas can be used for producing heat, electric power and vehicle fuel. Thus this process has the potential to significantly contribute to a shift from fossil to renewable energy (Insam et al., 2015). Digestate is the by-product of anaerobic digestion process and has different properties from the undigested material (Appels et al., 2011). This process is widely used in municipal wastewater biosolids treatment for stabilization and production of methane gas. Anaerobic digestion has been widely used for biodegradable wastes treatment due to the increasing demand on renewable energy and the energy-efficiency of this process (Iacovidou et al., 2012). It is considered as an important method to reduce the quantity of organic wastes by their use for energy and heat

production. Different types of organic material such as organic municipal waste, sewage sludge from wastewater treatment, waste from food processing industries and agricultural wastes (e.g., animal manure, biowastes, plants and crop residues) can undergo anaerobic digestion and are suitable feedstock for this process (Appels et al., 2011; Iacovidou et al., 2012). The anaerobic digestion of food wastes is considered as one of the effective methods of waste management (Iacovidou et al., 2012). The suitable treatments, disposal and proper reuse of the digested material help to avoid any negative environmental impacts (Abubaker et al., 2012). Moreover, the digestate can be utilized as a fertilizer for agricultural lands since it allows the recycling of plant nutrients and improves the structure of the soil as it contributes to soil organic matter influencing the biological chemical and physical soil characteristics as a soil amendment (Nkoa, 2014). This reduces the need of fossil fuel-dependent mineral fertilizers (Holm-Nielsen et al., 2009). Land application of digestate has become a common practice in several countries as it has been shown to improve the soil properties (Nkoa, 2014). Recently, anaerobic digestion process has attracted interest due to its multi-functionality and resulted in an increasing number of biogas plants and increasing production of renewable energy in Europe. Consequently the amounts of digestate have also increased (Weiland, 2010). The quality of the digestate and its composition of macronutrients, micronutrients and OM depend on the digestion process used and the composition of the raw material used, thus this impacts its agricultural application (Kumar, 2012).

Anaerobic digestion of animal manure before its agricultural use has positive impacts as the obtained digestate contains higher proportion of mineralized plant-available nutrients than the untreated manure. Moreover, anaerobic digestion results in a significant decrease in the odour and is able to decrease the pathogenic content at the common digestion temperature of 39 ^{0}C and even more if the thermophilic digestion temperature of 55 ^{0}C is applied (Franke-Whittle et al., 2014). Compared to mineral fertilization and undigested manure, the digestate enhances the microbial activity and biomass because they contain more mineral N and less organic C (Insam et al., 2015). The post-treatment of digestate, like solid-liquid separation or composting have been emphasized even though the anaerobic digestion does not have negative impacts on the soil organic C. This allows the retaining of the organic matter in soil (Insam et al., 2015). Abubaker et al., (2012) found that the use of digestate as organic amendments had positive impacts on wheat crop yields and soil microbial activity compared to mineral fertilizers.

1.4.3. Application of OWPs in agricultural lands

1.4.3.1. Impacts of OWP application on soil

The quality of soil has been described based on its physical and chemical properties; however, soil health widely depends on the soil organisms. The magnitude of nutrient accumulation and its distribution in the soil profile depends on several factors, like soil type, the climate, the frequency of application, and the properties of the digestate (Stinner et al., 2008). Moreover, OWPs enhance the nutrient recycling and thus decrease the use of mineral fertilizers (Gutser et al., 2005). Some studies suggested several positive impacts of the manure amendments on soil, such as the increase in microbial biomass that enhances soil bacteria, fungi and high microbial activity. Soil microbial activity is considered as a crucial factor for nutrient cycling, which should be considered to improve soil heath and crop growth. Manure application to cropland enhances the soil carbon content as the microbial activity promotes aggregate stability an soil fertility (Menta & Remelli, 2020). In addition, the application of organic fertilizers improves the soil quality by changing the structure and the diversity of soil microbial communities. Several advantages arise from the organic amendments on soil structure, water-holding capacity and microbial activity (Arthurson, 2009). **Figure 1.5** shows the benefits and risks associated with OWP recycling (Atalia et al., 2015). Beside the positive impacts of OWP recycling and agricultural application, it can have different health and environmental risks. For instance, some contaminants can accumulate in the soil, degrade water quality or be emitted into the atmosphere (Houot et al., 2002).

Decreasing organic matter content in agricultural soil has become a global concern due to its direct impacts on soil fertility and agricultural yield. As a result of increasing global population, the food security can be ensured by recycling of organic wastes, which is a sustainable solution to enhance the quality of the soil ecosystem degraded by the over use of chemical fertilizers and other agrochemicals in the past (Eden et al., 2017). The agricultural utilization of organic wastes represents a dual opportunity of soil conditioning and sustainable organic waste management that reduces the environmental deterioration due to their random disposal (Diacono & Montemurro, 2010).

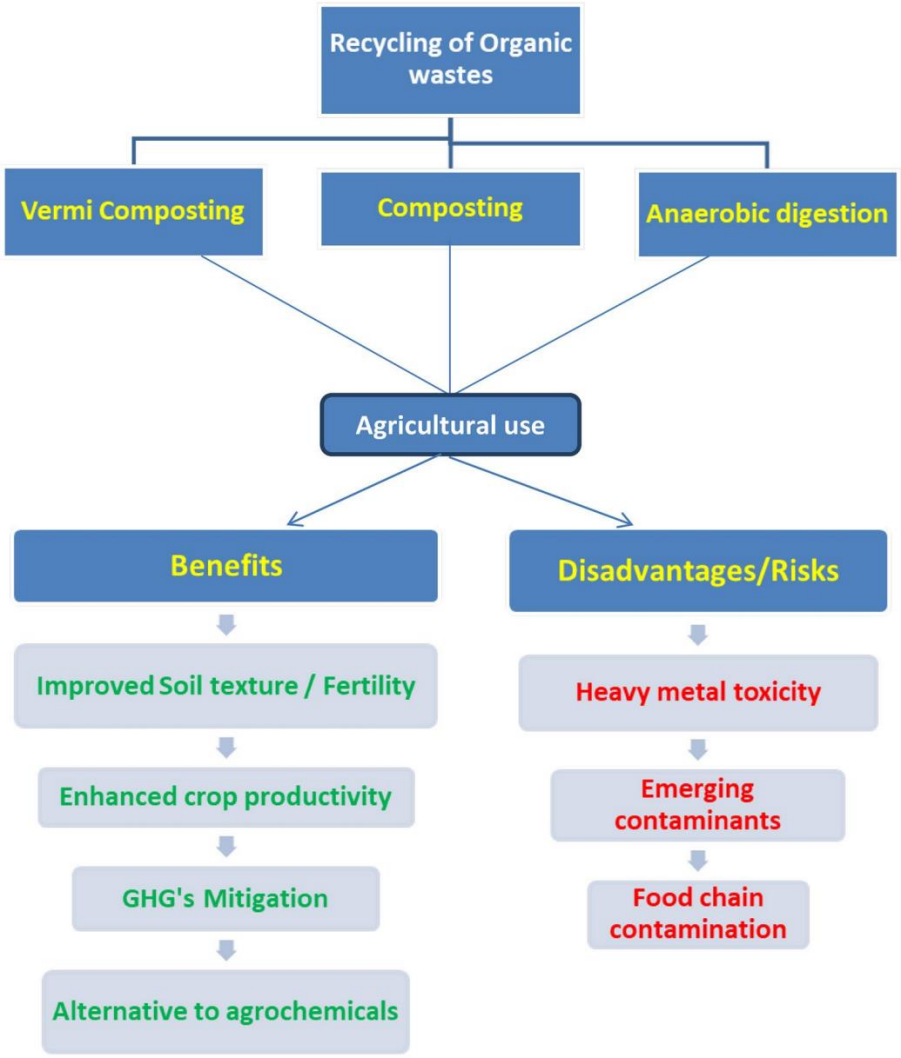

Figure 1.5 Agricultural recycling of OWPs and their associated advantages and disadvantages (Atalia et al., 2015).

1.4.3.2. Methods to reduce OWP emissions

In Europe, new legislation on environmental protection requires methods to reduce odour and ammonia emissions as a result of land application of OWPs. Several methods have been proposed to reduce emissions, among them, OWP treatment by anaerobic digestion (Feilberg et al., 2015) and the direct injection of digestate into the soil are considered as successful practices (Christodoulou & Stamatelatou, 2016; Collivignarelli et al., 2019; Feilberg et al., 2011; Orzi et al., 2018). The land application of OWPs can be done either by surface spreading or rapid mixing with soil after their spreading.

Regarding the other urban wastes such as green waste, the amount disposed in landfills will decrease by 50% before 2050 due to their increased use in agricultural crops (Kumar et

al., 2011). A study was performed to assess the advantages and disadvantages of the soil amendments of different organic wastes by Alvarenga et al., (2015). The authors characterized 8 different types of OWPs: (1) organic waste mixed with municipal solid waste compost, (2) municipal sewage sludge, (3) agricultural waste compost, (4) compost produced from agricultural waste and sewage sludge, (5) agro-industrial sludge, (6) municipal slaughterhouse sludge, (7) pig slurry digestate, and (8) paper mill wastes. The results of the study showed the positive impacts of the use of these organic waste amendments as they have high organic matter and nutrient (N, P and K) contents. Several risks have been proposed in this work (Alvarenga et al., 2015), such as the increase in soil salinity especially from the use of pig slurry, paper mill wastes and some compost samples; due to high electrical conductivity. In addition, SS has high concentrations of $N\text{-}NH_4^+$ leading to ammonia emissions and pathogenic microbes. Moreover, groundwater contamination due to the leaching of $N\text{-}NO_3^-$ from soil due to its high concentration in pig slurry digestate and high heavy metals except in compost produced from agricultural wastes and SS. Alvarenga et al., (2015) has recommended the SS composting due to its stabilization, sanitization and low metal content.

Land application of animal manure is a major source of odour emissions (Parker et al., 2013). Odour emissions constitute a problem as they affect the public health due to the diffusion of diseases and nuisance to the surrounding population. Different methods can be used for manure application on agricultural fields. Parker et al., (2013) performed a study to compare the VOC emissions using three application methods of swine manure (surface application, incorporation by disking 24 h following surface application and injection). The results showed that the injection of swine manure decreased the odorous aromatic compounds flux by 80 - 95% and the VOC flux decreased rapidly following the land application of swine manure. A new study has been performed to evaluate the impact of diet, land application method (surface-applied or incorporated), soil water conditions (saturated or wet), and time since manure application on VOC emissions from beef cattle manure (Woodbury et al., 2022). The results of this work showed that heptanoic acid, aromatics, indole and skatole contributed significantly to total odor activity value. In addition, the VOC emission fluxes were higher when the manure was surface-applied on the plots compared to its incorporation into the soil. This study highlighted the efficiency of incorporation of the manure soon after land application. Moreover, the authors suggested to delay land application when there is a high probability of rainfall for reducing the VOC emissions (Woodbury et al., 2022).

1.5. VOC emissions and new particle formation from OWPs

1.5.1. VOC emissions from agricultural recycling of OWPs

Agricultural practices are associated with considerable environmental burdens that affect the air quality, soil and water quality, directly or indirectly. Agriculture is considered as a major ground-level O_3 sink (Vuolo et al., 2017). VOCs emitted from terrestrial ecosystems have received much attention due to their contribution in atmospheric chemistry, soil processes and biotic interactions in soil. Several studies have been conducted to identify the sources and quantify the VOCs emitted from terrestrial ecosystems (Peñuelas et al., 2014; Singh et al., 2011). Most of these studies have focused on the natural ecosystem such as forest, grassland, wetland, etc.; and less attention has been paid on the VOC emissions from agricultural ecosystem. The global agricultural land area is around 4912 million hectares, comprising 37.4% of the global land area (FAO, 2013). Agricultural lands emit a large variety and amounts of VOCs (Leff & Fierer, 2008; Wang et al., 2015).

Agricultural activities such as the use of pesticides, fertilizer, machinery operation and livestock manure spreading emit a wide variety of pollutants such as ammonia, GHGs and VOCs. Previous studies have been performed to identify the atmospheric VOC emissions from fertilizers by performing laboratory studies and wind tunnel experiments (Kumar et al., 2011; Liu et al., 2018; Potard et al., 2017). The chemistry of some VOCs is less known compared to other agricultural pollutants, like ammonia and hydrogen sulphide (Feilberg et al., 2017; Ni et al., 2012). Several families of VOCs have been detected in OWP samples, such as organosulphur compounds (e.g., dimethyl and diethyl sulphide) (Byliński et al., 2019; Feilberg et al., 2015; Haider et al., 2022), terpenes (e.g., α-pinene, limonene) (Haider et al., 2022; Rincón et al., 2019), nitrogenated compounds (indoles), ketones and aldehydes (Haider et al., 2022; Sánchez-Monedero et al., 2018), and aromatic compounds (Abis et al., 2018; Haider et al., 2022; Nie et al., 2019).

While emission of nitrogen compounds from OWP is relatively well documented, there has been much less work on other VOC emissions. Recent measurements were performed in order to characterize VOC emissions from soil amended with different OWPs, such as municipal solid waste compost, green waste and sludge co-compost, bio-waste compost and farmyard manure (Abis et al., 2018). 21 VOCs that could be used to define emission profiles of different OWP treatments were isolated and can be considered as good markers of soil biological functioning. The results suggested that OWPs in soil affect the VOC emissions and the total flux was influenced by the quantity of organic matter and pH of the soil (Abis et al.,

2018). Potard et al., (2017) studied whether the amendments of pig slurry and methanized pig slurry affect the active bacterial communities and change the diversity and fluxes of VOCs emitted by soil. The results showed that the digested pig slurry reduces the VOC fluxes compared to the unamended plot and the pig slurry showed double fluxes due to high emissions of methanol. The results suggested that soil fluxes can be affected by additional fertilization and manure management in agriculture (Potard et al., 2017).

Rincón et al., (2019) has conducted an accurate and comprehensive study on gas emissions and odors from aerobic treatment of various organic matrices. The authors characterized the VOC and odour emissions upon composting of different digestates and solid waste. The identified VOCs belong to different chemical families of compounds that contributed differently to the overall cumulative mass of VOCs as illustrated in **Figure 1.6**. The chemical contribution of the identified chemical families is represented as "PCi" which is calculated based on a percentage basis, the cumulative mass production of a VOC or family of VOCs over the total production of VOCs (Rincón et al., 2019). For instance, substrates with a reduced vegetal content such as sewage sludge and agricultural waste like pig slurry and turkey manure showed low terpene emissions (PCi 0.07 – 21% of the total mass emissions). However, terpene showed elevated emissions (PCi 21-90%) from biowaste compost, green waste and the organic fraction of municipal solid waste. The main constituents of those samples were fruits, vegetables, leaves and food waste. Therefore, the high terpene emissions from the lignocellulosic material is explained by the decaying process of vegetable material and bacterial degradation of lignin and cellulose (Eitzer, 1995). Nitrogenated compounds and ammonia constituted the main emitted compounds from agricultural wastes, digestates and SS. SS was also dominated by the emissions of sulphide compounds (**Figure 1.6**) (Rincón et al., 2019). These VOCs are precursors of SOA and tropospheric O_3, resulting in environmental issues of air quality and climate (Atkinson, 2000). The composting emissions from food wastes and green wastes were dominated by terpenes, ketones, esters and alcohols (**Figure 1.6**) (Rincón et al., 2019).

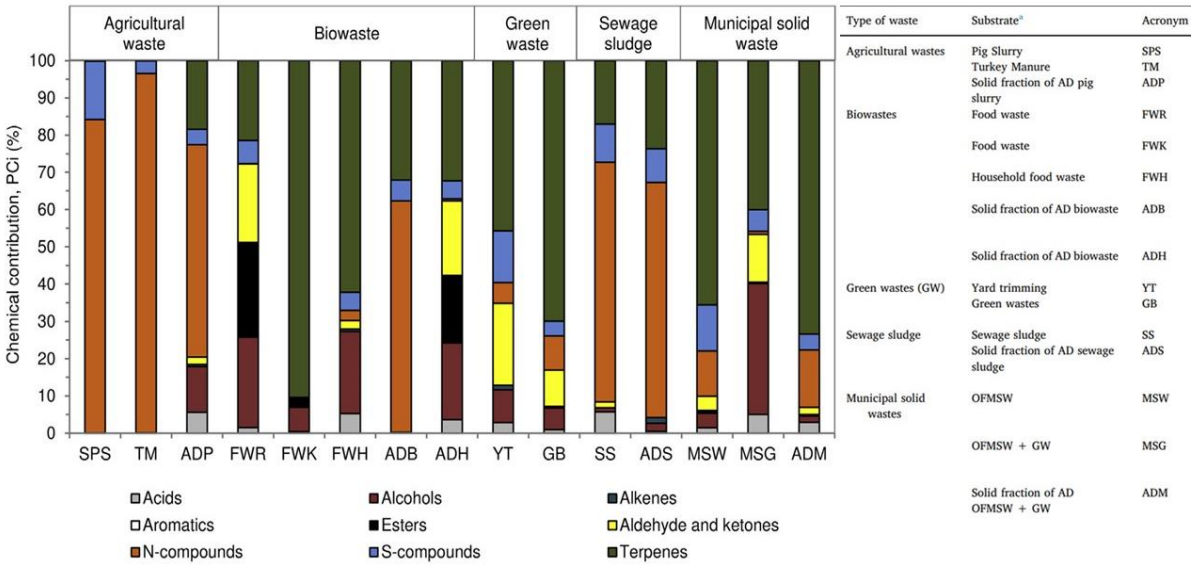

Figure 1.6 *Chemical contribution PC_i (%) of identified chemical families during the composting process of solid waste and digestates (Rincón et al., 2019).*

In the following two Sections, we will present an accurate bibliographic overview on the VOC emissions from SS and animal manure, as those OWPs will be the core subjects of this PhD thesis (**Chapters 3** and **4**). Additional literature details will be also given and discussed in **Chapters 3** and **4**.

1.5.1.1. VOC emissions from sewage sludge

The main organic compounds reported in the literature related to VOC emissions from SS are volatile sulphur compounds, volatile fatty acids, alcohols, aldehydes, ketones, alkanes, alkenes, terpenes and aromatics (Byliński et al., 2019; Fisher et al., 2017; Haider et al., 2022; Harrison et al., 2006; Nie et al., 2019; Rincón et al., 2019; Zhu et al., 2016a). There are very few studies quantifying the gaseous compounds emitted from SS, and those studies primarily address their odorant properties for identifying suitable odour abatement techniques (Byliński et al., 2019; Mustafa et al., 2017; Nie et al., 2018; Rincón et al., 2019). VOCs such as trimethylamine, acetic acid, limonene and ethylbenzene were identified at high levels in anaerobically stabilized sludge (Fisher et al., 2017). Oxygenated VOCs showed the highest concentration levels and acetone was the major species at the level of SS composting plant (Byliński et al., 2019).

Several studies performed on SS samples or SS compost showed the presence of different inorganic and sulphur organic compounds (hydrogen sulphide, methyl mercaptan, DMS, DMDS, carbon disulphide) produced by anaerobic microorganisms. Sulphur compounds are also produced by bacteria through the reduction of sulphate- and S-containing amino acids (Higgins et al., 2006; Zhu et al., 2016). These amino acids are monomers of protein extracted

from activated sludge and anaerobically digested sludge. Organic sulphur compounds from dewatered biosolids can be generated by the degradation of sulphur-containing amino acids and the methylation of sulphide and methanethiol. Furthermore, thermal treatment of SS leads to the emission of pollutants in the form of sulphur dioxide (SO_2) (Zhu et al., 2016), and SS can contain high concentrations of sulphur compounds, resulting in high emissions of SO_2 (Byliński et al., 2019; Ciuraru et al., 2021; Fisher et al., 2017; Haider et al., 2022; Nie et al., 2019; Rincón et al., 2019).

A recent study has been conducted to qualify and quantify the VOC emissions from different types of SS taken at different stages of treatment (Haider et al., 2022). The analyzed samples were collected from a WWTP located in France. This study revealed that SS samples emitted a large spectrum of VOCs where 380 compounds were detected, quantified and classified into different chemical groups. The identified chemical groups include: hydrocarbons, nitrogenated, oxygenated and organosulphur compounds. Several aromatic compounds and indoles (e.g. skatole) were emitted significantly from the undigested SS. Some of these VOCs can serve as precursor gases for atmospheric aerosol formation. The results of this work are described in details in **Chapter 3** of the manuscript.

1.5.1.2. VOC emissions from animal manure

New data and knowledge were obtained from experiments under laboratory and field conditions on VOC emissions from land application of animal manure (Ciganek & Neca, 2008; Feilberg et al., 2010, 2011, 2015; Ni et al., 2012; Ni et al., 2015; Woodbury et al., 2014, 2022). Ngwabie et al., (2008) have performed a 2-week measurement period in a large cowshed in Germany. The authors reported that the cowshed VOC emissions are dominated by OVOCs, such as methanol, ethanol, acetone, acetaldehyde and acetic acid. Other VOCs such as dimethyl disulphide (DMDS), cresol and trimethyl amine have been reported in manure samples (Beck et al., 2007; Feilberg et al., 2010, 2015; Filipy et al., 2006; Kammer et al., 2020; Rabaud et al., 2003). Filipy et al., (2006) identified the VOCs released in a lactating cow open stall and from a slurry wastewater lagoon using GC-MS. Results showed the identification of 82 VOCs at a lactating cow open stall and 73 were detected from a slurry wastewater lagoon. The emitted VOCs belong to different chemical classes such as alcohols, aldehydes, ketones, esters, ethers, aromatic hydrocarbons, halogenated hydrocarbons, terpenes, other hydrocarbons, amines, other nitrogen-containing compounds and sulphur-containing compounds. In this work, the emission rates of ethanol and dimethyl sulphide (DMS) were measured from the lactating stall area using an atmospheric tracer method. Also the emission rates of acetone, 2-butanone,

methyl isobutyl ketone, 2-methyl-3-butanone, DMS and DMDS were measured from the slurry waste lagoon using laboratory emission chambers (Filipy et al., 2006).

Several research investigated the effects of land application of liquid dairy and swine manure on odor emissions (Liu et al., 2018; Parker et al., 2013). Parker et al., (2013) used a small wind tunnel to investigate emissions of odorous VOC from land application of pig manure slurry. The detected VOCs included 8 volatile fatty acids (VFA), 5 aromatics and 2 sulphur compounds. The VOC flux versus time relationships for the 24 h period following land application followed the first order exponential decay model. The authors considered their measurement technique to have limited time resolution and did not include two potential key odor compounds, H_2S and methanethiol. Moreover, Feilberg et al., (2011) used a static chamber to investigate odorant emissions from field application of pig manure and found several potential key odorants (e.g., methanethiol, H_2S and 4-methylphenol), but also identified shortcomings of the static chamber (e.g., compound instabilities in the chamber). Feilberg et al., (2010) used PTR-MS to study the odorant emissions from intensive pig production facilities. The VOC emissions included carboxylic acids, alcohols, carbonyls, phenols, sulphur and nitrogenated compounds (Feilberg et al., 2010). Such VOCs can contribute to unpleasant odor problems, O_3 formation and fine particles affecting the regional air quality (Kammer et al., 2020; Nie et al., 2019; Yuan et al., 2017). Much of the previous research has focused on the odor characterization and VOCs emission rates from animal feeding operations. For instance, several studies were performed on the emissions from concentrated animal feeding operations (CAFOs) (Filipy et al., 2006; Ni et al., 2012; Sun et al., 2008; Yuan et al., 2017). Ngwabie et al., (2007, 2008) reported that VOC concentrations in dairy, sheep and pig CAFOs were the highest during animal waste removal and feeding, indicating that large emissions were related to these activities. While the contributions of different sources to individual VOC emissions from a facility are not accurately known (Ngwabie et al., 2008), a study was performed to characterize the chemical composition of VOC emissions and explore different sources within the facilities that contribute to VOC emissions (Yuan et al., 2017). Additionally, in this study, the reactivity of emitted VOCs toward photo-oxidants (OH and NO_3) has been studied (**Figure 1.7**). The results of this work showed that alcohols and carboxylic acids dominated the VOC concentrations and sulphur compounds showed the highest contributions.

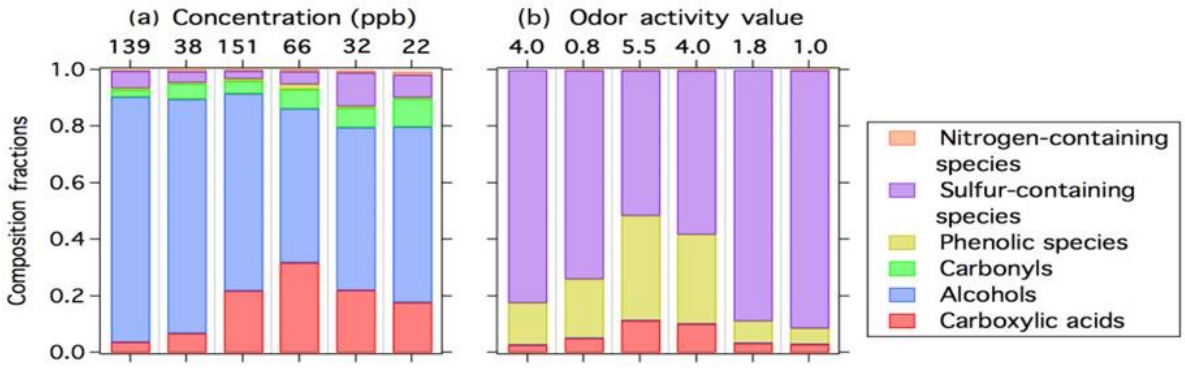

Figure 1.7 *(a) The fractional contributions of different VOC classes to the (a) total VOC concentrations and (b) odour activity value for the six concentrated animal feeding operation sites (Yuan et al., 2017).*

A recent field measurement campaign was conducted by Kammer et al., (2020) to characterize the gaseous and particulate emissions from an experimental farm in France containing a sheep pen and a dairy stable. The authors characterized more than 400 VOCs using the online and offline mass spectrometric techniques. The results showed that the diary stable emitted more VOCs than the sheep pen, with a maximum emissions of oxygenated compounds and hydrocarbons. The authors identified emission tracers for each pen and highlighted the sources of VOC emissions by correlation analysis. This was the first study that evaluated the emission rates for most of the identified VOCs with an overestimation by one order of magnitude.

1.5.2. New particle formation from OWPs

The measurements of VOCs from livestock fertilizers (Feilberg et al., 2015) or urban waste products (Nie et al., 2018) represent an essential data to better understand the formation and fate of SOA from agricultural practices. A recent study testing reduction scenarios of agricultural emissions, showed that agricultural practices such as livestock production and the use of nitrogen fertilizers impact near-surface air quality (Bauer et al., 2016). The authors showed that in many densely populated areas, aerosols formed from gases that are released by fertilizer application and animal husbandry can dominate over the combined contributions from all other anthropogenic pollution. The same modeling study showed that there are three regions in the world where agriculture represents a significant source of $PM_{2.5}$, namely Europe, North America and China (Bauer et al., 2016).

The regional observations of NPF processes are still little known. In agricultural areas, we have a limited understanding of the biosphere-atmosphere exchange of agriculturally emitted trace gases other than NH_3, and their contribution to SOA is missing (Aneja et al., 2009). It is recognized that agriculture contributes to primary aerosol emissions (Aneja et al., 2009) but to date there is only one estimate for the SOA formation from the precursor gases emitted from agricultural areas (Ciuraru et al., 2021). The importance of the effect of agriculture on atmospheric NPF is expected to vary regionally, as well as over the course of the year. In France, agriculture is estimated to generate around one-third of annual particle emissions (e.g., from livestock housing and tilling activities), but this estimate remains highly uncertain (Faburé et al., 2011). Agriculture has a remarkably large impact on $PM_{2.5}$ but is again highly uncertain both in terms of processes and quantification (Bauer et al., 2016). In areas with intense agricultural activity, the formation of SOA from precursors emitted by agricultural activities can dominate the other anthropogenic sources. However, the current knowledge mainly account for the effect of NH_3 on PM formation.

Feilberg et al., (2015) provided a time resolved data for a range of VOCs, NH_3 and H_2S. By performing ozonolysis experiments of manure slurry, the authors showed a consumption of trimethylamine emitted by manure due to its reaction with O_3. Murphy et al., (2007) reported that the ozonolysis of trimethylamine represents a significant source of SOA. Trimethylamine may be involved in the nucleation of new particles (Bergman et al., 2015). Different VOCs have been identified in OWPs (Section 1.5.1). Those VOCs represent SOA precursors; however, the chemical mechanisms in producing SOA from OWP samples and their chemical composition are not well understood. Moreover, our understanding of NPF is based mostly on measurements of particle size distribution with time, these measurements giving no information on the chemical mechanisms involving the particle nucleation and growth (Bzdek & Johnston, 2010).

Lelieveld et al., (2015), using an atmospheric chemistry model to investigate the link between premature mortality and emission source categories in urban and rural environments showed that agriculture has an impact on PM and, in many European countries, its contribution to $PM_{2.5}$ is 40% or higher. In these modeled agricultural emissions, the authors only consider the ammonia emissions that form inorganic $PM_{2.5}$. However, SOA formation from precursor VOCs emitted by agriculture was not estimated. This makes a part of the gap between the modeled and measured aerosols. The authors explained this by the underestimated agricultural sources (Lelieveld et al., 2015). Recently, we have conducted an accurate and comprehensive

study to identify the molecules that form new particles from SS in Ciuraru et al., (2021). In this study we suggested a detailed chemical mechanism underlying the particle formation and their initial growth. In addition, we reported the atmospheric particle formation solely from oxidized organic molecules and SO_2, both emitted from SS samples. To the best of our knowledge, this is the first time this aerosol formation phenomenon has been observed and quantified in an agricultural system (Ciuraru et al., 2021). Skatole or 3-methyl indole was demonstrated to be the key precursor gas that reacts with ozone and contributes to NPF in the presence of SO_2. Skatole belongs to an important class of atmospheric VOCs with high atmospheric emissions from land spreading of OWPs and contributes to odour nuisance (Feilberg et al., 2015; Liu et al., 2018). Our results of Ciuraru et al., (2021) are developed in **Chapter 5** of the manuscript.

1.6. Objectives and structure of PhD thesis

1.6.1. Objectives of the study

During these three years, this work has focused on different OWPs that serve as a source of VOC emissions and their role in new atmospheric secondary aerosols formation. This will provide new insights on the role of VOCs emitted by agricultural practices in the formation of SOA. The PhD objectives were hence constructed around three main scientific questions:

a. What are the VOCs emitted from treated and untreated sewage sludge samples? What are the effects of the treatment stage on the VOC composition and emission fluxes?
b. What are the chemical characteristics, composition, and emissions fluxes of the VOCs emitted from different animal manure samples?
c. How do different OWPs react toward ozone under controlled laboratory measurements and what are the key VOCs that serve as gas precursors and contribute to new particle formation?

Based on these, we studied the VOC emissions and their gas-phase oxidation products as a result of ozonolysis reactions from different organic waste samples (such as sewage sludge, animal manure and food biowaste) using proton transfer reaction quadrupole-ion-guide time-of-flight mass spectrometry (PTR-QiTOF-MS) and/or thermal desorption - gas chromatography - mass spectrometry (TD-GC-MS), and characterize the chemical composition of the newly formed aerosols by two-step laser mass spectrometry (L2MS) and Time-OF-Flight Secondary Ion Mass Spectrometry (TOF-SIMS).

1.6.2. Structure of the manuscript

The dissertation is structured into 6 Chapters. The **current (first) Chapter** presents the practical and scientific context of the work conducted during my PhD thesis. The definition of VOCs, their sources and atmospheric roles are briefly reminded. In addition, the role of VOCs in aerosol formation is introduced. A detailed bibliographic study is presented for the use of OWPs in agricultural fields and the previous works performed on the VOC emissions from different organic wastes.

The **second Chapter** gives an overview of the experimental techniques and set-ups employed in this work. A detailed description of the analyzed OWPs samples, along with the simulation chambers and analytical instruments used for the experiments is provided. Moreover, the methodology developed during this PhD thesis for mass spectrometric data analysis and used for the interpretation of experimental data is fully described in this Chapter.

The **third Chapter** presents a comprehensive study to qualify and quantify the VOC emissions from sewage sludge. In addition, we present the emission flux calculation for VOCs identified in sewage sludge samples. The Chapter ends with the discussion about the different identified chemical families of VOCs, with their atmospheric implications. Moreover, the impact of the treatment stage on the VOC composition and emissions has been discussed in this Chapter. The results provided in this Chapter have been recently published in *Science of the Total Environment* (Haider et al., 2022).

The online and offline characterization of VOCs emitted by animal manure is the subject of the **fourth Chapter**. Different animal manure samples collected from a farm located in Grignon, France were analyzed. The detailed chemical identification of VOCs emitted from each manure is possible by analysing the emitted gas phase using offline TD-GC-MS analysis. The discussion part of this Chapter includes each chemical family of compounds and focuses on some VOCs that are significant to atmospheric photochemistry. This Chapter ends with the statistical analysis performed on mass spectrometric data to unveil the similarities and differences between the manure samples. A scientific article including the results provided in this Chapter is under preparation.

The **fifth Chapter** is dedicated to study the reactivity of the emitted VOCs from different OWPs (sewage sludge, animal manure and food biowaste) toward ozone, potentially leading to new particle formation. In case of NPF, the newly formed aerosols were collected onto quartz fiber filters and their chemical composition was analyzed using the laser-based

mass spectrometric technique. The results in this Chapter cover NPF from undigested SS (already published in *npj Climate and Atmospheric Science* (Ciuraru et al., 2021)) and from biowaste (article in preparation).

The **sixth and final Chapter** proposes a general discussion, where we tried to gather all our results in a unique dataset, in order to derive the main conclusions and advances related to this PhD thesis. Special attention was paid to emission flux calculations. Finally, several perspectives related to the main outcomes of the thesis are proposed for future investigations.

Chapter 2

Materials and Methods

This Chapter provides a description of the experimental setup designed to study the emissions of volatile organic compounds and new particle formation upon ozonolysis of OWP samples. Various analytical mass spectrometric techniques were utilized to provide detailed information concerning the gas and particle phase compositions. The developed data processing methodology is described in details in this Chapter.

2.1. Sample description

2.1.1. Sewage sludge

The sewage sludge (SS) samples were taken from a wastewater treatment plant in France at the end of the following treatment stages: thickening (undigested SS – UDSS), anaerobic digestion (digested SS – DSS) and dewatering (samples with 30% and 60% of dryness - SS 30% and SS 60%, respectively) (**Figure 2.1**).

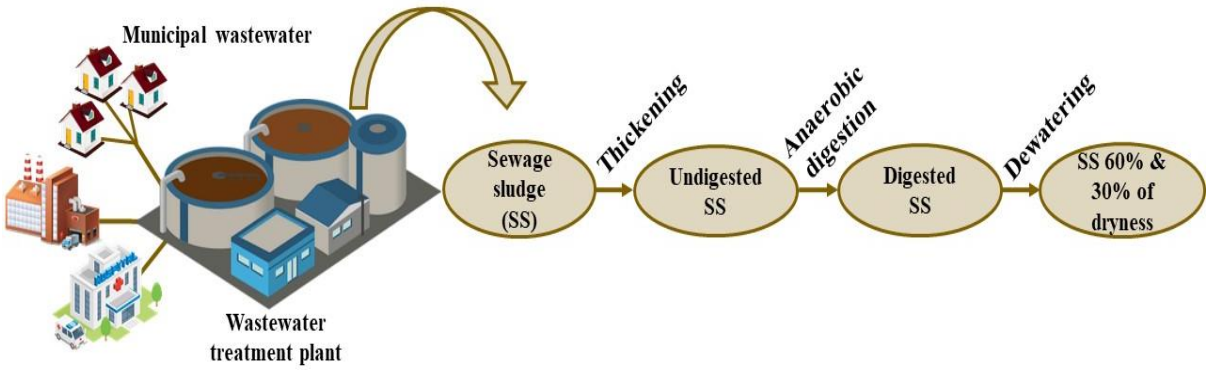

Figure 2.1 *Description of the SS samples collected from a wastewater treatment plant in France at different treatment stages.*

Sludge is formed during the biological treatment of wastewater, and then it is subjected to specific treatments to reduce its quantity and fermentability: thickening (undigested SS, UDSS), anaerobic digestion (digested SS, DSS) and dewatering which allows reaching up to 30% and 60% of dryness (SS 30% and SS 60%, respectively). The properties of bulk SS samples used in this study are listed in **Table 2.1**.

Table 2.1 *Physico-chemical properties of SS samples.*

Parameter (unit)	**Bulk sewage sludge**			
	UDSS	**DSS**	**SS 30%**	**SS 60%**
pH	8.4	8.5	6.1	7.3
Humidity (%)	96.3	97.1	80.6	15.6
Dry matter (%)	3.7	2.9	19.4	84.4
Organic matter (kg t^{-1})	26.0	19.0	126.0	604.0
Mineral material (kg t^{-1})	10.7	9.7	67.5	240.2
Organic nitrogen (g kg^{-1})	2.53	2.19	9.86	51.4
Total nitrogen (N) (g kg^{-1})	2.95	2.8	10.3	52.3
Organic carbon (kg t^{-1})	13.1	9.7	63.2	301.9
Sulphur trioxide (SO_3) (g kg^{-1})	0.84	0.78	5.7	23
Density (kg m^{-3})	1030	970	990	410
Ammoniacal nitrogen ($N\text{-}NH_4^+$) (g kg^{-1})	0.424	0.612	0.437	0.952

2.1.2. Animal manure

Four animal manure samples (horse, cow, sheep and goat manure) mixed with straw (shown in **Figure 2.2**) were collected from a farm located in Grignon, France (35 km west of Paris, 48050´28.89´´ N, 1056´56.03´´ E, altitude: 131 m above sea level) in December 2019 and analyzed.

horse manure cow manure sheep manure goat manure

Figure 2.2 *Animal manure samples spread on a stainless steel and placed in the simulation chamber.*

2.1.3. Other organic waste products (OWPs)

Different types of OWPs (food waste compost, digestate biowastes, cow manure, green waste compost and human urine) were analyzed. Food waste compost was collected from a company specialized in biowaste composting using an electromechanical machine. This compost was a result of 15 days of composting in the electromechanical apparatus followed by roughly 8

weeks of maturation on an open platform. The feedstocks were used as a ratio of 5:1 (w/w) of food waste (restaurants leftovers) and hardwood pellets. Digestate biowastes from restaurants food waste and supermarket leftovers were collected from a company located in France specialized in the collection and sorting of wastes. The digestate resulting from anaerobic digestion was pasteurized at 70^0C for about 1 hour before collection. Green waste compost was supplied from a local farmer (Ferme Martinière, Saclay) specialized in composting of green wastes from his farm and neighboring territories. The green wastes include grass or flower cuttings, hedge trimmings and brush. Human urine originated from a tank of a university building (Ecole des Ponts, Champs sur Marne) using a waterless male urinal for separated collection of urine. It was stored for roughly 2 years in the airtight tank.

A field campaign was done in Grignon on May 2021 where the samples were spread uniformly on 1 m^2 of soil cultivated with tomato (**Figure 2.3**). Following the spreading, the gas phase was sampled in bottles already put under vacuum. After that the collected gas phase was analyzed using a proton transfer reaction quadrupole-ion-guide time-of-flight mass spectrometer.

Figure 2.3 *Pictures of the field campaign performed in Grignon. The bottles used for gas phase sampling are shown. The spreading of each organic waste product sample on soil is illustrated.*

Those samples were also analyzed under controlled laboratory conditions. Each type of OWP was spread uniformly on a soil surface placed in an atmospheric simulation chamber. The

amounts of samples used in the chamber were estimated based on a given amount of OWP applied in agricultural fields (**Table 2.2**).

Table 2.2 *Real amounts of OWPs applied in the agricultural fields. The amounts used for chamber experiments were calculated relative to the surface area of the plate to spread the sample on (0.14 m^2).*

OWP type	Real amounts used agricultural fields	unit	Amounts used in the chamber experiments	unit
Green waste	20 to 30	t ha^{-1}	350	g m^{-2}
Cow manure	30	t ha^{-1}	420	g m^{-2}
Food biowaste compost	20	t ha^{-1}	280	g m^{-2}
Digestate biowastes	20 to 40	m^3 ha^{-1}	420	ml m^{-2}
Human urine	15 to 30	m^3 ha^{-1}	350	ml m^{-2}

2.2. Chamber experiments

The experiments described in this work were performed in the ECOSYS laboratory using poly(methyl methacrylate) chambers with Teflon walls in a temperature-controlled laboratory. ~~atmospheric simulation chambers.~~ In this study, two chambers were used: a 0.03 m^3 (0.2 m height, 0.27 m width, 0.55 m length) and a 0.18 m^3 (0.57 m height, 0.57 m width, 0.57 m length). The sample to be analyzed (e.g., SS, animal manure, biowaste, etc.) was uniformly spread on a stainless steel plate with an area of 0.14 m^2 and 0.32 m^2 for the 0.03 m^3 and 0.18 m^3 chambers, respectively.

During the experiments, the chamber was first purged with purified dry air. The high purity dry air was obtained either from Air Liquide bottle or air generator "F-DGSi Ultra Zero Air Total Gas Generator" (Ultra Zero Air Total Gas Generator) operating at 50 L min^{-1}. The dry air was passed through two Restek Super-Clean Gas Filter kits to ensure 99.9% pure gas for the experiments (Restek™ Super-Clean™ Gas Filters). The first (Restek, 22020) was used for hydrocarbons, moisture and oxygen impurities removal; while the second (Restek, 21991) ensured an additional hydrocarbon trap. The flow rate of the dry air into the chamber was 6 L min^{-1} and 8.6 - 10 L min^{-1} for the 0.03 m^3 and 0.18 m^3 chambers, respectively. The residence time or the cycle duration of the dry air in the 0.03 m^3 and 0.18 m^3 chambers was 5 min and ~18 - 20 min, respectively (see Annex 1, **Table A.1**). The time of the sample introduction into the chamber has been chosen as the initial time of the experiment. Accordingly, after three

cycles of dry air inside the chamber, specific concentrations of ozone were introduced into the chamber.

Figure 2.4 shows the experimental setup designed to study the gas and particle phases of one sample. At the inlet of the chamber, the dry air or O_3 were introduced. At the outlet of the chamber, the gas and particle phases were continuously sampled and analyzed. The gas phase analysis was performed using mass spectrometric techniques such as a proton-transfer-reaction quadrupole-ion-guide time-of-flight mass spectrometer (PTR-QiTOF-MS) and thermal desorption gas chromatography with mass spectrometry (TD-GC-MS). In addition, the amounts of SO_2, CO_2, H_2O, NH_3, NOx and O_3 at the entrance or exit of the chamber were monitored. The principle of operation of each instrument is described in the following Sections. The flow rate toward each instrument is given in **Figure 2.4**. In order to overcome the problem of overpressure inside the chamber, one Teflon tube was connected at the exit of the chamber (labelled as "Exhaust" in **Figure 2.4**). Besides our experiments, blank tests (i.e. without sample) were performed for both chambers to determine the background signals of the instrument (details in Annex 1).

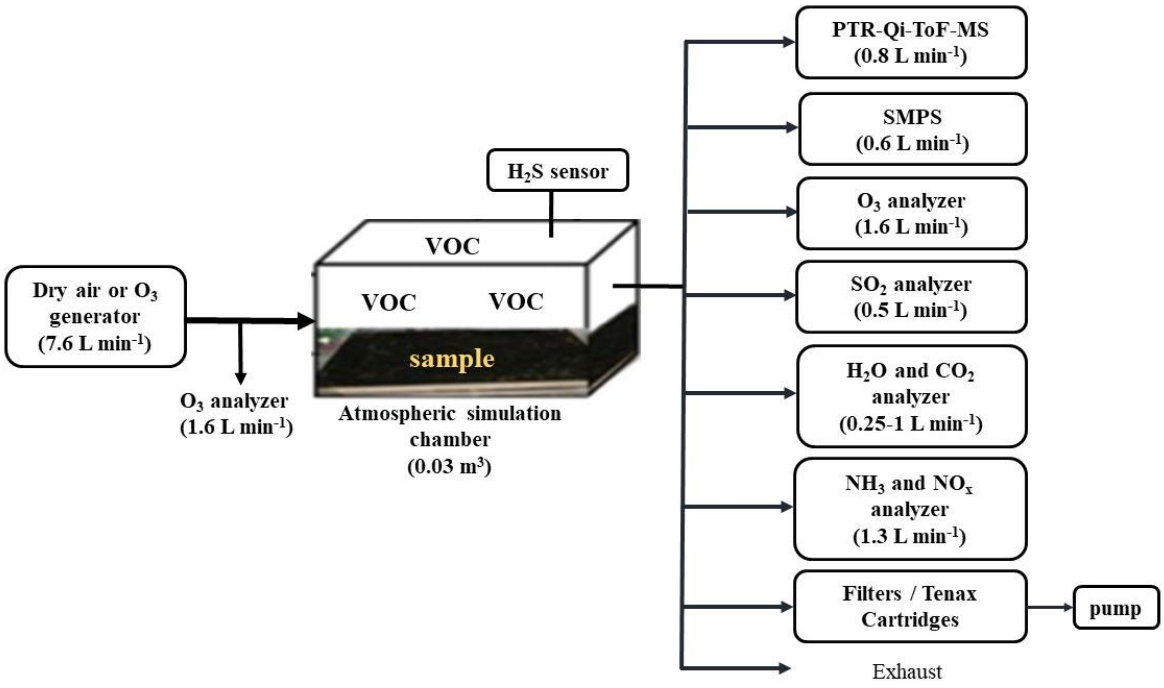

Figure 2.4 *Schematic representation of the experimental setup designed for the gas and particle phase analyses of a sample. The sampling can be done with or without O_3 addition into the simulation chamber. For some experiments, the hydrogen sulphide (H_2S) emitted from the samples has been measured using H_2S sensor placed inside the chamber. The flow rate toward each instrument is given in parentheses.*

2.2.1. SO_2 measurements

The sulphur dioxide (SO_2) emitted from the samples was measured using **SO_2 analyzer** (model 43C, Thermo Environmental Instrument). The measurement is based on fluorescence, where a ultraviolet (UV) light at a given wavelength is absorbed by the SO_2 molecules, which then decay to a lower energy state by emitting UV light at a longer wavelength (**2.1**). The emitted light is proportional to the concentration of SO_2 in the optical cell. The SO_2 measurement is performed at 1s time resolution in units of ppbv in ambient air (Sulphur Dioxide Monitor Instrument Handbook, 2016).

$$SO_2 + h\upsilon_1 \rightarrow SO_2^* \rightarrow SO_2 + h\upsilon_2 \quad \textbf{(2.1)}$$

2.2.2. Ozone production

Ozone (O_3) obtained by UV Ozone Generator (OSG-1, UVP) was injected into the chamber using purified dry air as a carrier gas. UV light in the spectral range 160 - 240 nm creates O_3 from the photolysis of the oxygen molecule (O_2). This photolysis (usually at 185 nm) dissociates the molecule (O_2) and creates oxygen atoms (O) that will then attach to any individual O_2 to create O_3 (Daumont et al., 1992).

2.2.3. Ozone measurements

A continuous monitoring of the mixing ratio (ppbv) of O_3 at the entrance and exit of the chamber was performed. This is based on the analytical technique known as UV absorption spectrophotometry by measuring the radiation emitted by a mercury lamp. The maximum absorption of O_3 is at a wavelength λ = 254 nm, which corresponds to the main emission line of mercury. Absorbance was measured alternately in a measuring cell (where O_3 circulates) and a reference cell (without O_3). The O_3 mixing ratio was calculated using the basic principle of Beer-Lambert law expressed in equation (**2.2**) (Trost & Fremgen, 2016):

$$\frac{I}{I_0} = \exp(-\sigma\, L\, C) \quad \textbf{(2.2)}$$

where I and I_0 are the light intensities measured in the measuring cell and the reference cell, respectively. σ is the absorption cross Section of O_3 at 254 nm ($114.7 * 10^{-19}$ cm^2, (Daumont et al., 1992)), L is the optical path of the cell (in cm) and C is the O_3 concentration (in molecule cm^{-3}). The mixing ratio of O_3 (ξ_{O3} in ppbv) is expressed using equation **2.3**.

$$\frac{I}{I_0} = \exp\left(-\frac{\sigma\, L\, P\, N_A\, \xi_{O3}}{10^{-9} R\, T}\right) \quad \textbf{(2.3)}$$

where N_A= Avogadro's number (6.02 * 10^{23} molecule mol^{-1}) and R is the ideal gas constant (8.314 m^3 Pa mol^{-1} K^{-1}). P (in Pa) and T (in K) are the pressure and temperature in the reference cell.

2.2.4. NOx and NH_3 measurements

The **Picarro G2103** gas concentration analyzer was used for some of our experiments. The instrument provides ultra-precise, real-time and stable measurement of ammonia (NH_3) and water (H_2O) vapour in parts-per-trillion (ppt) sensitivity. It incorporates coated (SilicoNert®) components in the critical gas pathway that reduce the propensity of NH_3 molecules to adsorb onto the pathway surfaces. This improves the measurement response time and eliminates measurement biases (PICARRO G2103 Ammonia Analyzer, Ambient, 2012).

In CRDS - Cavity Ring-Down Spectroscopy, the beam from a single-frequency laser diode enters a cavity defined by two or more high reflectivity mirrors. The Picarro analyzer uses a three-mirror cavity to support continuous travelling light wave. When the laser is on, the cavity quickly fills with circulating laser light. A fast photodetector senses the small amount of light leaking through one of the mirrors to produce a signal that is directly proportional to the light intensity in the cavity. When the photodetector signal reaches a threshold level (in a few tens of microseconds), the continuous wave (CW) laser is abruptly turned off. The light already within the cavity continues to bounce between the mirrors (about 100,000 times), but because the mirrors have slightly less than 100% reflectivity (99.999%), the light intensity inside the cavity steadily leaks out and decays exponentially to zero. This decay, or "ring down", is measured in real-time by the photodetector, and the time it takes for the ring down to happen is determined solely by the reflectivity of the mirrors (for an empty cavity). Consider that for a Picarro cavity of only 25 cm in length, the effective path length within the cavity can be over 20 km.

If a gas species that absorbs the laser light is introduced into the cavity, a second loss mechanism within the cavity (absorption) is now introduced. This accelerates the ring down compared to a cavity without any additional absorption due to a targeted gas species (e.g., NH_3). Picarro instruments automatically and continuously calculate and compare the ring down time of the cavity with and without absorption due to the target gas species (PICARRO G2103 Ammonia Analyzer, Ambient, 2012).

For some experiments, we used **Chemiluminescence Ammonia and nitrogen oxides analyzer** (Envea, air quality monitoring systems). The **AC32e-CNH3** consists of two

associated modules: the CNH3 module that allows the external $NH_3 \rightarrow NO$ thermal converter (measured parameter NH_3) plus the AC32e* chemiluminescence analyzer (measured parameters NO, NO_2 and NO_x) for stable and repeatable multi-gas measurements at very low levels. Chemiluminescence sensing is a light-based technology ideal for the measurement of ammonia, NO, NO_2 and total oxides of nitrogen (NO_x) in a wide range of combustion and emissions monitoring applications. Chemiluminescence detectors take advantage of NO and NO_2 chemical reactions that emit light. A volume of air is sent to a reaction chamber where O_3. In the chamber, NO reacts with O_3 and leads to the formation of NO_2 in a state excited which then emits energy in the form of light (photons) according to the following equations:

$$NO + O_3 \rightarrow NO_2^* + O_2 \quad (\mathbf{2.4})$$

$$NO_2^* \rightarrow NO_2 + h\upsilon \quad (\mathbf{2.5})$$

The quantity of photons thus produced is measured by a chemiluminescence detector (CLD). Chemiluminescence analyzers use a thermally stabilized photodiode to measure the intensity of the light produced by the reaction of NO with O_3. The intensity is directly proportional to the concentration of NO that was converted to NO_2 by the reaction. By converting NO_2 in the gas stream to NO, then reacting it with O_3, the total NO_x value can be calculated, allowing speciation of NO, NO_2 and total NO_x with a single analyzer ($NO_x = NO + NO_2$) (Chemiluminescence Ammonia and Nitrogen Oxides Analyzer).

2.2.5. Particle number concentration and size distribution

Particle mobility size spectrometers often referred to as Scanning Mobility Particle Sizers (model SMPS 3938, TSI) have found a wide application in atmospheric aerosol research. The number size distribution of atmospheric aerosol is a basic, but essential parameter required in calculations of the effects of aerosol on climate, human health and ecosystem (Wiedensohler et al., 2010). SMPS is based on the principle of the mobility of a charged particle in an electric field and used to measure the particle number concentration and size distribution.

The utilized SMPS combines a differential mobility analyzer (DMA; TSI 3085) and a condensation particle counter (CPC; TSI 3788). DMA allows the separation of particles according to electrical mobility, with only particles of a narrow range of mobility exiting through the output slit (Wiedensohler et al., 2010). Before the particles enter the DMA, they are brought to a bipolar charge equilibrium using a bipolar charger. Positive and negative ions are produced continuously in this charger by soft X-ray technique which generates the bipolar ions needed to achieve a steady-state charge distribution. The Model 3088 Advanced Aerosol

Neutralizer uses a low-energy (< 9.5 keV) soft X-ray source to generate high concentrations of ions with positive and negative polarity. The charged particles are then injected into the DMA and then laminarly merged with the particle-free sheath airflow. In the DMA, charged particles are separated as a result of the applied electrical field, giving the particles different trajectories according to their size. Only particles with a specific diameter are selected at a given electric field and then the particles are sent to the CPC (Wiedensohler et al., 2010). CPC determines the particle concentration at that size. Since the sampled particles are too small for detection, their size is increased by condensing water vapour. Then a photodiode can detect particles that diffuse radiation emitted by a laser.

The quality of mobility spectrometer measurements depends essentially on the stability of the aerosol and sheath flow rates, as well as the performance of the CPC. An error in the sheath flow rate of 1% corresponds to a shift of 1% in the selected electrical particle mobility. For the typical ratio of sample to sheath flow rates, 1:10, a leak in the loop of the sheath flow of 1% would cause a 10% error in the aerosol flow rate. Thus, the precision of the instrument is in the order of 1% on the number of particles and 10 % on the size. In this work, the sample flow rate was fixed at 0.6 L min^{-1} and sheath flow at 6 L min^{-1} to ensure a ratio 1:10 between aerosol and sheath flows in the DMA. This provides the measurements of the particle number and size distribution between 2.64 and 100 nm electrical mobility diameter. In the present study, it was assumed that the wall loss rate was constant during the experiments. Moreover, the possibility of particle loss in the tubing was considered.

2.2.6. Humidity and CO_2 measurements

Humidity and CO_2 mixing ratios were measured using a **LICOR (LI-840A)** instrument. The LI-840A CO_2/H_2O Gas Analyzer is an absolute, non-dispersive, infrared gas analyzer based upon a single path, dual wavelength and infrared detection system. The CO_2 and H_2O measurements are a function of the absorption of IR energy as it travels through the optical path. Concentration measurements are based on the difference in the IR absorption between reference and sample signal. Reference and sample channels measure infrared gas absorption in a single path using narrow band optical filters with selected bands. The CO_2 sample channel uses an optical filter centered at 4.26 µm, corresponding to an absorption band of CO_2. The reference channel for CO_2 has an optical filter centered at 3.95 µm, where CO_2 has no absorption. The H_2O sample channel uses an optical filter centered at 2.595 µm, corresponding to an absorption band of H_2O. The reference channel for H_2O has an optical filter centered at 2.35 µm, which is a non-absorbing spectral region for H_2O. Data output is provided in a digital

format through an RS-232 interface that supports connection to an external computer with a time resolution of 1s (LI-840A CO2/H2O Analyzer, 2016).

2.2.7. Particle sampling for off-line analysis

For particle phase analysis, the particle number concentration and size distribution was monitored using a scanning mobility particle sizer (SMPS). In the experiments where particle formation was observed, the freshly formed aerosols were collected onto quartz fiber filters (QFF, Pall Tissuquartz 2500 QAT-UP, cut to 14 mm diameter) using special pumps with specific flow rates (2-6 L min^{-1}). Blank QFFs were also prepared and stored in the same conditions as other samples, to be used as reference samples during the chemical analysis. The formed aerosols are chemically characterized using laser-based and secondary ions mass spectrometric techniques (see below).

2.3. Volatile organic compounds analysis

The analyses of VOCs emitted from the samples were performed using mass spectrometry – an analytical technique used to identify unknown compounds within a sample, thus helping to identify its chemical composition. Mass spectrometry has been developed and advanced during the last 50 years, and becoming the analytical method of choice in many scientific fields. The general principle of mass spectrometry is to create gas-phase ions, separate them in space or time based on their mass-to-charge ratio (*m/z*) and then measure their relative abundances (intensities). The gas phase ions are generated by a wide variety of suitable ionization methods such as electron impact, chemical ionization, thermal ionization, laser ionization, etc (Gross JH., 2004). Despite the large number of ionization methods and types of mass analyzers in use, all mass spectrometers follow the same basic scheme: they comprise of an ion source, a mass analyzer and a detector, which are operated under high vacuum conditions (Gross JH., 2004). The online gas analysis based on mass spectrometry using electron impact (EI) ionization suffers from the strong fragmentation of molecular ionic species. This fragmentation may complicate the quantitative analysis of the components present in a mixture of organic compounds under analysis (Hansel et al., 1995). Chemical ionization (CI) technique, first introduced by (Munson & Field, 1966), is based on the ionization of neutral molecules by chemical reactions in the gas phase.

Several approaches and tools can be used to detect VOC emissions in a laboratory system. Gas chromatography coupled with mass spectrometry (GC-MS) and proton transfer reaction mass spectrometry (PTR-MS) are the most frequent devices used to detect VOC

emissions. A flame ionization detector (GC-FID), a mass spectrometer (GC-MS) and a flame photometric detector (GC-FPD) can all be coupled with gas chromatography. These methods require VOC pre-concentration in absorption traps (e.g., solid phase micro-extraction-SPME) and they are time-consuming. PTR-MS, on the other hand, enables for real-time measurements of VOCs emitted from samples.

In the present study, VOC emissions from OWP samples were detected and quantified using a proton transfer reaction quadrupole-ion-guide time-of-flight mass spectrometer (PTR-QiTOF-MS). For some experiments, the gas phase was trapped on Tenax TA or carbotrap cartridges and analyzed by thermal desorption gas chromatography with mass spectrometry (TD-GC-MS)

2.3.1. Online VOC analyses by PTR-QiTOF-MS

A proton-transfer-reaction mass spectrometer (PTR-MS) system has been developed as a new method for quantitative trace gas analysis in the 1990s by Lindinger et al., (1998) at the Institut für Ionenphysik in Innsbruck. The first versions were based on quadrupole mass analyzers and furthermore, PTR-MS coupled with a time of flight detector was developed (Jordan et al., 2009). TOF mass analyzers typically provide high mass resolution and acquire the entire mass spectrum for every package of ions that is injected into the flight path (Jordan et al., 2009). High–resolution proton transfer reaction quadrupole-ion-guide time-of-flight mass spectrometry (HR-PTR-QiTOF-MS, Ionicon Analytik GmbH) is an online technique characterized by high sensitivity, selectivity and fast time response. It is mostly used for real time measurements and monitoring of VOCs at low detection limit (5 pptv) in gaseous samples (Hewitt et al., 2003; Jordan et al., 2009; Sulzer et al., 2014). This technique is widely invested for atmospheric research where significant advances occur concerning its specificity and the instrument response through the analysis of different atmospheric air samples (Edelenbos et al., 2012; Feilberg et al., 2010, 2011; Hewitt et al., 2003; Liu et al., 2018). **Figure 2.5** shows a schematic representation of the PTR-QiTOF-MS technique.

PTR-QiTOF-MS is composed of four main parts (**Figure 2.5**). The first is the hollow cathode ion source where the reagent ions (H_3O^+ in this case) are produced from water vapour using a hollow cathode discharge (illustrated in **Figure 2.6**). NO^+ and O_2^+ can be also produced but are considered as impurities (Jordan et al., 2009; Sulzer et al., 2014). H_3O^+ are transported into the drift tube reaction chamber where the sampled gas phase is also introduced (via a gas inlet system with adjustable flow of 0.8 L min^{-1}).

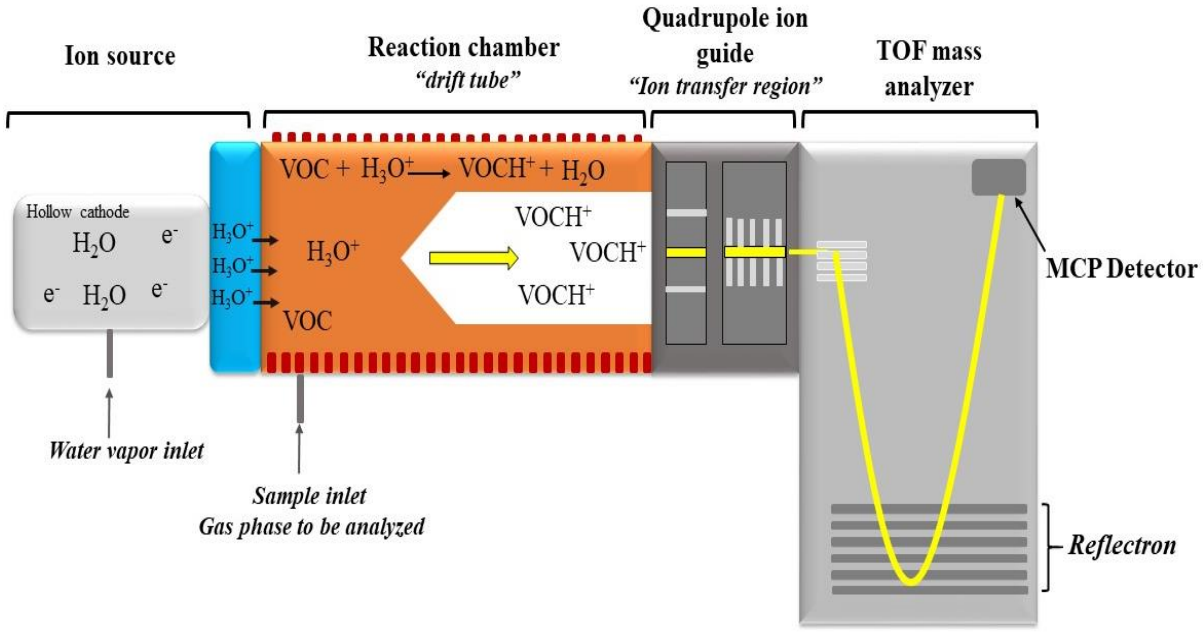

Figure 2.5 *Scheme of the PTR-QiTOF-MS technique that shows the four main parts of the technique. The transfer of protonated VOCs through the instrument is illustrated in yellow path.*

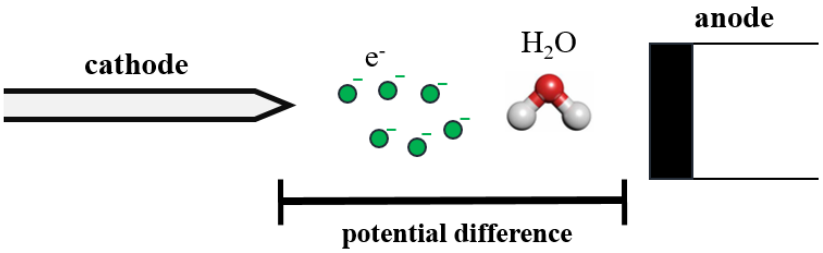

Figure 2.6 *Generation of reagent ions H_3O^+ in the hollow cathode ion source.*

PTR-QiTOF-MS uses low-energy soft chemical ionization, where the gas phase molecules are ionized by gentle proton transfer from the protonated water molecules (H_3O^+) into the molecule of interest (Hewitt et al., 2003). This low energy ionization results in relatively low levels of molecular fragmentation. This ionization happens in the drift tube (**Figure 2.5**). The main condition of this chemical ionization reaction to occur is that the compound must have a proton affinity (**PA**) greater than that of the water (i.e. ~ 697 kJ mol^{-1} or 7.22 eV) (Hansel et al., 1995; Hewitt et al., 2003). PA of a neutral atom or molecule is the negative of the enthalpy change in the gas phase reaction between a proton and the chemical species, usually electrically neutral species (Muller, 1994). H_3O^+ is the most suitable proton donor used in the analysis of air samples containing a wide variety of VOC traces for many advantages. First, H_3O^+ does not react with any of the natural components of air since they all have PA lower than H_2O

molecules (Hansel et al., 1995). Second, most of the organic compounds, including alcohols, aldehydes, aromatics, ketones, alkenes, amines, nitriles, sulphides and acids, have PA (> 700 kJ mol^{-1}) large enough (**Figure 2.7**) and therefore proton transfer occurs on every collision with rate constant (k) (typical values $1.5 * 10^{-9}$ cm^3 $s^{-1} \leq k \leq 4 * 10^{-9}$ cm^3 s^{-1}) (Hansel et al., 1995). Moreover, many of the proton-transfer processes are non-dissociative so that only one product ion species occurs for each neutral reactant as described in equation **2.6**. The molecule resulting from this interaction is positively charged with the mass of the parent ion, plus an additional proton ($VOCH^+$).

$$H_3O^+ + VOC \rightarrow VOCH^+ + H_2O \quad \textbf{(2.6)}$$

where H_3O^+ is the hydronium ion produced in the ion source, VOC is the compound emitted by our samples and introduced into the drift tube, and $VOCH^+$ is the product ion. NO^+ and O_2^+ can react with organic compounds which would interfere with the results so their concentrations in the drift tube are kept under 0.05% and 5% of H_3O^+, respectively (Yáñez-Serrano et al., 2021).

The drift tube is made of stainless steel rings separated by Teflon rings to isolate them electrically and coupled by a resistor chain to create an electric field. This electric field enhances the kinetic energy of the ions, causing hydrated ions to dissolve when they collide with the air. The water vapour present in the drift tube can bind with the hydronium ions (H_3O^+) and the product ($VOCH^+$) to form water clusters $H_3O^+(H_2O)_n$ and $VOCH^+(H_2O)_n$, respectively, where n is an integer.

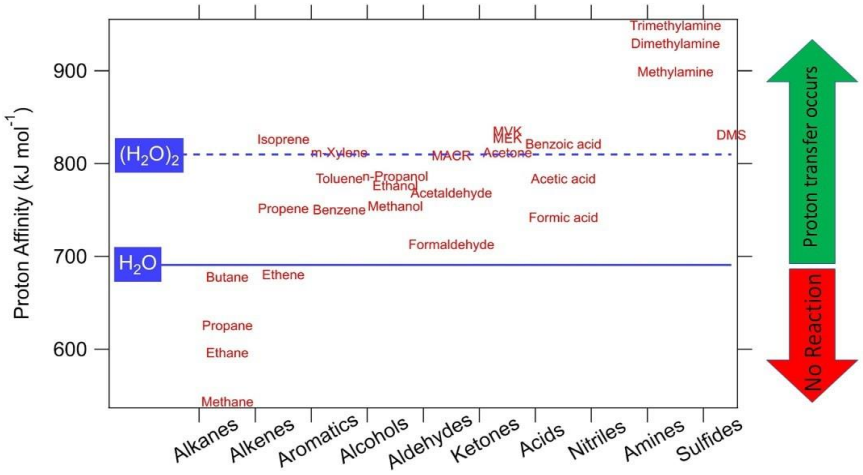

Figure 2.7 *Proton affinities of some common VOCs. Compounds having higher proton affinity than water undergo proton transfer reaction with H_3O^+ and are detectable in real-time with PTR-MS (Cappellin, 2018).*

Water clusters are the compounds that have bonded with a water molecule upon protonation. The formation of water cluster depends strongly on the drift tube pressure and electric field. To prevent the clustering and thus simplifying the mass spectrum, the reaction chemistry is performed in a drift tube so the cluster concentrations are reduced to a minimum by collision induced dissociation with air molecules in the drift tube. Drift tube reaction dynamics are characterized by the ratio of the electric field "E" (volts per centimeter) over the number density of gas "N" (cm^{-3}) in the drift tube according to equation (**2.7**). The units of this ratio are expressed in Townsend (Td), where 1 Td is equal to 10^{-17} V cm^2.

$$\text{Drift field strength} = \frac{E}{N} \text{ (V cm}^2\text{)} \qquad \textbf{(2.7)}$$

Temperature and pressure in the drift tube affect the number density of air. Increased electric field (higher Td) results in more energetic collisions and less clustering. Moreover, it causes greater degree of dissociative protonation and the creation of organic fragment ions. Such fragmentation is not desirable since the interpretation of the PTR-QiTOF mass spectrum relies upon its presentation as a simple $M+H^+$ mass spectrum where M is the molecular weight of a VOC.

In this work, PTR-QiTOF-MS was operated in standard conditions, where the pressure in the drift tube was tuned to 4 mbar, the temperature to 80 ^{0}C and the drift voltage to 1000 V, while the extraction voltage at the end of the drift tube (Udx) was set to 44 V. These conditions were set to ensure a constant E/N ratio at 132 Td. This value of E/N ratio limits fragmentation and lowers the sensitivity of the protonation rate to variations in relative humidity (Abis et al., 2018; Sulzer et al., 2014). All the above parameters were controlled in order to maintain constant ionization conditions within the drift tube.

Once the VOCs are ionized, they are accelerated in the drift tube and then injected into the quadrupole ion guide and electromagnetic lenses (i.e. a transfer region between the drift tube and the TOF mass spectrometer). This provides more effective transfer of the ions into the TOF analyzer. Quadrupole ion guides (and other means of transporting ions, such as ion funnel) are well known in mass spectrometers with atmospheric pressure ion source (Covey et al., 2009). The electromagnetic lenses focus the ions in the TOF mass spectrometer analyzer. The latter separates the ionized VOCs by inertia before their detection (Abis et al., 2018; Sulzer et al., 2014). The TOF tube is equipped with a V-shape reflectron where an electric field is applied. The applied electric field leads to the change in the trajectory of the ions by first slowing them down and then re-accelerating them toward the detector. This effectively

compresses the ion packets of the same mass to charge ratio (*m/z*) and improves mass resolution (over 4000 *m*/Δ*m*). The overall instrument mass resolution is defined as the peak *m/z* divided by the peak width at the half-maximum (FWHM) (Abis et al., 2018; Sulzer et al., 2014). **Figure 2.8** shows an example of an ion peak at *m/z* 132.08 detected by PTR-QiTOF-MS with its Gaussian fitting profile. The obtained value of the mass resolution (peak *m/z* / FWHM) is 4780 m/Δm for this peak.

The setup of the time of flight timing was: TOF extraction period 40000 ns, pulse width 2000 ns, trigger delay 100 ns. The number of channels was 240. This will end in a mass range measurement *m/z* 10 - 510. The time resolution is 1s. The *m/z* ratios of the ions are determined from the measured flight times and each extraction pulse generates a complete mass spectrum for the time interval (mass range *m/z* 10-510) chosen. Ions are detected with a multi-channel-plate (MCP) detector and a time-to-digital converter (Burle Industries Inc., Lancaster, PA, USA). The measurement period was set to 1 s, which means that each mass spectrum up to *m/z* 510 was recorded every one second. Raw PTR-QiTOF-MS data were recorded by TofDaq software (TofWerk AG, Switzerland). The methodology of processing the PTR mass spectra will be described in Section 2.5.

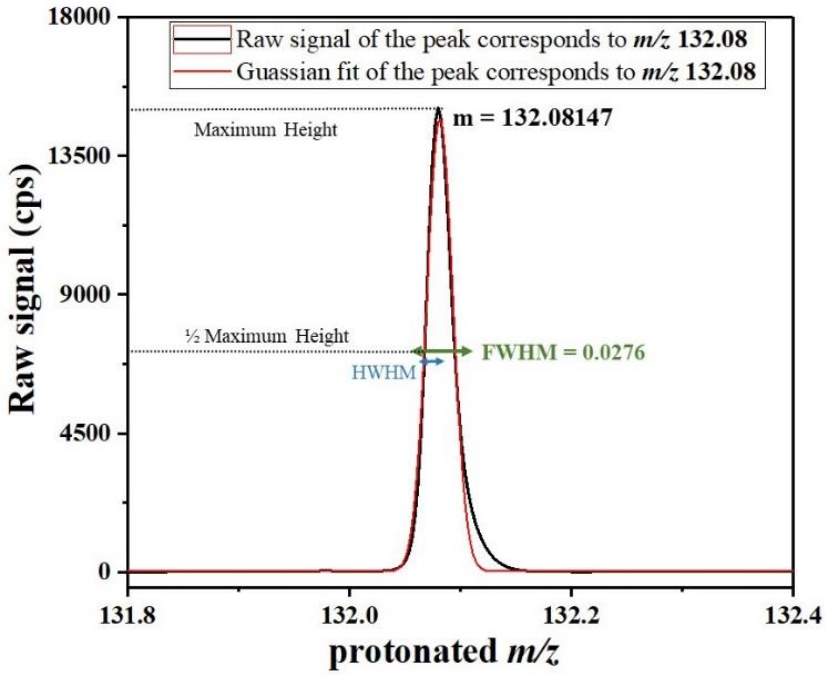

Figure 2.8 *Raw signal of an ion peak at m/z 132.08 detected by PTR-QiTOF-MS (black profile). The red profile corresponds to the Gaussian fitting of this peak. The center of the peak and the FWHM are calculated.*

The main advantages of PTR-TOF-MS are: (1) no sample preparation is needed, (2) high sensitivity for real-time VOC research, (3) high mass resolution, and (4) low limit of detection. In addition, some disadvantages are reported (1) events like fragmentation can occur as a result of the collision of the molecules within the drift tube (assumed negligible in our work), (2) the method requires calibration with gas standards for quantitative analysis, (3) the switching of the reagent ions is not straightforward and requires a stabilization period of several minutes, unlike selected ion flow tube-mass spectrometry (where the switching occurs within seconds), and (4) the instrument is not able to separate isomers and thus gives the concentration of all compounds of the same molecular weight. For this reason, PTR-MS is often coupled with a gas chromatographic analysis (Materić et al., 2015; Nie et al., 2019; Sulzer et al., 2014).

2.3.2. Off-line VOC analyses by TD-GC-MS

Gas chromatography-mass spectrometry (GC-MS) is an analytical method that combines the gas chromatography and mass spectrometry to identify different substances within a sample. GC-MS has been widely applied for drug detection, environmental analysis, biological and pesticides detection, petrochemical and hydrocarbons analysis and industrial applications (Al-Rubaye et al., 2017). In this work, off-line analyses were performed to obtain a more complete picture of the VOC emissions. The emitted VOCs were measured by Thermal Desorption - Gas Chromatography - Mass Spectrometry (TD-GC-MS) analysis. A schematic representation of TD-GC-MS instrument illustrated in **Figure 2.9** shows the different parts of the technique. Thermal desorption is a sample introduction technique for GC-MS where compounds of interest are thermally desorbed, over several minutes, and then retrapped on a cold trap in the thermal desorption instrument. The cold trap is a tube that contains packing material. It is rapidly heated and the VOCs are released and transferred through a heated transfer line to the GC (Materić et al., 2015).

The GC instrument includes a temperature-controlled oven (Materić et al., 2015) and an inert gas (e.g., He, N_2 or H_2) flowing through a capillary column (Al-Rubaye et al., 2017; David Sparkman et al., 2011). The capillary column is a very narrow tube with the stationary phase i.e. the film coating the inner wall of the tube. The properties of the capillary column such as its length, internal diameter and film thickness in addition to the type of the stationary phase (e.g., 5% phenyl polysiloxane) may alter the selectivity in GC analysis. The capillary column is the core of the GC system, where the separation of sample components takes place (Materić et al., 2015). The differential chemical mobility of the sample components is the basis of the separation process. Very similar chemical compounds such as isomers (e.g., α- and β-

pinene) interact differently with the stationary phase. Then those compounds elute from the column at different times which is called the retention time "RT" (Materić et al., 2015).

When GC is coupled to a mass spectrometer, the compounds that elute from the GC column are ionized using electrons (EI, electron ionization) or a chemical reagent (CI, chemical ionization) (Rockwood et al., 2018). The most useful ionization method is EI, in which the molecules are bombarded with free electrons that cause their fragmentation. This results in creating fragments of low *m/z*. The molecular fragmentation depends on the electron energy (typically 70 eV). The use of 70 eV facilitates the comparison of generated spectra with library spectra using software developed by the National Institute of Standards and Technology (NIST) (Materić et al., 2015). The ionized fragments are focused and accelerated into the mass analyzer, which is typically a quadrupole. Fragments with different *m/z* ratios will generate different signals, so any compound that produces ions within the mass range of the mass analyzer will be detected (Materić et al., 2015; Rockwood et al., 2018).

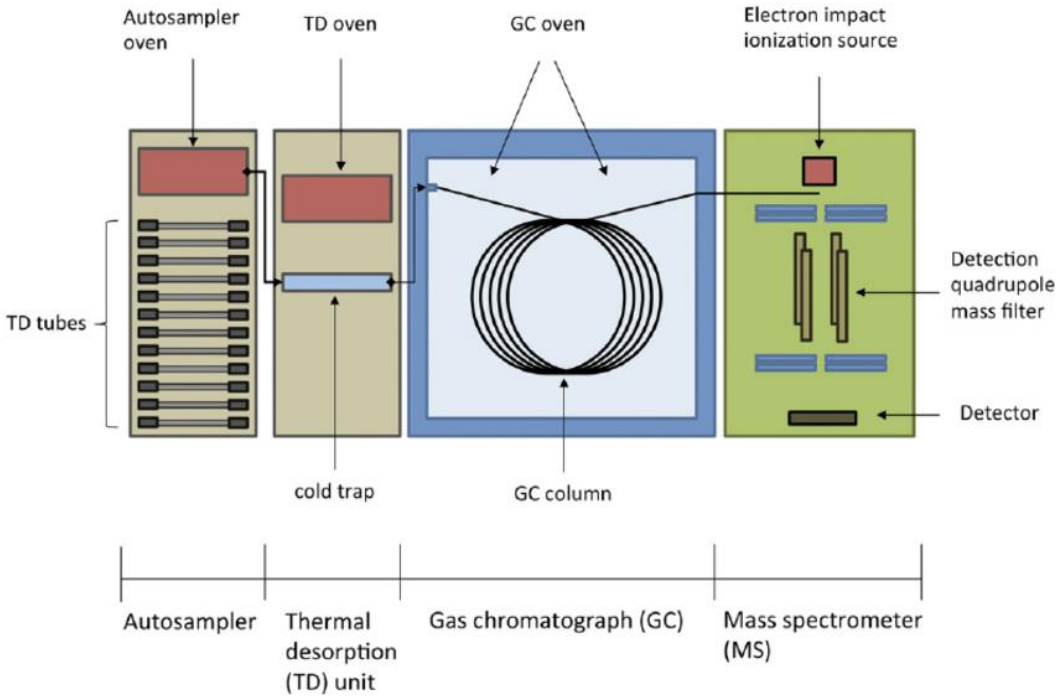

Figure 2.9 *Thermal desorption-gas chromatograph-mass spectrometer. The emitted VOCs were trapped on tubes are introduced into the autosampler. The autosampler collects a tube and heats it up according to the setup. Then the VOCs are retrapped onto material in the cold trap. The cold trap heats up rapidly and after that the VOCs are introduced into the GC column. Inside the GC column, the VOCs are separated and elute the column at different retention times. Following this, the VOCs are detected by a mass analyzer (Materić et al., 2015).*

During this PhD thesis, a series of analysis was performed to analyze the VOCs emitted from animal manure samples (described in Section 2.1.2). The emitted VOCs were trapped on Tenax TA cartridges, with a sampling time around 60-90 minutes at 0.5 L min^{-1}, and regulated with a mass flow controller (Bronkhorst). Before the experiment, the tubes were pre-conditioned by heating at 280 ^{0}C under a helium stream of 60 mL min^{-1} for 6 hours. After sampling, the cartridges were stored in the dark at 4 ^{0}C until their analysis. Tubes were desorbed using a thermo-desorption unit (Thermal Desorption Unit, TDU, Gerstel), which was programmed to desorb the tubes from 50 to 280 ^{0}C for 6 min at a rate of 60 ^{0}C min^{-1}. VOCs were cryo-focused in the Programmable Temperature Vapourization (PTV) at 5 °C using a Tenax liner. The separation of VOCs was carried out using an Agilent 7890B gas chromatograph on a capillary column (60 m length, 0.25 mm internal diameter, 1 μm film thickness). The oven temperature was initially set at 40 ^{0}C for 5 min, then heated to 60 ^{0}C at a rate of 11 ^{0}C min^{-1}. Helium was used as carrier gas. The detection of VOCs was done using an Agilent 5977A mass spectrometric detector. The EI mode was at +70 eV and the monitoring was from *m/z* 20 to 470. The ion source and quadrupole analyzer temperature were set at 230 and 150 ^{0}C, respectively.

The RT of compounds from the same chemical group were compared, to ensure that compounds with low boiling points were not eluted later than compounds with high boiling points. An example of the comparison between two compounds belonging to the ketone family is acetone C_3H_6O (*m/z* 58.0418, boiling point 55 ^{0}C), which is eluted in the minute 3.321, while 2-Tridecanone $C_{13}H_{26}O$ (*m/z* 198.1983, boiling point 263 ^{0}C) is eluted after 31.165 min. Rabaud et al., (2003) used two types of sorbent tubes: Carboxen and Tenax TA tubes that have different affinities and sorbed different types of compounds. Carboxen tubes sorbed compounds of low molecular weight and high volatility, while Tenax TA tubes captured larger compounds of intermediate volatility. Tenax TA has been determined to be a not suitable adsorbent for very VOCs (0 < boiling point < 50-100 ^{0}C) (Gallego et al., 2010). This is due to the displacement of the adsorbed volatile and polar compounds for non-polar high molecular weight pollutants (Zieba-Palus & Borusiewicz, 2006). However, Tenax TA tubes are considered one of the most widely used adsorbents for the preconcentration of VOCs (Ras et al., 2009).

TD-GC–MS data were processed by MassHunter (B.07.04.5560) software (Agilent Technologies Inc.). Automatic peak detection and mass spectrum deconvolution were performed using the Unknowns Analysis (B.06.00) module. Each compound was accompanied

by a deconvoluted spectrum, which was compared to the NIST (National Institute of Standards and Technology, 2011) mass spectra database to allow its identification. A minimum match factor of 70% between the observed and the reference mass spectra was required. Each compound was then manually scrutinized to confirm the proposed formula. For each proposed compound, the RT was analysed regarding its physico-chemical properties (e.g., boiling point). Identification of individual components was based on the comparison of calculated retention times with those of computer matching with commercial mass spectral library.

2.4. Aerosol characterization by off-line analysis

The chemical composition of the newly formed aerosols was studied using off-line mass spectrometric techniques: two-step laser mass spectrometry (L2MS) and Time-Of-Flight Secondary Ion Mass Spectrometry (TOF-SIMS).

2.4.1. Two-step laser mass spectrometry

The two-step Laser Mass Spectrometry (L2MS) couples three stages: laser desorption (LD), laser ionization (LI), and time-of-flight mass spectrometry (TOF-MS) (see **Figure 2.10** and **Figure 2.11**). This technique has been implemented at PhLAM laboratory for more than 15 years, and extensively used to characterize combustion products due to its high sensitivity and selectivity (Faccinetto et al., 2011; Mihesan et al., 2006). This technique has been thoroughly described elsewhere (Duca et al., 2019; Faccinetto et al., 2011). The following Sections describe briefly the principle of operation of L2MS.

2.4.1.1. Laser desorption

The transfer of molecules and atoms from a solid sample surface to the gas phase is done by a pulsed laser. Thermal desorption of neutral species occurs from the sample as a result of induced local heating. The fluence of the laser is defined as the pulse energy per unit of irradiated area. Depending on the fluence of the laser, “soft desorption” (represents the removal of only a fraction of the first monolayer from the sample surface) or “laser ablation” (refers to the removal of a sample micro-volume, leading to a crater formation) can occur. This parameter can be controlled to avoid fragmentation of molecules during the desorption process. Several parameters such as the sample properties (homogeneity, optical absorption coefficient, etc.) and the laser wavelength can influence the desorption process.

Prior to the analysis of the samples by L2MS, the collected filters were cut so that only a small piece was analyzed by L2MS and the other piece was kept in fridge at - 60 ^{o}C. The samples were then introduced into the transfer chamber (load-lock) connected to the analysis

chamber of the mass spectrometer. Throughout the experiment, the sample holder was cooled by liquid nitrogen to – 40 ^{o}C. This was done to avoid the sublimation of volatile compounds under vacuum (10^{-5} mbar) in the analysis chamber. We used in this study the 4th harmonic (λ= 266 nm) of an Nd:YAG laser (Quantel Brilliant, 4 ns pulse duration, 10 Hz repetition rate and beam diameter 530 µm) as desorption wavelength. Following the desorption step, the desorbed species expand in the vacuum orthogonal to the sample and form a "desorption plume". For the soft desorption used here, this plume is composed of neutral species, which must be ionized prior their separation and detection by the mass spectrome*ter*.

2.4.1.2. Laser ionization

The expanded plume is orthogonally irradiated by another UV laser (Nd:YAG, Quantel Brilliant, λ= 266 nm, 4 ns pulse duration, 10 Hz repetition rate and 0.2 cm beam diameter) (**Figure 2.10**). The delay between the desorption and ionization laser pulses is set to 4 µs. The energy of a 266 nm photon is 4.66 eV, thus a multi-photon ionization mechanism is used to generate the positive ions in this study (Duca et al., 2019).

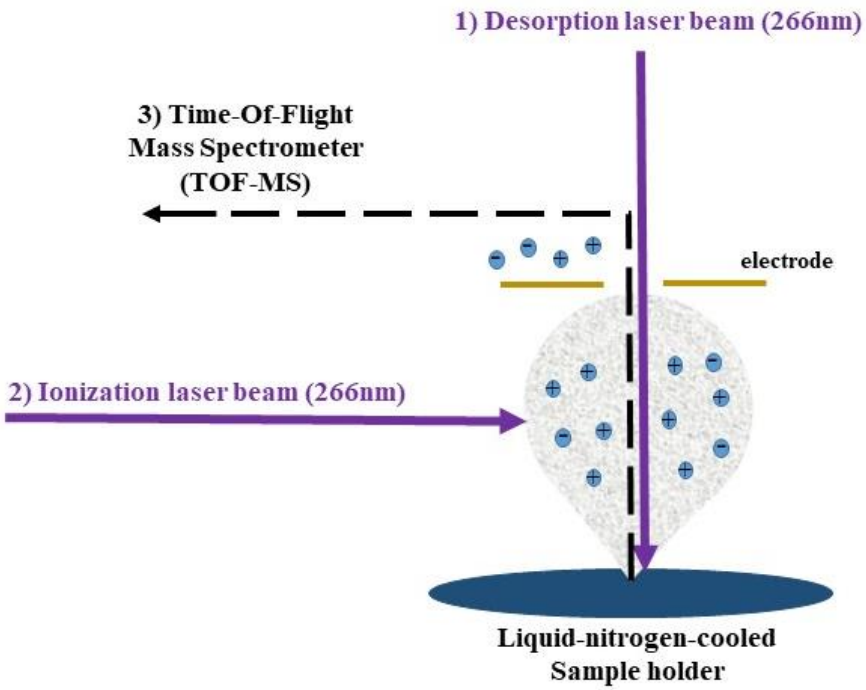

Figure 2.10 *Three stages involved in the L2MS technique: first, the sample is being irradiated with a desorption laser (first step), which allows the energy transfer to the sample surface and ejection of the molecules, which are then ionized by the ionization laser orthogonal to the desorption laser beam (second step), and finally, extraction of ions (positive or negative) is performed, in view of their m/z separation and detection in the TOF-MS.*

2.4.1.3. Time of flight mass spectrometer (TOF-MS)

The generated ions are then radio-frequency guided to a Helium (He) collision cell for thermalization, and then analyzed in the time-of-flight mass spectrometer. As described for PTR-QiTOF-MS, the principle of the TOF method is to separate ions of different mass to charge ratios during their flight in a free path of known length. An ion mirror (reflectron) slows the ions down and changes their trajectory towards the detector. The reflectron is used to improve the resolution by "compressing" ion packets of the same *m/z* ratio. The time passed in the reflectron compensates the time of flight difference of ions having the same m/z. The ions are spread with different kinetic energies at the ion source exit. This is the effect of initial position and velocity distribution, which are related to desorption and ionization events. The combination of collisional ion cooling, Radio Frequency (RF) trapping and Reflectron-TOF analyzer provides a mass resolution $m/\Delta m$ of ~ 15000 (Duca et al., 2019). The path of ions through the instrument is illustrated in **Figure 2.11**.

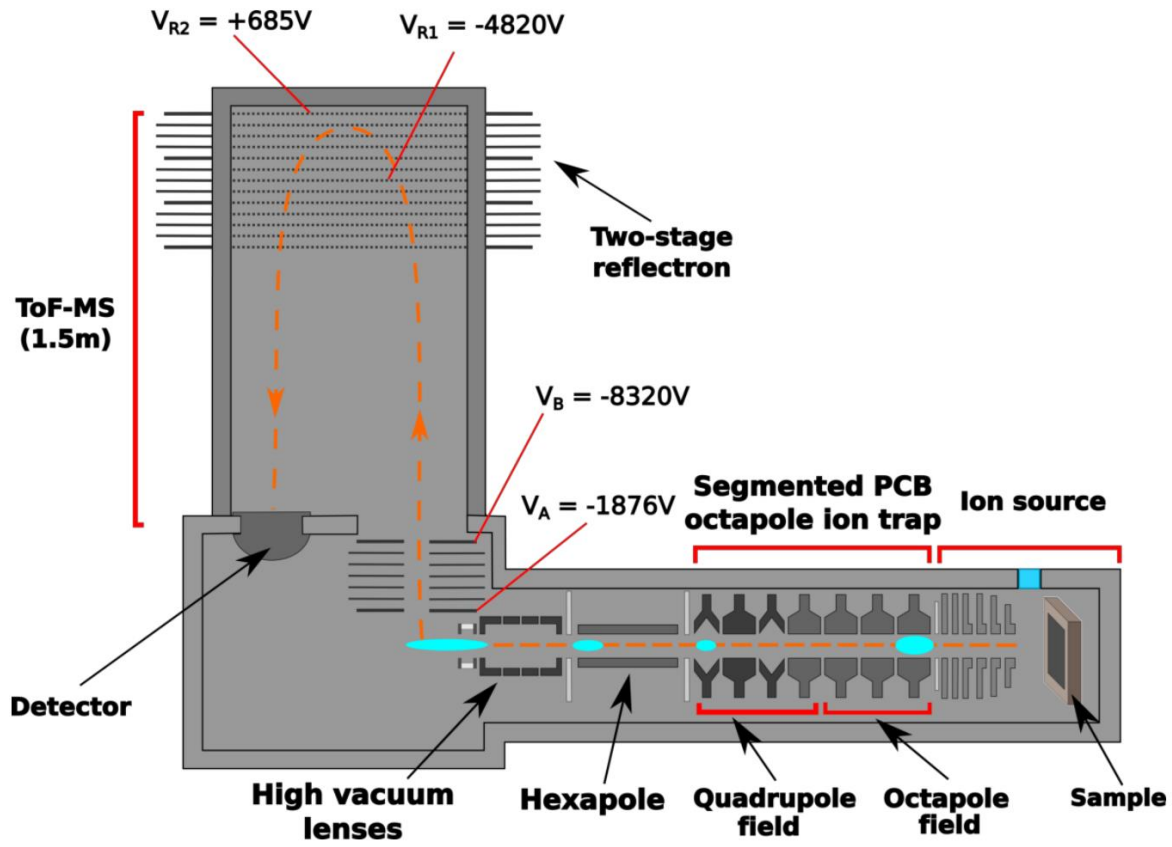

Figure 2.11 *Schematic representation of the L2MS set-up at PhLAM laboratory. The path of ions through the instrument is schematically illustrated by the orange dashed line. Time of flight mass spectrometer (TOF-MS).*

2.4.2. Time-of-flight secondary ion mass spectrometry

Time-of-Flight Secondary Ion Mass Spectrometry (TOF-SIMS) is a widely used technique for material characterization with high sensitivity to most elements of the periodic table. It has been widely used in several fields, such as material science, bioscience, industrial applications, etc. In this work, TOF-SIMS analysis is performed on a commercial TOF.SIMS 5 (Pidgeon et al., 2013) instrument produced by ION-TOF GmbH, available at the Regional Platform of Surface Analysis, University of Lille. For this instrument, the sample is attached to a sample holder and introduced through a load-lock into the analysis chamber with the residual pressure of ~ 10^{-7} mbar. The sample, placed on a mobile stage, can be visualized with an optical camera which allows the selection of the zone for the analysis.

The principle of operation of this technique is illustrated in **Figure 2.12**. Secondary ions are ejected from the sample surface by primary-ion bombardment in an ultrahigh vacuum environment. The ejected secondary ions are individually detected and recorded as a function of their *m/z*. The high sensitivity attainable by individual ion detection, and the high depth resolution are the principal attributes of SIMS.

SIMS can be operated in two working modes: static and dynamic. The static mode is used for the surface analysis (secondary ions originate from the top one or two monolayers of the sample), while the dynamic mode is used for the in-depth distribution analysis of trace elements (from few nm to few µm depth). In this study, we used the static mode which provides positive and negative mass spectra of the sample, to obtain the maximum amount of information on the sample. Bi_3^+ was chosen as primary ion source, since it has high ionization efficiency for organic species and a lower fragmentation probability of parent molecules. The energy of the primary ions is 25 keV with a current intensity of 0.3 pA (Irimiea et al., 2018, 2019).

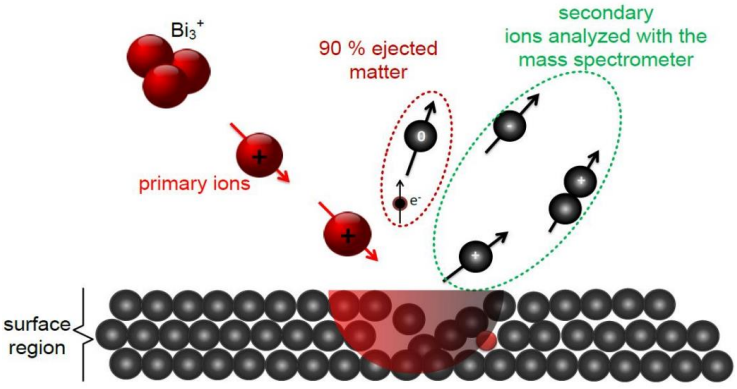

Figure 2.12 *SIMS working principle.*

The primary ions bombarded the selected surface and their energy is transferred to the atoms of the sample. The energy transfer initiates a cascade of collisions and results in the emission of sample atoms and molecules (sputtering). A small fraction of atoms and molecules are ionized and form the secondary ion beam, **Figure 2.12**. Secondary ions from the sputtered region are then extracted and accelerated toward the mass analyzer – a TOF-MS (V-mode, average resolution $m/\Delta m \sim 4000\text{-}6000$) (Irimiea et al., 2018, 2019). The obtained spectrum as calibrated using several known secondary ions (at least four ions evenly distributed across the whole mass range) using Surface Lab Software with at least five ions is used to convert the time-of-flight scale to mass scale. For this technique, the mass resolution is critically dependent on the roughness of the sample surface, i.e., low surface roughness is required in order to obtain high mass resolution (Irimiea et al., 2018). A mass spectrum obtained in this mode reveals characteristic molecular fragmentation patterns that help identify the chemical composition of the sample.

2.5. Data processing methodology of PTR mass spectra

Raw PTR-QiTOF-MS data were stored as hdf5 files that can be opened in PTR viewer 3.2.12 software (Ionicon analytik GmbH). During this PhD thesis, we developed a detailed methodology for PTR-TOF mass spectra data treatment, summarized in **Figure 2.13**. It can be applied directly to standard PTR-TOF mass spectra generated from commercial instruments, i.e. from raw spectra to data visualization/exploration and application of up-to-date data mining. For each step (**Figure 2.13**) we displayed the input data and the software used for analysis. It starts with the internal calibration of PTR-TOF-MS spectral data, followed by data pre-processing, such as de-noising and defining the regions of interest. Following these steps, we applied several procedures to acquire the qualitative and quantitative information of one sample. Advanced multivariate analysis were also applied to reveal the “hidden” trends among the analyzed samples. The following Sections will describe the methodology starting from mass calibration, assignment of mass peaks, concentration and emission flux calculation and statistical procedures.

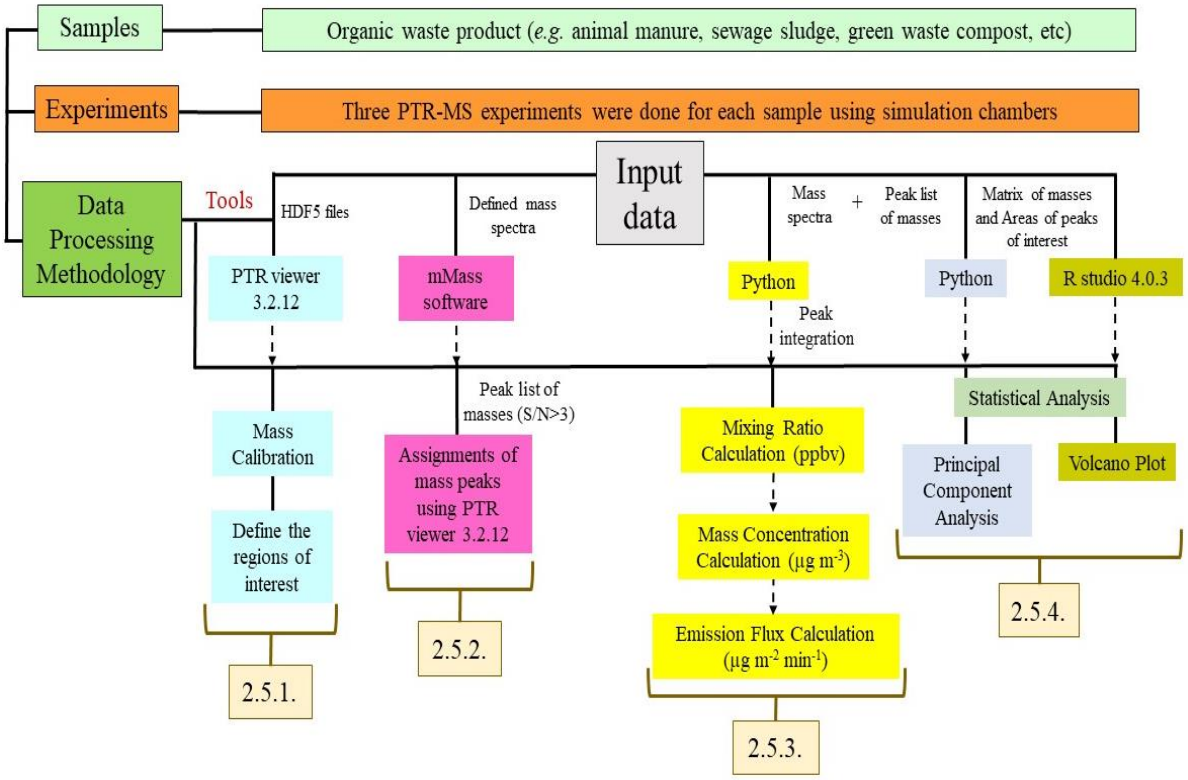

Figure 2.13 *Schematic representation of the data processing methodology developed to treat the raw data acquired by PTR-QiTOF-MS. Each part (column) of this methodology is detailed in the subSections (2.5.1 – 2.5.4) below.*

2.5.1. Mass calibration

The fundamental issues in mass spectrometry are mass calibration and mass accuracy. Indeed, through them the observed mass spectrometric peaks can be identified with the help of mass-to-charge ratios (*m/z*), isotope ratios and fragmentation pattern.

A TOF mass spectrum is composed of a series of peaks that correspond to the ion impacts on the detector. In TOF Mass Spectrometry, the mass-to-charge (*m/z*) of an ion is determined by measuring its time of flight (TOF). In a first step, the TOF information has to be converted into mass information. The relation between the *m/z* of an ion and the time it needs to arrive at the detector (TOF) is quadratic (Herbig et al., 2009):

$$m/z = A\,(t - t_o)^2 \qquad \textbf{(2.8)}$$

where A and t_o are parameters that only depend on the experimental conditions. In PTR-TOF-MS, single charge ions are detected (M^+) and all the detected ions are protonated $(MH)^+$ due to the soft chemical ionization occurring in the drift tube.

Mass accuracy of PTR-TOF-MS raw data is limited to external calibration that refers to fixing a proper set of calibration coefficients, which are employed during the entire duration of mass spectra acquisition. However, due to a lack of stability in instrumental parameters, external calibration in the commercial PTR-TOF-MS instrument does not guarantee mass accuracy for a sufficiently long time. A common solution to this problem is the use of internal calibrations based on the known exact mass of selected ions present in all mass spectra.

In the case of PTR-MS useful choices are, for instance, oxygen isotope of the ion source $H_3{}^{18}O^+$ (*m/z* 21.022) and protonated acetone, $C_3H_6O\text{-}H^+$ (*m/z* 59.0449) which are always present at reasonable concentrations. Another internal standard calibrant PerMaSCAL ($C_6H_4I_2$, 1,3-diiodobenzene, Permeation add-on for Mass Scale Calibration of PTR-MS, IONICON) was used for calibrations. This compound gives two peaks at *m/z* 330.848 ($C_6H_4I_2\text{-}H^+$) corresponding to the parent molecule and *m/z* 203.943 ($C_6H_4I\text{-}H^+$) corresponding to a fragment (– I). Thus, we chose four peaks at masses 21.0220, 59.0449, 203.943 and 330.848 as calibration peaks in the calibration of the dataset. The internal calibration then proceeds straightforwardly using the above formula to fit theoretical *m/z* values versus the measured TOF of the selected calibration peaks (illustrated in **Figure 2.14**).

The internal calibration of our data begins with the determination of the calibration peak centroids. TOF values are estimated by determined peak centroid using for example a Gaussian function to fit the peak shape. The selection of calibration peaks is very accurate such that it is important to avoid saturated peaks and low intensity peaks, for which the centroids cannot be properly determined. In practice, we consider only well-separated peaks of which the maximum height lies in the 10 - 1000 cps range in order to limit errors due to asymmetry in the peak shape. This ensures that the peak centroid can be properly estimated. In other words, to perform correct calibration, the peak height must be large enough for the peak to be well shaped and small enough to avoid saturation effects (Cappellin et al., 2011). Calibration peak centroids give the (uncalibrated) TOF values to be used together with the exact *m/z* values, to fit the parameters of the above equation (**2.8**).

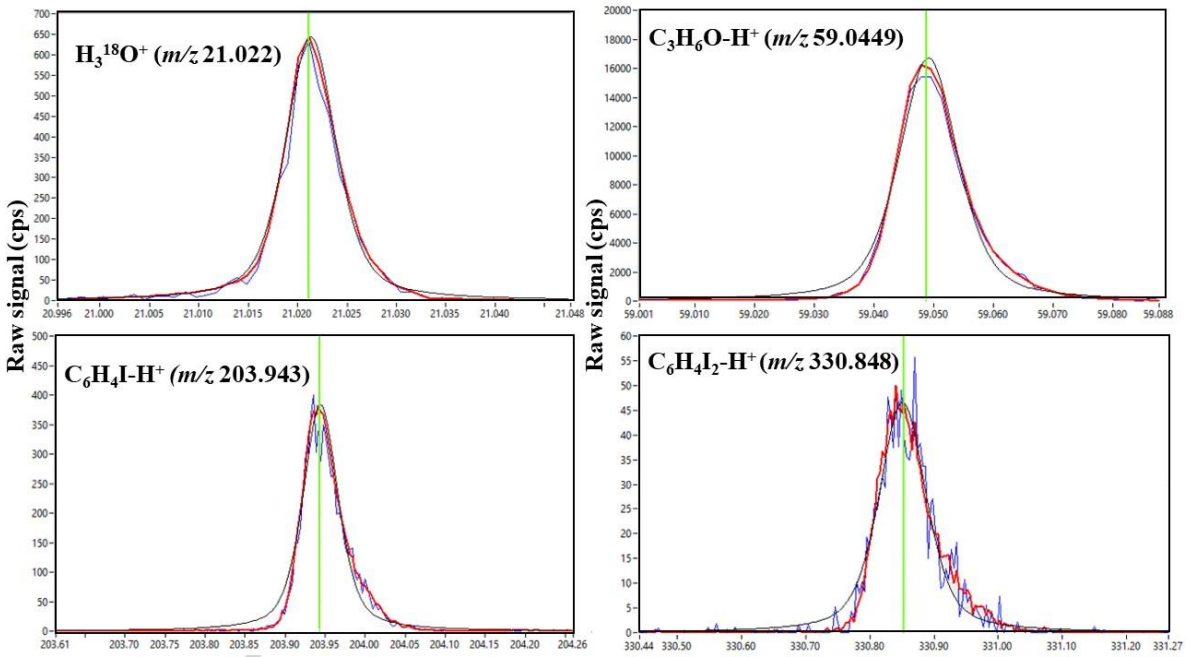

Figure 2.14 *The four calibration peaks at nominal masses 21, 59, 204 and 331 used for the calibration of the PTR-MS dataset. The black curve shows the average of 10 consecutive spectra; the Gaussian fit of each peak is illustrated in red. The peak centroid is displayed using the green line.*

The accuracy and mass resolution of the recorded spectrum can be affected by the electronic jitter – small fluctuations in the voltage of the accelerating electrodes causing a linear shift of the recorded spectrum. If the jitter effect is not taken into account, this will lead to an artificial increase in peak width and decrease of the mass resolution. In order to obtain a higher mass resolution, the shift induced by the electronic jitter must be eliminated before the calibration, effectively aligning all the spectra. The signal can be noisy and the peaks in a single spectrum might be poorly defined. The mass calibration algorithm needs well-defined peaks in order to work correctly. Using PTR viewer 3.2.12 software (Ionicon analytik GmbH), we have the possibility to let the software take an average of the spectra of a certain number of consecutive cycles. Thus, the random noise is reduced and the quality of the signal is improved by simply averaging over the spectra. However, the averaging procedure is appropriate only if the spectra are properly aligned on the TOF scale (Cappellin et al., 2011). Accordingly, before applying the mass calibration procedure described above, the alignment of the spectra was checked between 10 individual spectra and there was no shift between them. Thus, the mass calibration was made using an average of 10 successive spectra (in this work) in order to improve the signal-to-noise (S/N) ratio using the PTR viewer 3.2.12 software.

After mass calibration, the regions of interest (in the time evolution of the signals monitored throughout the experiment) were defined. In this study, we are interested in two regions (an example is illustrated in **Figure 2.15**): the first one is before O_3 addition into the chamber (denoted as R1). To define this region, the signal of a particular ion was monitored until it reached a steady state (usually after 3 cycles of dry air in the chamber, around 20 min), **Figure 2.15**. The second region is after O_3 addition into the chamber (denoted as R2) in **Figure 2.15**. This region is usually selected after 20 min of O_3 addition. Following this step, two averaged mass spectra (average of 120 mass spectra) were extracted from R1 and R2. The same procedure was applied for the three replicates performed for each sample.

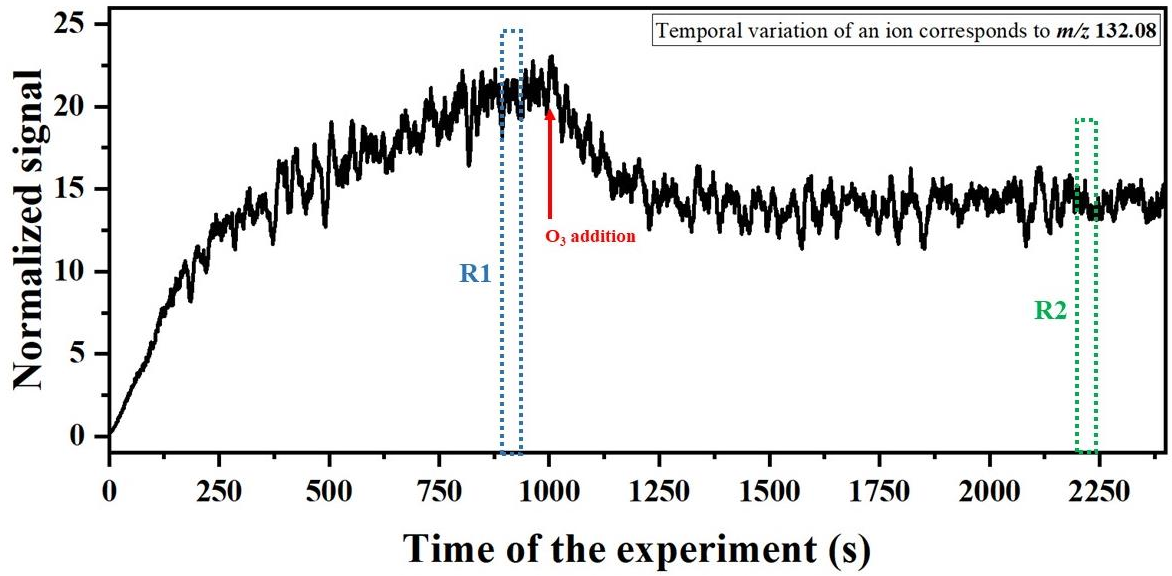

Figure 2.15 *Temporal variation of the signal at m/z 132.08 assigned as $C_9H_9NH^+$. The x-axis represents the time of the experiment and the y-axis represents the normalized signal of the m/z 132.08 peak relative to H_3O^+. The time of O_3 addition is indicated using red arrow. The blue box represents the defined region of interest (R1) chosen when the signal reached a steady state (before ozone addition). The green box represents the defined region of interest (R2) chosen after around 20 min of O_3 addition.*

2.5.2. Assignment of mass peaks

An example of PTR-QiTOF mass spectrum is illustrated in **Figure 2.16**. The peak position is determined by the *m/z* value of the $VOCH^+$. To identify the emitted VOCs, the three averaged mass spectra exported before the O_3 addition (R1, **Figure 2.15**) from the three replicates of one sample were used. A peak table was created for each sample using the mMass software (Strohalm et al., 2010) by selecting the peaks with a S/N > 3.0 one by one from the three

averaged spectra. The mass range chosen for analysis was between *m/z* 31 and 400. Signals identified as instrumental background or related to water clusters such as *m/z* 37.03, *m/z* 38.03, *m/z* 39.03 and *m/z* 55.03 were excluded from the data analysis. By the end of this step, separate peak tables were created for each type of analyzed samples.

Once the peak list of masses for each sample was ready, the "Spectra Analyzer" tool within the PTR viewer 3.2.12 software (Ionicon, Analytik GmbH) was subsequently used to identify the chemical molecular formula corresponding to each protonated molecular ion in the peak lists. By using this tool, we manually selected the peak chosen for identification. The identification of the molecular formula corresponding to each ion peak was performed by searching for the possible combination of elements that led to the closest molecular weight. We selected the following elements for the whole set of peaks: C, H, O, N, S and Cl. Subsequently, we got a list of proposed molecular formulas that best matched the selected exact *m/z*.

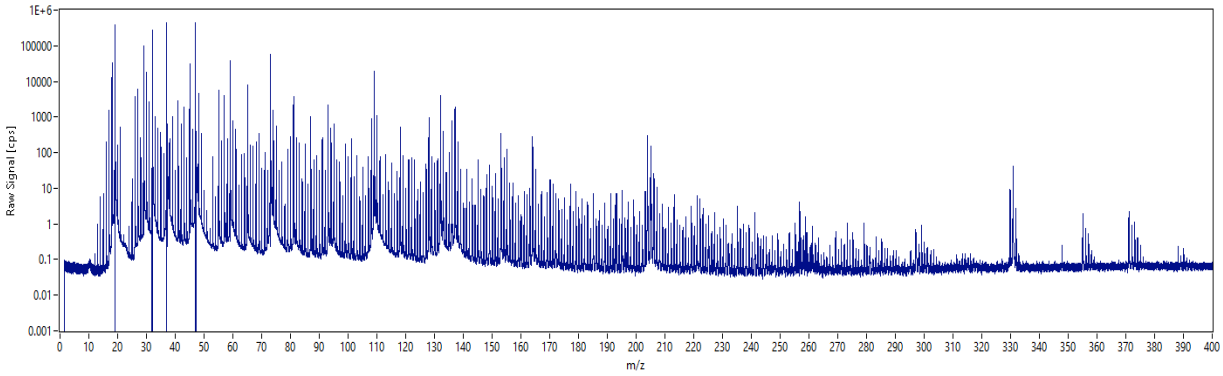

Figure 2.16 *Example of a PTR-QiTOF mass spectrum obtained from biowaste sample.*

In this work, we assigned each detected peak to a single compound. The molecular formula assignment of detected peaks (with S/N > 3.0) was selected based on several criteria. First, the exact *m/z* value which is represented by the uncertainty of assignments (in ppm). This uncertainty was calculated as the difference between the mass of the proposed formula and exact mass of the peak to be assigned. Second, the theoretical isotopic distribution of the associated molecular formula was checked. Third, the coherence of atoms contained in each proposed molecular formula, with respect to chemical rules such as valence of atoms, was crosschecked against NIST Webbook (Yáñez-Serrano et al., 2021). For some ions, we assigned the molecular formulas based on literature. Moreover, compound cross-validation with other available techniques such as TD-GC-MS would thus remain important to confirm that the mass monitored with PTR-MS corresponds to the reported compound. However, there are cases

where literature or offline analysis are not available, such as for compounds that have not been reported previously. In such cases, assignments of mass peaks were performed with high care trying to fit the four previously described criteria.

To illustrate the above criteria, we chose a multi-peak at nominal *m/z* 95 (example in **Figure 2.17**). The first peak corresponds to *m/z* 94.99 and the second one to *m/z* 95.04. To find the best molecular formula which corresponds to *m/z* 94.99, we checked its matching with three protonated ions ($C_2H_3O_2ClH^+$, $C_5H_2SH^+$ and $C_2H_6S_2H^+$).

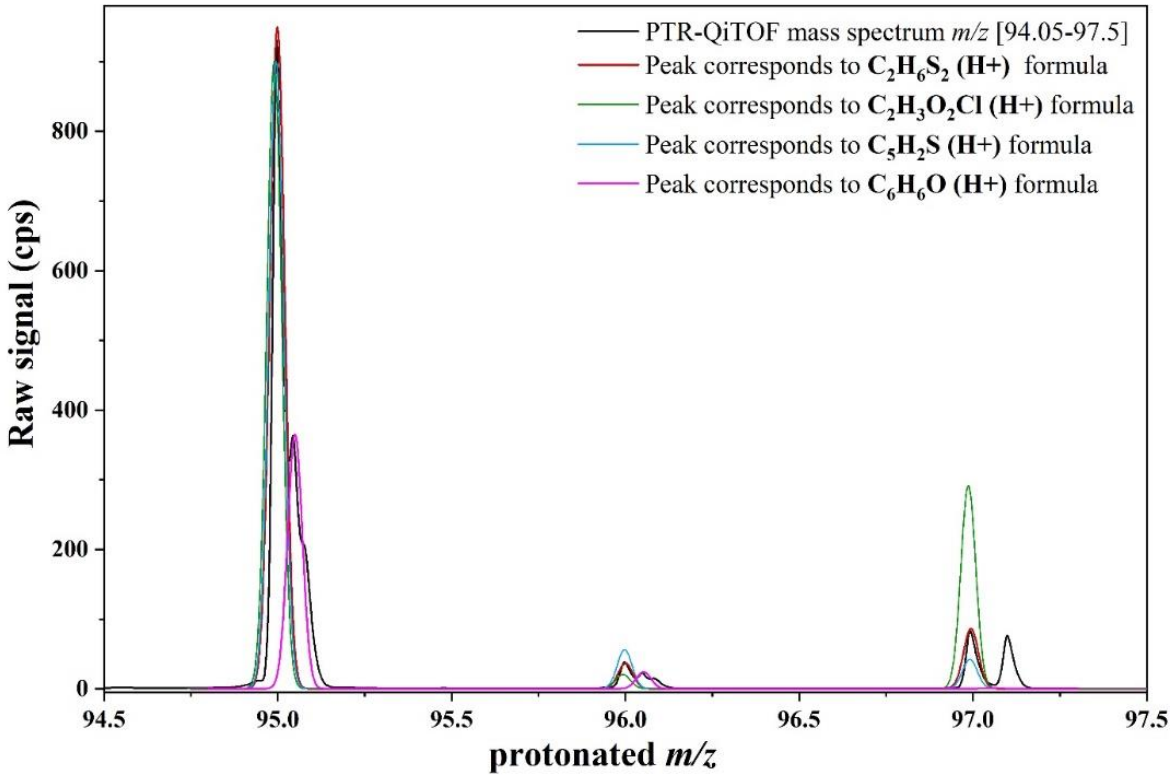

Figure 2.17 *Example of a PTR-QiTOF mass spectrum at the mass range [94.5-97.5] (shown in black). The isotopic pattern of each proposed protonated molecular formula is shown using colours (see the legend).*

For $C_2H_3O_2Cl(H^+)$ (green peak, **Figure 2.17**), the major isotopic peak (at *m/z* 94.99) shows matching between its exact mass and the peak to be assigned (*m/z* 94.99). However, the exact mass of the isotopic peak at *m/z* 96.99 is 24% of the main peak (*m/z* 94.99). This does not match with the peak to be assigned. For $C_5H_2S(H^+)$ (blue peak, **Figure 2.17**), it does not show isotopic agreement (in terms of intensities) with the peak to be assigned. The last formula $C_2H_6S_2(H^+)$ (red peak, **Figure 2.17**) shows perfect matching in its exact mass and isotopic distribution (of the major and minor abundant isotopes). Moreover, this compound has been widely reported in literature to be one of the major emitted VOCs from agricultural wastes

(odorous compound). Accordingly, the ion which corresponds to *m/z* 94.99 has been assigned as $C_2H_6S_2(H^+)$. Another example is given for a peak at *m/z* 95.04 that has been assigned to $C_6H_6O(H^+)$ (pink peak, **Figure 2.17**). Following this procedure, the vast majority of the detected peaks (> 90%) were assigned to a suitable molecular formula and only a few were unassigned. In this work, the average mass uncertainty of the assignments was better than 20 ppm. By PTR-QiTOF-MS, a wide range of compounds was monitored, however, the detected signals were chemically assigned instead of actual identification because this technique is mass selective and isomers cannot be separated.

2.5.3. Mixing ratio, mass concentration and emission flux calculations

Beside the identification of compounds by their molecular formula, PTR-QiTOF-MS allows for the quantification of the compounds emitted from the samples. In order to calculate the mixing ratio of gases that enter the PTR in parts per billion by volume (ppbv), a series of calculations were performed. They were based on the well-known conditions in the drift tube such as pressure, temperature, voltages, length and protonation reaction constant. The mixing ratio of detected ions was calculated using the integrated peak area and applying the equation (**2.9**) described in (Abis et al., 2018; Cappellin et al., 2011; Lindinger et al., 1998) :

$$\text{Mixing ratio (ppbv)} = 1.6575799*10^{-11} * \frac{\text{Udrift [V]Tdrift}^2\text{[K]}}{\text{k pdrift}^2\text{[mbar]}} * \frac{\text{Raw signal of VOCH}^+}{\text{Raw signal of H3O}^+} * \frac{\text{TR(H3O}^+)}{\text{TR(VOCH}^+)} \quad \textbf{(2.9)}$$

where $1.657 * 10^{-11}$ is a constant (see Annex 2, **Figure A.3**), U_{drift} is the voltage of the drift tube (**1000 V**), T_{drift} is the temperature in the drift tube (**353 K**), p_{drift} is the pressure in the drift tube (**4 mbar**). k is the protonation rate constant (**$2 * 10^{-9}$ cm^3 s^{-1}** assumed equal for all compounds). The raw signals of H_3O^+ and $VOCH^+$ represent the integrated peak area, calculated using Python 3.9, of H_3O^+ and $VOCH^+$ peaks, respectively.

TR_{H3O+} and TR_{VOCH+} are the transmission factors for protonated ion of H_3O^+ and $VOCH^+$, respectively. The raw signal (cps) of a compound estimates the number of ions detected by MCP. This raw signal must be corrected to transmission in order to calculate the number of ions generated in the drift tube. The obtained value is called "corrected raw signal". This approach is accurate since not all ions are transported through the lens system and ion extractor with the same efficiency. The transmission curve is constructed by analyzing gas standard containing compounds with varying mass ranges in order to calculate the "absolute" transmission of each standard. After that, we can calculate the relative transmission to the standard with highest absolute transmission. However, a bottle with many standards is not available; accordingly, we used the initial Ionicon transmission curve (exported from PTR

viewer 3.2.12 software) (**Figure 2.18, a**). To calculate the transmission of all detected ions, we fit this curve to nonlinear regression Exponential plateau (**Figure 2.18, b**). We chose this kind of fitting since we have a dataset with X (*m/z*) and Y (transmission) values. Transmission plateaus at a certain value Y=1 which means that for *m/z* >181 the transmission is 1. Thus, all the $VOCH^+$ of *m/z* > 181 generated in the drift tube are detected by MCP detector. The equation of transmission as a function of *m/z* of detected ion was applied for all the masses inserted in the peak list.

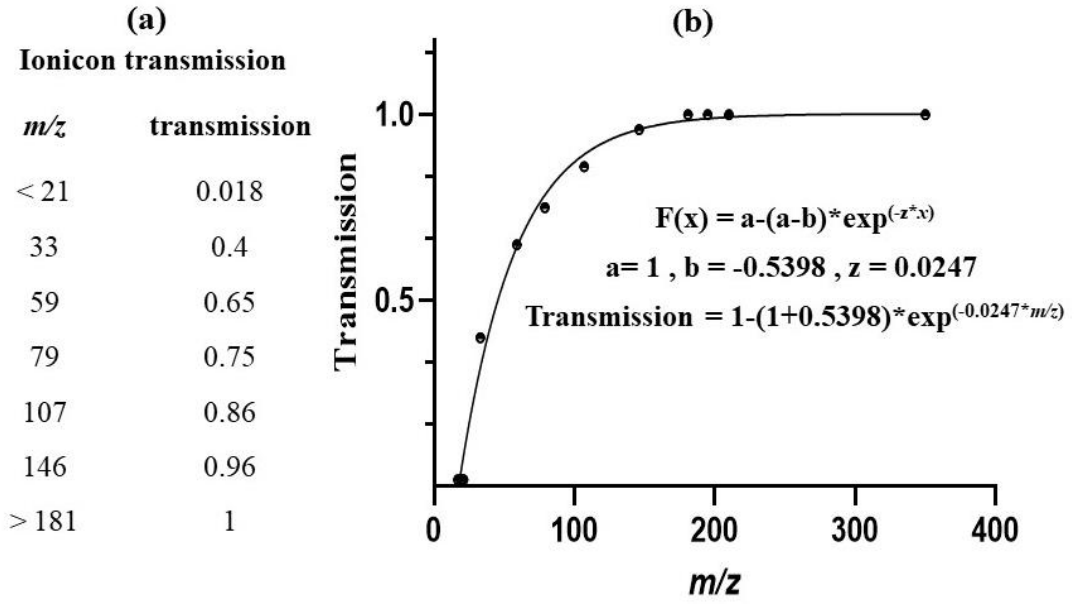

Figure 2.18 *(a) IONICON data for transmission and (b) nonlinear regression exponential plateau of the transmission function. The equation of transmission as a function of m/z is given.*

In order to account for the normal loss in sensitivity of PTR-QiTOF-MS, due to the MCP degradation over time, the change of $H_3{}^{18}O^+$ produced in the drift tube, or other factors, we used a calibration procedure to determine the uncertainty associated with concentration calculations. This calibration was performed using a standard bottle containing benzene, toluene, ethylbenzene and xylene (BTEX) as reference compounds. The mixing ratio of these compounds was modulated using a dilution system with a standard cylinder containing 102 ppbv of benzene, 96 ppbv of toluene and 336v ppb of ethylbenzene (BTEX, Messer®). We used the same synthetic air for the dilution system as the one used for chamber experiments. This dilution was performed to obtain different concentrations of standard compounds. The correction factor for mixing ratio was calculated as the slope of the regression between measured mixing ratio with the standard transmission provided by Ionicon and theoretical mixing ratio, and forcing a zero intercept (**Figure 2.19**). This calibration coefficient obtained

was then used to correct the $VOCH^+$ mixing ratios measured during the experiments. This calibration has been performed regularly to ensure the stability of the instrument. The procedure was applied for the three compounds cited above for the calibration. We found that the correction factor was 2.4 ± 0.02. This correction was applied to all masses in the peak list created for each sample. Finally, we chose the signal of toluene for this correction factor calculation since this compound is neither fragmented nor overlapped with other compounds. The signal of toluene is isolated unlike that at *m/z* 107 where it corresponds to ethylbenzene and xylene; in addition, ethyl benzene is totally fragmented to give benzene. In PTR-MS, the measurement accuracy in mixing ratio is determined by propagating the errors from all parameters used in the calculation, which usually comes out to about 30-50% (de Gouw et al., 2003).

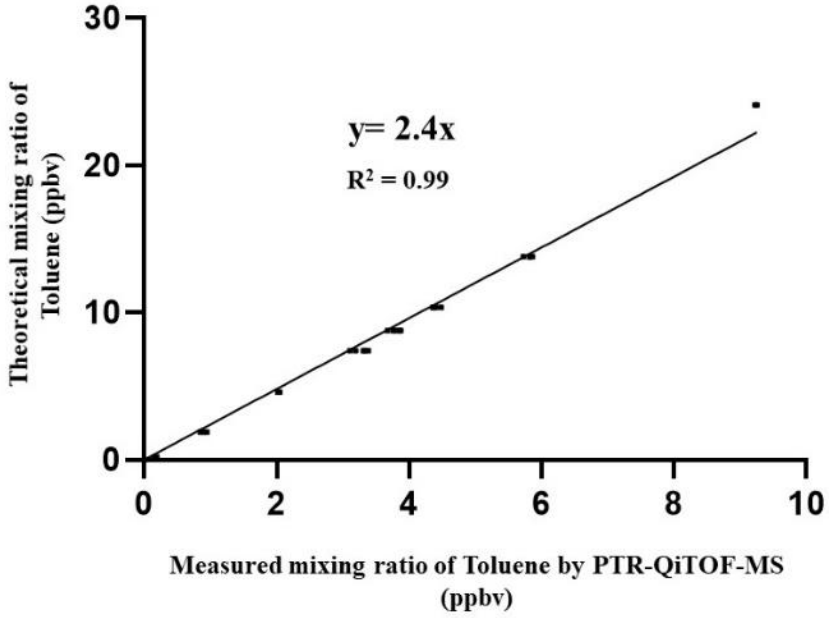

Figure 2.19 *The theoretical mixing ratio of toluene as a function of its measured mixing ratio by PTR-QiTOF-MS (forcing a zero intercept).*

The concentration of a species in atmosphere is expressed either as number concentration (C_i or [i] in molecule cm^{-3}), or mixing ratio (r_i, % or ppm or ppb or ppt) or mass concentration (C_{mi} in µg m^{-3}). To convert the mixing ratio (r_i, ppb) of a given compound to mass concentration (C_{mi} in µg m^{-3}) the following rule was applied:

$$\mathbf{C_{mVOC}} = \frac{\mathbf{rVOC} * \mathbf{10^{-9}} * \mathbf{Cair} * \mathbf{MVOC} * \mathbf{10^{6}}}{\mathbf{N_A}} \mathbf{x\ 10^{6}} \qquad \mathbf{(2.10)}$$

where, C_{mVOC} is the mass concentration of the VOC of interest (in µg m^{-3}), r_{VOC} is the mixing ratio of VOC (measured by PTR-QiTOF-MS), M_{VOC} is the molar mass of VOC in g mol^{-1}, C_{air} is the concentration of air at STP (T_0 = 25°C and P=101325 Pa), N_A is the Avogadro's number ($6.02*10^{23}$ molecule mol^{-1}). C_{air} is calculated from ideal gas law PV= nRT using P=101325 Pa, T=298 K which gives $C_{air} = 2.5*10^{19}$ molecule cm^{-3}. Then,

$$\mathbf{C_{mVOC}\ (\mu g\ m^{-3}) = \frac{rVOC * 10^{-9} * 2.5 * MVOC * 10^{6}}{6.02 * 10^{23}} * 10^{6}} \qquad \mathbf{(2.11)}$$

Finally, the mass concentration of each assigned VOC as follows:

$$\mathbf{C_{mVOC}\ (\mu g\ m^{-3}) = 0.0415 * r_{VOC} * M_{VOC}} \qquad \mathbf{(2.12)}$$

The comparison between samples was based on the emission fluxes of the compounds. In order to calculate the emission flux, the emission surface was taken into account, as well as the airflow rate through the chamber and the mass concentration of the emitted VOC. The emission flux of each VOC was calculated using the following equation:

$$\mathbf{F_{VOC} = Q/A * C_{VOC}} \qquad \mathbf{(2.13)}$$

where F (µg m^{-2} min^{-1}) is the flux of the assigned VOC, Q (m^3 min^{-1}) is the air flow rate through the chamber, and A (m^2) is the geometric surface area of the plate where the sample is placed. C_{VOC} (µg m^{-3}) is the averaged mass concentration of a VOC obtained from the three replicates performed for each sample.

As we have three replicates for each sample, we calculated the average mixing ratio, average mass concentration and average emission flux of each detected compound. Multiple data (average of 120 mass spectra) were recorded and all were considered for calculating the precision (degree of repeatability). This precision contains the error due to samples (heterogeneity of the samples, distribution on surface, amounts used, etc), the uncertainty due to concentration calculation (e.g., uncertainty in reaction rate constant used for the PTR reactions assumed equal for all compounds), and the systematic error. Systematic errors show the minimum error that will be involved in every measurement due to uncertainty in calibration, instrumental response and loss in sampling line. All the error bars reported in the figures show precision i.e. the total uncertainty or the standard deviation of the outputs obtained from the three replicates of each sample such as mass concentration and emission fluxes. The comparison between samples was done using the emission flux despite the difference in the samples' quantities, where this parameter was not considered for flux calculation. Experiments

were performed (not shown here) to determine the impact of the sample surface and its quantity on the emission flux of compounds. Several quantities of the sample were used and spread on the same surface area for analysis. The results showed that the emission flux of the compounds depends on the geometric surface of the sample but not on the quantity used for the experiments. Accordingly, the emission flux of the compounds were used to compare between samples even though the quantity of the sample used was not taken into account for this calculation.

2.5.4. Statistical procedures

The analysis of mass spectrometric data requires an appropriate technique based on the structure of mass spectrometric database. The latter is composed of a number of mass spectra each containing up to thousands of peaks. Statistical tools, such as multivariate analysis, can be used in this case to reduce the dimensionality of the data and organize it into several clusters containing similar spectra or mass peaks (Duca et al., 2019). In this Section, statistical techniques that have been adopted by the ANATRAC group (PhLAM laboratory) for the analysis of mass spectrometric data, allowing us to identify convoluted patterns and extract "hidden" relationships, are described.

2.5.4.1. Principal Component Analysis

The mass spectra of gas-phase analyzed by chemical ionization reaction mass spectrometers (PTR-MS) feature hundreds of mass peaks, which complicate their interpretation. PTR-MS spectra are high-dimensional vectors that can be more efficiently analyzed if the dimensionality is reduced by suitable data compression methods such as principal component analysis (PCA) (Aprea et al., 2006). Data compression is useful in comparing multiple mass spectra while retaining the majority of the original information. PCA is a powerful statistical tool for classifying samples and revealing trends and patterns in databases. It is also used to improve the readability of very complex data (Abdi & Williams, 2010; Adam et al., 2007; Tanaka, 1988).

In this work, PCA was performed on a matrix containing the integrated peak areas (variables) against the mass spectra of the samples. A special preparation procedure was applied on mass spectrometric data prior applying PCA (Tanaka, 1988): calibration of mass scale, baseline removal, construction of a peak list, peak area integration and normalization. All mass spectra were normalized relative to the total ion count (TIC). All mass peaks that have S/N > 3 are considered and then the areas are integrated. The variance of the integrated area

usually has a *L-shape* distribution, caused by a big difference in signal intensities of mass peaks, which is unacceptable for any statistical analysis techniques (Bradley, 1982). A suitable method for converting the data to a bell-shaped distribution is by calculating the decimal logarithm of the data set, a procedure that preserves all the information about the covariance between mass peaks (François Vermeulen, 2020).

Principal components are calculated using the covariance matrix of initial variables (Tanaka, 1988). The eigenvectors of this matrix represent the directions of the axes with the largest variance (i.e. directions of PCs). Eigenvalues are the coefficients attached to eigenvectors that give the amount of variance carried by each component. Given a data set X with p observations and n variables, the first principal component PC1 is represented by the linear combination of the original variables $X_1, X_2, \ldots, X_n$:

$$PC1 = \omega_{11}X_1 + \omega_{12}X_2 + ... + \omega_{1n}X_n \quad \textbf{(2.14)}$$

where $\omega_1 j$ are the elements of the first eigenvector and can be used to interpret the meaning of the PC. Most of the time, the interpretation of PCs is instead performed with loadings, as their magnitude is representative of the covariances /correlations observed between the initial variables:

$$loadings = eigenvectors \cdot \sqrt{eigenvalues} \quad \textbf{(2.15)}$$

The variables (i.e. mass peaks) that have the largest effect on each PC are identified using a loadings plot, which depicts the loading of all the initial variables (**Figure 2.20**). A higher loading indicates that the variable strongly influences the PC. Moreover, the sign of the loading is important as it shows the correlation among variables.

The number of PCs represents the number of variables in the data. PCs are ranked in accordance with their significance (i.e. the first PC accounts for the largest possible variance in the data set). Therefore, selecting only the first m components allows to reduce the dimensionality of the data set while still preserving the majority of the variance (i.e. information). Thus, it is important to properly choose the number of PCs that are considered. A common practice in determining the optimal number of PCs is to use the scree plot, which represents the percentages of explained variance by each PC (proportional to its eigenvalue), ordered from the largest to the smallest, and to identify the point where the slope significantly changes. Only the components before the change point (called ”elbow“) are considered (Abdi & Williams, 2010; Peres-Neto et al., 2005). Example of a scree plot (obtained from our data)

is illustrated in **Figure 2.21**. For this particular scree plot, we have two elbows (the point where the slope changes). Considering the last elbow, the first three PCs are located before the "elbow" and, therefore contain the majority of meaningful data.

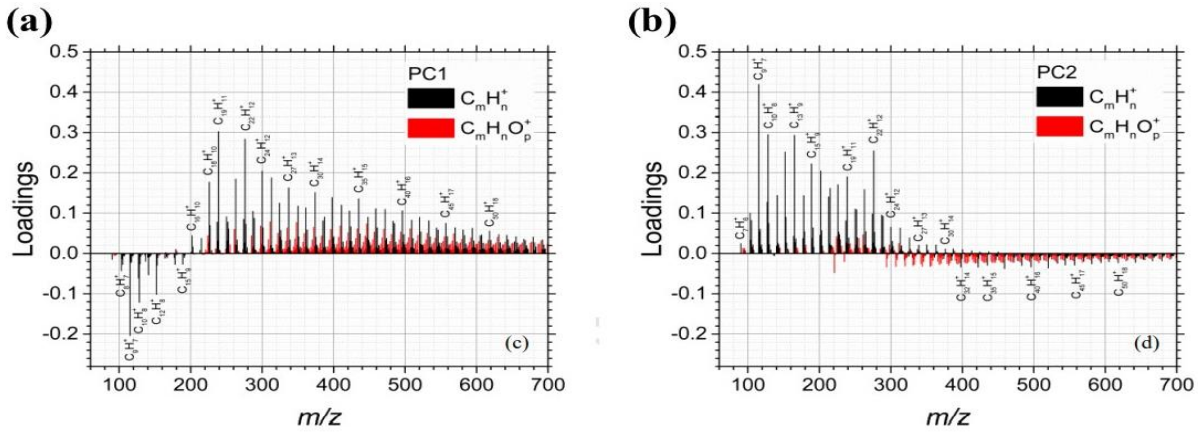

Figure 2.20 *Example of a loadings plot showing the contribution of each mass peak to the value of the (a) first and the (b) second PCs. The contribution of hydrocarbons and oxygenated species are shown in different colours. The physical meaning of each principal component can be determined based on the loadings plot (Irimiea et al., 2019).*

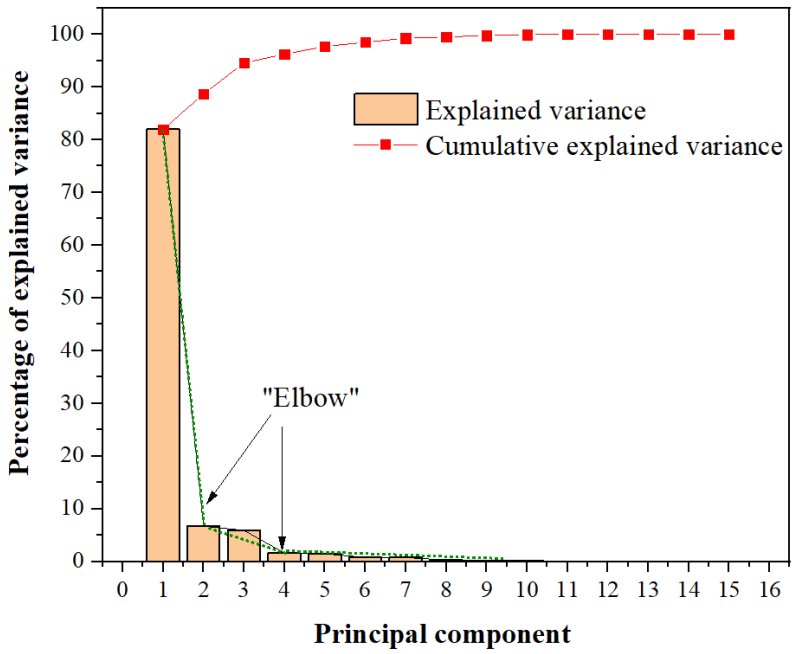

Figure 2.21 *Example of a typical scree plot showing the contribution of each PC and the cumulative contribution of all PCs to the explained variance. The trend line of the components is shown in green with "elbow" point highlighted.*

By projecting all the observations onto the low-dimensional (two or three dimensions) sub-space and plotting the results, it is possible to visualize the structure of the investigated data set. The coordinates of the observations (mass spectra in our case) on this plane are called scores, and hence the plotting of such a projected configuration is known as a score plot (**Figure 2.22**). The combination of the score and loadings plots allows to determine the contribution of initial variables (i.e. mass peaks) to all the observations (i.e. mass spectra) (Abdi & Williams, 2010; Peres-Neto et al., 2005).

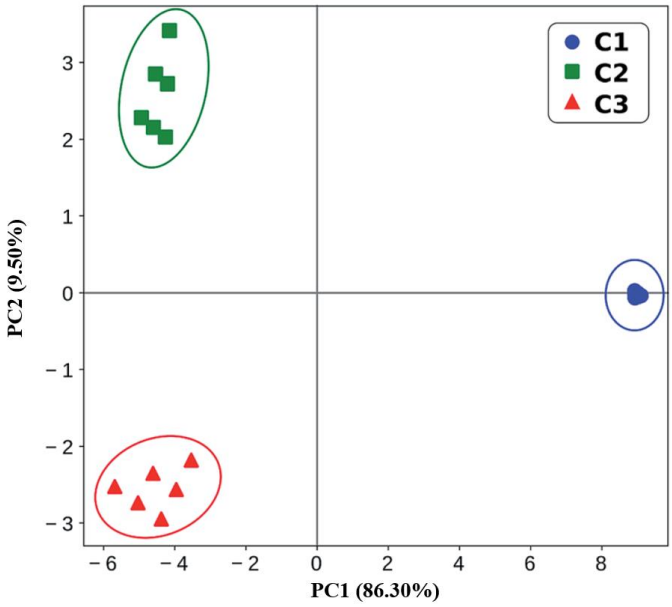

Figure 2.22 *Example of a score plot showing the projection of the observations (mass spectra) on the first two principal components. The observations (spectra) can be easily grouped into three distinct clusters (C1, C2 and C3) (Duca et al., 2019).*

2.5.4.2. Volcano plot

When comparing only two sample-sets (e.g., two samples), not all species will have a significant enough variation. For datasets characterized by a large number of variables (detected masses) and a relatively small number of observations (samples, mass spectra) it is important to choose a proper method of identifying variables that are the most different between two observations, i.e., that contribute the most to their "differential expression". The two usual methods of identifying the most different variables within a data set are the fold-change and the t-statistics, each one with its own advantages and drawbacks. The fold-change represents the magnitude of the change in the signal of the same variable between two different observations: FC1−2 = S2/S1 (e.g., the signal of an organic compound emitted from a sample 2 to that of sample 1). The fold-change, however, does not take into account the noise often

present in mass spectra; moreover, its value becomes less important with the increasing variance. Even though the t-statistics take into account the noise, less reliability is expected for small datasets. To obtain a robust visualization of the "differential expression" of two observations (e.g., with/without O_3), a combination of the two methods can be used, leading to a volcano plot. In statistics, a volcano plot is a kind of scatter plot that is applied to quickly seek out changes in large data sets composed of replicate data. It plots fold-change versus significance on the x and y-axes, respectively. A volcano plot combines a measure of statistical significance from a statistical test (e.g., a *p* value from an ANOVA model) with the magnitude changes, enabling quick visual determination of these data-points that represent large magnitude changes that are also statistically significant. To improve the readability of the plot when the variance in the data set is rather high, the fold-change (FC) can be replaced by its logarithm ($\log_2$ (FC)).

A volcano plot consists of three main regions (**Figure 2.23**): i) the region where the data-points have either a small magnitude of change (< 1) or are not statistically significant (p-value > 0.05 or $-\log_{10}$(p-value) > 1.3) – usually displayed in grey, ii) data-points with high contribution to the first sample with a high statistical significance, iii) data-points with high contribution to the second sample with a high statistical significance. Since only the last two regions (ii and iii) contain statistically significant information, they need to be used for making meaningful conclusions about the mass spectrometric data.

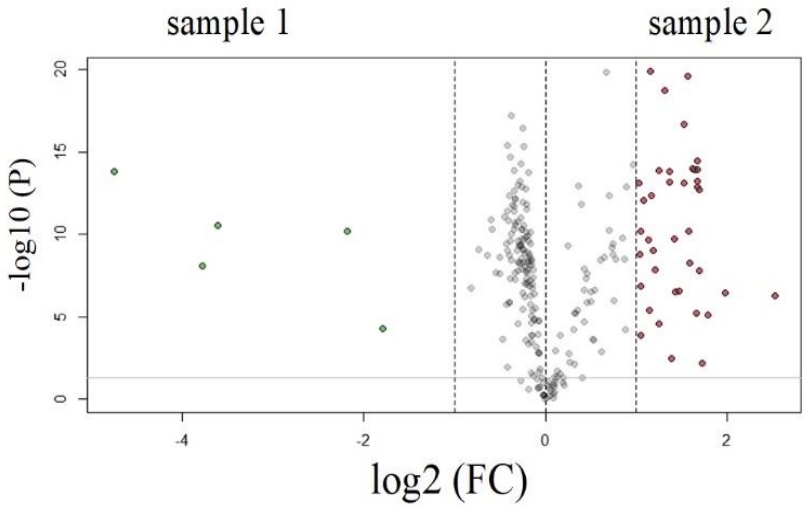

Figure 2.23 *Example of a volcano plot illustrating the three main regions: (i) points with either a small fold change or statistical significance – grey markers, (ii) with high contribution to the sample 1 with a high statistical significance – green markers, and (iii) points with high contribution to the sample 2 with a high statistical significance – red markers.*

2.5.5. Double Bond Equivalent

In the analysis of the molecular formula of organic molecules, the degree of unsaturation also known as the index of hydrogen deficiency (IHD) or double bond equivalent (DBE) or unsaturation index, is a calculation that determines the total number of rings and π bonds. A formula is used in organic chemistry to obtain possible molecular structure assignments. The DBE method is used in several fields, as in petroleomics to separate and sort petroleum components (Dobbins et al., 1998). The DBE value of $C_cH_hN_nO_oS_s$ is calculated as follows:

$$\mathbf{DBE = c - h/2 + n/2 + 1} \qquad \mathbf{(2.16)}$$

where c, h and n are the number of carbon, hydrogen and nitrogen atoms inside the molecular formula. DBE is independent of the number of oxygen and sulphur atoms in the molecules (Sabbah et al., 2021). DBE represents the level of unsaturation of the molecules that determines the total number of rings and double or triple bonds (π-bonds) involving carbon atoms (because each ring or double bond results in a loss of two hydrogen atoms) (Dobbins et al., 1998). As the number of H atoms in a molecule decreases, the level of unsaturation increases and hence leads to higher DBE values. By using the DBE method, several classes of hydrocarbons are obtained (illustrated in **Figure 2.24**). DBE versus C number plot is used in mass spectrometry to simplify the visualization and for understanding of complex HC mixture.

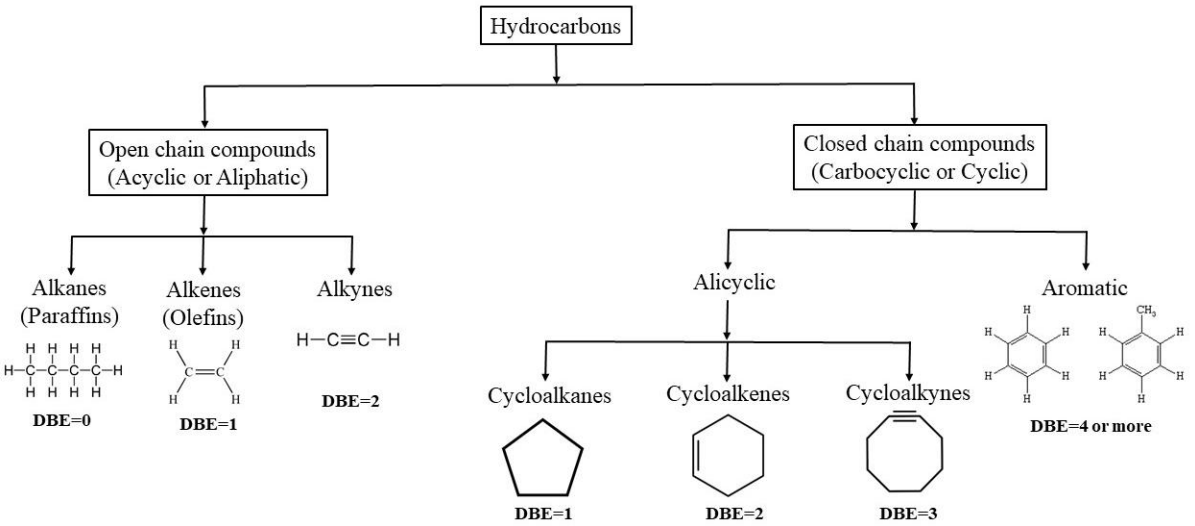

Figure 2.24 *Sub-classification of hydrocarbons. Example of each subclass is shown with the value of its corresponding double bond equivalent value (DBE).*

In **Figure 2.25**, Sabbah et al., (2017) represented the DBE versus C number for the detected species. Several series of compounds are aligned horizontally and spaced by one or n carbon numbers. A homologous series of compounds with different degrees of alkylation (substitution

of peripheral H by CH_3 groups leading to no change in the DBE) has constant DBE value but different carbon numbers. This type of series is illustrated in **Figure 2.25** by dashed lines. In this work, DBE method was applied to our PTR-QiTOF mass spectra rich in hydrocarbons. After identifying the masses by their molecular formula, we calculated the DBE value for each molecule with chemical formula C_xH_y. Several classes of hydrocarbons were illustrated in OWP samples. Therefore, DBE representation can be used to simplify the analysis of a complex mixture through classification.

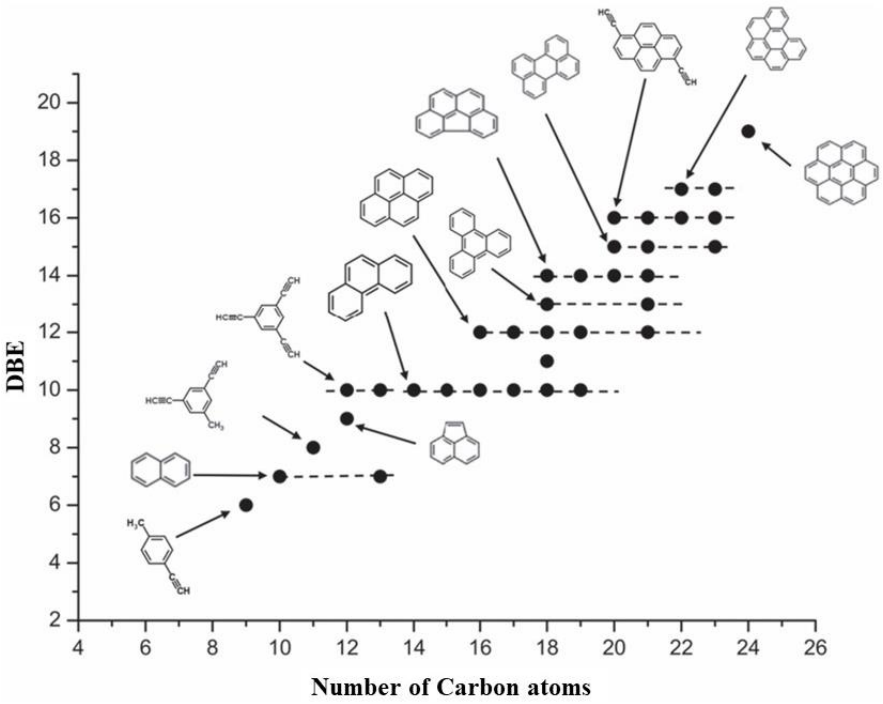

Figure 2.25 *DBE vs. carbon number plot showing the polycyclic aromatic hydrocarbons (PAHs) detected in a meteorite and their related products. Dashed lines on the diagram display species having the same DBE value and differing in the alkylation degree (substitution of H atom by CH_3) (Sabbah et al., 2017).*

Chapter 3

Chemical identification and quantification of volatile organic compounds emitted by sewage sludge

3.1. Introduction

Sewage sludge (SS) refers to the residual, solid, semi-solid or liquid material that is generated at wastewater treatment plants (WWTPs) as treatment by-products of wastewaters released from various sources (e.g., homes, industries, medical facilities, street runoff, etc.) (Christodoulou & Stamatelatou, 2016; Harrison et al., 2006). In Europe, investments in municipal wastewater treatment have been very important in the last decade, but this increasing number in WWTPs arises secondary environmental concerns due to the accumulation of sludge resulting from wastewater treatment processes. SS treatment in WWTPs usually includes thickening, digestion and dewatering, which separate the solid and liquid components of the sludge to be easily handled for final disposal (Hall, 1995; Iticescu et al., 2018; Jamil Khan et al., 2006). The SS that leaves the WWTPs has a high content of water (up to 90%) (Gomez-Rico et al., 2008). Thus, sludge treatment is focused on minimizing its weight and volume to reduce transportation and disposal costs, and on reducing potential health risks of disposal options. Thickening is often the first step in a sludge treatment process. Sludge is stirred to form larger and more rapidly settling aggregates. In general, this operation is performed by simple decantation or flotation, or by dewatering and centrifugation, which allows reaching a dryness of 1 to 10%. Many sludge are treated using a variety of digestion techniques, the purpose of which is to reduce the amount of organic matter and the number of disease-causing microorganisms present in the solids. The most common treatment options include anaerobic digestion, aerobic digestion and composting. Sludge digestion offers significant cost advantages by reducing sludge quantity by nearly 50% and providing biogas (like methane) as a valuable energy source. Anaerobic digestion is a biological process of sludge stabilization carried out in the absence of oxygen. This treatment leads to the transformation of organic matter into water, CO_2 and CH_4 by anaerobic microorganisms (Hall, 1995; Iticescu et al., 2018; Jamil Khan et al., 2006). Thermal drying of sludge is a necessary intermediate common to all disposal methods, as it makes it possible to stabilize the sludge, reduce its volume and hygienize the product (Gross, 1993; Gomez-Rico et al., 2008).

The agricultural reuse of SS should be prioritized as recommended by the European Commission in the Circular Economy Action Plan (Collivignarelli et al., 2019). This use of SS

has been preferred in France where nearly 60% of SS is applied to soil as organic fertilizer providing nutrients for crops, soil buffer and soil amendment (Milieu et al., 2010). SS should be treated prior its agricultural application such as by anaerobic digestion, composting or chemical treatment (Christodoulou & Stamatelatou, 2016; Collivignarelli et al., 2019). The composition of anaerobically digested sludge increases its potential as soil amendment and/or fertilizer. For this reason, in Europe, particularly in the Mediterranean region where the high summer temperatures combined with the intensive cultivation practices promote a constant decrease in the soil organic matter, 40% of SS is used as a soil organic amendment due to its high organic matter content (Lamastra et al., 2018). The use of SS in agriculture has been disciplined as each European member state has issued a national legislation based on the European directive 86/278/EEC (Collivignarelli et al., 2019; Capua et al., 2020). Nowadays 42% of the annual production of the urban sludge is spread on agriculture land without prior treatments and 30% after composting (Houot et al., 2014). The characteristics of SS play a significant role when considering the ultimate land application. There are different methods for SS application on soils depending on the total solid content of SS. For instance, liquid or low-solid sludge can be generally injected into the soil to provide better aesthetics. On the contrary, dewatered or semisolid sludge can be spread on the surface and subsequently plowed into the soil (Iticescu et al., 2018). Moreover, the spreading occurs at different climatic condition (e.g., temperature and humidity) and on different types of soils (e.g., soil pH, texture and carbon content) (Colón et al., 2014).

Within certain limits, SS may play a role of pH regulator (Iticescu et al., 2018). While the use of SS to bring nutrients and organic matter could be beneficial for the soil, it also represents a risk due to the content of contaminants like heavy metals, organic compounds and pathogens. Moreover, SS emits large amounts of H_2S and NH_3 and volatile organic compounds (VOCs) into the atmosphere that are generally associated with odorous nuisance and health risks (Mustafa et al., 2017; Nie et al., 2019). VOCs and semi-VOCs contained in SS may have a harmful impact on the natural environment and human health (Kotowska et al., 2012). Some of those compounds undergo biodegradation during the process of wastewater treatment; others remain in the SS in an unchanged form. A large number of VOCs are formed during metabolic activity of the bacteria that decompose the sludge organic matter in the processes performed at WWTPs and appear as intermediates metabolites (Gomez-Rico et al., 2008). Due to their volatile character, some of these compounds escape to the atmosphere during the SS treatment processes (Kotowska et al., 2012).

In the literature on the subject, only a small number of research papers have been devoted to characterizing the VOCs from SS (Abis et al., 2018, Kotowska et al., 2012; Rincón et al., 2019). Generally, most of the studies related to VOCs emitted from SS are focused on its composting (Shen et al., 2012; Zhang et al., 2013; Zhu et al., 2016) or at the level of WWTPs (Nie et al., 2019; Widiana et al., 2019). In addition, some studies have been performed to study the emission characteristics of VOCs during thermal drying of sludge (Deng et al., 2009; Gomez-Rico et al., 2008). For instance, Gomez-Rico et al., (2008) have studied the impacts of drying temperature on the total number of identified compounds and total yield of VOCs. The authors reported that the drying temperature slightly affects the yield of some individual compounds (such as dimethyl tetrasulphide and propylchlorotoluene). Other studies were related to the emissions during dewatering processes, although the temperature is lower than for thermal drying and thus the emissions of VOCs due to vapourization during the drying are supposedly lower (Gomez-Rico et al., 2008). However, detailed researches on the species and emission characteristics of VOCs from sludge with different degrees of dryness were not investigated yet and these characteristics may have significant agricultural purposes.

To date, there is only one estimation of secondary aerosol formation from precursor gases emitted from the agricultural sector (Ciuraru et al., 2021). This recent study performed on undigested SS samples showed atmospheric particle formation from oxidized organic molecules and SO_2, which are both emitted by SS (Ciuraru et al., 2021). These SOA are readily formed from ozonolysis of skatole emitted by the SS. The authors suggest that this additional VOC source (e.g., skatole) may have a significant influence on atmospheric particle formation during the spreading periods as a high nucleation rate can locally and briefly induce the formation of a significant annual source of particles (Ciuraru et al., 2021).

There is an urgent need for more comprehensive quantitative information on VOCs emitted by SS as aerosol precursors and their comparability at different treatment stages. This comparability would help to identify the impact of sludge treatment on VOC emissions and thus reducing the environmental risk of land applied sludge. The present study extensively characterized the volatile organic compound emissions upon thickening, anaerobic digestion and dewatering of SS and compared them with undigested samples. The results of this study provide an accurate inventory reference for the VOC emissions from SS samples and specific tracers for each type of treatment.

3.2. Materials and methods

The materials and methods were presented in **Chapter 2**, only a brief reminder is presented here on specific details related to the studies described in this Chapter.

3.2.1. Sample description

The SS samples were taken from a wastewater treatment plant in France at the end of the following treatment stages: thickening (undigested SS – UDSS), anaerobic digestion (digested SS – DSS) and dewatering (samples with 30% and 60% of dryness - SS 30% and SS 60%, respectively) (**Figure 2.1**). The main physicochemical properties of the bulk SS samples used in this study are listed in **Table 2.1**. The samples were stored at 4 ^{0}C before the experiments. For the experiments, 500 g of the solid samples (SS 30% and SS 60%), 500 mL of DSS and 1 L of UDSS were used.

3.2.1. Chamber experiments

Experiments were performed in poly(methyl methacrylate) chambers with Teflon walls in a temperature-controlled room. The experimental setup designed for those experiments is illustrated in **Figure 2.4**. In this work, two chambers were used: a 0.03 m^3 and a 0.18 m^3. The sample was uniformly spread on a stainless steel plate with an area of 0.14 m^2 and 0.32 m^2 for the 0.03 m^3 and 0.18 m^3 chambers, respectively. The thickness of the spread sample was 3-4 mm. Three replicates were performed for each sample under the same experimental conditions. During the experiments, the chamber was purged with purified dry air at 6 L min^{-1} and 8.6 L min^{-1} flow rates for the 0.03 m^3 and 0.18 m^3 chambers, respectively. The cycle of the dry air or its residence time in the 0.03 m^3 and 0.18 m^3 chambers was 5 min and ~20 min, respectively (see Annex 1, **Table A.1**). The VOCs were analyzed online using a proton transfer reaction mass spectrometer. In addition, the amount of SO_2, CO_2 and H_2O emitted from the sample was continuously monitored. Ammonia was measured only for one experiment due to the availability of the equipment. Blank tests (i.e. without sample) were performed for both chambers (Annex 1).

3.2.2. PTR-Qi-TOF-MS measurements

The emitted VOCs were measured in real-time using online proton transfer reaction quadrupole-ion-guide time-of-flight mass spectrometry (PTR-Qi-TOF-MS, Ionicon Analytic GmbH). In this work, the PTR-Qi-TOF-MS was operated under the standard conditions described in Section 2.3.1. The measurement period was set to 1s, which means that one mass spectrum of range *m/z* 10-510 was recorded every second. Raw PTR-Qi-TOF-MS data were

recorded by TOFDaq software (TOFWerk AG, Switzerland). PTR-Qi-TOF mass spectra were processed using the PTR viewer 3.2.12 (Ionicon analytik GmbH) and the mMass software (Strohalm et al., 2010). Mass calibrations were performed following the procedure described in Section 2.5.1. In PTR-Qi-TOF-MS, single charge ions are detected and all the detected ions are protonated $(MH)^+$ due to the proton transfer reaction occurring in the drift tube.

The signal of a particular ion was monitored until it reached a steady state (usually after 3 cycles of dry air in the chamber) then 120 mass spectra were extracted from the region where the signal was stable (e.g., **Figure 3.1**). The same procedure was applied for the three replicates.

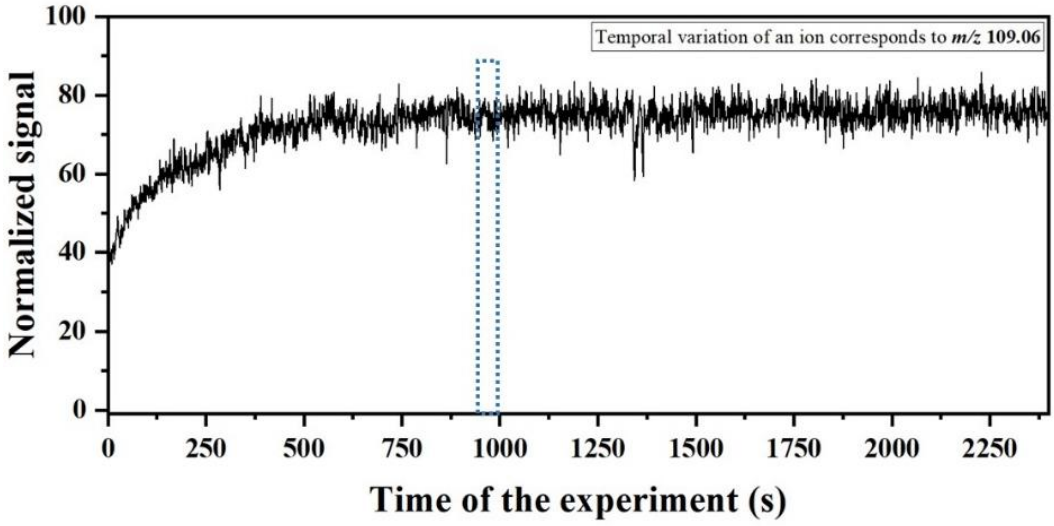

Figure 3.1 *Example of a temporal variation of an ion signal corresponding to m/z 109.06 assigned as $C_7H_8OH^+$ (protonated cresol). The region marked in blue box corresponds to 120 mass spectra chosen for further data analysis.*

To identify the emitted VOCs, a peak table was created for each sample using the mMass software (Strohalm et al., 2010) by selecting the peaks with a S/N > 3.0 from the three averaged spectra. The mass range chosen for analysis was between *m/z* 31 and 400. Signals identified as instrumental background or related to water clusters such as *m/z* 37.03, *m/z* 38.03, *m/z* 39.03 and *m/z* 55.03 were excluded from the data analysis. The PTR viewer 3.2.12 software (Ionicon analytik GmbH) was subsequently used to identify the chemical molecular formula corresponding to each protonated molecular ion in the peak lists following the procedure described in Section 2.5.2. Following this step, the averaged mass spectra were used to calculate the average mass concentration and emission flux of the emitted compounds (details in Section 2.5.3). The comparison between samples was based on the emission fluxes of the compounds, which was calculated taking into account the emission surface, airflow rate

through the chamber and the mass concentration of the emitted VOC. Even though the quantities of the samples were different as a function of their degree of dryness, this parameter was not used to calculate the fluxes.

3.2.3. Statistical analysis

Statistical analysis of the emitted VOCs was performed to identify the chemical compounds that characterize the differences between the samples and mark each treatment step. In this work, PCA was performed with a matrix containing the integrated peak areas (variables) against the mass spectra (observations). The volcano plot was performed for identifying the chemical compounds that contribute to the diversity between two samples. Python and R software (R Studio version 4.0.3) were used to perform PCA and volcano plot, respectively. For more details on statistical analysis, see Section 2.5.4.

3.3. Results

3.3.1. VOCs emitted by the different samples

An example of a PTR-Qi-TOF average mass spectrum for each sample is given in **Figure 3.2**. The molecular formula assignment of detected peaks (for S/N > 3.0) was selected based on the criteria described in Section 2.5.2.

Following this procedure, the vast majority of the detected peaks (> 90%) were assigned to a suitable molecular formula and only a few were unassigned (**Table 3.1**). PTR-QiTOF-MS does not allow unambiguous recognition of the compounds, such as isomers. However, for the assignments under discussion, we tentatively identified the structural formula based on the literature (Byliński et al., 2019; Fisher et al., 2017; Harrison et al., 2006; Kotowska & Isidorov, 2012; Mustafa et al., 2017; Nie et al., 2018; Rincón et al., 2019). The average mass uncertainty of the assignments was less than 20 ppm. The assigned peaks correspond to either a VOC or its ^{13}C-containing isotopic peak. The total number of assigned VOCs in UDSS, DSS, SS 30% and SS 60% were 233, 193, 192 and 186, respectively. A total of 380 distinct compounds were detected and quantified in all SS samples using PTR-QiTOF-MS, with 81 compounds commonly found in all samples. The list of assigned 380 VOCs detected in all SS samples is given in Annex 3, **Table A.2**. Among all samples, UDSS was the largest emitter (233 VOCs) with 93 compounds specific for this sample. The number of compounds emitted exclusively from DSS, SS 30%, and SS 60% was 30, 22 and 32, respectively (**Table 3.1**). These compounds may hence be specific tracers for each type of SS emissions and are listed in **Table A.2**.

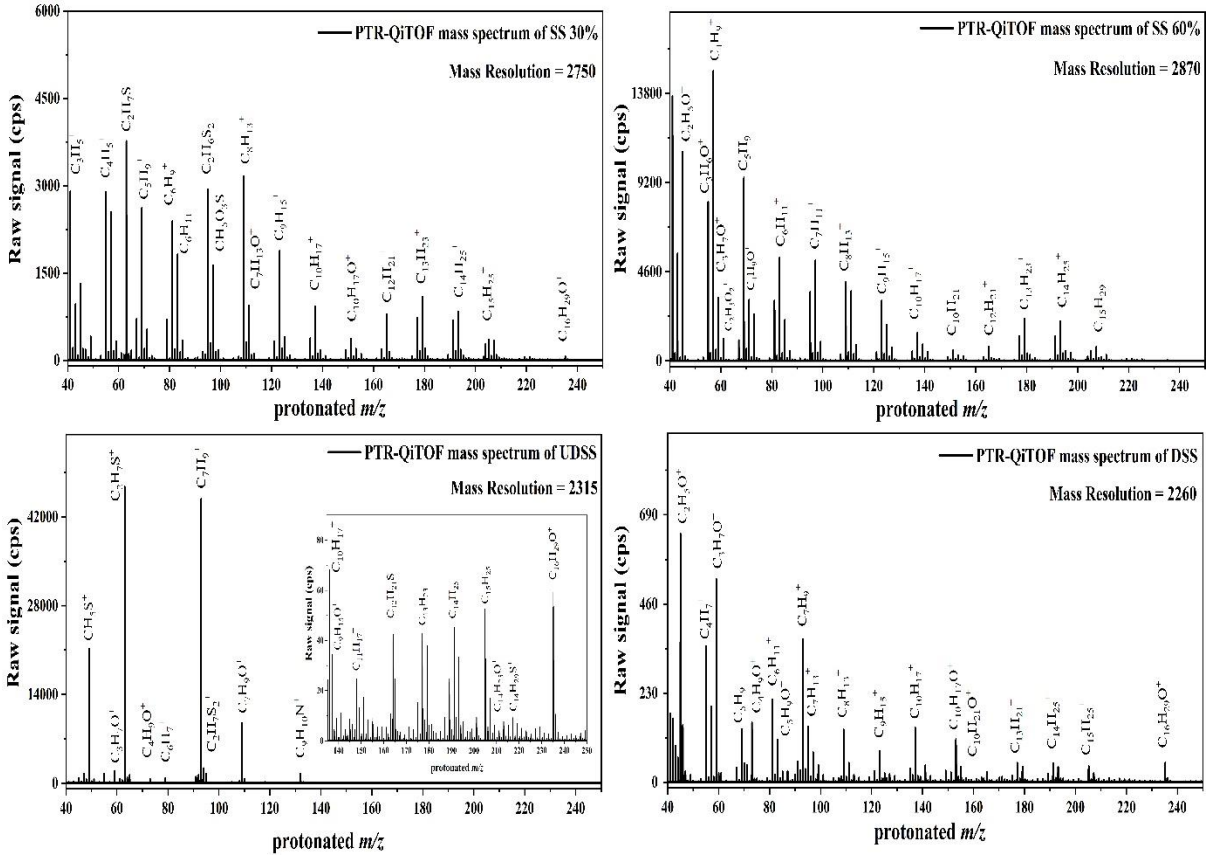

Figure 3.2 *PTR-QiTOF average mass spectrum for each sample and the chemical assignments of some protonated mass peaks. All the assigned molecular formulas are protonated ($VOCH^+$).*

Table 3.1 *PTR-QiTOF-MS results for SS samples analysis. The numbers in bold correspond to the total number of assigned VOCs in each sample.*

Sample name	# of detected peaks	# of assigned peaks	# of unassigned peaks	# of peaks corresponding to VOCs	# of peaks corresponding to ^{13}C isotopes	# of emission tracers
UDSS	305	285	20	**233**	52	93
DSS	287	259	28	**193**	66	30
SS 30%	331	286	45	**192**	94	22
SS 60%	303	275	28	**186**	89	32

The assigned VOCs were classified into the following chemical groups: Hydrocarbons (*HC*), Oxygenated compounds (*O-compounds*), Sulphur compounds (*S-compounds*), Nitrogenated compounds (*N-compounds*), and Other compounds (*Others*: chemical compounds containing more than one heteroatom in their molecular formula, e.g., C_3H_7NO, $C_3H_7NO_2$, C_5H_6OS, $C_9H_{17}NS$, C_5H_7NOS, etc.). The number of compounds assigned to each chemical group is

shown in **Figure 3.3**. The speciation of VOCs varied among the analyzed samples. For instance, the DSS showed more HC and fewer O-compounds and N-compounds compared to UDSS. The dewatering step increased the number of HC; about half of the assigned molecular formulas in SS 30% and SS 60% being HC.

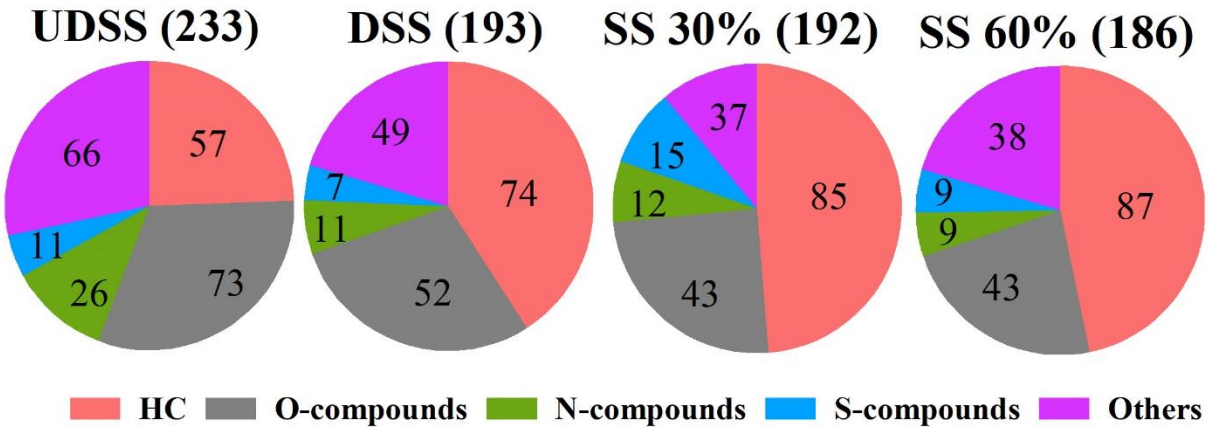

Figure 3.3 *The number of compounds assigned for each chemical group in each sample. The total number of assigned VOCs in each SS is given in parentheses.*

3.3.2. Emission characteristics of VOCs

The mass concentration of the assigned VOCs was estimated based on their mixing ratio and considering the molecular weight of the compound. The total mass concentration of each chemical group was calculated by summing the concentrations of the individual compounds in each chemical group. The chemical groups contributed to a different extent to the total concentration of VOCs (**Figure 3.4**). HC was the chemical group with the highest concentration in all samples. The second most abundant group in SS 60% and DSS was O-compounds (1425 ± 739 and 511 ± 171 µg m^{-3}, respectively). In contrast, in UDSS and SS 30%, S-compounds represented the second most abundant group (1038 ± 448 and 372 ± 131 µg m^{-3}, respectively). The concentrations of other compounds containing more than one heteroatom in their molecular formulas were the lowest in all samples (less than 300 µg m^{-3}) and their contribution to total concentration was less than 20%.

The emission fluxes of VOCs and the total emission flux of each chemical group are shown in **Table 3.2**. The highest VOC emission fluxes were observed in the SS 60% with 328 ± 65 µg m^{-2} min^{-1}, followed by SS 30%, UDSS and DSS samples with 168 ± 39, 94 ± 21 and 69 ± 25 µg m^{-2} min^{-1}, respectively. Compounds having the highest emission flux in all samples were HC. The emission fluxes of O-compounds followed the trend: SS 60% > SS 30% > DSS

> UDSS. The compounds designated as *others* were highly emitted from DSS (12 ± 3 µg m^{-2} min^{-1}), compared to the other samples.

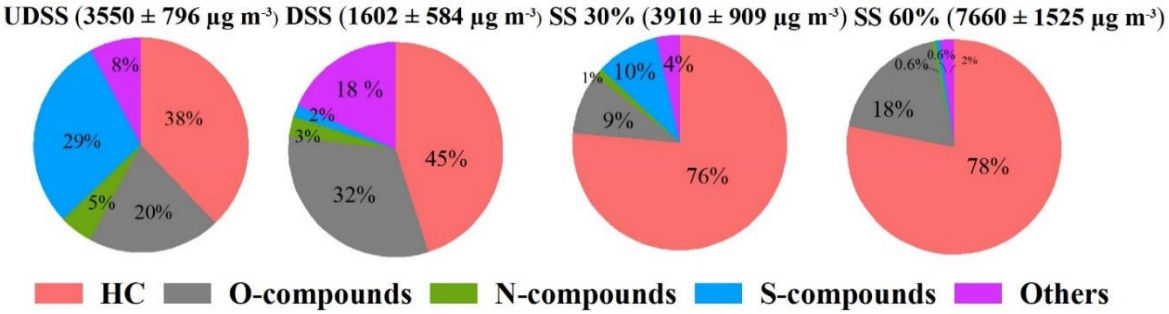

Figure 3.4 *Percentage contribution of each chemical group to the total mass concentration of assigned VOCs. The total concentration of VOCs obtained in each sample is given in parenthesis.*

Table 3.2 *Total emission flux of each chemical group found in SS samples. The standard deviation of the average emission flux obtained from the three replicates of each sample is displayed.*

Sample name	**Total emission flux of VOCs (µg m^{-2} min^{-1})**	**Total emission flux of each chemical group (µg m^{-2} min^{-1})**				
		HC	O-compounds	N-compounds	S-compounds	Other compounds
UDSS	94 ± 21	36 ± 1	19 ± 6	4.77 ± 1.47	28 ± 12	7.37 ± 0.59
DSS	69 ± 25	31 ± 14	22 ± 7	2.08 ± 0.62	1.2 ± 0.3	12.48 ± 3.04
SS 30%	168 ± 39	128 ± 27	16 ± 5	2.12 ± 0.35	16 ± 6	6.01 ± 0.65
SS 60%	328 ± 65	256 ± 32	61 ± 32	1.87 ± 0.39	2.0 ± 0.2	7.06 ± 0.77

The emission flux of each sulphuric and nitrogenated compound is illustrated in **Figure 3.5**. Comparable emission fluxes of N-compounds were found in DSS, SS 30% and SS 60%, while they showed the highest in UDSS (4.77 ± 1.47 µg m^{-2} min^{-1}). This was explained by a high contribution of an ion corresponding to *m/z* 132.08 and assigned as $C_9H_9NH^+$, with an emission flux 2 ± 1 µg m^{-2} min^{-1}. The highest emission fluxes of S-compounds were observed in UDSS (28 ± 12 µg m^{-2} min^{-1}); this was attributed to the strong emissions of CH_4S, C_2H_6S and $C_2H_6S_2$.

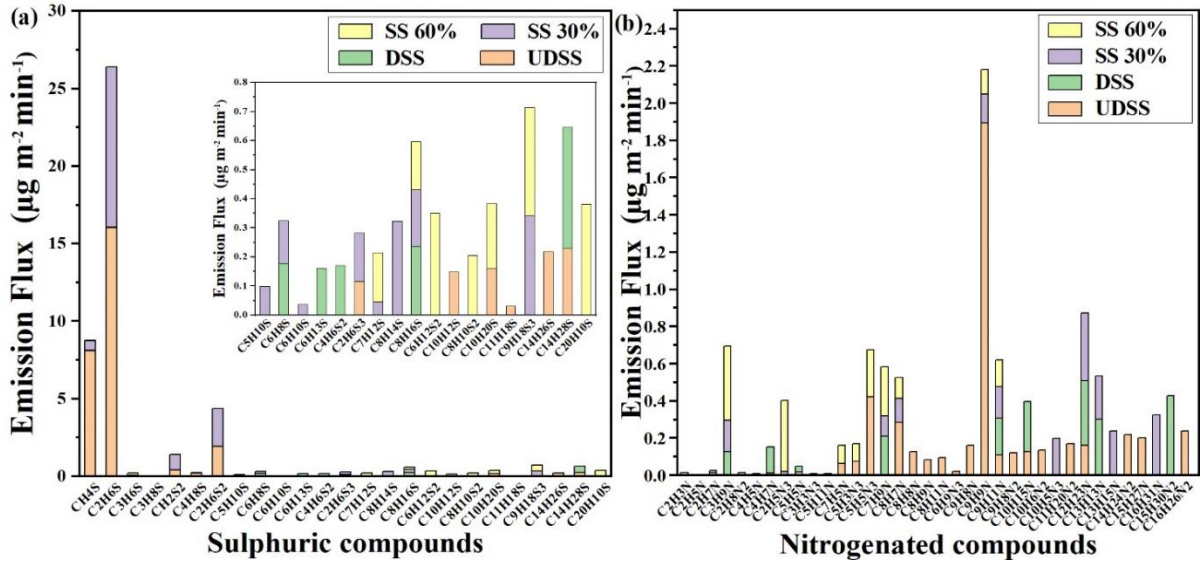

Figure 3.5 *(a) Emission fluxes of sulphur compounds emitted from SS samples. The zoomed inset to the right shows sulphur compounds with fluxes < 1 µg m^{-2} min^{-1}. (b) Emission fluxes of nitrogenated compounds emitted from SS samples.*

3.3.3. Classification of HC by the double bond equivalent method

DBE analysis was performed on the HC emitted from all samples in this work. A detailed description of this method is provided in Section 2.5.5. The obtained DBE values ranged from 1 to 8 with six sub-classes of HC: aliphatic (linear alkenes or alkynes), alicyclic (cycloalkanes, cycloalkenes, or cycloalkynes), aromatic (benzene and its derivatives), terpenes and polycyclic aromatic hydrocarbons (PAHs). In this work, 95 compounds were assigned as HC in all samples. The DBE value of each HC was calculated (listed in Annex 3, **Table A.3**). The DBE versus the C number of all assigned HC is illustrated in **Figure 3.6**. DBE value increased with the decreasing number of H atoms in the molecular formula (from C_nH_{2n} to C_nH_{2n-12}).

A homologous series of compounds with different degrees of alkylation (substitution of peripheral H by CH_3 groups leading to no change in the DBE) had constant DBE value but different C numbers. For each series, the proposed general molecular formula and the corresponding DBE value is indicated in **Figure 3.6**. The emitted HC were either cyclic, include π-bonds or both (see **Figure 2.24**). Several aliphatic and alicyclic compounds with $1 \leq$ DBE ≤ 3 were found. Such compounds might be alkenes, alkynes, dienes, cycloalkanes, cycloalkenes, cycloalkynes or polyenes. Peaks at *m/z* 69.06, 137.13 and 205.19 were assigned to $C_5H_8H^+$, $C_{10}H_{16}H^+$ and $C_{15}H_{24}H^+$, respectively and identified as terpenes (situated on the dashed line in **Figure 3.6**). In this study, 47 compounds of the emitted HC were aromatic with $4 \leq$ DBE ≤ 8.

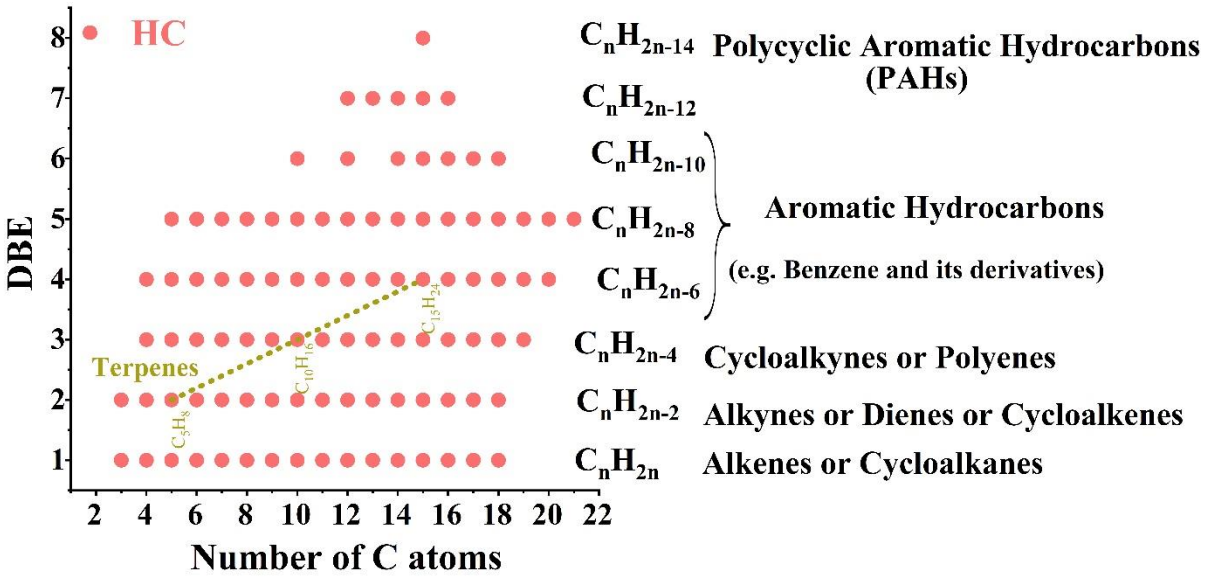

Figure 3.6 *DBE vs. the number of carbon (C) atoms plot for the HC emitted from all SS. The proposed molecular formula of the compounds having the same DBE and differing by one C number is shown to the right with the possible sub-class(es) name. Compounds identified as terpenes are highlighted by a dashed line on the diagram.*

The bar graph representation of the HC sub-classes identified using DBE analysis is displayed in **Figure 3.7 (a)**.

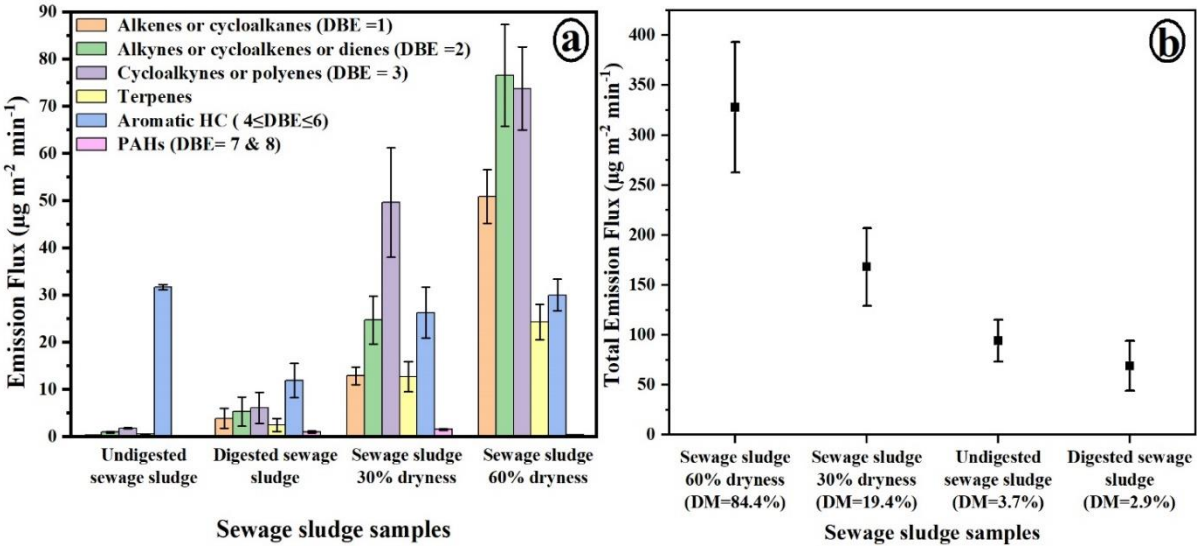

Figure 3.7 *(a) Classification of HC detected in each SS using the DBE method. The total emission flux of HC sub-classes in each sample is illustrated. The error bars shown in the figure represent the standard deviation of the average emission flux obtained from the three replicates of each sample. (b) Total emission flux of VOCs emitted from each SS versus the dry matter content of the sample.*

The total emission fluxes of HC sub-classes are displayed. Aromatic compounds dominated the emissions among the HC from UDSS (31.96 ± 0.55 µg m^{-2} min^{-1}). The emissions of aromatic compounds were the highest for UDSS, followed by SS 60%, SS 30% and DSS. DBE = 2 compounds were emitted dominantly from SS 60% (76.58 ± 10.77 µg m^{-2} min^{-1}). SS 30% was characterized by the high emissions of HC with DBE = 3 (49.68 ± 11.59 µg m^{-2} min^{-1}). Terpenes showed the highest emissions from SS 60% (24.37 ± 3.74 µg m^{-2} min^{-1}). Their emission flux was about the half in SS 30% (12.73 ± 3.17 µg m^{-2} min^{-1}) and lower in DSS and UDSS (2.53 ± 1.34 and 0.55 ± 0.04 µg m^{-2} min^{-1}, respectively). The total emission flux of HC emitted from each sample decreased with the decrease in its dry matter content (**Table 3.2**). Similarly, the total emission flux of VOCs decreased as the dry matter content of the SS sample decreased (**Figure 3.7, b).**

3.3.4. Sample comparison

To better uncover the similarities and differences between analyzed SS, PCA was performed based on the samples' mass spectra. The first three principal components, PC1, PC2 and PC3, comprised 71.30%, 17.17% and 9% of data variation, respectively. Together they accounted for 97% of the total variance and were enough to discriminate between the samples. Thus, PC1, PC2, and PC3 were considered for data interpretation. The four samples were well separated in the PC2 *vs.* PC1 and PC3 *vs.* PC1 score plots illustrated in **Figure 3.8**.

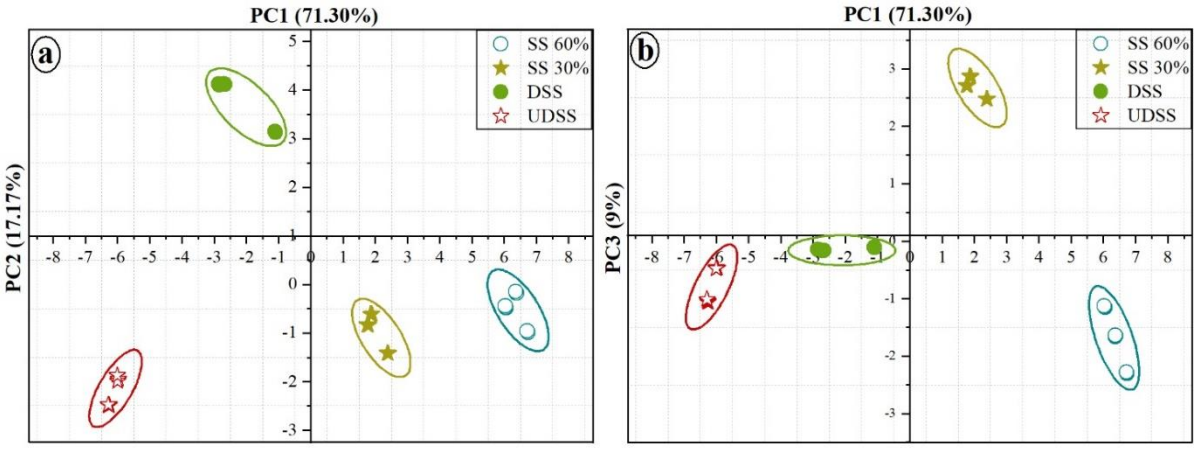

Figure 3.8 *Score plots of (a) PC2 vs. PC1 and (b) PC3 vs. PC1 for SS samples. The percentage contribution of each PC to total variance is given in parenthesis. The ellipses highlight data points coming from the same SS and are added for visual purposes only.*

Positive PC2 separated DSS from the other samples (**Figure 3.8**). The corresponding loading plot (**Figure 3.9, b**) suggested that DSS was highly influenced by N&O-compounds

and oxygenated VOC (OVOC) emissions. The negative value of PC2 separated UDSS from the other samples. The loading plot (**Figure 3.9, b**) showed that UDSS was characterized by S-compounds. Thiazole compounds such as C_3H_3NS, C_5H_7NS, C_6H_7NS, $C_{10}H_7NS$ and $C_8H_7NS_2$ showed high contribution in UDSS. Dewatered samples (SS 30% and SS 60%) were separated from UDSS and DSS by PC1. Based on the loading plots (**Figure 3.9, a**), SS 60% and SS 30% were associated with HC, O-compounds and S-compounds. PC3 (~9%) allowed for better discrimination between SS 60% and SS 30% than PC1 and PC2. From PC3 loading plot (**Figure 3.9, c**), SS 60% received a high contribution from OVOCs while SS 30% was dominated by S-compounds.

In order to determine how the treatment stage affects the profile of VOC emissions, the samples collected at consecutive treatment steps were compared: DSS versus UDSS to identify the impact of anaerobic digestion and SS 30% and SS 60% versus DSS to uncover the impact of the dewatering step. The results are illustrated by volcano plots in **Figure 3.10**. The assignments of detected ions having high statistical significance and logarithm of fold change > +1 (red circles) or < -1 (green circles) are provided in Annex 3, **Table A.4**. UDSS was characterized by S-compounds while DSS was associated with OVOCs (**Figure 3.10, a)**. This supported the PCA results. In addition, three compounds showed high significance and fold change in UDSS compared with DSS: C_7H_8, C_9H_9N and C_7H_8O. The comparison between dewatered sludge and DSS is illustrated in **Figure 3.10 (b and c)**. SS 30% was dominated by S-compounds and HC compared with DSS, while SS 60% was influenced by O-compounds and HC. The dewatered samples were also compared to determine the impact of dry matter on VOC emissions (**Figure 3.10, d)**. The results show that SS 30% was characterized by high S-compound emissions; while SS 60% was influenced by OVOCs.

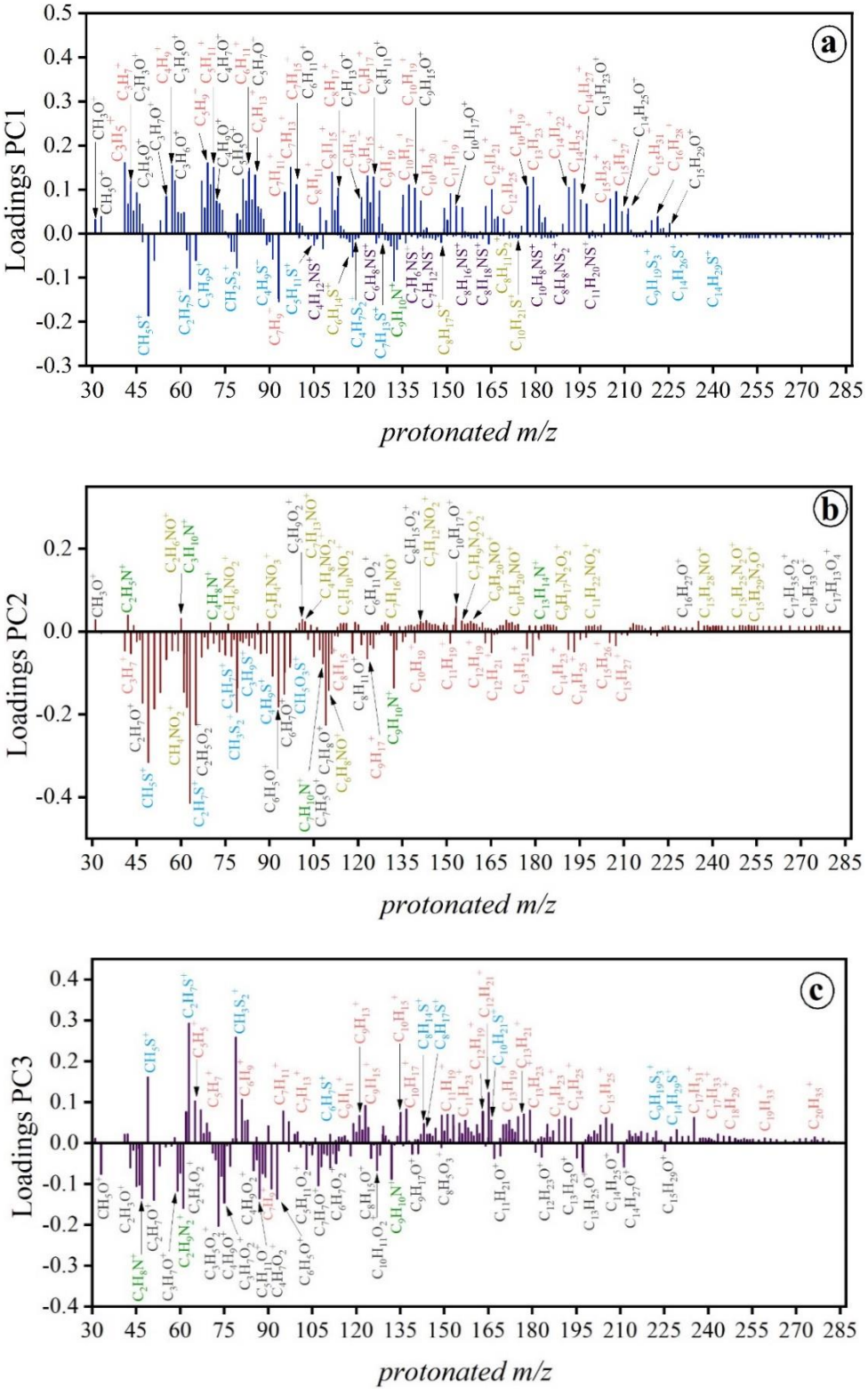

Figure 3.9 *Loading plots for the (a) PC1, (b) PC2 and (c) PC3 obtained from the mass spectra of SS samples. The protonated molecules ($VOCH^+$) contributing to positive and negative values of each PC are shown. All the assigned molecular formulas are protonated ($VOCH^+$). HC (light red), oxygenated (dark grey), nitrogenated (green), sulphuric (blue), nitrogen and oxygen*

containing (yellow) and other compounds containing more than one heteroatom in the molecular formula (violet) are displayed.

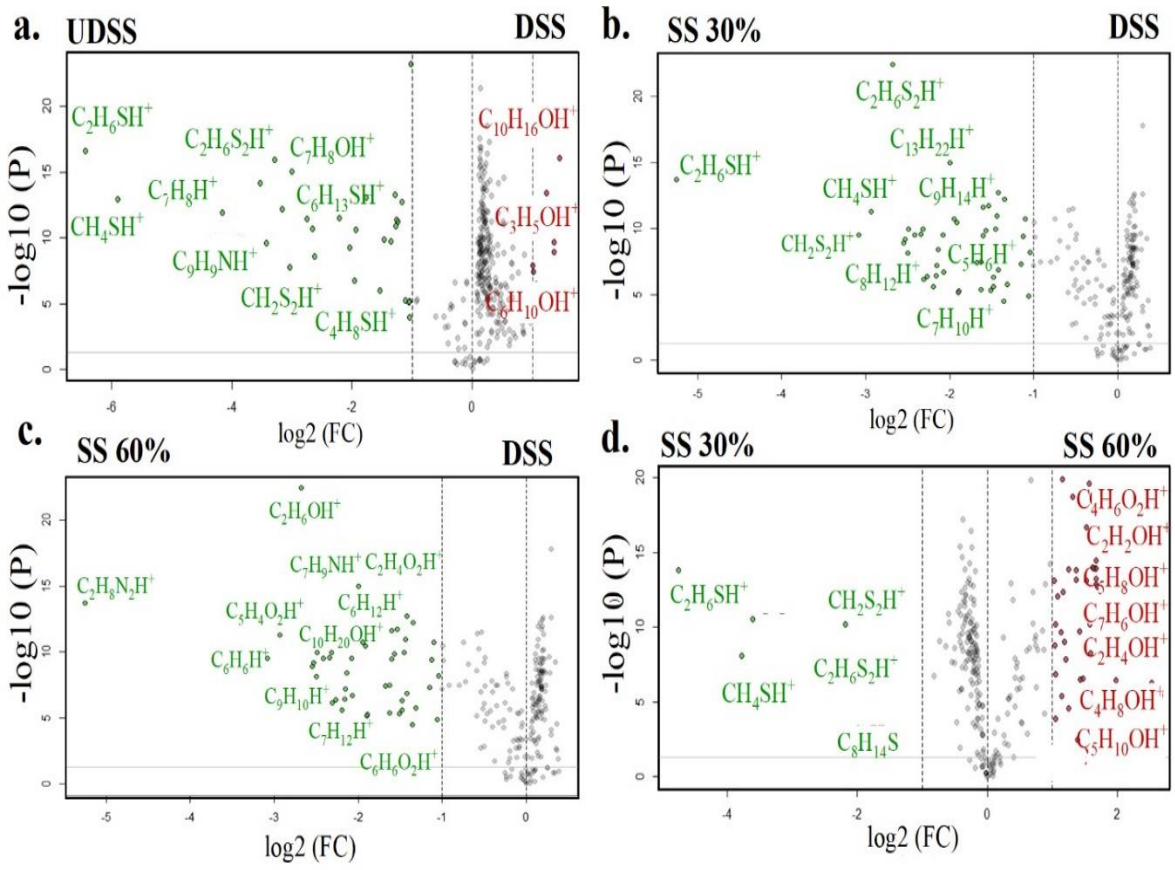

Figure 3.10 *Volcano plots showing the «differential expression» of detected chemical compounds in (a) UDSS and DSS (b) SS 30% and DSS, (c) SS 60% and DSS, and (d) SS 30% and SS 60%. Grey points correspond to chemical species that have either a low statistical significance or low fold change, and thus do not contribute to the separation between the two samples. The chemical assignments of protonated molecules ($VOCH^+$) are shown. Red circles represent the significant mass peaks with logarithm of fold change > +1 and green circles represent the significant peaks with logarithm of fold change <-1.*

3.4. Discussion

Table 3.3 summarizes the main characteristics of each SS sample. The assigned VOCs were classified into five major chemical groups (1) HC, (2) S-compounds, (3) O-compounds, (4) N-compounds and (5) other compounds. In the following Sections, the results of this study were discussed by the chemical group and based on comparison with the literature.

Table 3.3 *Characteristics of the analyzed SS samples. The total number of VOCs, number of emission tracers, total mass concentration, and total emission fluxes as well as the percentage of dry matter in each SS are displayed. The uncertainty in the calculation is given next to each value.*

Sample name	Number of assigned VOCs	Number of emission tracers	Total mass concentration of assigned VOCs (µg m^{-3})	Total emission flux of assigned VOCs (µg m^{-2} min^{-1})	Dry matter (%)
UDSS	233	93	3550 ± 796	94 ± 21	3.7
DSS	193	30	1602 ± 584	69 ± 25	2.9
SS 30%	192	22	3910 ± 909	168 ± 39	19.4
SS 60%	186	32	7660 ± 1525	328 ± 65	84.4

3.4.1. Hydrocarbons

Compounds assigned as HC had the highest emission fluxes in all samples. PTR-Qi-TOF-MS helps to determine the molecular formula of a compound but not its chemical structure. Such identification is possible by combining complementary analytical techniques, such as GC-MS (Ni et al., 2012). In this work, the DBE method was applied to classify the assigned HC into smaller sub-classes of compounds with the same DBE value but different degree of alkylation. To our knowledge, DBE analysis is performed here for the first time on PTR-Qi-TOF-MS data. In this study, no linear alkanes with DBE = 0 were found. This could be explained by their PA lower than that of water, therefore the proton transfer reaction with H_3O^+ is not an effective ionization mechanism for their detection (Amador-Muñoz et al., 2016). However, this does not exclude their emissions from our samples as several linear alkanes were detected in SS using GC-MS (Fisher et al., 2017; Kotowska & Isidorov, 2012; Nie et al., 2018). Mustafa et al., (2017) related the presence of alkanes to the decomposition of organic matter in SS. Our results showed that for example the aliphatic and alicyclic compounds showed highest emission flux in digested samples compared to undigested samples while aromatic compounds showed the highest emission flux in UDSS. Moreover, the increased number of assigned HC in the dewatered sludge compared to the UDSS and DSS can be explained by the much higher organic matter content of the dewatered samples (**Table 2.1**).

3.4.1.1. Aliphatic and alicyclic compounds

A group of 16 aliphatic compounds (C_3 - C_{18}) with DBE = 1 (alkenes or cycloalkanes) were found in all samples. SS 60% showed the highest emission flux (50.93 ± 5.64 µg m^{-2} min^{-1})

compared to 12.93 ± 1.83, 3.95 ± 2.08, 0.35 ± 0.03 µg m^{-2} min^{-1} from SS 30%, DSS and UDSS, respectively. This variation was mainly attributed to a compound detected at *m/z* 57.06 and assigned as $C_4H_8H^+$, comprising 34% of the total aliphatic compound emission flux in SS 60%. Other aliphatic compounds with high emission fluxes in SS 60% were C_3H_6, C_5H_{10} and C_6H_{12}. Compounds assigned as C_8H_{16} and C_9H_{18} were identified as ethyl cyclohexane and propyl cyclohexane, respectively, in anaerobically stabilized biosolids subjected to aging by Fisher et al., (2017). These compounds were highly emitted from SS 60% compared to the other samples. Compounds such as $C_{10}H_{20}$, $C_{11}H_{22}$ and $C_{12}H_{24}$ identified as pentyl cyclopentane, pentyl cyclohexane and hexyl cyclohexane, respectively, were found in SS from municipal WWTPs (Kotowska & Isidorov, 2012).

Fifteen compounds with DBE = 2 that were alkynes, dienes or cycloalkenes were found in all samples. These compounds showed high emissions from SS 60% (76.58 ± 10.77 µg m^{-2} min^{-1}), this was attributed to the high emissions of compounds C_3H_4, C_7H_{12}, C_4H_6, C_6H_{10}, C_8H_{14} and C_9H_{16}, contributing to 85% of the total emissions of compounds with DBE = 2 from SS 60%. C_8H_{14} and C_9H_{16} were identified as 1-methyl-2-methylenecyclohexane and methyl-(methylethylidene) cyclohexane, respectively (Fisher et al., 2017). 15 compounds having DBE = 3 (cycloalkynes or polyenes) with the highest emissions from SS 60% of 73.81 ± 8.83 µg m^{-2} min^{-1} were also detected. Therefore, SS 60% showed the maximum emission flux of aliphatic or alicyclic compounds compared to the other three samples.

3.4.1.2. Terpenes

Three ions at *m/z* 69.07, 137.13 and 205.19 assigned as $C_5H_8H^+$, $C_{10}H_{16}H^+$ and $C_{15}H_{24}H^+$, respectively were emitted from all SS samples. These compounds were identified as terpenes, a class of compounds with the formula $(C_5H_8)_n$, which are typical unsaturated HC and frequently attributed to biogenic origin. SS 60% showed the highest emission flux of terpenes (24.37 ± 3.73 µg m^{-2} min^{-1}), **Figure 3.7 (a)**. Terpenes such as isoprene (C_5H_8), monoterpenes ($C_{10}H_{16}$) and sesquiterpenes ($C_{15}H_{24}$) were identified in SS samples (Byliński et al., 2019; Fisher et al., 2017; Nie et al., 2018; Kotowska & Isidorov, 2012). The use of fragrant aromatic detergents and green waste were considered potential sources of terpenes and HC (Mustafa et al., 2017). Several studies showed terpenes and aromatic compounds emission from SS samples and composting processes (Schiavon et al., 2017; Tsai et al., 2008; Zhang et al., 2013; Zhu et al., 2016). In this work, terpenes contributed slightly to the total mass concentration of VOCs, ranging from 0.58% - 7.42% for different samples. This is consistent with the results reported by Rincón et al., (2019), where terpenes emission varied from 0.07% - 21% of the total mass

concentration from samples characterized by a reduced content of vegetal materials, such as pig slurry, turkey manure and solid fraction of anaerobically digested pig slurry and SS. High terpenes emission (21-90%) was observed from samples with lignocellulosic content such as biowastes and green wastes (Rincón et al., 2019). The decaying process of vegetable material, bacterial degradation of lignin and cellulose and aerobic degradation of organic matter resulted in high terpene emissions (Eitzer, 1995; Moreno et al., 2014; Schiavon et al., 2017). Their organic matrices were mainly constituted of fruits, vegetables, leaves, brush and food waste (Eitzer, 1995). $C_{10}H_{16}$ was identified as limonene (cyclic monoterpenes) in SS at different processing units of the composting plant (dewatering room, dewatered sludge, blender room, fermentation workshop and product) with measured concentrations of 5.2 ± 0.5, 23.0 ± 4.4, 290.1 ± 109.1, 252.6 ± 120.9, and 27.9 ± 6.2 μg m^{-3}, respectively (Nie et al., 2018). In this work, $C_{10}H_{16}$ was emitted from all SS samples. Concentrations measured at SS 60% and SS 30% gas phase emissions were 28.29 ± 13.09 and 6.83 ± 0.52 μg m^{-3}, respectively. They were relatively higher than the concentrations of dewatered sludge measured by Nie et al., (2018). The composition of composting materials and the deodorants used in the composting plant were considered the main origin of limonene in the composting plant (Nie et al., 2018).

3.4.1.3. Aromatic compounds

Most of the detected HC (37 compounds) were aromatic with $4 \leq DBE \leq 6$. Those compounds had at least one aromatic ring and suffered from extensive dehydrogenation as revealed by the group of peaks illustrated in **Figure 3.6**. In contrast to aliphatic and alicyclic compounds, aromatic compounds showed the highest emission flux in UDSS (31.72 ± 0.55 μg m^{-2} min^{-1}) followed by SS 60%, SS 30% and DSS. The high emissions of aromatic compounds from UDSS were attributed to a compound $C_7H_8H^+$ detected at *m/z* 93.07 with a concentration of 981 ± 5 μg m^{-3}. It constituted 82% of the total aromatic compound emissions from UDSS. C_7H_8 was identified as toluene in SS (Byliński et al., 2019; Fisher et al., 2017; Harrison et al., 2006; Kotowska & Isidorov, 2012; Nie et al., 2018). Toluene dominated the aromatic compounds emitted from SS analyzed at different processing units of the composting plant (dewatering room, dewatered sludge, blender room, fermentation workshop and product) (Nie et al., 2019). The measured concentrations of toluene were 262 ± 116, 118 ± 12, and 57 ± 15 μg m^{-3} in the fermentation workshop, dewatered sludge and dewatering room, respectively (Nie et al., 2019). The amount of toluene emitted from UDSS exceeded the values reported by Byliński et al., (2019). The authors showed a fluctuation in toluene mixing ratios between 1 ppb and 27 ppb during the measurement period of samples collected from WWTPs in Poland (Byliński et al.,

2019). Toluene is widely used in industrial environments and it can be easily biodegraded under aerobic conditions (Wilson et al., 1994). This might explain the high emissions of toluene from UDSS. In addition, the very high concentration of toluene might be associated with a specific industrial discharge to these WWTPs. Moreover, Chiriac et al., (2011) reported that spices and other household products are the main sources of toluene.

Other compounds such as $C_{10}H_{12}$, $C_{10}H_{14}$, $C_{15}H_{22}$, $C_{16}H_{26}$ and $C_{17}H_{28}$ were emitted from all samples. Such compounds were reported in SS samples (Byliński et al., 2019; Fisher et al., 2017; Kotowska & Isidorov, 2012; Nie et al., 2018; Nie et al., 2019, Rincón et al., 2019). Benzene and its derivatives (e.g., C_8H_{10} and C_9H_{12}), identified in SS using off-line GC-MS measurements (Fisher et al., 2017; Kotowska & Isidorov, 2012), were found in our samples. Toluene, benzene, ethylbenzene and xylene (BTEX) have been widely found in the gas-phase emissions from SS (Wilson et al., 1994; Zhu et al., 2016). BTEX and C_9H_{12}, found in all our samples, were frequently attributed to anthropogenic sources and reported inside farm buildings (Ciganek & Neca, 2008; Kammer et al., 2020). BTEX was produced in large quantities and is extensively employed in a broad spectrum of industrial applications, primarily as solvents, components of gasoline, and in the production of other chemicals. For example, toluene is present in many consumer products, including household aerosols, paints, varnishes, adhesives and glues (Mrowiec et al., 2005). Five PAHs with $7 \leq DBE \leq 8$ showed the lowest emission fluxes among all HC. Among all PAHs, only $C_{15}H_{18}$ was identified in SS samples as 1,6-dimethyl-4-(1-metyhylethyl) naphthalene (Kotowska & Isidorov, 2012).

3.4.2. Volatile organic sulphur compounds (VOSCs)

Sulphur in the sludge mainly exists in the form of organic sulphur or sulphur oxides, such as thioamino acids, sulphonic acids and sulphate (Xue et al., 2021). The emission of sulphur compounds could be associated with the biodegradation of sulphur-containing amino acids such as methionine and cysteine (Higgins et al., 2003; Mackie et al., 1998; Schiavon et al., 2017). This conversion leads to the formation of volatile organic sulphur compounds VOSCs and H_2S under anaerobic conditions (Du & Parker, 2012). In this work, twenty-five detected peaks were assigned as VOSCs. UDSS and SS 30% showed higher emission fluxes of VOSCs compared to the other samples (**Table 3.2**).

A compound detected at *m/z* 63.02 was assigned to the protonated form of $C_2H_6SH^+$. C_2H_6S was emitted from all samples except SS 60%. It was identified as dimethyl sulphide (DMS) and the most abundant VOSC in UDSS (604 ± 311 μg m^{-3}) and SS 30% (241 ± 109 μg m^{-3}). CH_4S was emitted from all samples and identified as methanethiol (or mercaptan) in SS

(Byliński et al., 2019; Fisher et al., 2017; Nie et al., 2018). It was the second most abundant VOSC in UDSS (304 ± 112 μg m^{-3}). CH_2S_2 and $C_2H_6S_2$ were emitted from UDSS and SS 30%. $C_2H_6S_2$, identified as dimethyl disulphide (DMDS) in SS (Byliński et al., 2019; Fisher et al., 2017), was measured in this work with an average concentration of 72 ± 18 and 57 ± 12 μg m^{-3} in UDSS and SS 30%, respectively. It was around half the average concentration measured by Nie et al., (2019); 144 ± 37 μg m^{-3}. This difference might be related to the high photochemical reactivity of DMDS, thus it would be expected that most of DMDS could be lost prior to sample introduction into the chamber. In addition, DMDS was found to be the dominant pollutant in other studies (Ding et al., 2015; Duan et al., 2014). $C_2H_6S_3$ and CH_4O_3S, identified as dimethyl trisulphide (DMTS) and methane sulphonic acid, respectively in SS (Fisher et al., 2017), were emitted from UDSS and SS 30%. Yao et al., (2019) reported the dominance of methanethiol and DMS among the sulphur compounds in municipal solid waste disposal plants. In the current study, CH_4S (methanethiol), C_2H_6S (DMS), CH_2S_2 and $C_2H_6S_2$ (DMDS) constituted 96% and 91% of total VOSC emission flux in UDSS and SS 30%, respectively. These VOSCs have been selected as core indicators for odour nuisance in SS (Byliński et al., 2019; Fisher et al., 2017; Nie et al., 2018). This might explain the intense odour of UDSS sample as those compounds were highly emitted from this sample.

3.4.3. Oxygenated volatile organic compounds (OVOCs)

In this work, 104 VOCs were assigned as OVOCs. Their highest emission flux was observed in SS 60%, followed by DSS, UDSS and SS 30% (**Table 3.2**). Among OVOCs, 59% of compounds contained one O atom, 30% contained two O atoms and 6% and 5% included three and four O atoms, respectively. This indicated that the emitted OVOCs were not highly oxidized. Accordingly, OVOCs were classified into different groups based on the number of O atoms in the molecular formula. The first group of compounds having the molecular formula $C_nH_{2n}O$ and characterized by CH_2 repetitive unit was tentatively identified as carbonyl compounds (i.e. aldehydes or ketones). The second group included compounds with molecular formula $C_nH_{2n-2}O$ and were either unsaturated or cyclic carbonyl compounds. The last group of compounds ($C_nH_{2n}O_2$) were either carboxylic acids or esters.

A compound detected at *m/z* 45.03 was assigned as $C_2H_4OH^+$. C_2H_4O was emitted from all samples with high emissions from SS 60% (14.87 ± 8.35 μg m^{-2} min^{-1}). This compound was identified in stabilized dewatered sludge and anaerobically stabilized biosolids as acetaldehyde (Byliński et al., 2019; Fisher et al., 2017). Two compounds at *m/z* 33.03 and *m/z* 47.05 were assigned as CH_4OH^+ and $C_2H_6OH^+$, respectively. CH_4O was emitted from all samples except

SS 30%. It showed a relatively high emission flux from SS 60% (7.42 ± 4.19 μg m^{-2} min^{-1}) when compared with DSS and SS 60%. C_2H_6O was only emitted from DSS and SS 60%. CH_4O and C_2H_6O were identified in SS as methanol and ethanol, respectively (Byliński et al., 2019; Fisher et al., 2017; Kotowska & Isidorov, 2012). Methanol and ethanol were the end products of various organic metabolic processes (Kotowska & Isidorov, 2012). Methanol was found in green waste as the most relevant alcohol and it was an intermediate product of microbial metabolism of wood and plants (Rincón et al., 2019). C_3H_6O (*m/z* 59.05) was emitted from all samples and identified as acetone. It was reported to be the most abundant OVOC in SS samples (Byliński et al., 2019; Fisher et al., 2017; Kotowska & Isidorov, 2012; Nie et al., 2018). Another compound C_4H_8O (*m/z* 73.06) was emitted from all our samples and identified as 2-butanone (Byliński et al., 2019; Fisher et al., 2017; Harrison et al., 2006; Nie et al., 2018). The concentrations of C_4H_8O in this work were comparable with that measured in SS analyzed at different processing units of the composting plant (< 200 μg m^{-3}) (Nie et al., 2019). $C_2H_4O_2$ (*m/z* 61.03) was emitted from all samples and it was identified as acetic acid in SS samples (Byliński et al., 2019; Fisher et al., 2017). Acetic acid was one of the main VOC contributors in composting gas emissions of SS and it could be associated with anoxic conditions and partial anaerobic organic matter degradation (Byliński et al., 2019). The emission of OVOCs is primarily caused by the breakdown of lipids and proteins during composting (Mackie et al., 1998). In addition, the decomposition by-products of easily degradable organic matter in waste were the potential sources of OVOCs (Scaglia et al., 2011). In the current study, the highest OVOC emission fluxes were found in SS 60%, collected at the last step of SS treatment. Our findings agreed with other studies, where the OVOCs dominated the emissions during waste maturation and from sludge obtained at the last steps of treatment (Davoli et al., 2003; Nie et al., 2019).

Three ions detected at *m/z* 95.05, 123.08 and 109.06 were assigned as $C_6H_6OH^+$, $C_8H_{10}OH^+$ and $C_7H_8OH^+$, respectively. Those compounds (C_6H_6O, $C_8H_{10}O$ and C_7H_8O) were emitted from UDSS. C_7H_8O was identified as 3-methylphenol (Harrison et al., 2006; Kotowska & Isidorov, 2012) or cresol (Mackie et al., 1998). C_6H_6O and $C_8H_{10}O$ were identified as phenol and 2-ethylphenol, respectively (Mackie et al., 1998). Cresol, phenol and 2-ethylphenol were known to be associated with urea and feces as a result of the metabolic degradation of aromatic amino acid tyrosine (Chen et al., 2004; Mackie et al., 1998). Thus, the three compounds were of identical biological origin. This could explain the exclusive emissions of C_6H_6O along with

C_7H_8O and $C_8H_{10}O$ from UDSS. Therefore, these compounds could be considered as emission tracers for UDSS.

3.4.4. Nitrogenated organic compounds

Thirty-six nitrogenated compounds were found in this study (**Figure 3.5, b**). Among them, only one compound was emitted from all samples ($C_9H_{11}N$, *m/z* 134.10) and 26 compounds were emitted only from UDSS. The maximum emission fluxes of N-compounds were observed in UDSS (4.77 ± 1.47 μg m^{-2} min^{-1}) and the other samples showed almost the same levels (**Table 3.2**). C_3H_9N (*m/z* 60.08) was emitted from all samples except UDSS. This compound showed the maximum emission flux in SS 60% at 0.398 ± 0.215 μg m^{-2} min^{-1}. C_3H_9N was identified in SS samples as trimethyl amine (TMA) by TD-GC-MS (Fisher et al., 2017; Kotowska & Isidorov, 2012). Rosenfeld et al., (2001) reported that TMA was produced from the biological degradation of proteins and emitted from land application of dewatered sludge. This is consistent with our results as TMA showed higher emissions from SS 60% compared to SS 30% and DSS. The presence of TMA in sludge subjected to dewatering might be due to the degradation of polymers used in this process as suggested by Fisher et al., (2017). In addition, animal excrements such as feces and urine released large amounts of TMA into the atmosphere (Sintermann et al., 2014).

Several N-compounds were tentatively identified as small amines such as C_2H_5N, C_2H_7N and C_3H_9N. Others were associated with one or more aromatic rings and belong to indoles, pyridine, quinolone, etc (e.g., C_7H_9N, $C_9H_{11}N$, C_5H_5N and $C_{13}H_{13}N$). The ions $C_2H_3NH^+$, $C_5H_5NH^+$ and $C_7H_5NH^+$ were assigned to acetonitrile, pyridine and benzonitrile, respectively (Byliński, et al., 2019; Fisher et al., 2017). Two volatile organic aromatic compounds assigned to the protonated form of $C_9H_9NH^+$ (*m/z* 132.08) and $C_8H_7NH^+$ (*m/z* 118.06) were emitted from all samples except DSS. The highest emission flux of these two compounds was in UDSS. C_8H_7N and C_9H_9N were identified as indole and skatole (3-mehyl indole), respectively (Ciuraru et al., 2021; Gebicki et al., 2016; Mackie et al., 1998; Ni et al., 2012). Indole and skatole were the major end-products of tryptophan metabolism (Mackie et al., 1998). They have been selected as major malodorous compounds that contributed to the strong odour nuisance in animal waste facilities and SS treatment plants (Gebicki et al., 2016; Ni et al., 2012).

3.4.5. Other gas phase emissions

Several compounds containing more than one heteroatom in their molecular formula were found in this work. Among these, significant concentrations of compounds containing both N and O atoms (N&O-compounds) were detected. The emission fluxes of N&O-compounds were the highest in DSS (11.54 ± 2.85 μg m^{-2} min^{-1}), followed by SS 60% (5.63 ± 0.68 μg m^{-2} min^{-1}), UDSS (5.60 ± 0.4 μg m^{-2} min^{-1}) and SS 30% (5.48 ± 0.59 μg m^{-2} min^{-1}). $C_6H_{11}NO$ (*m/z* 114.09) was identified as caprolactam, which is a cyclic amide of caproic acid (Kotowska & Isidorov, 2012). It was emitted from DSS only with a concentration of 3.71 ± 0.89 μg m^{-3}. $C_{12}H_{15}N_3O_6$ was emitted from all samples with emission flux < 0.5 μg m^{-2} min^{-1} and identified as a fragrance material (Harrison et al., 2006).

In addition to VOC measurements, the mixing ratio of SO_2 emitted from each sample was measured. The results showed that UDSS was characterized by the highest SO_2 emissions (4.5 ppb), which was almost double compared to DSS (2.6 ppb), SS 30% (2.6 ppb) and SS 60% (2.1 ppb). Moreover, in our study, NH_3 emissions were measured only for DSS. The average mixing ratio of NH_3 emitted from DSS was 3239 ppm. Lim et al., (2018) reported NH_3 as one of the main odour compounds.

3.4.6. Impact of treatment stage on VOC emissions

The impact of SS treatment at the level of the WWTP is illustrated in **Table 3.4**. Our results showed that the anaerobic digestion decreased the total number of emitted VOCs and the dewatering step had little impact. This impact was also observed on the number of emission tracers, where UDSS showed the maximum number (93) compared with the anaerobically digested and dewatered samples. Chen et al., (2014) studied the impact of the SS drying process on odour and VOC emissions. The authors illustrated that the total organic compounds in the sludge were significantly lower after drying. In this work, the total emission flux of VOCs increased with the increase in the dry matter content. For instance, DSS had the lowest dry matter content (2.3%) and showed the lowest emission flux of VOCs. However, after dewatering to reach 60% of dryness, the emission flux of VOCs was the highest. This was interrelated to the highest organic matter content in this sample (60.4%) (**Table 3.3**). The HC emission flux increased with the increase in the dry matter of the sample (**Table 3.2**).

Table 3.4 *The tendency of VOC variation based on the treatment step and dry matter content.*

	Number of VOCs	**Number of emission tracers**	**Total emission flux of VOCs**	**VOC chemical class**
Anaerobic digestion	↓	↓	-	↓ Aromatics, ↓ VOSC, - OVOC
Dewatering to 30% dryness	-	-	↑	↑ Aromatics, ↑ VOSC, - OVOC
Dewatering to 60% dryness	-	-	↑	↑ Aromatics, ↓ VOSC, ↑ OVOC
Dry matter content (↑)	↓	↓	↑	↑ Aromatics, ↓ VOSC, ↑ OVOC

(↓): decrease, (↑) increase, (-) no or little impact.

The emissions of aromatic HC were comparable between UDSS and dewatered sludge, while in DSS it was almost one-third lower. This indicated that anaerobic digestion reduced the aromatic compound emissions, while dewatering had a lower impact. This reduction could result from their biodegradation during the treatment process. Anaerobic digestion uses the process of fermentation to break down organic matter from SS in order to produce biogas. The anaerobic digestion leads finally to H_2, CH_4 and CO_2 as the desired products, while organic acids, NH_3, H_2S are intermediate products. It starts with hydrolysis, follows with acidogenesis and acetogenesis, and finishes with methanogenesis (Du & Parker, 2012). These processes might produce HC either by the reduction of CO_2 or by the reduction of organic acids. During hydrolysis the complex organic compounds are solubilized and converted into smaller size organic compounds (Di Capua et al., 2020). These processes break down the chemical compounds to produce HC.

Anaerobic digestion decreased the VOSC emissions by 96%. The reduction in VOSC emissions could be explained either by their loss during the anaerobic digestion treatment process or their degradation by bacterial action. The emissions of VOSCs from SS 30% increased by 92% then decreased (in SS 60%). Sulphur compounds might not totally be lost but incorporated in the sludge by bacterial action during anaerobic digestion.

The impact of dry matter was illustrated upon a comparison between dewatered samples. SS 30% showed higher emissions of VOSCs compared to SS 60%. Gomez-Rico et al., (2008) have reported that the temperature does not have a significant effect on the number

of identified compounds nor on the total yield of VOCs found. This is consistent with our results as both dewatered sludge showed comparable total number of emitted VOCs. Moreover, Gomez-Rico et al., (2008) reported the impact of the temperature on the yield of individual compounds such as sulphur compounds. The emission of sulphur compounds increased with the increase in the temperature during SS treatment (Mrowiec et al., 2005). This phenomenon has also been explained by Ding et al., (2015) who studied the effect of thermal drying temperature and processing time on VOC emissions from sludge. This study revealed that higher emissions of pollutants and VOSCs were observed at higher drying temperatures. In addition, the concentration of odours, total VOCs and amines changed with the drying temperature (Ding et al., 2015). A similar aspect was also reported by Deng et al., (2009) where the authors investigated the VOCs released during the sludge drying process under 140 – 170 ^{o}C. Consequently, the higher drying temperature leads to higher emissions of pollutants and odorants. This agrees with our results as SS 30% showed higher VOSC emissions than SS 60%. SS 30% might be subjected to lower drying temperature compared to SS 60%, which resulted in higher emissions of VOSCs from SS 60% during the dewatering step. Both samples emitted lower sulphur compounds with respect to UDSS. This indicated that a big part of soluble fractions of sulphur form was separated from the sludge during dewatering, thus dewatered sludge contained less sulphur than the raw sludge.

The high contribution of OVOCs in SS 60% could be explained by more heterogeneous oxidation reactions occurring at the sample surface. Thus, the composition of gas-phase emissions from dewatered sludge was affected by the sludge characteristics, moisture content, and drying conditions, such as temperature, time and drying process type. The thermal drying of SS could involve the release of VOCs that were contained in the sludge and evaporated due to thermal effect (Anderson et al., 2002; C. Gross, 1993; Gomez-Rico et al., 2008). Several studies investigated the gas-phase emissions during the thermal drying process (Anderson et al., 2002; Deng et al., 2009; Ding et al., 2015; Gomez-Rico et al., 2008), but to our knowledge, detailed quantitative and qualitative research on the VOC emissions from sludge subjected to dewatering treatment have not been investigated yet. Such characteristics may be important for agricultural purposes. The four types of analyzed SS can be applied in agricultural field, however the way and amounts of applied sludge depends on the soil, crop, local conditions and government regulations.

3.5. Conclusions and environmental implications

This study gives comprehensive qualitative and quantitative information on VOCs emitted by SS. We showed that SS samples emitted a large spectrum of VOCs. In this work, 380 compounds were detected and quantified, with 81 compounds commonly found in all samples. The assigned VOCs were classified into the following chemical groups: hydrocarbons, oxygenated, sulphuric, nitrogenated and "other" compounds (containing distinct heteroatoms in the molecular formula). Different sub-classes of HC were identified using the DBE method, which is applied for the first time on PTR mass spectra. Some aliphatic and alicyclic compounds, many aromatic HC and terpenes were found. From the DBE analysis, the efficiency of this method to simplify the analysis of a complex mixture through classification was illustrated. HC showed maximum emissions among all VOCs in all samples. OVOCs were dominant in SS 60% while VOSC showed elevated emissions from UDSS.

The total VOC emissions increased with the increase in the dry matter and organic matter contents of SS samples. Several sulphur compounds found in our samples (e.g., DMS, DMDS, methanethiol, etc) can participate in the (photo)chemical reactions in the atmosphere (Shon et al., 2005). The emissions of sulphur compounds were reduced after the anaerobic digestion and dewatering to higher degrees of dryness (60%). The results showed that anaerobic digestion and dewatering had positive impacts in decreasing the potential emissions of VOSC and aromatic compounds that can serve as SOA precursors and affect the atmospheric chemistry. For example, terpenes such as limonene were found in this work. Limonene, which has a high level of chemical reactivity (Ni et al., 2015; Nie et al., 2019), contributes to the atmospheric reactivity of VOCs and contributes to ozone and aerosol formation in atmosphere (Ni et al., 2015; Nie et al., 2019). Moreover, amines (TMA), indoles and skatole can be important species for atmospheric chemistry, as they can lead to secondary organic aerosol formation (Ciuraru et al., 2021; Yao et al., 2018; Yu et al., 2012). Recently, skatole emitted from UDSS at emission flux of 50 $\mu g\ m^{-2}\ min^{-1}$ was demonstrated as a key gas-phase precursor for SOA formation in the presence of ozone and SO_2 (Ciuraru et al., 2021). Accordingly, the significant emissions of skatole from UDSS can contribute to particle formation in the presence of photo-oxidants (such as ozone) as this sample also emitted significant amount of SO_2 compared to the other three samples.

Laboratory measurements using atmospheric simulation chambers can provide information to support field measurements and recommendations for VOC abatement in WWTPs. The results of this work provide an accurate inventory reference for the VOC

emissions from SS samples. The comparability of SS emissions at different treatment stages helps identify the impact of sludge treatment at WWTPs on VOC emissions. The environmental risk of land-applied sludge might be reduced upon treatment due to the decrease of individual VOC emissions.

Chapter 4

Online and offline chemical characterization of volatile organic compounds emitted by animal manure

4.1. Introduction

Manure is an organic matter that is used as organic fertilizer and soil conditioner in agriculture (Tester, 1990). High attention has been raised on the odorous gases produced from animal manure due to the increasing number in animal husbandries (Woodbury et al., 2014). Common forms of animal manure include farmyard manure (FYM) or farm slurry (liquid manure). Agricultural manure in liquid form, known as slurry, is produced by more intensive livestock rearing systems where concrete or slats are used, instead of straw bedding (Liu et al., 2018).

Land application of animal manure is a source of very complex mixtures of pollutants such as dust, bacteria, mold, endotoxins, GHG, NH_3 and PM that can affect air quality on local and regional scales (Woodbury et al., 2014). Methane (CH_4) and nitrogen oxides (NO_x) are the major products resulting from manure degradation, while methane contributes to the accumulation of GHG in troposphere (Mackie et al., 1998). Livestock is also a strong emitter of carbon dioxide (CO_2) (Hempel et al., 2016) and NH_3 (Schmithausen et al., 2018; Yao et al., 2018). Zhang et al., (2017) suggested that manure nitrogen production at a global scale is expected to increase due to the growing demand of livestock population with a high impact on GHG balance in terrestrial ecosystems. In Europe, agriculture contributes to more than 90% of total nitrogen emissions, with animal manure constituting the main source of NH_3 (EEA, 2008). NH_3 from agricultural activities has become a public concern as it impacts health and can cause acidity of the natural environment and formation of atmospheric aerosols (Atkinson, 2000; Kammer et al., 2020; Mackie et al., 1998). Animals consume considerable amounts of protein and other nitrogenated compounds with their feed. A portion of this protein is deposited into the body or secreted in milk, meat or eggs. However, the conversion of feed to animal product is often inefficient, with 50 - 80% of the nitrogen being excreted in animal feces and urine (Mackie et al., 1998). Nitrogen excreted in feces originated from feed and endogenous sources. The nitrogen excreted from undigested feed or endogenous sources is mainly in the form of protein (amino acids). The fecal nitrogen is 50% organic nitrogen and 50% NH_3. After excretion, nitrogenated compounds in the mixture of feces and urine undergo degradation by bacterial effect (Mackie et al., 1998).

Beside the valuable use of manure as fertilizer, in the last decades, animal manure has been considered as a pollutant and a nuisance as a result of intensive animal production and the diversity in the composition of manure (Williams, 1995). Environmental pollution from animal manure has become a global concern and is much serious in countries having a high number of animals with a limited land base for manure disposal. Land application of excessive quantities of nutrients affects negatively on air and water contaminations. For instance, N leaching is a major N pollution concern on livestock farms and P entering surface waters from land application of animal manure can stimulate the growth of algae and aquatic plants (Mackie et al., 1998).

In Europe, agriculture contributes to more than 90% of total nitrogen emissions, with animal manure constituting the main source of ammonia (European Environment Agency (EEA), 2008). NH_3 from agricultural activities has become a public concern as it impacts health and can cause acidity of the natural environment and formation of atmospheric aerosols (Atkinson, 2000; Kammer et al., 2020; Mackie et al., 1998). In addition to ammonia, application of manure is a source of odor nuisance and several techniques, such as direct slurry injection into the soil have been introduced to reduce the odorant emissions (Feilberg et al., 2010). When manure undergoing degradation has a surface exposed to atmosphere, volatile products and intermediates are emitted into the environment (Mackie et al., 1998). The odors generated from manure and its decomposition during collection, handling, and storage and spreading are considered offensive. Under moisture and temperature conditions, manure is subjected to anaerobic digestion and results in the generation of odorous volatile compounds (Mackie et al., 1998). Anaerobic digestion of animal manure before its use as a fertilizer has positive impact, as the obtained digestate has higher proportions of mineralized plant-available nutrients than untreated manure. Moreover, digestion results in a significant odor reduction as reviewed by Insam et al., (2015).

The odorant emissions consist of a complex mixture of VOCs and hydrogen sulphide (H_2S), which adversely affect air quality and health risks (Ciganek & Neca, 2008; Feilberg et al., 2010; Woodbury et al., 2014). Mackie et al., (1998) has reported that the incomplete anaerobic fermentation of waste by bacteria is the main source of odorant VOC emissions. The emitted VOCs belong to six major chemical groups: VFA, volatile amines, indoles, phenols and sulphur compounds (Feilberg et al., 2010, 2011; Mackie et al., 1998; Woodbury et al., 2014, 2022). Increasing and significant progress has been made in recent years in research of

VOC emissions from livestock production. Several technologies were developed and applied for more efficient VOC sampling and measurements.

To achieve a complete screening of VOCs, it is recommended to conduct studies combining both on-line (PTR-MS) and off-line (GC-MS) techniques (Ni et al., 2012). VOCs emissions from intensive pig production have been investigated using the combination of on-line and off-line techniques, but the range of detected compounds was limited due to the use of a quadrupole PTR-MS (Feilberg et al., 2010). A complete VOC identification list was proposed in few studies (Ciganek & Neca, 2008; Schiffman et al., 2001; Yuan et al., 2017) and there are also a limited number of investigations on the VOC emission factors and fluxes from farm buildings and animal manure samples under laboratory conditions. Most of the reported studies to date have dealt with pig, dairy or poultry farming, but little is known about other livestock. Ni et al., (2012) reviewed 100 studies of VOC emissions at swine facilities and there are three studies dealing with VOC emissions from sheep farming (Kammer et al., 2020; Ngwabie et al., 2007; Yuan et al., 2017). In a recent field measurement campaign, more than 400 VOCs were characterized using the online and offline mass spectrometric techniques (Kammer et al., 2020). The results showed that the diary stable emitted more VOCs than the sheep pen, with a maximum emission of oxygenated compounds and hydrocarbons. The authors identified emission tracers for each pen and highlighted the sources of VOC emissions by correlation analysis. This was the first study that evaluated the emission rates for most of the identified VOCs, and the authors suggested more studies in different periods and farms about emissions (Kammer et al., 2020). Beside the full scale field trials, emissions can be studied at laboratory scale using small model systems with an artificial air exchange that can be designed to simulate ambient conditions as far as possible (Dorno et al., 2013). This is useful for investigating emission fluxes under controlled laboratory conditions and obtaining qualitative and quantitative data for gaseous emissions from animal manure. This detailed chemical analysis is necessary to assess suitable odor abatement technologies and to study the atmospheric reactivity of the VOCs. This can be developed from more knowledge regarding the chemical characterisation of VOCs emitted from manure and their reactivity with photo-oxidants (e.g., OH radicals and O_3).

In this context, an experimental study was performed on different types of animal manure samples (cow, horse, sheep and goat) in order to assess an inventory of VOCs produced by these animal manures. The aim of our laboratory study was to thoroughly investigate, identify and quantify the VOCs emitted by the samples. The chemical composition of VOCs

using atmospheric simulation chambers under controlled laboratory conditions combined to on-line (Proton Transfer Reaction-Quadrupole ion guide-Time of Flight Mass Spectrometry, PTR-QiTOF-MS) and off-line (Thermal Desorption-Gas Chromatography-Mass Spectrometry, TD-GC-MS) measurements were explored.

4.2. Materials and Methods

Four animal manure samples (horse, cow, sheep and goat manures) shown in **Figure 2.2** collected from a farm located in Grignon, France were analyzed. The samples were stored at 4 ^{0}C before the experiments. The samples were analyzed using the two chambers described in Section 2.2: 0.03 m^3 and 0.18 m^3. Three replicates were performed for each sample. Two experiments were in the 0.18 m^3 chamber with 1 kg of the sample spread uniformly on 0.32 m^2 surface area. The third experiment was performed in the 0.03 m^3 chamber with 500 g of sample spread on 0.14 m^2 surface area. The thickness of the spread sample was 3-4 mm. The experiments were performed using the same protocol described in Section 2.2. The emitted VOCs were analyzed online by PTR-QiTOF-MS and were also trapped on Tenax TA cartridges (at 0.5 L min^{-1} for 60 – 90 minutes) for offline TD-GC-MS analysis. The principles of operation of these mass spectrometric techniques were described in Section 2.3. In parallel to these experiments, we regularly performed blank tests without sample and blank cartridges were analyzed using TD-GC-MS to check the impurities. The amounts of SO_2 (model 43C, Thermo Environmental Instruments) and NH_3 (Picarro G2103) emitted by the sample and the relative humidity (RH) were monitored. The principle of operation of each instrument is described in Section 2.2.

In this work, the PTR-QiTOF-MS was operated under standard drift tube conditions (4 mbar and 80 ^{0}C) using a drift voltage of 1000 V, which gives an E/N number of 132 Td. Raw PTR-QiTOF-MS data were processed using the methodology described in Section 2.5. From each experiment, a mass spectrum (average of 120 mass spectra) was extracted from the region where the signal was stable (e.g., **Figure 2.15**). The same procedure was applied for the three replicates. The S/N > 3.0 peak list was constructed using the mMass software (Strohalm et al., 2010). The mass range chosen for analysis was between *m/z* 31 and 400. Signals identified as instrumental background or related to water clusters such as *m/z* 37.03, *m/z* 38.03, *m/z* 39.03 and *m/z* 55.03 were excluded from the data analysis. The PTR viewer 3.2.12 software (Ionicon analytik GmbH) was used to identify the chemical molecular formula corresponding to each protonated molecular ion in the peak lists following the procedure described in Section 2.5.2.

Following this step, the averaged mass spectra were used to calculate the average mass concentration and emission flux of the emitted compounds (details in Section 2.5.3).

The PTR-QiTOF mass spectra were compared using principal component analysis. Statistical analysis of the emitted VOCs were performed to identify the chemical compounds that characterize the differences between the samples and mark the chemical compounds for each manure type. In this work, PCA was performed with a matrix containing the integrated peak areas (variables) against the mass spectra (observations) using Python. For more details on statistical analysis, see Section 2.5.4.

4.3. Results

4.3.1. Detection of VOCs by PTR-QiTOF-MS

A dataset consisting of gas-phase emissions as a function of time was obtained for each type of manure by PTR-QiTOF-MS. An example of PTR-QiTOF mass spectrum for each sample is illustrated in **Figure 4.1**. The *x-axis* is the detected protonated *m/z* and the *y-axis* represents the signal in counts per second (cps). The mass range shown is from *m/z* 40 to 250, since most of the assigned VOCs belong to this region.

Following the procedure described in Section 2.5.2, the vast majority of the detected peaks (> 90%) were assigned to a suitable molecular formula and only a few were unassigned (**Table 4.1**). For instance, the peak list corresponding to cow manure included 255 mass peaks. Among those, 233 mass peaks were assigned based on the criteria described in Section 2.5.2. The assigned peaks corresponded to either a VOC (224 VOCs) or its ^{13}C isotopic peak (9 peaks). For cow manure, only 22 mass peaks were unassigned to a molecular formula and designated as unknown compounds. The average mass uncertainty of all assignments among the four samples was less than 30 ppm. The total number of assigned VOCs in cow, horse, goat and sheep manures were **224**, **233**, **254** and **257**, respectively. Only the assigned VOCs were considered for further data analysis, which includes chemical classification, quantification and statistical analysis.

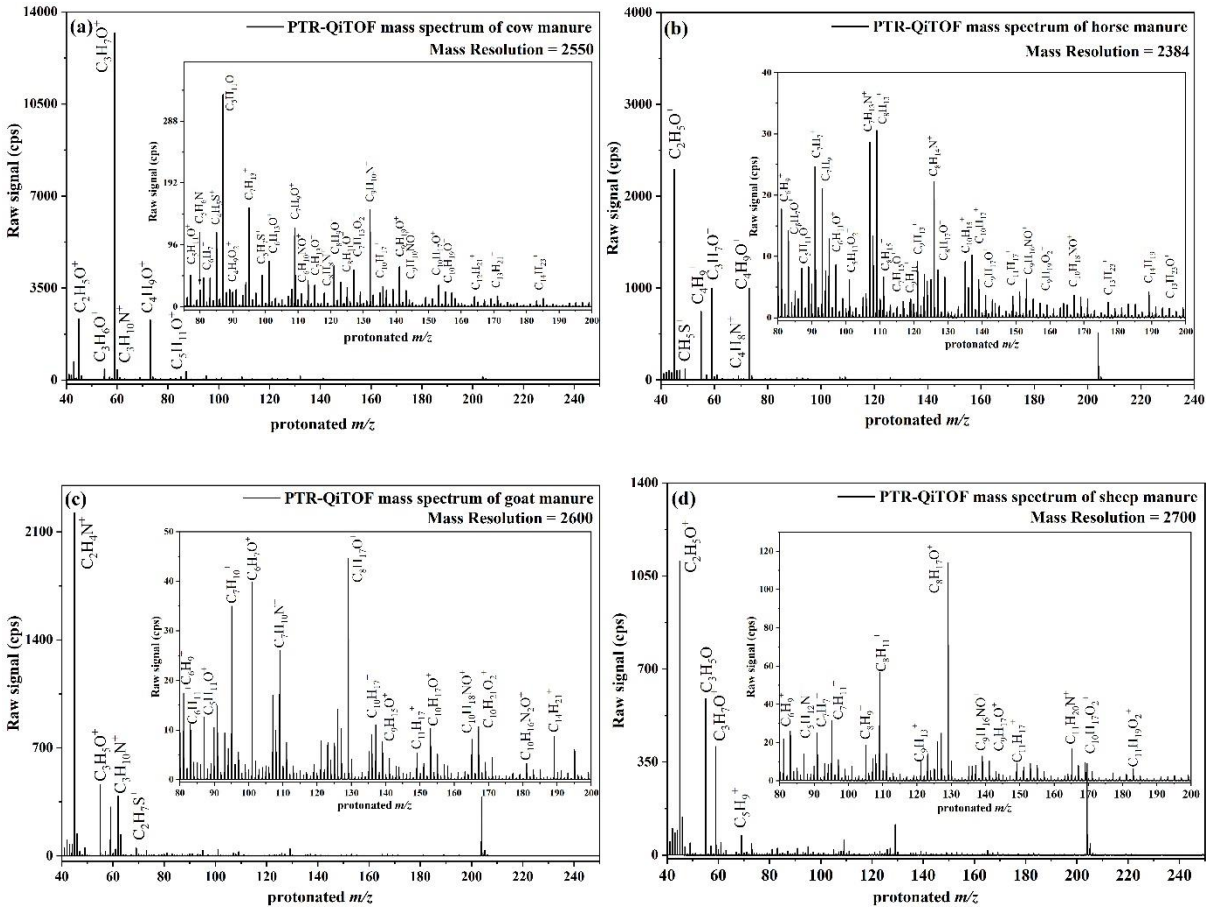

Figure 4.1 *PTR-QiTOF average mass spectrum for (a) cow, (b) horse, (c) goat and (d) sheep manures. The m/z [40-250] range is shown. A zoomed in portion for mass range m/z 80-200 is illustrated for each spectrum for better representation. All the assigned molecular formulas are protonated VOCH$^+$. The average mass resolution for each spectrum is shown.*

Table 4.1 *PTR-QiTOF-MS results for animal manure samples analysis. The numbers in bold correspond to the total number of assigned VOCs in each sample.*

Manure type	# of detected peaks	# of assigned peaks	# of unassigned peaks	# of peaks corresponding to VOCs	# of peaks corresponding to ^{13}C isotope	Average mass uncertainty (ppm)
Cow	255	233	22	**224**	9	~ 29
Horse	243	235	8	**233**	2	~ 13
Goat	274	258	16	**254**	4	~ 16
Sheep	276	262	14	**257**	5	~ 17

The bar graph illustrated in **Figure 4.2** shows the total number of VOCs detected and quantified using PTR-QiTOF-MS as well as the number of compounds exclusively emitted by every

manure sample. In this work, **385** compounds were detected and quantified in all samples using PTR-QiTOF-MS, with **115** compounds commonly found in all samples. The list of assigned 385 VOCs detected in all samples is given in Annex 4, **Table A.5**. Among all samples, sheep manure showed the highest number of VOCs (257 VOCs) with 25 compounds specific for this sample. Comparable emissions with sheep manure were observed from goat manure, with 254 VOCs and 21 specific compounds. Cow manure emitted 224 compounds and showed the highest number of emission tracers (57 VOCs, **Figure 4.2**). 22 VOCs were specific for horse manure emissions among the 233 assigned VOCs. Compounds that were exclusively emitted by one sample could be interpreted as its emission tracers and are listed in **Table A.5**.

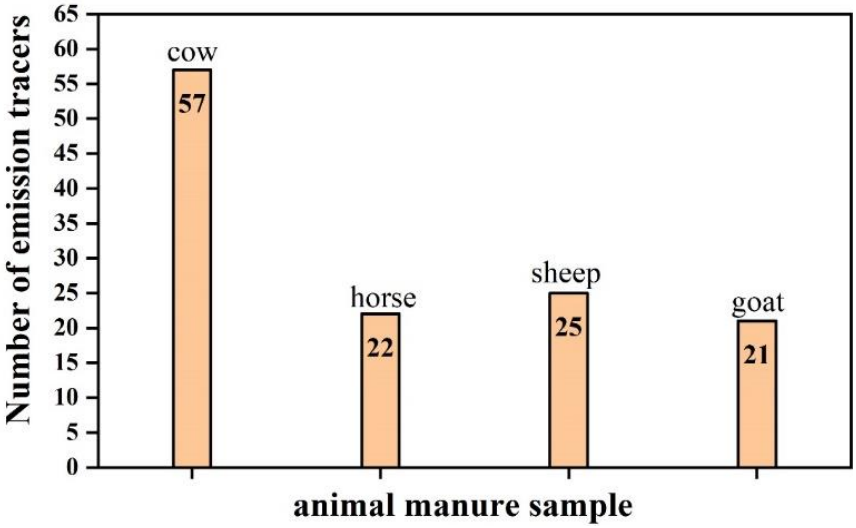

Figure 4.2 *Bar graph showing the number of emission tracers for each sample detected and quantified using PTR-QiTOF-MS. The exact number with the sample name are displayed.*

The assigned VOCs detected by PTR-QiTOF-MS were classified based on their corresponding chemical group: hydrocarbons (*HC*), oxygenated compounds (*O-compounds*), nitrogenated compounds (*N-compounds*), sulphur compounds (*S-compounds*), *halogenated compounds* (including at least one halogen atom) and *others* (containing distinct heteroatoms in their molecular formula). The number of compounds assigned to each chemical group is illustrated in **Figure 4.3**. The distribution of the chemical families of VOCs varied among the analyzed samples. Among all assigned VOCs, oxygenated compounds (or OVOCs) were the dominant in all samples. The maximum number of emitted OVOCs was in sheep manure (90), followed by goat, horse and cow manures, respectively. The number of assigned HC was almost the same in all samples. The highest number of N-compounds was in goat manure. Cow

manure showed the maximum number of S-compounds. A few number of halogenated compounds was also found (< 1% of the assigned molecular formula).

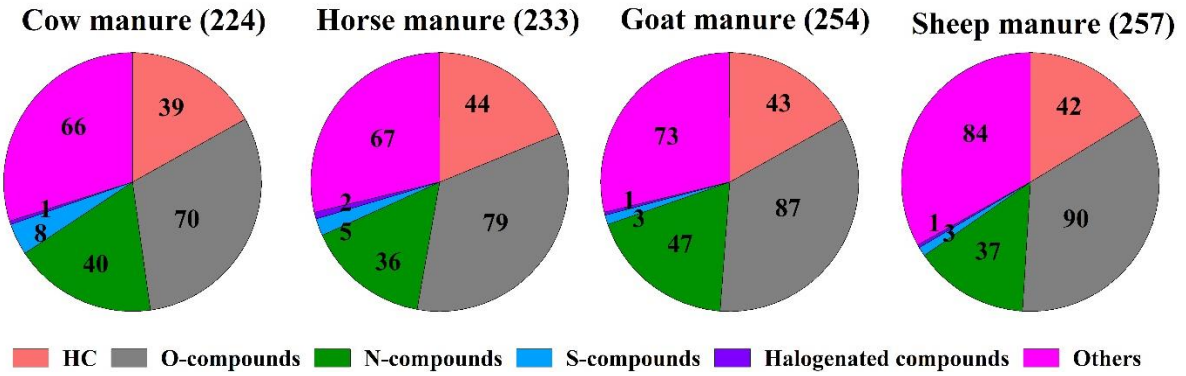

Figure 4.3 *The number of compounds assigned for each chemical group in each sample using PTR-QiTOF-MS. The total number of assigned VOCs is given in parentheses.*

4.3.2. Identification of VOCs by TD-GC-MS

The assignments of detected ions by PTR-QiTOF-MS were based on TD-GC-MS measurements performed for each sample and on the existing knowledge on emissions from manure samples and livestock production from the literature. An example of gas chromatogram obtained from TD-GC-MS analysis of the four manure samples is illustrated in **Figure 4.4**. In this work, we used Tenax tubes for VOC trapping and all the detected compounds were in the *m/z* range 40-500 except the two masses below *m/z* 40, represented by *m/z* 30 and 34 for formaldehyde and hydrogen sulphide, respectively.

The TD-GC-MS results are given in **Table 4.2**. Using offline measurements, the VOCs were identified based on their physico-chemical properties (e.g., boiling point), thus the number of identified compounds was usually higher than the number of detected masses. Accordingly, for each detected mass we could have different structural formula known as isomers, i.e. compounds having the same molecular formula but different structural formula. For instance, in sheep manure, 224 masses were detected which corresponded to 304 chemical compounds. One example could be given for a mass 156.1514u with molecular formula $C_{10}H_{20}O$ corresponding to 3 isomers (2-decanone, 3-decanone, decanal). The total number of identified compounds in cow, horse, goat and sheep manures were 307, 290, 300 and 304, respectively.

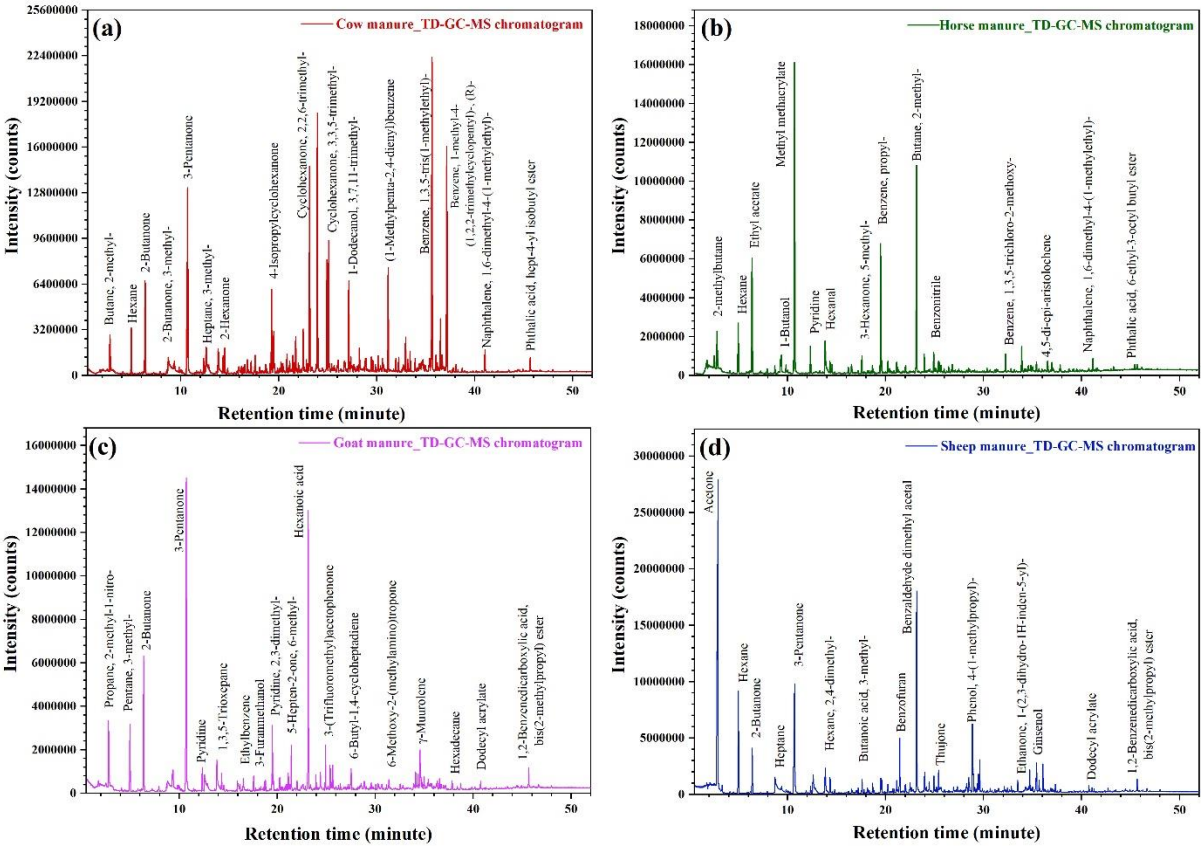

Figure 4.4 *Gas chromatogram obtained from offline TD-GC-MS for (a) cow, (b) horse, (c) goat, and (d) sheep manures. The x-axis represents the retention time (minutes) and the y-axis represents the intensity (counts). Some chemical compounds identified based on their retention time are displayed.*

Table 4.2 *The number of detected masses and identified compounds by TD-GC-MS analysis of animal manure samples.*

Manure type	# of detected masses	# of identified compounds
Cow	214	307
Horse	212	290
Goat	200	300
Sheep	224	304

Compounds identified in each sample using TD-GC-MS were classified based on their chemical group, **Figure 4.5**. Similar chemical groups of compounds obtained for the assigned VOCs by the PTR-QiTOF-MS technique were found using TD-GC-MS analysis. The distributions of the chemical families of identified compounds were roughly similar in the horse and sheep manures, and slightly different from the other two samples. OVOCs dominated the

identified compounds in all samples. Those OVOCs were identified as alcohol, ketone, aldehyde, carboxylic acid, ester, etc. Comparable number of identified HC was found in horse, goat and sheep manures and it was higher than that identified in cow manure.

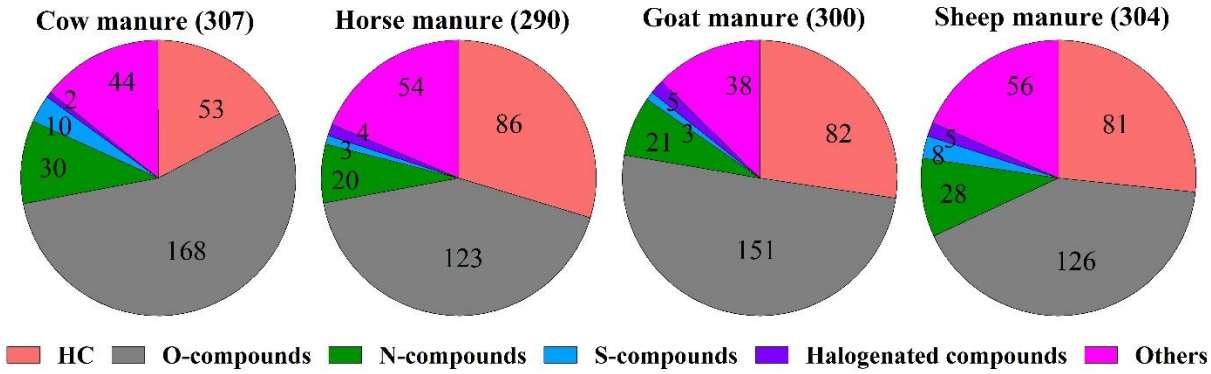

Figure 4.5 *The distribution of compounds identified by TD-GC-MS among the chemical groups. The total number of identified compounds is given in parentheses.*

4.3.3. Comparison between measurement techniques

The combination between the PTR-QiTOF-MS and TD-GC-MS techniques helped for supplementary screening of VOC emitted from manure samples. The number of detected masses in both techniques (**Table 4.3**) underlined the consistency of the identification process considering that these measurement techniques are independent. For instance, using PTR-QiTOF-MS, 224 molecular formulas were successfully attributed in cow manure. 70 molecular formulas among 224 detected by PTR-QiTOF-MS were also identified using off-line TD-GC-MS. Note that according to TD-GC-MS, some molecular formulas identified with the PTR-QiTOF-MS corresponded to several compounds. For instance, the ion corresponding to *m/z* 127.112 was assigned to emission of $C_8H_{14}O$ using PTR-QiTOF-MS. By TD-GC-MS analysis, 4 isomers were identified for this formula (6-methyl-5-hepten-2-one, 2,2,5-trimethyl-cyclopentanone, 2-methyl-cycloheptanone and 3-methyl-3-hepten-2-one,). Thus, there were certainly more compounds than the number of molecular formulas assigned with the PTR-QiTOF-MS.

Table 4.3 *Comparison between PTR-QiTOF-MS and TD-GC-MS techniques. The numbers of masses and identified compounds by each technique are shown. The number of common masses detected by both techniques is displayed.*

Manure type	**PTR-QiTOF-MS**		**TD-GC-MS**		**PTR-QiTOF-MS & TD-GC-MS**
	# of detected masses	# of assigned VOCs	# of detected masses	# of identified compounds	# of masses detected by both techniques
Cow	255	224	214	307	70
Horse	243	233	212	290	64
Goat	274	254	200	300	65
Sheep	276	257	224	304	66

4.3.4. Comparison between samples

The gas phase emissions from all samples measured by PTR-QiTOF-MS were compared using PCA in order to classify the samples and uncover the similarities and differences between them. Once the chemical formulas have been assigned and identified based on TD-GC-MS results, the contribution of each compound, or group of highly correlated species, could be determined with PCA. The majority of the variance within the data set is explained by only a few principal components (PC) (compared to hundreds of initial variables), in this case the first two PCs accounted for ~ 89% of the variance and were enough to discriminate between the four manure types. Thus, the number of dimensions of the original data was reduced to two. The score plot that represents the first PC (PC1) and second PC (PC2) is illustrated in **Figure 4.6**.

PC1 contributed to ~ 82% of the total dataset variability, thus it was able, on its own, to separate all the samples. From the score plot, cow manure was isolated from other manures and separated by PC1. However, PC2 separated horse and sheep manures from goat manure. The contribution of mass peaks to each PC was represented by their loadings. Therefore, the meaning of each component could be inferred from its corresponding loadings plot shown in **Figure 4.7** (PC1 – blue line, PC2 – brown line).

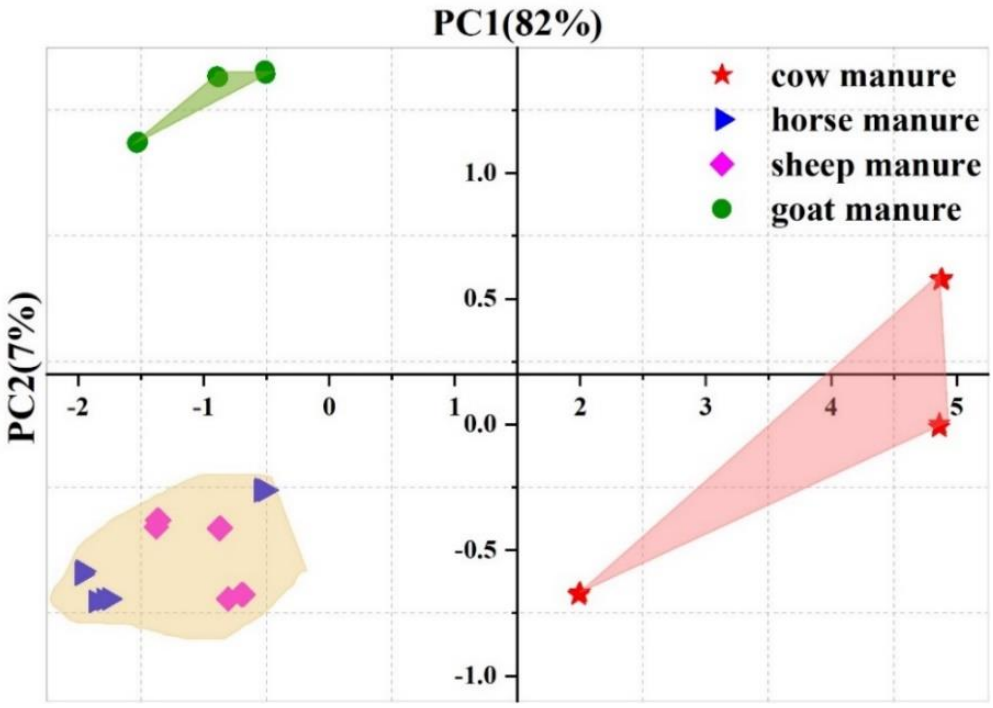

Figure 4.6 *Score plot of PC2 vs. PC1 for animal manure samples. The percentage contribution of each PC to the total variance is given in parenthesis. The points of the same colour correspond to data recorded for the same sample.*

The positive value of PC1 (**Figure 4.7, a**) was associated primarily with the contribution of oxygenated compounds "C_xH_yO" (e.g., alcohols, phenols, ketones, aldehydes) and nitrogenated compounds "C_xH_yN" (e.g., trimethyl amine "C_3H_9N" and 3-methylindole - skatole "C_9H_9N"). PC1 received a high negative contribution from two sulphur compounds (methanethiol "CH_4S" and dimethyl sulphide "C_2H_6S"). PC2 accounted only for 7% of the variance and it received very small contribution of oxygenated and nitrogenated compounds. The positive value of PC2 (**Figure 4.7, b**) was determined by the contribution of nitrogen- and oxygen-containing compounds of molecular formula "$C_nH_mO_pN_o$" and sulphur compounds "$C_xH_yS_z$". The negative value of PC2 was dominated by oxygenated and nitrogenated compounds which showed high contribution to positive value of PC2.

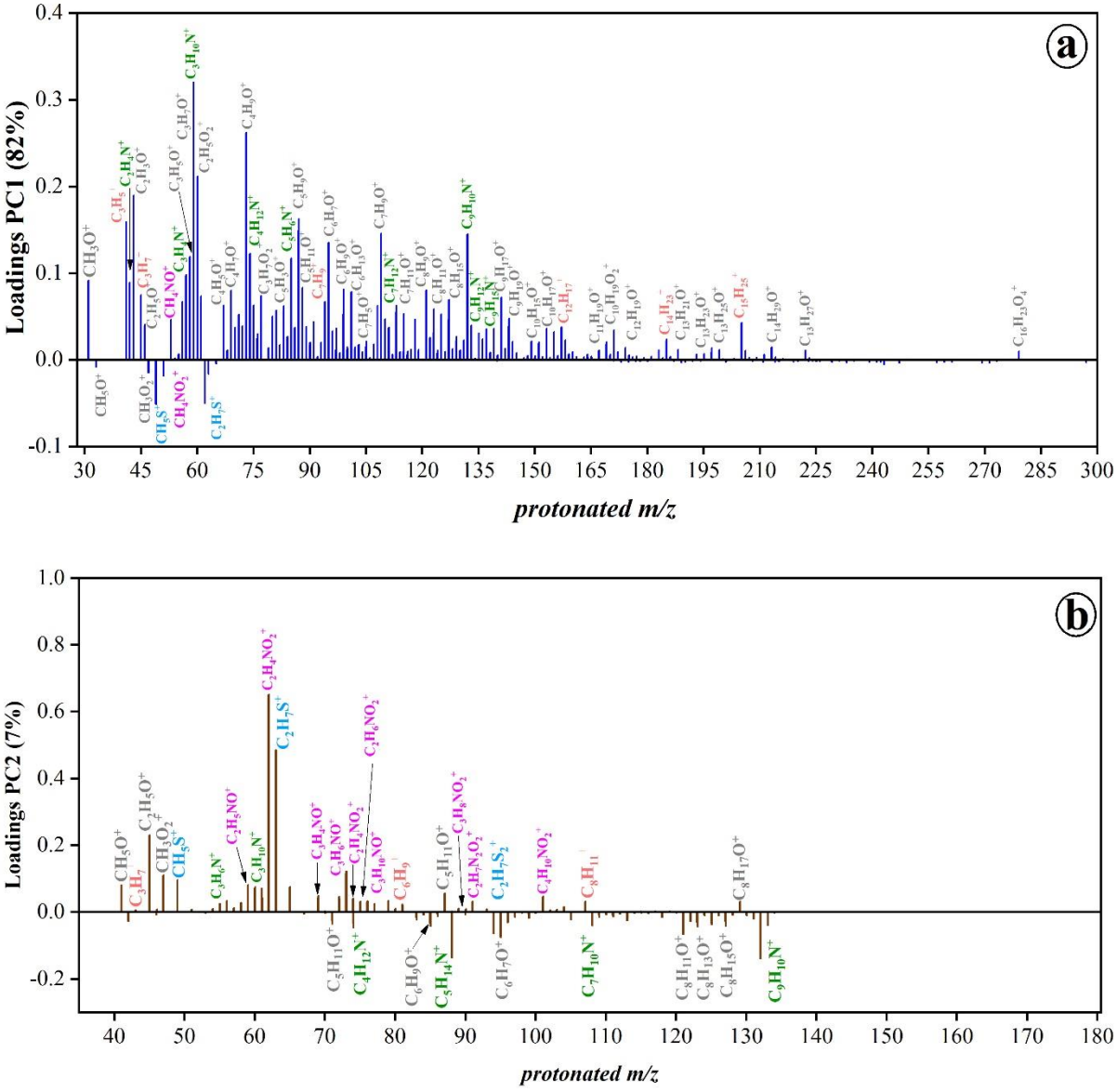

Figure 4.7 *Loading plots for the (a) PC1 and (b) PC2 obtained from the PTR mass spectra of animal manure samples. Chemical compounds contributing to positive and negative values of each PC are shown. The protonated molecules ($VOCH^+$) contributing to positive and negative values of each PC are shown. Hydrocarbons (light red), oxygenated compounds (dark grey), nitrogenated compounds (green), sulphur compounds (blue) and nitrogen- and oxygen-containing compounds (pink) are displayed.*

4.3.5. VOC emission characteristics

The mass concentration of the assigned VOCs was estimated based on their mixing ratio obtained from PTR-QiTOF-MS and considering the molecular weight of the compound. The total mass concentration of each chemical group was calculated by summing the concentrations of the individual compounds in each chemical group. The chemical groups contributed to a

different extent to the total concentration of VOCs (**Figure 4.8**). The maximum concentrated chemical group in all samples corresponded to OVOCs. The second most abundant group in all samples corresponded to compounds that include distinct heteroatoms in their molecular formula (other compounds). Comparable concentrations of HC and N-compounds were observed in each sample.

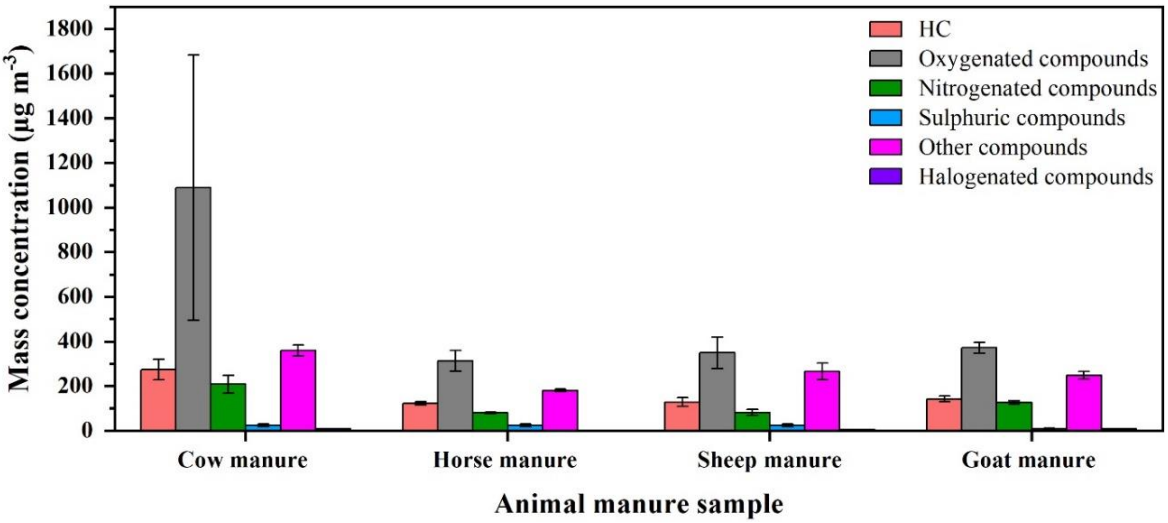

Figure 4.8 *Mass concentration of each chemical group of compounds in each sample. The error bars shown in the figure represent the standard deviation of the average mass concentration obtained from the three replicates of each sample.*

The total emission flux of all assigned VOCs was calculated. The highest VOC emission fluxes were observed for the cow manure with 66 ± 26 µg m^{-2} min^{-1}, followed by goat, sheep and horse manures with 32 ± 5, 31 ± 11, and 25 ± 5 µg m^{-2} min^{-1}, respectively. **Table 4.4** shows the total emission flux of each chemical group. Cow manure showed higher emission fluxes of VOCs compared with other samples; specifically, OVOCs and HC showed maximum emissions from cow manure (36 ± 19 µg m^{-2} min^{-1} and 10 ± 2 µg m^{-2} min^{-1}, respectively), and their emissions from the other samples were comparable. The emission flux of N-compounds was as follows: cow > goat > horse or sheep manures. The compounds designated as *others* were highly emitted from cow manure (12.59 ± 2.18 µg m^{-2} min^{-1}), compared to the other samples. Little emissions of sulphur and halogenated compounds were observed from all samples.

Table 4.4 *Total emission flux of each chemical group found in manure samples. The standard deviation of the average emission flux obtained from the three replicates of each sample is displayed.*

Manure type	**Total emission flux of each chemical group (μg m^{-2} min^{-1})**					
	HC	O-compounds	N-compounds	S-compounds	Other compounds	Halogenated compounds
Cow	10 ± 2	36 ± 19	7.21 ± 1.84	0.86 ± 0.12	12.59 ± 2.18	0.28 ± 0.05
Horse	4.29 ± 0.21	11 ± 3	2.80 ± 0.47	0.86 ± 0.12	6.30 ± 1.09	0.34 ± 0.05
Sheep	4.62 ± 1.63	12 ± 5	2.93 ± 1.06	0.86 ± 0.12	9.51 ± 3.21	0.21 ± 0.07
Goat	4.92 ± 0.66	13 ± 2	4.41 ± 0.63	0.33 ± 0.14	8.64 ± 1.36	0.28 ± 0.05

The assigned OVOCs were further sub-classified by the number of oxygen atoms in the molecular formula. Around half of the assigned OVOCs in horse, sheep and goat manures contained one oxygen atom with molecular formula C_xH_yO; however, they constituted 77% in the cow manure. The percentage contribution of each OVOC class was calculated and is displayed in **Figure 4.9**.

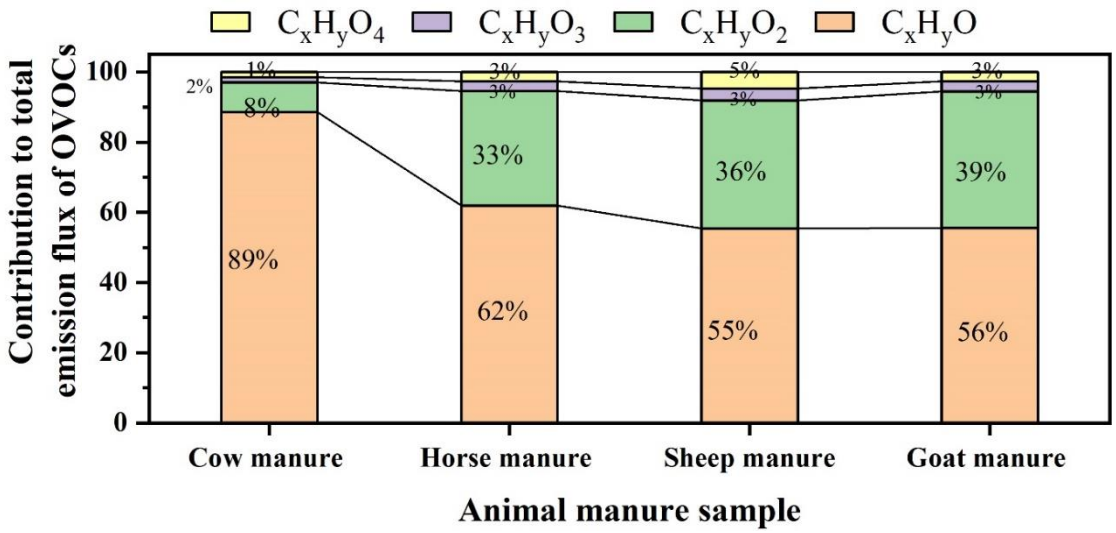

Figure 4.9 *Contribution of each OVOC sub-class to total OVOC emission flux from each sample. The legend shows the colour used for each subclass represented by a general molecular formula.*

Cow manure showed different distribution of OVOCs by their number of oxygen atoms compared to the other three samples. Compounds containing one oxygen atom with molecular

formula C_xH_yO showed maximum emission flux from cow manure, while its contribution to OVOCs in the other three samples was comparable. Compounds with two oxygen atoms with molecular formula $C_xH_yO_2$ showed similar contribution to OVOC emission fluxes in horse, sheep and goat manures. Very low contribution from compounds containing more than two oxygen atoms were observed in samples.

4.4. Discussion

The gas phase was analyzed using PTR-QiTOF-MS and TD-GC-MS. The TD-GC-MS data was mainly used for the assignment of *m/z* values detected in PTR-QiTOF-MS to specific compounds and to provide additional chemical identification of the VOCs. The detected VOCs were classified into six chemical groups (1) HC, (2) Oxygenated, (3) Nitrogenated, (4) Sulphur (5) Halogenated and (6) Other compounds. Beside VOCs analysis, other gas phase measurements, for instance SO_2, H_2O and NH_3 emissions, were also performed for each sample (**Table 4.5**). In the following Sections, the results are discussed based on the chemical family of VOCs with more focus on some compounds that are considered characteristic emissions from manure and important for atmospheric chemistry. The results under discussion were compared with the literature.

Table 4.5 *Average RH, NH_3 and SO_2 emission concentrations for each manure sample.*

Manure type	RH (%)	NH_3 (ppb)	SO_2 (ppb)
Cow	2.02	7093	3.84
Horse	1.75	6352	1.02
Sheep	1.59	18278	1.28
Goat	1.59	10225	9.45

4.4.1. Hydrocarbons

A total of 88 HC have been detected using online and/or offline methods in animal manure samples. Among the 88 HC, 27 compounds were detected using PTR-QiTOF-MS, 34 compounds were identified by TD-GC-MS and 27 compounds were detected using both techniques. The DBE analysis described in Section 2.5.5 was performed on the 88 HC found in this work. For each HC, the DBE value was calculated and the plot DBE versus the number of carbon atoms is illustrated in **Figure 4.10**. The obtained DBE values ranged from 0 to 10. HC with DBE = 0 are identified using TD-GC-MS as linear alkanes. Examples such as 3-methyl hexane (C_7H_{16}), 3-methyl pentane (C_6H_{14}), 6-methyl tridecane ($C_{14}H_{30}$), hexadecane ($C_{16}H_{34}$), pentadecane ($C_{15}H_{32}$), etc. were detected using TD-GC-MS analysis. Those

compounds which were not detected using PTR-QiTOF-MS as linear alkanes (with high masses) have lower PA than water. This explained their detection only using TD-GC-MS which is based on the physical properties of a compound (i.e. boiling point) and not their PAs, which is the main condition for the proton transfer reaction to occur in the drift tube.

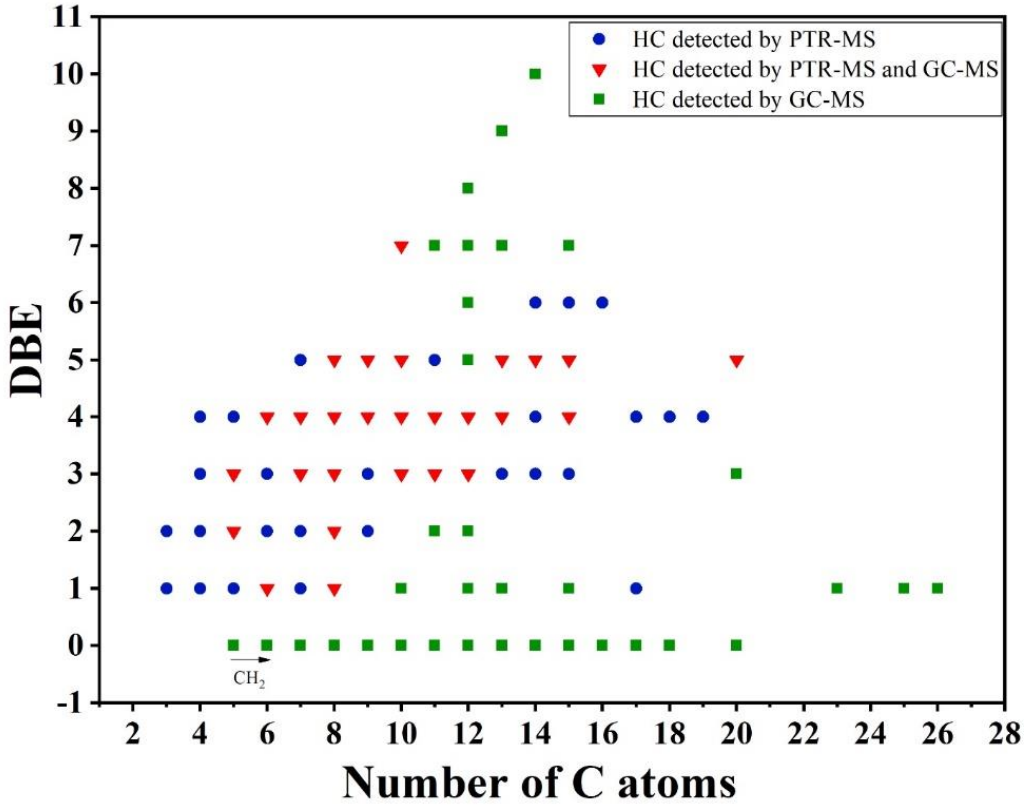

Figure 4.10 *DBE vs. the number of carbon atoms plot for the HC emitted from manure samples and detected using PTR-QiTOF-MS (blue circles), TD-GC-MS (green squares) and both techniques (red triangles).*

Using DBE analysis, HC were classified into different sub-classes with the same DBE value but different alkylation degree (compounds situated in the same straight line in **Figure 4.10**). Compounds with DBE=1 were either alkenes or cycloalkanes such as 10-methyl-3-undecene ($C_{12}H_{24}$) and 1,5-dimethyl cyclooctane ($C_{10}H_{20}$). Other compounds with DBE=2 were either alkynes, cycloalkenes or dienes such as 1,3-octadiene (C_8H_{14}). Cycloalkynes or polyenes having DBE=3 such as 6-butyl-1,4-cycloheptadiene ($C_{11}H_{18}$) and 3-ethylidenecyclohexene (C_8H_{12}). Most of the detected HC in this work were aromatics with DBE $\geq$ 4. Moreover, 4 compounds identified as terpenes were emitted from all manure samples and identified using both online and offline analysis.

The emission fluxes of the assigned HC detected using PTR-QiTOF-MS were estimated. **Figure 4.11** shows the bar graph representation of the HC sub-classes identified using DBE analysis. HC detected using PTR-QiTOF-MS belong to five sub-classes: aliphatic (linear alkenes or alkynes), alicyclic (cycloalkanes, cycloalkenes, or cycloalkynes), aromatic (benzene and its derivatives) and terpenes. The total emission fluxes of HC sub-classes are displayed. Aromatic compounds dominated the emissions among the HC in all samples. The emissions of compounds with DBE = 3 arouse dominantly from cow manure (2.8 ± 0.6 µg m^{-2} min^{-1}). Moreover, cow manure was characterized by elevated emissions of terpenes (1.71 ± 0.36 µg m^{-2} min^{-1}) while they were comparable in the other samples. Comparable numbers of VOCs were assigned as HC in all samples (**Figure 4.3**). The highest emission flux of HC was observed for cow manure at 10 ± 2 µg m^{-2} min^{-1}. The emission flux of HC in the other three samples were comparable (**Table 4.4**).

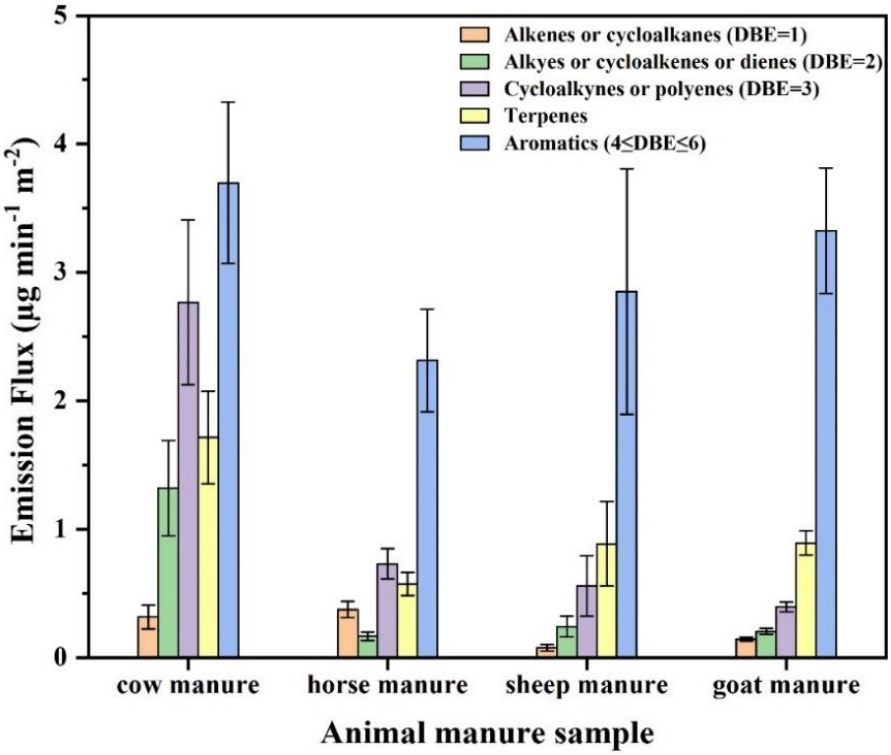

Figure 4.11 *Classification of HC detected by PTR-QiTOF-MS in each manure sample using the DBE method. The total emission flux of each sub-class is illustrated. The error bars shown in the figure represent the standard deviation of the average emission flux obtained from the three replicates of each sample.*

The fluxes of BTEX and terpene compounds emitted from the four samples are illustrated in **Figure 4.12**. Benzene (C_6H_6, *m/z* 79.05), toluene (C_7H_8, *m/z* 93.07), ethylbenzene

and xylene (C_8H_{10}, *m/z* 107.09) were emitted from the four samples and detected using PTR-QiTOF-MS and TD-GC-MS. Ions corresponding to *m/z* 69.07, 137.12, 205.19 and 273.26 were assigned as $C_5H_8H^+$ (isoprene), $C_{10}H_{16}H^+$ (monoterpenes, D-limonene and 3-carene), $C_{15}H_{24}H^+$ (sesquiterpenes) and $C_{20}H_{32}H^+$ (diterpenes). Based on TD-GC-MS, more than 20 compounds were identified as sesquiterpene isomers.

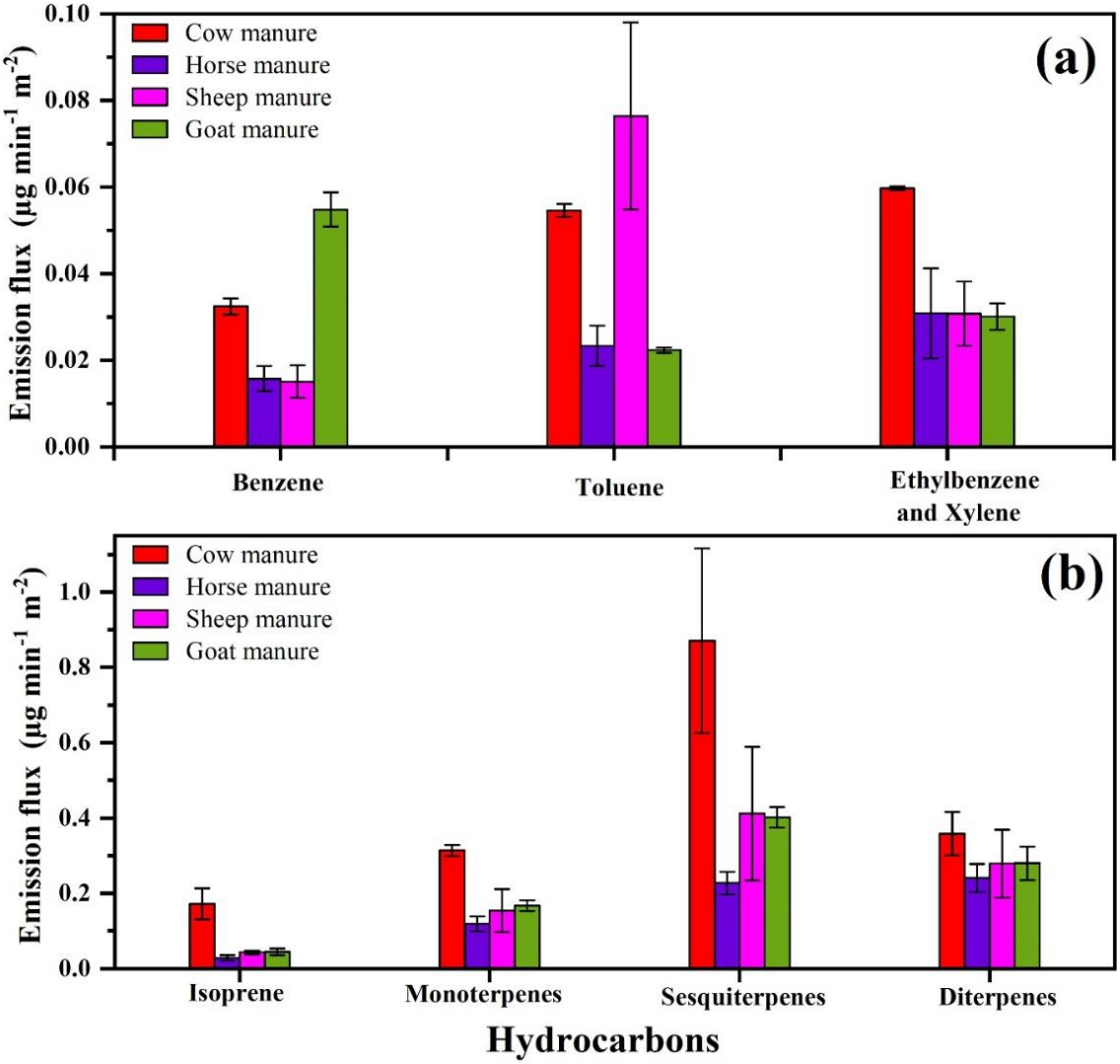

Figure 4.12 *Emission flux of (a) BTEX and (b) terpene compounds emitted from manure samples. The error bars represent the standard deviation of the three replicates.*

Benzene showed the maximum emissions from goat manure, while sheep manure was characterized by the highest emissions of toluene. Ethylbenzene and xylene showed the highest emissions in cow manure, while they were equally emitted from the other three samples. BTEX was already reported inside farm buildings (Ciganek & Neca, 2008). Kammer et al., (2020) reported the emissions of markers of anthropogenic combustion tracers such as BTEX,

trimethyl benzene, propyl benzene and NO_x from dairy stable and sheep pen. The authors found no correlation between NO_x and BTEX and thus they assumed that BTEX compounds were originated from the sheep pen. The emissions of BTEX compounds in our work are considered low compared to those reported by Kammer et al., (2020). This difference could be explained by the conditions of the study, as Kammer et al., (2020) performed field experiments, while we performed chamber experiments. Kammer et al., (2020) assumed that anthropogenic sources such as farming activities inside the farm buildings are the main sources of BTEX compounds (Kammer et al., 2020).

Terpenes are usually attributed to biogenic emissions (Büyüksönmez & Evans, 2007; Kumar et al., 2011; Sánchez-Monedero et al., 2018). Terpene emissions dominated the total concentrations of emitted VOCs (about 50% of the total amount of VOC) in a composting pile at different stages of the process (Sánchez-Monedero et al., 2018). Terpene emissions were lower than 1 µg m^{-2} min^{-1} in our samples (**Figure 4.12**). They showed the highest emissions from cow manure, followed by goat, horse and sheep manures. Terpenes were emitted from yard waste compost and are considered the natural compounds released from the feedstock (Eitzer, 1995). Moreover, Büyüksönmez & Evans, (2007) showed terpenes as the single most important compounds emitted from the feedstock tested in the study. In this work, the contribution of terpenes to the total flux of VOCs was 2.6%, 2.5%, 1% and 2.8% in cow, horse, sheep and goat manures, respectively. This contribution is very low compared to the contribution of terpenes to total flux of VOCs emitted from green waste compost piles of different ages (10%) (Kumar et al., 2011). Knowing that the analyzed manure samples were mixed with straw, this difference is related to the type of the emitter, as straw (of plant origin) is not considered to be a strong terpene emitter, as shown by Beck et al., (2007). Sesquiterpenes were the 2nd highest emitted compounds from sheep and goat manure, while their rank was 6th and 10th in cow and horse manures, respectively.

4.4.2. Oxygenated compounds

In this work, the highest number of VOCs was assigned as OVOCs in the four samples. OVOCs showed the maximum emission fluxes among the identified chemical families of compounds. The highest emission flux was observed in cow manure at 36 ± 19 µg m^{-2} min^{-1}. The OVOCs emission fluxes in horse, sheep and goat manures were comparable at 11 ± 3, 12 ± 5 and 13 ± 2 µg m^{-2} min^{-1}, respectively. In this work, the detected OVOCs contained from one to four oxygen atoms, this indicated that the emitted OVOCs were not highly oxidized. A vast majority of the assigned OVOCs by PTR-QiTOF-MS were identified using TD-GC-MS analysis. Based

on the two instruments, we observed many characteristic groups of OVOCs in significant proportion in cow manure: alcohols, carboxylic acids, carbonyls (ketones and aldehydes), ethers and esters. Several studies have shown that OVOCs, such as methanol, ethanol, acetone, and acetic acid dominate dairy cattle emissions (Ngwabie et al., 2008; Sun et al., 2008). Yuan et al., (2017) reported the dominant contribution of oxygenated compounds such as alcohols and carbonyls to the total concentration of emitted VOCs from different concentrated animal feeding operation sites (**Figure 1.2**). Moreover, Zhang et al., (2019) showed the dominance of OVOCs such as ethanol, acetone and 2-butanone among the VOC emissions from swine manure biogas digestate storage. Ngwabie et al., (2007) have identified methanol, acetaldehyde, ethanol, acetone and isopropanol in sheep house at a mixing ratio > 14 ppb with the highest amount of ethanol at 6571 ppb.

4.4.2.1. Emissions of alcohols and carbonyl compounds

Compounds assigned as C_xH_yO contributed to 89%, 62%, 55% and 56% to the total emission flux of OVOCs in cow, horse, sheep and goat manure. Cow manure showed the highest emission flux of C_xH_yO at 31.80 ± 18.59 µg m^{-2} min^{-1} due to the high emissions of three compounds C_3H_6O (*m/z* 59.04), C_4H_8O (*m/z* 73.06) and C_7H_8O (*m/z* 109.07). Those compounds were identified by TD-GC-MS as follows: C_3H_6O (acetone), C_4H_8O (butanal and 2-butanone) and C_7H_8O (anisole, p-cresol and benzyl alcohols) and contributed alone to 58% of the total C_xH_yO emissions flux. C_7H_8O was identified as 4-methylphenol in sheep house at a mixing ratio of 3.9 ppb (Ngwabie et al., 2007). Butanal and butanone were classified as the 2nd most emitted VOCs from cow manure. C_4H_8O was identified in the dwelling houses and stables of dairy and cattle farms in Northern Germany (Beck et al., 2007). Animal exhalation is the main emission source of this compound.

The highest emissions of acetone were observed from cow (1st most emitted), followed by horse, goat and sheep manures. Acetone, butanal and butanone were emitted from all samples. Kammer et al., (2020) have reported that acetone and trimethylamine were the most emitted VOCs after ethanol and methanol in sheep pen. This order of emissions was not the same in sheep manure in this work. This difference can be related to several factors such as (i) the measurement conditions, field or laboratory study, (ii) the different approached in emission flux calculations, and (iii) the sources of emitted VOCs as some emissions are correlated to respiration (acetone), agricultural practices, animal and excreta emissions (Kammer et al., 2020; Ngwabie et al., 2008).

Methanol (CH_4O, *m/z* 33.03) was emitted from all samples except the cow manure. It was the most emitted VOC in horse and goat manures (2.13 ± 0.26 and 2.61 ± 0.38 µg m^{-2} min^{-1}, respectively). Our values were almost double compared to those reported by Liu et al., (2018), 1.2 µg m^{-2} min^{-1}, emitted following the land application of pig manure. Acetaldehyde (C_2H_4O, *m/z* 45.03) was emitted from all samples. It was the 1st most emitted compound from sheep manure. Acetaldehyde showed almost the same emission fluxes at 0.8 ± 0.5 µg m^{-2} min^{-1} in horse and sheep manures, while in cow manure its emission flux was 0.3 ± 0.2 µg m^{-2} min^{-1}. The lowest emission flux of 0.063 ± 0.006 µg m^{-2} min^{-1} was observed in goat manure. The low emissions of acetaldehyde are consistent with other studies where this compound was not reported as the one of the most important VOCs (Filipy et al., 2006; Ngwabie et al., 2008; Sun et al., 2008). However, acetaldehyde emissions were higher from pig manure land application (16.7 µg m^{-2} min^{-1}) (Liu et al., 2018). Very low emission flux (< 0.01 µg m^{-2} min^{-1}) of ethanol (C_2H_6O, *m/z* 47.05) was found in the four samples. An ion corresponding to *m/z* 87.08 assigned as $C_5H_{10}OH^+$ has been found in all samples using PTR-QiTOF-MS. Several candidates for $C_5H_{10}O$ were identified using TD-GC-MS such as 3-methyl butanal, 3-methyl-2-butanone, 2-pentanone, pentanal and 3-pentanone. These compounds were also reported in lactating cow open stall, cattle farms and intensive pig production (Beck et al., 2007; Feilberg et al., 2015; Filipy et al., 2006).

4.4.2.2. Emissions of carboxylic acids and esters

Compounds assigned as $C_xH_yO_2$ showed comparable contributions to total emission flux of OVOCs in horse, sheep and goat manures (33%, 36% and 39%, respectively). The lowest was observed in cow manure at 3.02 ± 0.65 µg m^{-2} min^{-1}. $C_xH_yO_2$ were identified as carboxylic acids, esters or ethers by TD-GC-MS analysis. CH_2O_2 (*m/z* 47.02) identified as formic acid (Feilberg et al., 2015) was emitted from all samples with the same emission flux of 0.02 µg m^{-2} min^{-1}. Acetic acid (protonated ion $C_2H_4O_2H^+$, *m/z* 61.03) was emitted from all samples. The highest emission flux of acetic acid was observed in cow manure at 0.0989 ± 0.0548 µg m^{-2} min^{-1}, which is very low compared with its emission from swine manure slurry (3 - 24 µg m^{-2} min^{-1}) (Parker et al., 2013). This compound has been proposed as cowshed emission tracer in (Feilberg et al., 2015; Rabaud et al., 2003). Acetic acid was the 3rd most concentrated VOC in the dairy stable, sheep pen and outdoor according to Kammer et al., (2020). Moreover, acetic acid was characterized by high fluxes from the waste of lactating cows as reported by (Shaw et al., 2007). $C_3H_6O_2$ (*m/z* 75.04) was identified as propanoic acid and 1-hydroxy-2-propanone by TD-GC-MS analysis. These compounds were emitted from all samples, with the highest

emission flux in cow manure (0.07 ± 0.06 µg m^{-2} min^{-1}). Propanoic acid was reported in the literature as characteristic compound of cow and sheep pen emissions (Ngwabie et al., 2007, 2008). Liu et al., (2018) reported very high emission flux of propanoic acid (1012 µg m^{-2} min^{-1}) during the 37 h application of pig manure slurry. However, this compound showed little emissions (~ 9 µg m^{-2} min^{-1}) after swine manure slurry application (Parker et al., 2013). The higher emissions, compared with our values, could be related to the type of the manure and the field measurement compared to our controlled laboratory experiments. This compound was also reported in swine slurry emissions with an average emission flux of 2.6 µg m^{-2} min^{-1} during 4 weeks of swine slurry application (Parker et al., 2013). Benzoic acid (protonated ion $C_7H_6O_2H^+$, *m/z* 123.05) was emitted from all samples except cow manure. This compound results from the metabolic degradation of an amino acid phenylalanine as reported by Mackie et al., (1998).

Volatile fatty acids (VFA) such as heptanoic acid ($C_7H_{14}O_2$), hexanoic acid ($C_6H_{12}O_2$), isobutyric acid ($C_4H_8O_2$) and isovaleric acid ($C_5H_{10}O_2$) were found in this work. These VFAs were reported by Woodbury et al., (2022) to show notable contributions to total odor activity value. Heptanoic acid and hexanoic acid were emitted from all samples except cow manure. Isobutyric acid and isovaleric acid were emitted from all samples.

4.4.2.3. Emissions of phenols

The emission flux of 3 phenols identified in manure samples is illustrated in **Figure 4.13**. C_7H_8O was found in all samples except sheep manure using PTR-QiTOF-MS. C_7H_8O was detected by the TD-GC-MS analysis as p-cresol and anisole in all samples.

C_7H_8O showed the highest emission flux in cow manure at 1.39 ± 1.35 µg m^{-2} min^{-1} and it was the 3rd most emitted VOC from this sample. An ion corresponding to *m/z* 95.08 was assigned to C_6H_6O emissions from all samples, with different fluxes. The highest emission flux of phenol was observed in cow manure at 0.525 ± 0.189 µg m^{-2} min^{-1}. Horse and sheep manures showed the same emission flux of phenol (0.02 ± 0.01 µg m^{-2} min^{-1}), while goat manure showed the lowest emission flux (0.127 ± 0.009 µg m^{-2} min^{-1}). Phenol was emitted from surface-application or injection of swine manure slurry into soil in a study performed by Parker et al., (2013) at an emission flux of 4.02 and 0.86 µg m^{-2} min^{-1}, respectively. Mackie et al., (1998) explained that cresol is produced during the microbial degradation of tyrosine (amino acid) and associated with the production of phenol. Consequently, phenol and cresol emissions show

strong correlation. Based on this, we can explain the relatively high emission fluxes of phenol and cresol from the manure samples under study.

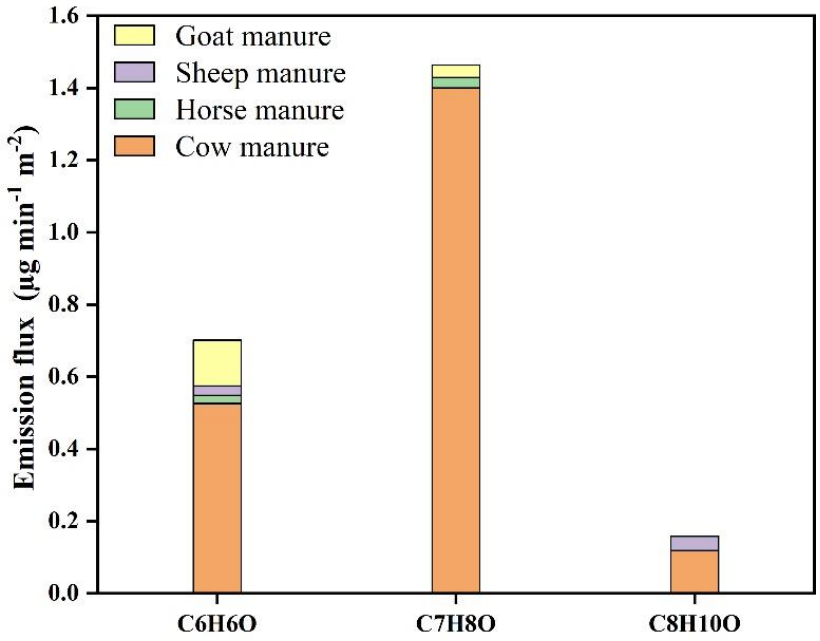

Figure 4.13 *Emission flux of phenols identified in manure samples.*

Another phenolic compound detected at *m/z* 123.08 was assigned to the protonated form of $C_8H_{10}O$ and identified in cow and sheep manures as 1-methoxy-4-methyl-benzene and 4-ethylphenol. Phenolic species were demonstrated by Yuan et al., (2017) to dominate the reactivity of emitted VOCs to NO_3 radicals (**Figure 1.2**). This compound constituted only a few percentage of emissions from CAFOs (Yuan et al., 2017). Phenols content increases with the increasing amount of the dietary protein of cows. An ion detected at *m/z* 123.08 was assigned as being the protonated form of $C_8H_{10}O$. This compound was emitted from cow and sheep manure at emission fluxes 0.12 ± 0.02 and 0.039 ± 0.016 µg m^{-2} min^{-1}, respectively. TD-GC-MS identified two compounds corresponding to $C_8H_{10}O$, 1-methoxy-4methyl-benzene and 3-ethylphenol.

4.4.3. Nitrogenated compounds

Several nitrogenated compounds were found in animal manure samples. Based on emission flux calculations, nitrogenated compounds showed the maximum emission flux in cow manure at 7.21 ± 1.87 µg m^{-2} min^{-1}, followed by goat, sheep and horse manures (**Table 4.4**).

4.4.3.1. Emissions of ammonia, dimethylamine and trimethylamine

NH_3 was by so far the most abundant gaseous compound measured in the emissions from the manure application (Williams, 1995). NH_3 is an important end product of the biological and

chemical breakdown of manure protein, uric acid and urea decomposition (Mackie et al., 1998). NH_3 can volatilize into the atmosphere depending on the pH, temperature and moisture. This enhances the deposition of sulfate and nitrate, leading to acid rain that acidifies the soil (Atkinson, 2000).

Quantitative analysis of NH_3 using the H_3O^+ ionization mode in PTR-QiTOF-MS is difficult due to its interaction with the surface of many materials and the high water solubility of NH_3 which promotes the back reactions of NH_4^+ to NH_3 (Norman et al., 2009). A modified approach of PTR-MS to measure NH_3 has been presented by Norman et al., (2007). This approach is based on the chemical ionization of NH_3 using oxygen (O_2) as a source gas to produce O_2^+ as ionizing reagent instead of H_3O^+. The O_2^+ ions react with the NH_3 molecules through the electron transfer reaction $O_2^+ + NH_3 \rightarrow NH_3^+ + O_2$. For this ionization mode the corrected term of the instrument is ETR-MS (Electron Transfer Reaction Mass Spectrometer) as it uses electron transfer instead of proton transfer. The use of O_2^+ for chemical ionization allows for fast, highly sensitive and specific measurements of gas-phase NH_3 (Norman et al., 2007). This approach was not applied in our work and the H_3O^+ was used as ionizing reagent for the purposes described in Section 2.3.1. Moreover, the objective of this work was to chemically characterize the VOC emissions from manure samples, where most of VOCs of interest can be measured using the proton transfer approach of the instrument. In this study, NH_3 was measured by the Picarro instrument. The results showed the highest emission of NH_3 from sheep manure (18278 ppb), followed by goat, cow and horse manures at 10225, 7093, and 6352 ppb, respectively.

The signal at *m/z* 18 was assigned to NH_3 (NH_4^+ ion), thus the temporal evolution of NH_3 could be followed using PTR-QiTOF-NMS to compare the trend of emissions to that obtained by Picarro measurements. An example of the temporal evolution of NH_3 measured in the four manure samples by PTR-QiTOF-MS is illustrated in **Figure 4.14 (a)**. The y-axis represents the signal of NH_3 (normalized relative to H_3O^+ counts per second) and the x-axis represents the time of the experiment. According to PTR-QiTOF-MS results, cow manure showed the highest normalized signal of NH_3. The temporal variation of NH_3 mixing ratio measured by Picarro was also illustrated for the four samples in **Figure 4.14 (b)**. The y-axis represents the mixing ratio of NH_3 (ppb) and the x-axis represents the time of the experiment. Although PTR-MS is not quantitative for NH_3, the temporal evolution of its signal can be followed and compared to that obtained by Picarro. Similar trends of NH_3 emissions were observed using PTR-MS and Picarro as shown in **Figure 4.14**.

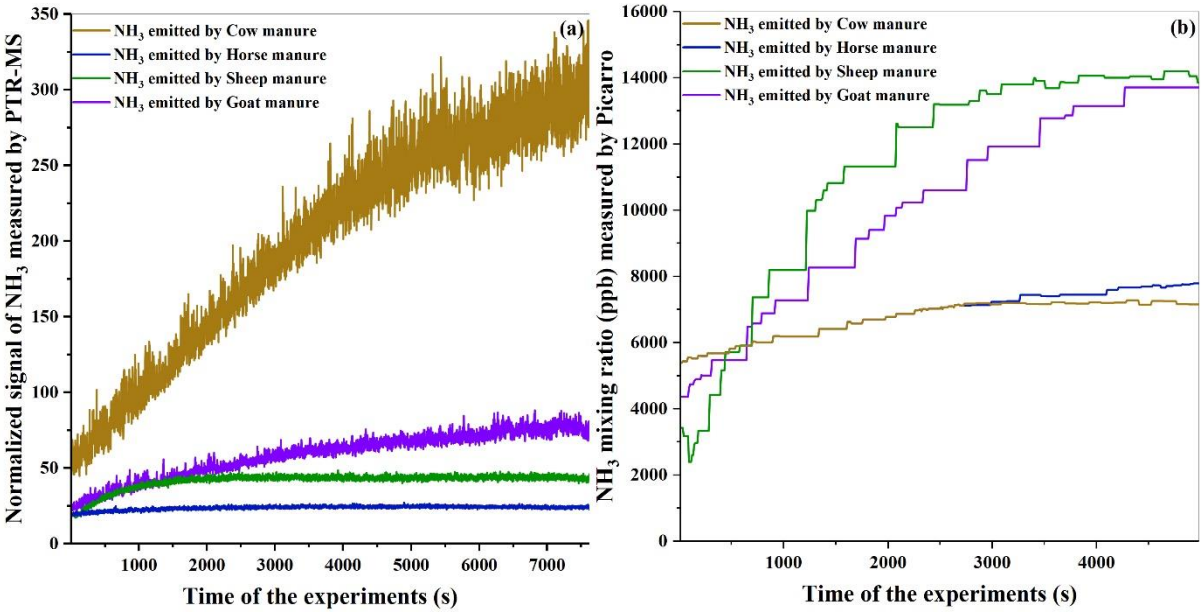

Figure 4.14 *(a) Temporal evolution of NH_3 signal measured using PTR-QiTOF-MS and (b) temporal evolution of NH_3 mixing ratio measured by Picarro, for the four manure samples.*

An ion corresponding to *m/z* 46.06 was assigned to the protonated form $C_2H_7NH^+$ of dimethylamine (DMA) (Kammer et al., 2020). This compound was emitted from all samples except horse manure. A multipeak at the nominal mass *m/z* 60 was also detected. The first ion signal at *m/z* 60.05 corresponded to ^{13}C isotope of protonated acetone ($C_3H_6OH^+$, *m/z* 59.04). The second signal at *m/z* 60.08 was assigned to $C_3H_9NH^+$. Feilberg et al., (2015) applied a correction of the signal of $C_3H_9NH^+$ to the ^{13}C isotopomer of acetone since the PTR-MS with a quadrupole mass analyzer was used, with lower resolution than the instrument used in our work. The average resolution of PTR-MS instrument used in our study was estimated to ~5000, which was enough to separate the two compounds, as in the case of the multipeak at nominal mass 60. C_3H_9N has been identified as trimethylamine (TMA) in (Beck et al., 2007; Feilberg et al., 2015). In this work, TMA was only detected by PTR-MS and not detected in TD-GC-MS. This phenomenon has been explained by Feilberg et al., (2015) as TMA only elutes from the specific GC column in the first few runs of a column. The maximum emission flux of TMA was observed in cow manure at 0.3 ± 0.2 µg m^{-2} min^{-1} followed in sheep, goat and horse manures at 0.043 ± 0.017, 0.018 ± 0.007 and 0.008 ± 0.002 µg m^{-2} min^{-1}. TMA was also observed by Liu et al., (2018) after land application of pig manure slurry with an emission flux of 8.9 µg m^{-2} min^{-1}. This emission is relatively high compared to our samples emissions. This can be related to the type of manure, concept of the study and emission fluxes calculations.

Sintermann et al., (2014) showed that dairy excreta (urine + feces) are the main source of NH_3, DMA and TMA in dairy farming. TMA is a volatile aliphatic amine species, released from agricultural activities, and has been found to be the dominant gas-phase aliphatic amine (compared to methylamine and DMA) at agricultural sites (Sintermann et al., 2014). Gas-phase DMA and TMA participate in nucleation, have high potential efficiency for secondary particle formation and can undergo condensation onto existing aerosol particles (Lee et al., 2019; Sintermann et al., 2014).

4.4.3.2. Emissions of indoles

Two aromatic nitrogenated compounds, with protonated ions $C_8H_7NH^+$ (*m/z* 118.06) and $C_9H_9NH^+$ (*m/z* 132.08) detected by PTR-MS, were found in the four samples (**Figure 4.15**). Using TD-GC-MS data, C_8H_7N was identified as indole in all samples. C_9H_9N was identified as 4-methylindole in cow, horse and goat manure, while in sheep manure it was identified as 6-methylindole. The emission flux of indole was almost the same in all sample (~ 0.96 ± 0.01 µg m^{-2} min^{-1}). 4-methylindole showed the highest emission flux in cow manure at 1.3 ± 0.4 µg m^{-2} min^{-1}, followed by sheep and horse manures at 0.11 ± 0.03 and 0.098 ± 0.017 µg m^{-2} min^{-1}, respectively. 4-methylindole was the 4th most emitted compound from cow manure. 6-methylindole was emitted only from sheep manure, thus it can be considered as emission tracer of this manure. Indole (C_8H_7N) was emitted at an emission flux of 2.3 µg m^{-2} min^{-1} after the land application of pig slurry manure (Liu et al., 2018). This emission flux was lower, 0.564 and 0.035 µg m^{-2} min^{-1}, after surface-application or injection of swine manure slurry into soil, respectively (Parker et al., 2013).

Several indoles were widely reported in the literature and are considered odorant compounds emitted from livestock production and after the land application of different animal manure types (Feilberg et al., 2010, 2011; Liu et al., 2018; Ni et al., 2012; Parker et al., 2013; Woodbury et al., 2022). Indole and skatole are the principal end-products of tryptophan metabolism (Mackie et al., 1998). Cresol, indoles and phenols have high odor activity value and are reported as strong odorant compounds that contribute to odor nuisance (Feilberg et al., 2010, 2011; Kammer et al., 2020; Mackie et al., 1998). Moreover, indole and skatole were reported as the main aromatic compounds and contributed significantly, 14.7% and 8.84%, respectively, to odor activity values from land application of beef cattle manure (Woodbury et al., 2022). A recent study showed the new particle formation from skatole ozonolysis in the presence of SO_2, which are both emitted by sludge samples (Ciuraru et al., 2021). The authors

suggested skatole as an additional VOC source that may have a significant influence on atmospheric particle formation during the spreading periods of sludge (Ciuraru et al., 2021).

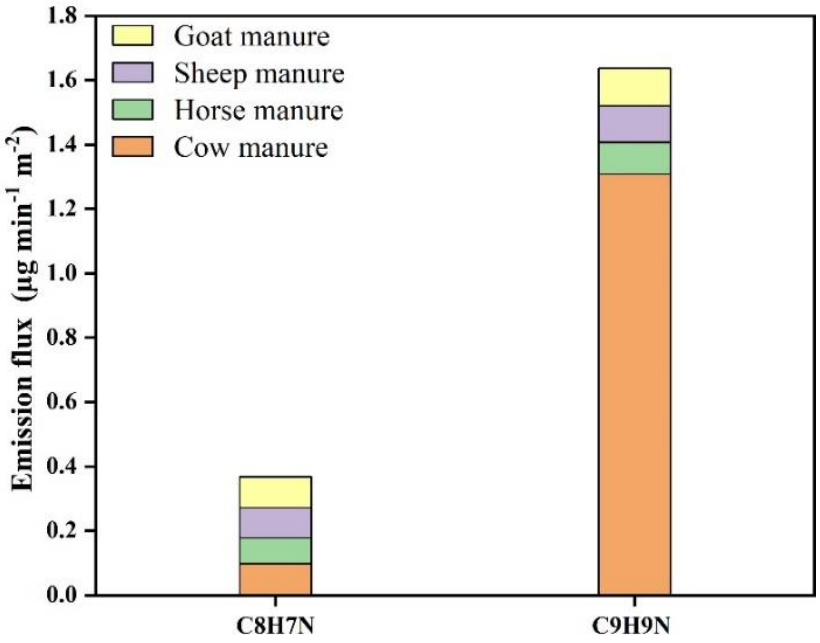

Figure 4.15 *Emission flux of indoles identified in manure samples.*

4.4.4. Sulphur compounds

A total of 12 sulphur compounds were found in manure samples using PTR-QiTOF-MS. Sulphur compounds were emitted in relatively low amounts from the analyzed manure samples. Equal total emission flux of these compounds were found in cow, horse and sheep manures, while a lower flux was emitted from the goat manure (**Table 4.4**). The emission flux of each sulphur compound in manure samples is displayed in **Figure 4.16**. Sulphur compounds are a part of the essential amino acids methionine, cysteine, homocysteine and taurine that come from the proteins livestock are fed with (Higgins et al., 2004; Zhu et al., 2016).

Two sulphur compounds were detected in the emissions of all samples at *m/z* 49.01 and 63.02 as CH_4SH^+ and $C_2H_6SH^+$ ions, respectively. CH_4S was identified as methanethiol by TD-GC-MS and showed the lowest emission flux in cow manure (0.047 ± 0.023 µg m^{-2} min^{-1}). Our value was higher compared to the pig manure emissions (0.02 µg m^{-2} min^{-1}) reported by Liu et al., (2018). C_2H_6S was identified as dimethyl sulphide (DMS) (Beck et al., 2007; Feilberg et al., 2015), with the highest emission flux observed from goat manure at 0.22 ± 0.12 µg m^{-2} min^{-1}. This exceeds the value reported by Liu et al., (2018) in swine manure slurry application at 0.06 µg m^{-2} min^{-1}. DMS can be oxidized to methanesulphonic acid and eventually sulphuric acid, which can contribute to the formation of cloud condensation nuclei (CCN) and aerosols

when combined with NH_3 (Filipy et al., 2006). A compound detected at *m/z* 94.99 and assigned to the protonated form of $C_2H_6S_2$ was found the PTR mass spectra of horse manure emissions, while by TD-GC-MS, $C_2H_6S_2$ was observed in the gas phase emissions of all samples. It was assigned to dimethyl disulphide (DMDS). DMDS was reported by Parker et al., (2013) as an odorant compound emitted following pig manure slurry surface-application or injection into soil, with emission fluxes of 0.086 and 0.037 μg m^{-2} min^{-1}, respectively. DMDS was emitted at very low flux from horse manure at 0.06 ± 0.01 μg m^{-2} min^{-1}. Moreover, DMDS is characterized by high photochemical reactivity. Thus its lack of detection by PTR-MS measurements of cow, sheep, and goat manures would be expected, as most of DMDS could be lost prior to the sample introduction into the chamber.

Methanethiol, DMS and DMDS are potentially odorous compounds that could produce odor problems at farm buildings as they are characterized by low human odor detection thresholds (Filipy et al., 2006; Schiffman et al., 2001). Six sulphur compounds assigned as $C_4H_4SH^+$, $C_5H_6SH^+$, $C_5H_8SH^+$, $C_6H_8SH^+$, $C_6H_{12}SH^+$ and $C_7H_{10}SH^+$ ions were observed only for the cow manure and they can be considered as emission tracers. CS_2 (*m/z* 76.95) was observed only in goat manure using PTR-MS while it was identified as carbon disulphide in the gas phase emissions of sheep manure using TD-GC-MS. Carbon disulphide, DMS and DMDS were found to be the dominant VOCs in the indoor and outdoor parts of animal farms (Ciganek & Neca, 2008).

In this work, hydrogen sulphide (H_2S) was not detected due to the deficiency in PTR-QiTOF-MS system. This compound has relatively low PA (691 kJ mol^{-1}) compared to water (705 kJ mol^{-1}), moreover it is difficult to measure it using PTR-MS due to humidity-dependent backward reaction of protonated H_2S (Hansen et al., 2012). Feilberg et al., (2010) described a correction of the measurement of H_2S by PTR-MS, but this method was not applied in our work. Accordingly, the emissions of H_2S from the analyzed manure samples was not excluded, as it was emitted from sheep manure based on TD-GC-MS. H_2S is a major sulphur compound emitted from livestock production. Feilberg et al., (2017) showed that agriculture constituted the most important sulphur source category in Denmark, a country with intensive livestock production. H_2S can undergo several oxidation reactions in atmosphere with photo-oxidants such as OH radicals, NO_3 radicals and O_3. The ultimate end-product of gas phase H_2S oxidation in the atmosphere is SO_2, which can oxidize and ends up as aerosol sulphate (Atkinson et al., 2004). The absence of H_2S detection by TD-GC-MS analysis of cow, horse and sheep manure

emissions can be explained by its oxidation upon contact with air as it was suggested by (Feilberg et al., 2015) prior to the sample introduction into the chamber.

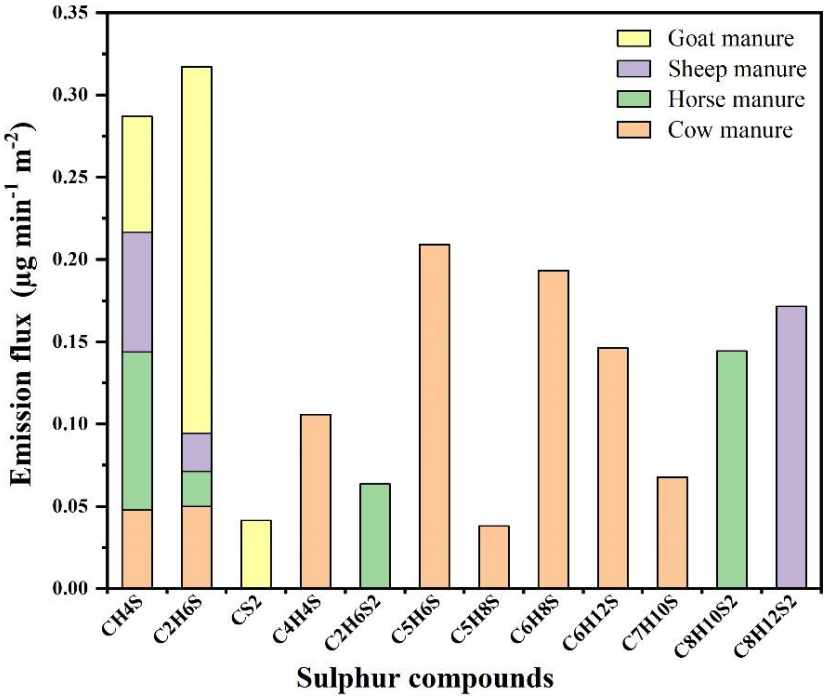

Figure 4.16 *Emission flux of sulphur compounds found in the four manure samples.*

The microbial oxidation of H_2S at the manure-air surface has been observed to occur at a rate of few seconds, which is significantly faster than typical chemical oxidation (Kühl & Jørgensen, 1992). Due to the rapid oxidation and loss of H_2S, it is not possible to exclude its emission from the manure samples under this study.

4.4.5. Emissions of halogenated and other compounds

A total of 10 halogenated compounds were found in manure samples using the combination of online and offline analysis. **Table 4.6** shows the list of halogenated compounds with the corresponding molecular formula, molecular weight and the chemical identification done using TD-GC-MS analysis. Halogenated compounds showed almost the same emission fluxes in all samples (**Table 4.4**). Halogenated compounds were generated from substances such as food additives, chemical cleaning agents and coatings (Duan et al., 2014). Some potential sources of halogenated compounds are industrial solvents, paint remover, refrigerants, soaps, paints and varnish (Allen et al., 1997; Orzi et al., 2018). Moreover, the emissions of halogenated compounds are contributed from both degradable and nonbiodegradable compounds (Liu et al., 2009). Halogenated compounds should gain special attention because they might pose high toxicological risk to workers and local inhabitants (Scheutz et al., 2008).

Table 4.6 *Halogenated compounds detected by TD-GC-MS and PTR-QiTOF-MS techniques.*

Molecular formula	Molecular weight	Chemical identification	Manure samples with compound detected
C_2H_3F[a]	46.022	Flouroethene	horse and sheep
C_2H_5F[a]	48.038	Flouroethane	goat
C_6H_5Cl[a]	112.008	Chlorobenzene	cow, horse, goat
C_7H_7Cl[a]	126.024	Benzyl chloride	sheep
$C_2H_3Cl_3$[a]	131.930	1,1,1-trichloroethane	cow, horse, sheep, goat
$C_8H_{17}Cl$[a]	148.102	2-chlorooctane	goat
CCl_4[a]	151.875	Carbon tetrachloride	horse, sheep, goat
$C_7H_{13}Br$[a]	176.020	1-bromo-4-methyl- cyclohexane	sheep
$C_7H_6OCl_2$[b]	176.989	-	horse, goat
$C_7H_5OCl_3$[b]	210.951	-	cow, horse, sheep

[a] *Compound detected by TD-GC-MS*

[b] *Compound detected by PTR-QiTOF-MS*

4.4.6. Sample comparison

PCA was applied to reduce the dimensionality of the data set and uncover the hidden trends. The PTR-QiTOF mass spectra of the four samples were compared. For this comparison, only the assigned VOCs that were 224, 233, 254 and 257 in cow, horse, sheep and goat manures were considered. The results of PCA are shown in Section 4.3.4. Based on the interpretation of score plots and loading plots (**Figure 4.6** and **Figure 4.7**), cow manure was isolated from the other three samples. This separation was associated primarily with the contribution of oxygenated compounds with one O atom (e.g., acetone, butanal, 2-butanone, p-cresol, anisole, 4-isopropylcyclohexanone, formaldehyde, phenol, acetophenone, etc.) as illustrated in **Figure 4.7 (a)**. In addition, nitrogenated compounds showed significant contribution in cow manure compared to other samples. For instance, dimethylamine, trimethylamine, indole and 3-metthyl indole were highly emitted from this sample (**Figure 4.7**, **a)**. Horse and sheep manures seemed to be very similar in the chemical composition of the gas phase emissions. They were separated from goat manure by the effect of PC2 (**Figure 4.6**). Goat manure received high contribution from nitrogen and oxygen containing compounds such as CH_3NO_2, C_2H_4NO, $C_2H_3NO_2$ and C_3H_3NO (**Figure 4.7**, **b)**.

Mackie et al., (1998) reported in their review the biological origin of key odor components in livestock waste. The biological origin of four principal classes of odor

compounds, namely volatile fatty acids, ammonia and volatile amine, indoles and phenols and volatile sulphur-containing compounds were reviewed. Phenols and indoles are excreted in feces and result from the same biological origin as described by Smith & Macfarlane, 1996. The microbial production of indoles and phenols results from amino acid metabolism. For instance, phenol and hydroxylated phenol-substituted fatty acids are the main products of tyrosine fermentation. Phenyl acetate and phenyl propanoate are produced from phenylalanine, whereas indole and 3-methylindole (skatole) are the main end-products of tryptophan metabolism (Mackie et al., 1998; Yuan et al., 2017). The metabolic pathways involved in the formation of phenolic and indolic compounds by intestinal anaerobic bacteria could explain the correlation between those compounds and their dominance in cow manure compared to the other samples (Smith & Macfarlane, 1996).

4.5. Conclusions and perspectives

Detailed chemical analysis of the gas phase emissions from different types of animal manure were provided in this study. A total of 385 compounds were detected and quantified using PTR-QiTOF-MS technique. The detailed chemical identification of VOC emitted from each manure was possible by analysing the emitted gas phase using offline TD-GC-MS analysis. Significant match was observed between the results of PTR-QiTOF-MS and TD-GC-MS. This highlighted the efficiency of combining online and offline analysis to better characterize VOC emissions, especially from samples enriched with VOCs such as animal manure.

The assigned VOCs were classified into different chemical families of compounds. Oxygenated compounds (e.g., ethanol, acetone, cresol, acetic acid, acetaldehyde, phenol, hexanoic acid, isobutyric acid, isovaleric acid, etc.), nitrogenated compounds (ammonia, dimethylamine, trimethylamine, etc.), sulphur compounds (methanethiol, DMS, DMDS, etc.), aromatic compounds (phenol, indoles and skatole), terpenes (isoprene, D-limonene, 3-carene, sesquiterpenes, etc.) and halogenated compounds were found in this work. The highest VOC emission fluxes were observed from the cow manure with 66 ± 26 µg m^{-2} min^{-1}, followed by goat, sheep and horse manures with 32 ± 5, 31 ± 11 and 25 ± 5 µg m^{-2} min^{-1}, respectively. OVOCs were the dominant compounds in all samples. They showed the highest contribution to total VOCs emission fluxes in all samples.

The performed statistical analysis demonstrated that cow manure emissions were isolated from the other three types of manures. Cow manure was characterized by oxygenated and nitrogenated compounds. Horse and sheep manures seemed to be very similar, while the

goat manure was associated with an increased contribution of oxygen and nitrogen containing compounds. Various compounds considered as strong odorants were found in this work. Compounds such as aromatic (indole and skatole), DMS, DMDS, methanethiol, cresol, phenol were emitted from manure samples. The detailed chemical analysis of manure emissions performed by laboratory measurements using atmospheric simulation chambers can provide information to support field measurements and recommendations for potential VOCs and odorants emitted from animal manure used in agricultural fields. This study provides a detailed inventory of VOCs with their emission fluxes and mass concentrations from each type of manure. The laboratory setup used in the current work can be used for future studies of the effects of manure treatment (such as by anaerobic or aerobic digestion) on gaseous emissions. Moreover, several factors such as animal diets, waste handling practices, feed, housing and climate can be taken into account.

Chapter 5

Reactivity of volatile organic compounds emitted by organic waste products toward ozone and secondary organic aerosol formation

5.1. Introduction

The large number of VOCs with different physico-chemical properties emitted from agricultural areas makes the research on VOC emissions challenging (Harrison et al., 2006). To date, a significant number of VOCs has been detected from OWP samples, such as organosulphur compounds (e.g. DMS and DMDS) (Byliński et al., 2019; Feilberg et al., 2015; Haider et al., 2022), terpenes (α-pinene, limonene) (Haider et al., 2022; Rincón et al., 2019a), nitrogenated compounds (indoles), aromatic compounds (Abis et al., 2018; Haider et al., 2022; Nie et al., 2019), and ketones and aldehydes (Sánchez-Monedero et al., 2018). **Figure 5.1** displays the distribution of the main chemical families of VOCs emitted from the piles at different stages of municipal solid waste composting process. The identified chemical families belong to differently families of compounds and contributed differently to the total concentration of VOC (Sánchez-Monedero et al., 2018). Some VOCs can represent SOA precursors; however, the chemical mechanisms in producing SOA using atmospheric emissions of OWP samples, as well as their chemical composition, are not well understood. Moreover, our understanding of NPF is based mostly on measurements of particle size distribution evolution with time, these measurements giving no information on the chemical mechanisms on how nucleation and growth occur (Bzdek & Johnston, 2010).

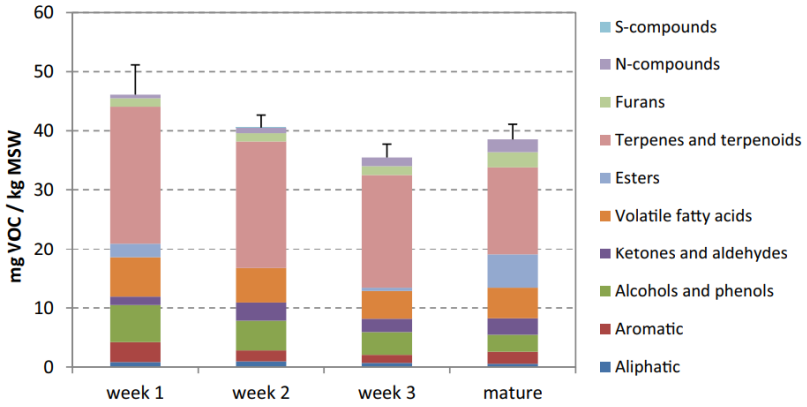

Figure 5.1 *Quantification of the total amount and chemical families of the VOCs identified in the piles at different stages of municipal solid waste composting process (Sánchez-Monedero et al., 2018).*

In this context, the objectives of our work have been (i) to study the role of OWPs as a source of VOCs that are reactive to O_3 contributing to NPF, (ii) to propose a chemical mechanism for the NPF from precursor gases, and (iii) to study the chemical composition of the newly formed aerosols using off-line mass spectrometric techniques (L2MS and TOF-SIMS). A first study performed in our laboratory (Ciuraru et al., 2021) investigated atmospheric particle formation from oxidized organic molecules and SO_2, both emitted by undigested SS samples. In a second step, we investigated the reactivity toward O_3 and NPF from VOCs emitted by the other types of OWPs studied in this thesis. These ozonolysis experiments we performed are summarized in **Table 5.1**.

Table 5.1 *Description of the ozonolysis experiments on various OWP samples.*

OWP type	Name of sample	PTR-MS measurements	GC-MS cartridge	Particle formation
SS from WWTP1	Undigested SS	Yes	Yes	٧
SS from WWTP2	UDSS	Yes	No	٧
	DSS	Yes	No	-
	SS 30%	Yes	No	-
	SS 60%	Yes	No	-
Animal manure	Cow	Yes	Yes	-
	Horse	Yes	Yes	-
	Sheep	Yes	Yes	-
	Goat	Yes	Yes	-
Food biowaste	Digestate biowastes	Yes	No	٧

The ozonolysis experiments of OWPs: undigested SS collected from WWTP1, SS (UDSS, DSS, SS with 30% and 60% of dryness) collected from WWTP2, animal manure (cow, horse, sheep and goat manures) and digestate biowastes were performed in the two atmospheric simulation chambers available at ECOSYS, as described in Section 2.2. Prior to each ozonolysis experiment, the chamber was carefully cleaned to obtain the residual particle number concentration to lower than one particle cm^{-3}. Upon introduction of the samples in the chamber, a strong initial emission of VOCs was observed, then the signals in the mass spectrum stabilized reaching a steady state. Once the steady state was reached, the samples were exposed to O_3 and the signals of the emitted VOCs were monitored. No OH or Criegee intermediate scavengers were added and no seed aerosol was used. For each sample, the gas-phase and the oxidation products resulting from ozonolysis reactions were analyzed by PTR-QiTOF-MS (see

Section 2.3.1). For some samples, TD-GC-MS analysis was performed on collected cartridges to detect and assign VOCs and their oxidation products (**Table 5.1**). The particle number concentration and size distribution were measured using the SMPS 3938 (TSI), described in Section 2.2.5. In case of new particle formation, the freshly formed particles were collected on quartz-fiber filters (see Section 2.2.5) and further analyzed using the L2MS and TOF-SIMS techniques (details in Section 2.4).

As we showed in the previous Chapters, multiple VOCs were identified in the studied OWP emissions, belonging to various chemical families such as aliphatic HC, alicyclic HC, aromatic HC, terpenes, alcohols, aldehydes, ketones, carboxylic acids, indoles, phenols and sulphur compounds, etc. In this Chapter, we try to identify the main compounds involved in NPF from OWP emissions. For this, the signals of the emitted VOCs were monitored and the temporal evolutions of all ion signals were carefully verified and interpreted. Thus, to achieve the objectives of this work, we focused on VOCs that showed significant reactivity to O_3 or formed as a result of ozonolysis.

5.2. Experimental observations of skatole emissions and ozonolysis leading to new particle formation

Based on the PTR-QiTOF-MS measurements, the only decreasing ion signal upon introduction of ozone was detected at *m/z* 132.08 and assigned as $C_9H_9NH^+$. Through complementary chromatographic analyses (TD-GC-MS and UHPLC-HRMS), the corresponding molecule was identified as 3-methylindole or skatole (Ciuraru et al., 2021). Skatole is one of the major malodorous compounds contributing to the odor problem of animal production facilities and SS treatment plants as it is emitted by bacterial degradation in a slurry (Gebicki et al., 2016; Ni et al., 2012).

The temporal evolution of skatole over the entire time of the experiments was therefore monitored for all samples using PTR-QiTOF-MS (**Figure 5.2**). Upon sample introduction into the chamber, a strong burst release of skatole was observed from cow manure (**Figure 5.2, a**; red line), UDSS (**Figure 5.2, b**; violet line) and digestate biowastes (**Figure 5.2, c**; brown line). Extremely low emissions of skatole were observed from other types of SS (DSS, SS 30% and SS 60%) and animal manure (horse, sheep and goat manures). Following the O_3 introduction into the chamber, skatole showed a significant reactivity to O_3, as the signal decreased within few seconds of O_3 addition. Skatole is known as a very reactive nucleophile that can easily undergo electrophilic substitution reactions (Sundberg, 1970). One study reported a reaction

rate constant in the aqueous phase for skatole with O_3 of 4.5 x 10^6 M^{-1} s^{-1} at pH = 6.7 (Wu & Masten, 2002). The stoichiometric factor is 0.9 which means that 1 mole of O_3 is needed for the ozonolysis of 0.9 mol of skatole (Wu & Masten, 2002). In addition, the reaction rate constants of indolic compounds in water increases with pH. In this work, the rate constant of 5 * 10^{-15} cm^3 $molecule^{-1}$ s^{-1} based on our skatole experiments was estimated. Thus skatole is a highly reactive compound towards O_3, resulting in a lifetime of ~ 3 min at ambient O_3 concentrations.

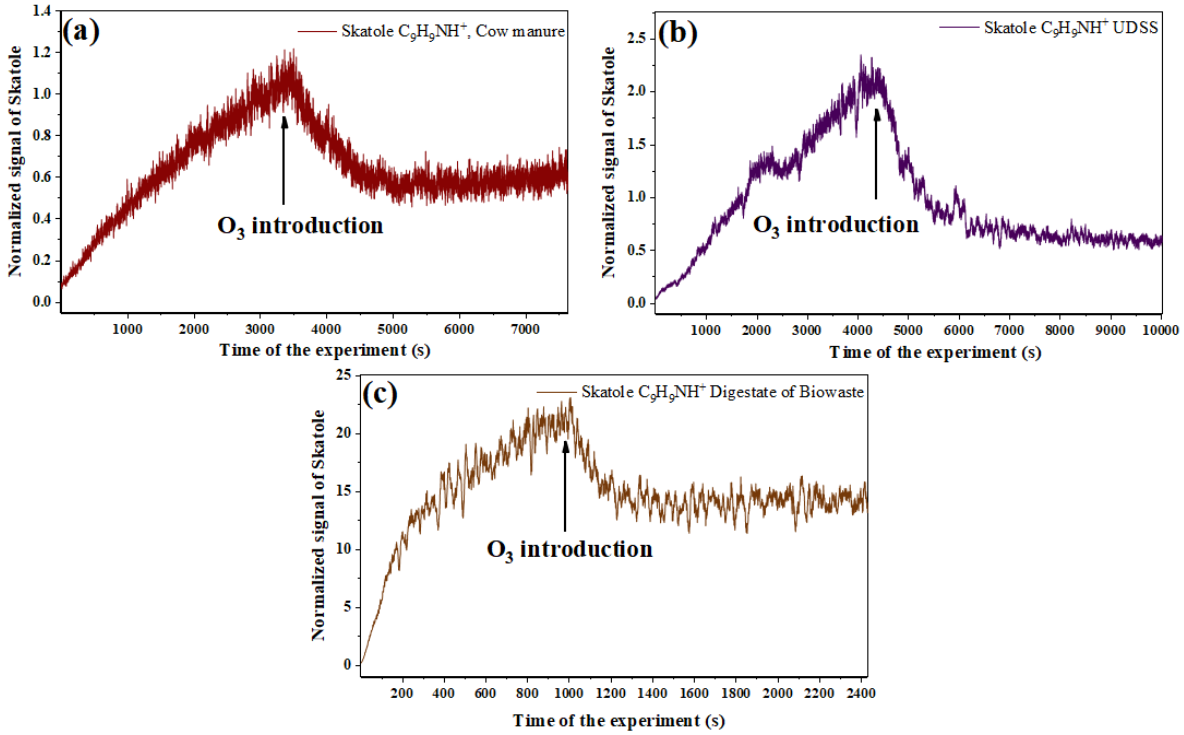

Figure 5.2 *Temporal evolution of the signal corresponding to skatole (m/z 132.08 $C_9H_9NH^+$) emitted from (a) cow manure, (b) UDSS and (c) digestate biowaste samples over the entire experimental time. The y-axis represents the normalized signal relative to the ion counts of H_3O^+ and the x-axis represents the time of experiment in second. The time of O_3 addition is indicated using vertical black line.*

The ozonolysis experiment of undigested SS taken from WWTP1 is illustrated in **Figure 5.3**. The amount of SO_2 and O_3 emitted by the sample as well as the amount of O_3 injected into the chamber were monitored (**Figure 5.3, b**). Within few seconds of initial exposure to O_3, the signal of skatole decreased, and those of gas-phase oxygen- and nitrogen-containing detected at *m/z* 136.08 $C_8H_9NOH^+$ and *m/z* 164.07 $C_9H_9NO_2H^+$, increased (**Figure 5.3, c**). According to GC-MS performed before and after ozonolysis and liquid chromatography performed on

collected particles, the *m/z* 164.070 $C_9H_9NO_2H^+$ ion was associated with 2-acetyl phenyl formamide (Ciuraru et al., 2021). Instantaneous particle formation was observed after O_3 injection. The particle number and size distributions (**Figure 5.3, a**) were measured over the size range 2 - 64 nm in electrical mobility diameter, indicating newly formed particles. During these experiments, the particle number concentration reached a maximum of 10^6 particles cm^{-3} within less than 2 min (**Figure 5.3, a**). Accordingly, the particle nucleation rate was 1.1 * 10^6 cm^{-3} s^{-1} during the NPF. After longer reaction times, the particles grew in size, while their number remained constant or slightly decreased due to coagulation and/or losses by adsorption to the walls. This behavior of the particle number concentration and size distribution was observed to be constant for experiments lasting for about 5 hours.

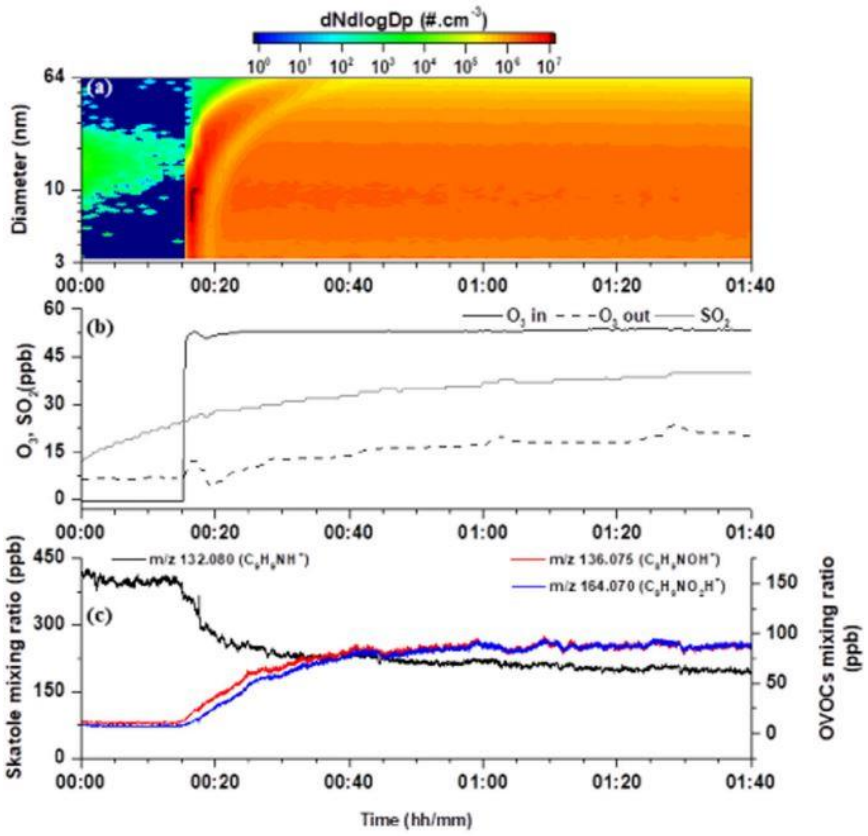

Figure 5.3 *Undigested SS (from WWTP1) ozonolysis experiment. (a) Temporal evolution of the particle number concentration and size distribution. The ordinate represents the electrical mobility diameter (nm), and the colour scale represents the particle number concentration. (b) Temporal evolution of O_3 entering the chamber (black line, O_3 in), O_3 measured at the exit of the chamber (black dotted line, O_3 out) and SO_2 (grey line). (c) Temporal evolution of m/z 132.080 $C_9H_9NH^+$ (black line, left axis), m/z 136.075 $C_8H_9NOH^+$ (red line, right axis) and m/z 164.070 $C_9H_9NO_2H^+$ (blue line, right axis) (Ciuraru et al., 2021).*

During the experiments, it has been observed that only ~35 ppb of O_3 were needed for ozonolysis to form particles (**Figure 5.3, b**). In addition, we performed more experiments with higher amounts of O_3 (250 ppb) and the results showed no difference in particle number concentration or size distribution. This might indicate that the reaction was limited by the residence time (5 min) inside the chamber. Moreover, our experiments showed that the consumption of skatole was fast but not complete and the newly formed reaction products reached a steady state within less than 15 min. This might be explained by the high kinetic rate constant for the ozonolysis reaction of skatole but might also indicate that oxidation can occur in both gaseous and condensed phases (walls, SS surface or secondary aerosols).

The behaviour of skatole emissions and NPF due to ozonolysis was observed only for undigested sludge (collected from WWTP1 and WWTP2), and not for the other SS samples. The ozonolysis experiment of UDSS from WWTP2 is illustrated in (**Figure 5.4**). The size distribution and the number concentration of the newly formed particles spanned the entire measured size range from 2 to 64 nm in electrical mobility diameter (**Figure 5.4**). The new particles reached a maximum of 10^5 particles cm^{-3}.

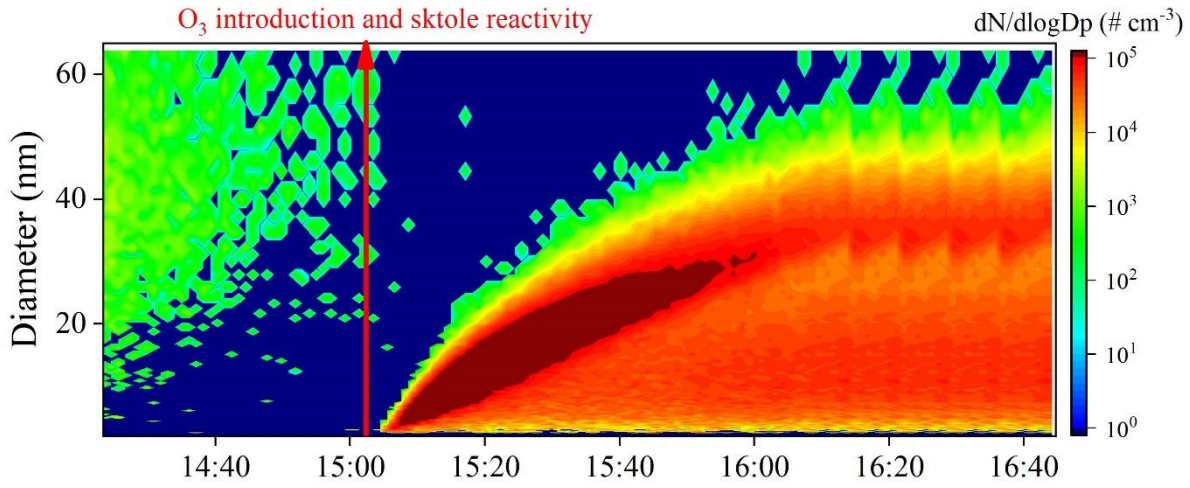

Figure 5.4 *Typical UDSS ozonolysis (from WWTP2) experiment. Temporal evolution of the particle number concentration and size distribution measured by SMPS. The ordinate represents the electrical mobility diameter (nm), and the colour scale represents the particle number concentration. The time of O_3 addition is indicated using vertical red line.*

Significant skatole emissions were also observed from digestate biowastes as displayed in **Figure 5.5**. The amount of SO_2 emitted from the sample was monitored during the experimental time and the maximum emitted amount was ~ 105 ppb (**Figure 5.5, b)**. After O_3 addition, the signal of skatole decreased and that of $C_8H_9NOH^+$ and $C_9H_9NO_2H^+$ increased

(**Figure 5.5, a)**. The particle number concentration reached a maximum of 10^4 particles cm^{-3} within few minutes of O_3 injection (**Figure 5.5, c)**. As shown in **Figure 5.5 (d)**, we monitored the particle number concentration and their size distribution at higher diameter ranged from 2 to 100 nm. The particles grew in size, while their number concentration remained constant thereafter or slightly decreased. This can be explained by the particle coagulation and condensation of semi-volatile compounds on the formed particles, leading to growth of particles into the chamber and a shift to larger diameters.

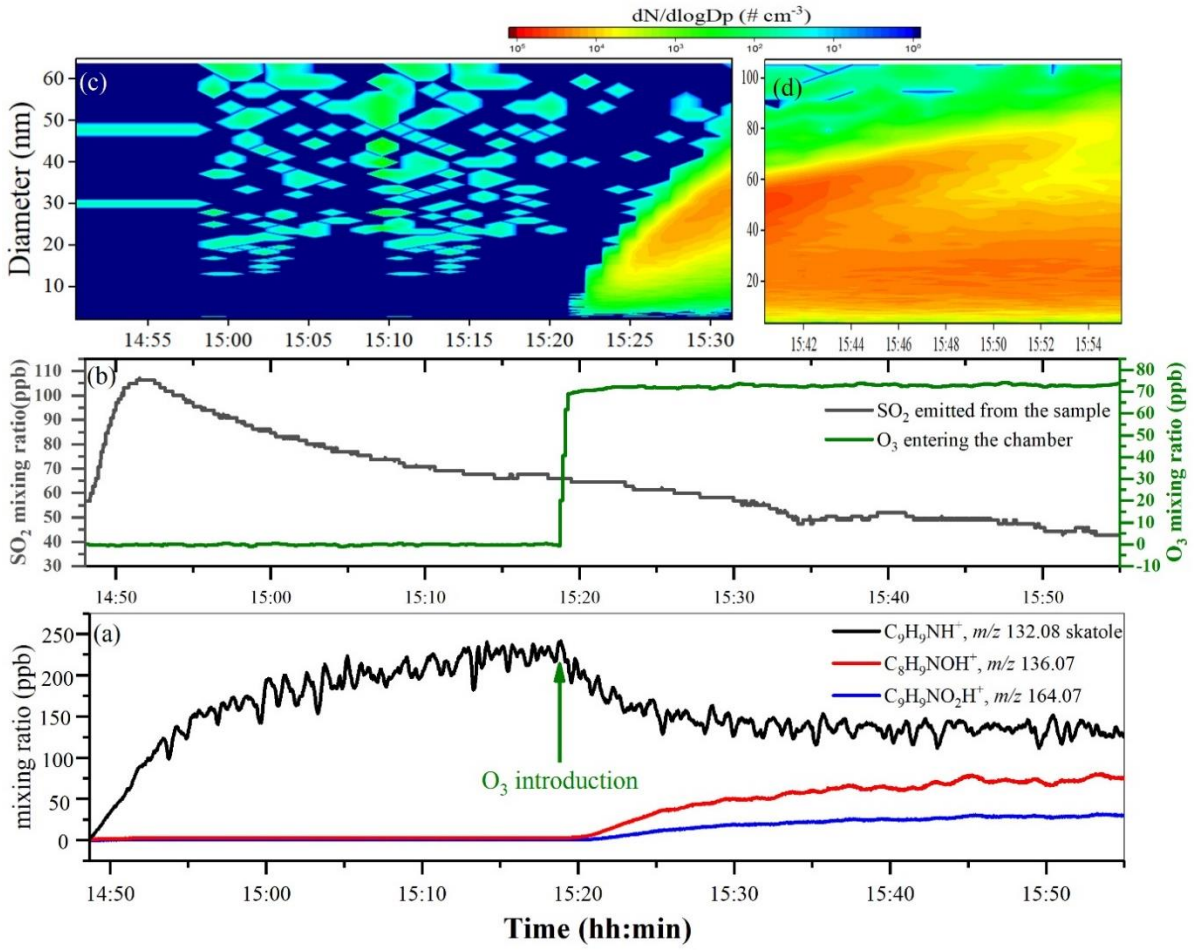

Figure 5.5 *Digestate biowastes ozonolysis experiment. (a) Temporal evolution of m/z 132.08 $C_9H_9NH^+$ (black line), m/z 136.07 $C_8H_9NOH^+$ (red line) and m/z 164.07 $C_9H_9NO_2H^+$ (blue line). The time of O_3 addition is highlighted by the vertical green line. (b) Temporal evolution of O_3 entering the chamber (green line, O_3 in) and SO_2 emitted by the sample (grey line). Temporal evolution of the particle number concentration and size distribution for particle diameter (c) 2-65 nm and (d) 3-103 nm. The ordinate represents the electrical mobility diameter (nm), and the colour scale represents the particle number concentration.*

5.3. New particle formation mechanism

5.3.1. Criegee ozonolysis

The ozonolysis of skatole proceeds via the Criegee mechanism which involves an initial addition of O_3 to the double bond and leads to a primary ozonide $C_9H_9NO_3$ (a molecule where the carbonyl oxide and carbonyl moieties are attached together as part of the same molecule) (**Figure 5.6**). The ozonolysis of endocyclic compounds can add several functional groups without loss of carbon number, leading to the formation of secondary ozonides, which have been shown to contribute significantly to SOA (Kroll & Seinfeld, 2008). The primary ozonide decomposes into stabilized Criegee intermediates either (i) by cleavage of the O-O bond proximal to the methyl group, or (b) by cleavage of the O-O bond distal from the methyl group (**Figure 5.6**). The first intermediate can proceed by hydrogen shift reactions to form ketonic hydroperoxides ($C_9H_9NO_3$) or can isomerize to form dioxirane ($C_9H_9NO_3$) (Donahue et al., 2011). The first Criegee intermediate can react with a carbonyl and form the secondary ozonide $C_9H_9NO_3$ (*m/z* 179.057) and then it can oxidize SO_2 and form the 2-acetyl phenyl formamide $C_9H_9NO_2$ (*m/z* 163.063) and SO_3 which hydrolyses to form H_2SO_4 (Mauldin et al., 2012). Sulphuric acid is a key atmospheric nucleation species (Boy et al., 2012). Mauldin et al., (2012) have shown that reactions of Criegee intermediates, formed due to alkene ozonolysis, with SO_2 can be significantly fast and lead to SO_3 formation.

The second intermediate can form aldehydic hydroperoxides or cyclizes to form secondary ozonide ($C_9H_9NO_3$, *m/z* 179.057) (**Figure 5.6**). Both intermediates can form a secondary ozonide via recyclization. The secondary ozonide can react with water to form a molecule possessing a carbonyl group and a hydroxy-hydroperoxide group ($C_9H_{11}NO_4$). The latter compound can lose H_2O_2 and form 2-acetyl phenyl formamide ($C_9H_9NO_2$, *m/z* 163.06). The oxidation of 2-acetyl phenyl formamide leads to oxocarboxylic acid, which has been detected in the aerosol chemical composition by L2MS (see below). Hydroxy-hydroperoxide group can also lose water, and thus 2-acetyl phenyl formamide is directly formed. Moreover, SO_2 can also partition into aerosols to form HSO_3^- (TOF-SIMS, see below), which can further react with organic peroxides generated by skatole ozonolysis. It is now well known that the oxidation of SO_2 by stabilized Criegee intermediates is the main source of atmospheric H_2SO_4 via SO_3 formation and hydrolysis (Mauldin et al., 2012).

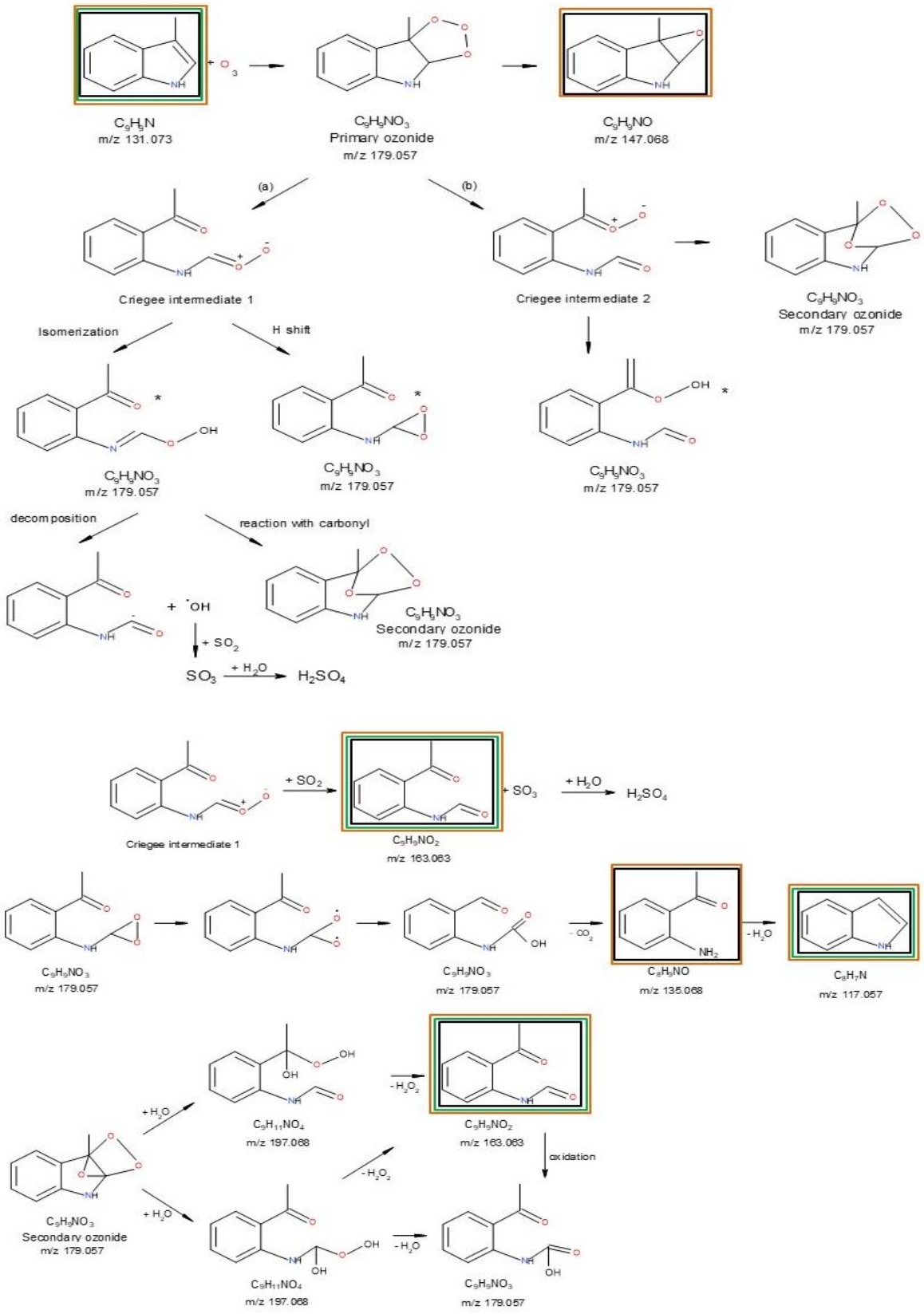

Figure 5.6 *Proposed ozonolysis mechanism of skatole. The compounds detected by PTR-QiTOF-MS are marked in black, those detected by TD-GC-MS in green and those detected by UPHLC-HRMS in orange (Ciuraru et al., 2021).*

The previous theoretical studies using computational methods at the quantum level helped to identify which species are the most favourable for nucleation formation (Radola et al., 2021). The results showed that the interaction of skatole with sulphuric acid is weak. Moreover, the oxidized $C_9H_9NO_2$ and $C_9H_9NO_3$ molecules are the main participants in the formation of critical nuclei with sulphuric acid in the atmosphere having thus a critical role in SOA formation (Radola et al., 2021). Thus, in VOC-rich environment, the oxidation of SO_2 by a stabilized Criegee intermediate is a significant source of atmospheric sulphuric acid (Boy et al., 2012). Based on the experiments and the theoretical calculations we propose that the oxidized reaction products together with SO_2 participate in the first step of the nucleation process.

5.3.2. Role of SO_2, RH and NH_3 in NPF

The proposed binary reaction mechanism which involves the organics and SO_2 via sulphuric acid formation has been supported by conducting an experiment on a commercially available skatole sample placed in the chamber. In this experiment, we tested the effect of SO_2, H_2O and NH_3 on the NPF. The results are illustrated in **Figure 5.7**. Following O_3 addition, a slight increase in $C_8H_9NOH^+$ and $C_9H_9NO_2H^+$ was detected, while no particle formation was observed. After SO_2 injection into the chamber, increase of $C_9H_7NOH^+$ and $C_8H_9NOH^+$, together with new particle formation were observed. Thus, this illustrates the role of SO_2 in the particle formation and demonstrates the proposed ozonolysis mechanism (**Figure 5.6**).

Sulphuric acid is identified as the major precursor vapour enhancing atmospheric NPF (Riccobono et al., 2012; Yao et al., 2018) due to its low vapour pressure, thus it is able to form small particles and condense onto them effectively. In addition, when H_2SO_4 is stabilized by a base, such as ammonia or amine, the rate of NPF is enhanced (Almeida et al., 2013; Kürten et al., 2016). Recently, low volatility highly oxygenated products have been found as oxidation products of many VOCs (Bianchi et al., 2019; Ehn et al., 2014). Those low volatility highly oxygenated products were discovered to contribute to particle formation and growth in the absence of H_2SO_4 under chamber experiments (Riccobono et al., 2012; Schobesberger et al., 2013). Thus, our obtained results showed the prompt of NPF event only with the addition of SO_2 into the chamber.

An additional argument for the fundamental role of SO_2 in the NPF process is that no particle formation was observed from cow manure samples. The ozonolysis experiment is illustrated in **Figure 5.8**. Following the sample introduction into the chamber, the signal of

skatole increased and reached a steady state then decreased after O_3 addition. The signals of $C_8H_9NOH^+$ and $C_9H_9NO_2H^+$ showed sharp increase within a few seconds of initial exposure of cow manure to O_3. Those two compounds in addition to skatole oxide ($C_9H_9NOH^+$, *m/z* 148.075) were also detected in the gas-phase sampled after O_3 addition and analyzed by TD-GC-MS. C_8H_9NO, C_9H_9NO and $C_9H_9NO_2$ were identified as 1-(2-aminophenyl) ethanone, 2,6-dimethylphenyl isocyanate and 2-acetyl phenyl formamide, respectively. The low SO_2 emissions (~ 4 ppb) (**Figure 5.8, b**) from the cow manure sample, compared with undigested sludge and digestate biowaste ones, thus explains the absence of NPF for this OWP.

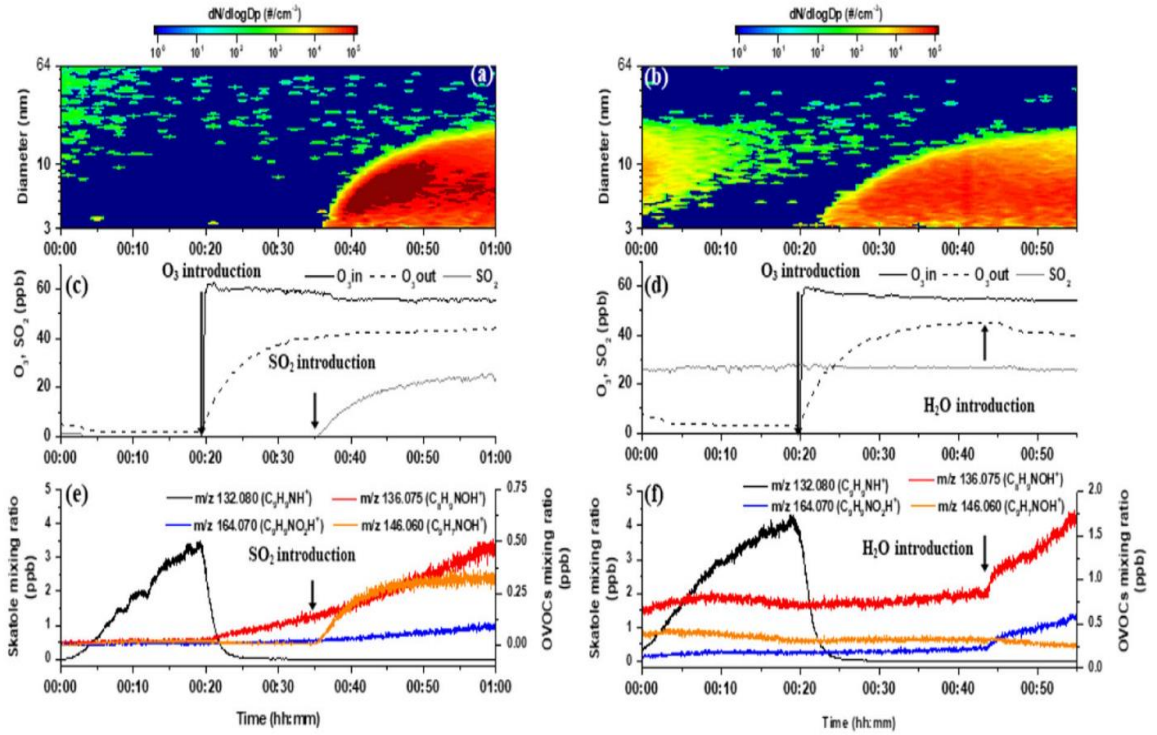

Figure 5.7 *Ozonolysis experiment of skatole. (a,b) Temporal evolution of particle number concentration and size distribution. (c,d) Temporal variation of SO_2 (grey line), ozone entering the chamber (black line) and ozone measured at the exit of the chamber (black dottet line). (e,f) Temporal evolution of skatole (black line, left axis), $C_8H_9NOH^+$ (m/z 136.08), $C_9H_7NOH^+$ (m/z 146.06, orange line) and $C_9H_9NO_2H^+$ (m/z 164.07, blue line). The tie of SO_2 an H_2O addition into the chamber are indicated using black vertical line (Ciuraru et al., 2021).*

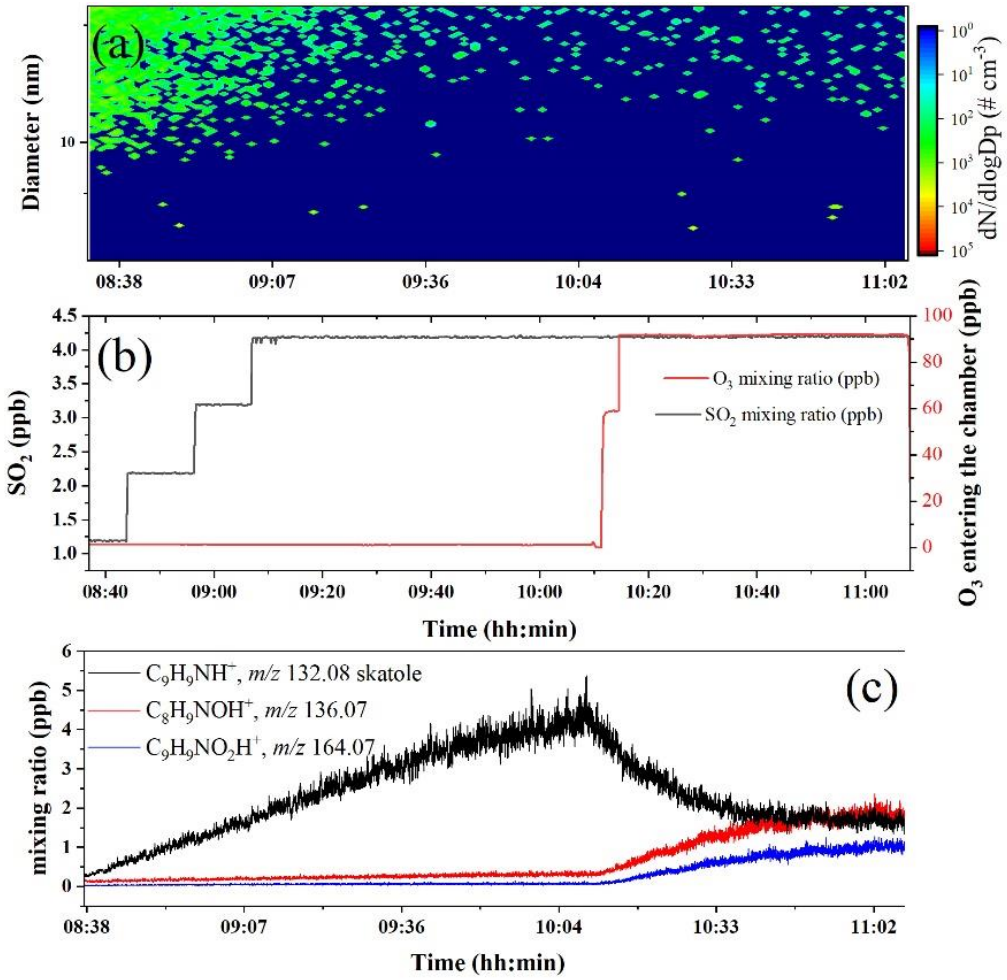

Figure 5.8 *Typical cow manure ozonolysis experiment. (a) Temporal evolution of the particle number concentration and size distribution. The ordinate represents the electrical mobility diameter (nm), and the colour scale represents the particle number concentration. (b) Temporal evolution of O_3 entering the chamber (red line, O_3 in) and SO_2 emitted by the sample (grey line). (c) Temporal evolution of m/z 132.08 $C_9H_9NH^+$ (black line), m/z 136.07 $C_8H_9NOH^+$ (red line) and m/z 164.07 $C_9H_9NO_2H^+$ (blue line).*

Finally, the impact of H_2O on NPF was also demonstrated by introducing water vapour into the chamber (from dry conditions to 90% RH). This led to a slight increase in $C_8H_9NOH^+$ and $C_9H_9NO_2H^+$ signals and a slight decrease in that of $C_9H_7NOH^+$, while no effect was observed on the NPF event and the particle number concentration. Similarly, the role of ammonia was tested and the results showed that it had no effect on NPF. The results of those experiments demonstrated that the NPF mechanism involves the nucleation initiated by sulphuric acid formed from the oxidation of SO_2 by stabilized Criegee intermediates.

5.4. Preliminary investigations on particle chemical composition

During this work, new particles formed as a result of UDSS ozonolysis were collected onto quartz-fiber filters for off-line mass spectrometric analysis (L2MS and SIMS). The mass of particles deposited onto the filters was estimated prior to off-line analysis. We calculated the maximum deposited mass assuming that the efficiency of collection was 100%. Taking into account the sampling time and the flow rate of the pump to which the sample holder was connected, we calculated the maximum mass that could be deposited on the filter by:

$$\text{max mass } (\mu g) = M\ (\mu g\ m^{-3}) * V\ (m^3)$$

$$\text{max mass } (\mu g) = M\ (\mu g\ m^{-3}) * T\ (min) * Q(L\ min^{-1}) \quad \textbf{(5.1)}$$

where *max mass* is the maximum mass that could be deposited on the filter (µg), *M* is the average total mass concentration of particles obtained from SMPS data (µg m^{-3}), *V* (m^3) is the sampled volume, obtained by multiplying the time of collection *T* (min) by the flow rate *Q* of the pump (L min^{-1}). **Table 5.2** summarizes the results for the five filters collected from UDSS NPF experiments. Assuming that we have a uniform deposition of the particles on the filter surface (area of $1.54*10^{-4}$ m^2), we can calculate the amount of particulate matter probed by the laser spot (which has a diameter of 530 µm, i.e. an area of $0.22*10^{-6}$ m^2) using equation **5.2.**

$$\text{Amount of matter probed by the laser} = \frac{\text{total mass of particles} * \text{area of laser spot}}{\text{Filter surface area}} \quad \textbf{(5.2)}$$

Table 5.2 *Calculation of maximum mass of particles deposited on the filters (assuming a collection efficiency of 100%) and calculation of the particle mass available per laser spot.*

Ozonolysis experiment	Sample	Chamber volume (L)	T (min)	Q (L min^{-1})	Total mass concentration (µg m^{-3})	Max mass (ng)	Mass per laser spot (pg)
UDSS WWTP1	F1	30	255	3.3	2.9	2240	3200
	F2	30	52	3.3	2.9	478	683
UDSS WWTP2	F3	30	181	2	0.12	43	61
	F4	180	131	3	0.14	55	79
	F5	180	300	3	0.33	297	424

The results reported in **Table 5.2** show (maximum) laser probed PM mass in the pg range. The L2MS technique was already proved to reach sub-femtomole (i.e. sub-pg for the molecules addressed here) limit of detection (LOD). However this was obtained on PAH detection

through a resonant two-photon ionization mechanism (Faccinetto et al., 2015). Here the probed molecules are different, which might turn their detection (for such low amounts of deposited matter, particularly for the F3, F4 and F5 filters) into a challenging task.

We first performed L2MS analysis for newly formed particles collected onto F1 and F2 using the readily available 266 nm ionization wavelength. The L2MS spectra obtained are illustrated in **Figure 5.9** (Ciuraru et al., 2021). We detected a high number of oxidized and bifunctional species on the filter-sampled particles. Using L2MS analysis, we revealed the formation of oxidized compounds not detected in the gas phase by PTR-QiTOF-MS or GC-MS.

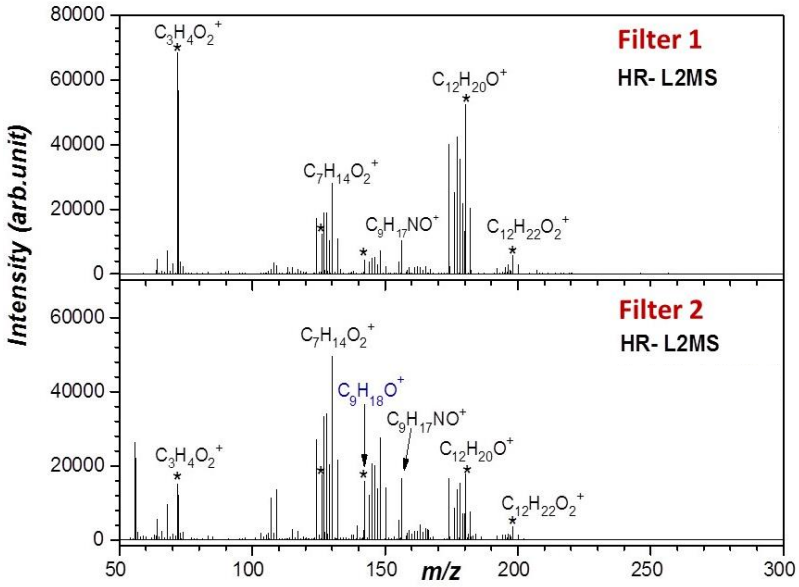

Figure 5.9 *L2MS spectra of the newly formed particles collected onto quartz-fiber filters (Filter 1, top and Filter 2 bottom).The peaks used for the mass calibration are marked using stars (Ciuraru et al., 2021).*

The observed compounds by L2MS were classified into different groups: a first group of compounds containing the carbon skeleton of skatole with inserted oxygen atoms (e.g., C_9H_9NO, $C_9H_9NO_2$, $C_9H_9NO_3$), a second group resulting from ring opening showing the successive oxidation processes (e.g., $C_9H_{17}NO$, $C_{11}H_{22}NO_2$), a third group with oxygen attached to the six-member ring (e.g., $C_8H_{13}NO_2$), and a fourth group with nitrogenated compounds (e.g., $C_9H_9N_2$, $C_{11}H_{20}N_2$, $C_{14}H_{21}N_2$). Multiple ozonolysis reactions are possible due to the presence of multiple double bonds in skatole and this could explain the growing of SOA. The reaction products might continue to evolve chemically and lead to a decrease in volatility and rapid partitioning to the particulate phase. Using L2MS and UHPLC-HRMS, we detected

2-acetyl phenyl formamide ($C_9H_9NO_2$) in the particulate phase as it was also detected in the gas phase after ozonolysis using PTR-QiTOF-MS and TD-GC-MS measurements.

In this work, we proposed a Criegee mechanism in which the SO_2 emitted by OWP samples reacts with Criegee intermediates and produces sulphuric acid. In order to confirm this, chemical analysis of the newly formed aerosols collected onto quartz-fiber filters was also performed using SIMS in negative ion polarity. The results displayed in **Figure 5.10** show the presence of characteristic H_2SO_4 peaks such as SO_3^- and HSO_4^-. In addition, those two ions (SO_3^- and HSO_4^-) have been detected in the SS bulk samples analyzed by SIMS, as illustrated in **Figure 5.11**. In the present study, no sulphur organic compounds were detected, but the possibility of organosulphates fragmentation in SIMS contributing to the observed SO_3^- signal cannot be excluded.

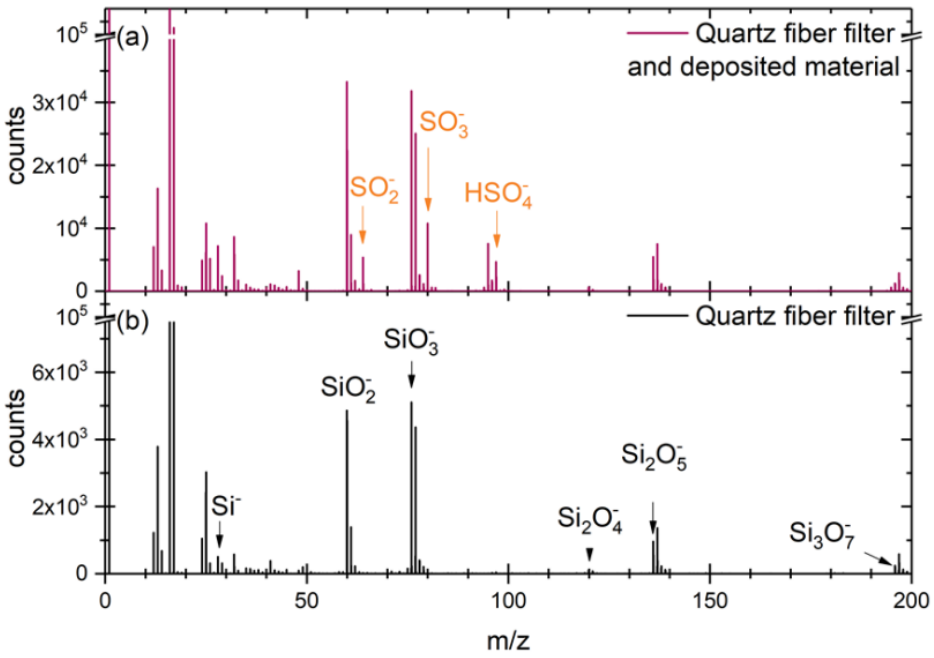

Figure 5.10 *(a) Negative SIMS spectrum of the SOA deposited onto QFF. The spectrum of a blank QFF (b) is given for comparison (Ciuraru et al., 2021).*

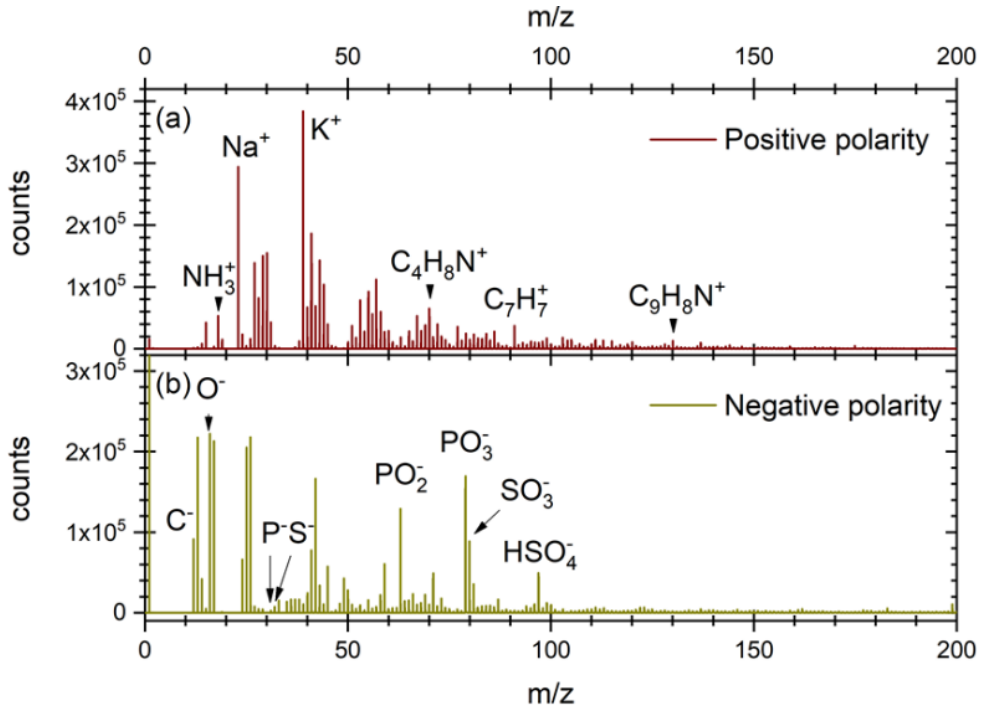

Figure 5.11 *SIMS spectra of bulk SS in positive (a) and negative (b) ion polarities. $C_9H_8N^+$ corresponds to a skatole fragment and is detected along with other nitrogenated fragment ions. Sulphate and phosphate ions are detected in negative polarity (Ciuraru et al., 2021).*

The L2MS analyses performed to date on the F3, F4 and F5 filters were unsuccessful. This is probably due to the low amount of deposited material available per laser spot, as explained above, which would in turn give a LOD for the addressed molecules in this desorption/ionization L2MS configuration in the range of few fmol per laser shot. Further efforts are envisaged by changing the ionization mechanism through the use of VUV wavelengths (157 nm and 118 nm) already available in the PhLAM Laboratory.

5.5. Conclusions

The temporal evolution of VOCs emitted from various OWP samples placed in the atmospheric chambers was monitored. Thus, in this work, we focused on VOCs that showed significant reactivity to O_3 or formed as a result of ozonolysis. Among all the detected VOCs, only skatole signal decreased following the O_3 addition into the chamber.

Significant skatole emissions were observed from the undigested sludge, cow manure and digestate biowastes. Extremely low emissions of skatole were observed from other types of SS (DSS, SS 30% and SS 60%) and animal manure (horse, sheep and goat manures). Following the O_3 introduction into the chamber, skatole showed a significant reactivity to O_3, as the signal decreased within few seconds of O_3 addition. The ozonolysis of skatole resulted

in the formation of various reaction products observed in the gaseous and particulate phases. Among them, we identified the 2-acetyl phenyl formamide as the main skatole ozonolysis product.

New particle formation events were observed following the ozonolysis of undigested sludge and digestate biowaste samples only. Accordingly, in this work, we have proposed a Criegee mechanism of the new particle formation following skatole ozonolysis and formation pathways of 2-acetyl phenyl formamide. This mechanism involves indoles (i.e. skatole) of agricultural origin. Also, we showed the oxidation of SO_2 by stabilized Criegee intermediates as the main source of atmospheric H_2SO_4 via SO_3 formation and hydrolysis.

We performed a study on a commercially available skatole sample to verify the Criegee mechanism and to test the effect of SO_2, H_2O and NH_3. Our obtained results showed the prompt of NPF event only with the addition of SO_2 into the chamber which demonstrated the proposed Criegee ozonolysis mechanism. In addition, the fundamental role of SO_2 in the NPF process was investigated by cow manure ozonolysis, which showed no NPF event following skatole ozonolysis. This was explained by the very low amount of SO_2 compared to undigested sludge and digestate biowaste samples.

The newly formed particles were collected onto filters for off-line mass spectrometric (L2MS and SIMS) analysis. We detected a high number of oxidized and bifunctional species on the filter-sampled particles formed from the ozonolysis of undigested sludge (WWTP1). Different groups of compounds were detected using L2MS (e.g., C_9H_9NO, $C_9H_9NO_2$, $C_9H_9NO_3$, $C_{11}H_{22}NO_2$, $C_8H_{13}NO_2$, $C_{14}H_{21}N_2$, etc.). Beside L2MS analysis, we analyzed the deposited aerosols using SIMS. We observed the presence of characteristic H_2SO_4 peaks such as SO_3^- and HSO_4^- peaks. Therefore, our obtained SIMS results serve as an additional argument for the proposed Criegee mechanism in which the SO_2 emitted by OWP samples reacts with Criegee intermediates and produces sulphuric acid. We also performed some preliminary tests for the aerosols formed from UDSS (WWTP2) ozonolysis; however, no results were obtained from L2MS analysis. Further efforts are needed to optimize the ionization scheme and also to design a sampling system for improved SOA collection and define appropriate sampling parameters (details in **Chapter 6**).

Conclusions and perspectives

Chapter 6

General discussion, conclusions and perspectives

This Chapter is divided into two main sub-Chapters: (i) general discussion and conclusions, where we summarize the main results of our work and the major advances related to this PhD thesis; we merged all our results in a unique dataset to give a complete overview of the main outcomes of this thesis, and (ii) several perspectives in view of the scientific literature available to date.

6.1. General discussion and conclusions

The main objectives of this PhD work were to identify and quantify the VOC emissions from OWPs and to study their ozone reactivity and NPF. Accordingly, this research was structured into two main topics. The first topic is related to the characterization of VOCs emitted by different types of OWPs. The combination of various mass spectrometric techniques and advanced statistical tools in this work resulted in a comprehensive identification and quantification of a large number of VOCs. The measurements of VOCs emitted from OWPs are essential to better understand the formation and fate of SOA from agricultural practices (OWP recycling). For this reason, the second part of the thesis is dedicated to study the reactivity of the VOCs emitted from OWP samples toward ozone and elucidate the new particle formation mechanisms. We recently published a study that demonstrated the NPF from organic gas precursor (i.e. skatole) and SO_2, both emitted from sewage sludge (SS) samples. The experiments performed during this PhD thesis are summarized in **Table 6.1**. The description is given based on the structure of this manuscript, where the results on VOC analyses were given in **Chapters 3** and **4**, while those for SOA formation were presented in **Chapter 5**.

Conclusions and perspectives

Table 6.1 *Summary of the experiments performed during this PhD thesis.*

Chapter title	Site	Experimental conditions	Number of samples (N) and replicates (R)	VOC emissions analysis	Type of OWPs	Measurements
Chapter 3 - Chemical identification and quantification of volatile organic compounds emitted by sewage sludge	Waste water treatment plant in France	Simulation chamber under controlled laboratory conditions	N = 4 R= 3	• Total VOC mass concentration • Total VOC emission flux • DBE analysis • PCA • Volcano plot	• UDSS • DSS • SS 30% dryness • SS 60% dryness	VOCs: PTR-QiTOF-MS
Chapter 4 - Online and offline chemical characterization of volatile organic compounds emitted by animal manure	Farm located in Grignon	Simulation chamber under controlled laboratory conditions	N = 4 R= 3	• Total VOC mass concentration • Total VOC emission flux • DBE analysis • PCA	• Cow manure • Horse manure • Sheep manure • Goat manure	VOCs: PTR-QiTOF-MS and TD-GC-MS
Chapter 5 - Organic waste products: reactivity of volatile organic compounds toward ozone and secondary organic aerosol formation	France	Simulation chamber under controlled laboratory conditions	N = 9 R = 3	• Total VOC emission flux • Temporal evolution of VOCs • Reactivity of VOCs to ozone	• Sewage sludge • Animal manure digestate biowaste	VOCs: PTR-QiTOF-MS and TD-GC-MS (animal manure) Particles: SMPS, L2MS and SIMS

6.1.1. Chemical identification and quantification of VOCs emitted by OWPs

Various SS samples collected at different stages of treatment from a WWTP located in France were analyzed (UDSS, DSS, SS 30% and SS 60% of dryness). The detailed analysis and obtained results were described in **Chapter 3** of this manuscript. In addition, the VOC emissions from different animal manure samples collected from a farm located in Grignon, France were measured. Moreover, the VOC emissions form digestate biowastes were analyzed and the results are briefly summarized here. The sample to be analyzed was spread on a stainless steel plate (0.14 or 0.32 m^2 surface area) and placed in an atmospheric simulation chamber (0.03 or 0.18 m^3). The identification of VOCs was performed based on mass spectrometric techniques such as PTR-QiTOF-MS and TD-GC-MS. TD-GC-MS was performed only for animal manure samples. The assignment of the detected mass peaks to known molecules was cross-validated according to the literature. The quantification and the calculation of VOC emission fluxes were done based on PTR-QiTOF-MS analysis. The comparison between samples was based on the emission fluxes of the compounds taking into account the airflow rate through the simulation chamber and the mass concentration of the emitted VOC.

A dataset consisting of gas-phase emissions as a function of time was obtained for each sample by PTR-QiTOF-MS. The PTR mass spectra obtained were treated following the methodology described in **Chapter 2** of the manuscript. The vast majority of the detected peaks (> 90%) was assigned to suitable molecular formulas. **Table 6.2** shows the main results of PTR-QiTOF-MS analysis. This study showed that SS, animal manure and digestate biowaste samples emitted a large spectrum of VOCs where 380, 385 and 221 compounds were assigned and quantified, respectively. Among the SS samples, UDSS showed the highest emission of VOCs (i.e. 233 VOCs), while sheep manure showed the highest emission among the animal manure samples (i.e. 254 VOCs).

The assigned VOCs were classified into different chemical families: hydrocarbons, oxygenated, sulphuric, nitrogenated, and “other” compounds (containing distinct heteroatoms in the molecular formula). Two halogenated compounds were detected only in animal manure samples using PTR-QiTOF-MS ($C_7H_6OCl_2$ and $C_7H_5OCl_3$). The number of compounds assigned to each chemical group is shown in **Table 6.3**. The distribution of VOC chemical groups varied among the analyzed samples.

Table 6.2 *PTR-QiTOF-MS results for OWP samples. The numbers in bold correspond to the total number of assigned VOCs in each sample.*

OWP type	Sample name	# of detected peaks	# of assigned peaks	# of unassigned peaks	# of peaks corresponding to VOCs
Sewage sludge (SS)	UDSS	305	285	20	**233**
	DSS	287	259	28	**193**
	SS 30%	331	286	45	**192**
	SS 60%	303	275	28	**186**
Animal manure	Cow	255	233	22	**224**
	Horse	243	235	8	**233**
	Goat	274	258	16	**254**
	Sheep	276	262	14	**257**
Food biowaste	Digestate biowaste	280	245	35	**221**

Table 6.3 *The distribution of compounds identified by PTR-QiTOF-MS among chemical families in the studied samples. The total number of assigned compounds is bolded.*

OWP type	Sample name	VOCs	HC	Oxygenated compounds	Nitrogenated compounds	Sulphuric compounds	Other compounds
Sewage sludge (SS)	UDSS	**233**	57	73	26	11	66
	DSS	**193**	74	52	11	7	49
	SS 30%	**192**	85	43	12	15	37
	SS 60%	**186**	87	43	9	9	38
Animal manure	Cow	**224**	39	70	40	8	66
	Horse	**233**	44	79	36	5	67
	Goat	**254**	43	87	47	3	73
	Sheep	**257**	42	90	37	3	84
Food biowaste	Digestate biowaste	**221**	39	73	34	18	57

The total emission flux of all assigned VOCs in each sample was calculated. **Figure 6.1** shows the total emission flux of the identified classes of VOCs in OWP samples. Digestate biowastes showed the highest VOC emission flux (737 ± 242 µg m^{-2} min^{-1}), followed by SS samples (659 ± 150 µg m^{-2} min^{-1}) and animal manure (154 ± 47 µg m^{-2} min^{-1}). SS samples were characterized by the highest emission flux of HC (451 ± 74 µg m^{-2} min^{-1}). Digestate biowaste showed the

highest emission flux of oxygenated VOCs with 626 ± 465 µg m^{-2} min^{-1} (OVOC, mainly ethanol, butanone, acetone, cresol, methanol, etc.). Nitrogenated compounds with 229 ± 207 µg m^{-2} min^{-1} (mainly skatole, trimethylamine, etc.), followed by HC with 123 ± 53 µg m^{-2} min^{-1} (C_6H_8, C_4H_6, monoterpenes, etc.), were also found in digestate biowastes. We also detected sulphur compounds that showed the highest emission from SS samples with 47 ± 18 µg m^{-2} min^{-1} (mainly DMS, DMDS and methanethiol), followed by animal manure with 2.9 ± 0.5 µg m^{-2} min^{-1} and digestate biowastes with 0.11 ± 0.04 µg m^{-2} min^{-1}. Volatile sulphur compounds must be integrated to odor and chemical monitoring as they are toxic even at low concentrations (Rosenfeld et al., 2007). In addition, sulphur compounds emitted from OWPs such as SS, animal manure and food wastes showed the highest contribution to odor (Ni et al., 2015; Rincón et al., 2019a; Yuan et al., 2017). Nie et al., (2019) showed elevated emissions of sulphur compounds such as DMS, DMDS, methanethiol and ethanethiol from SS samples analyzed at different processing units of composting plant, as in the case of our SS samples compared to other OWPs.

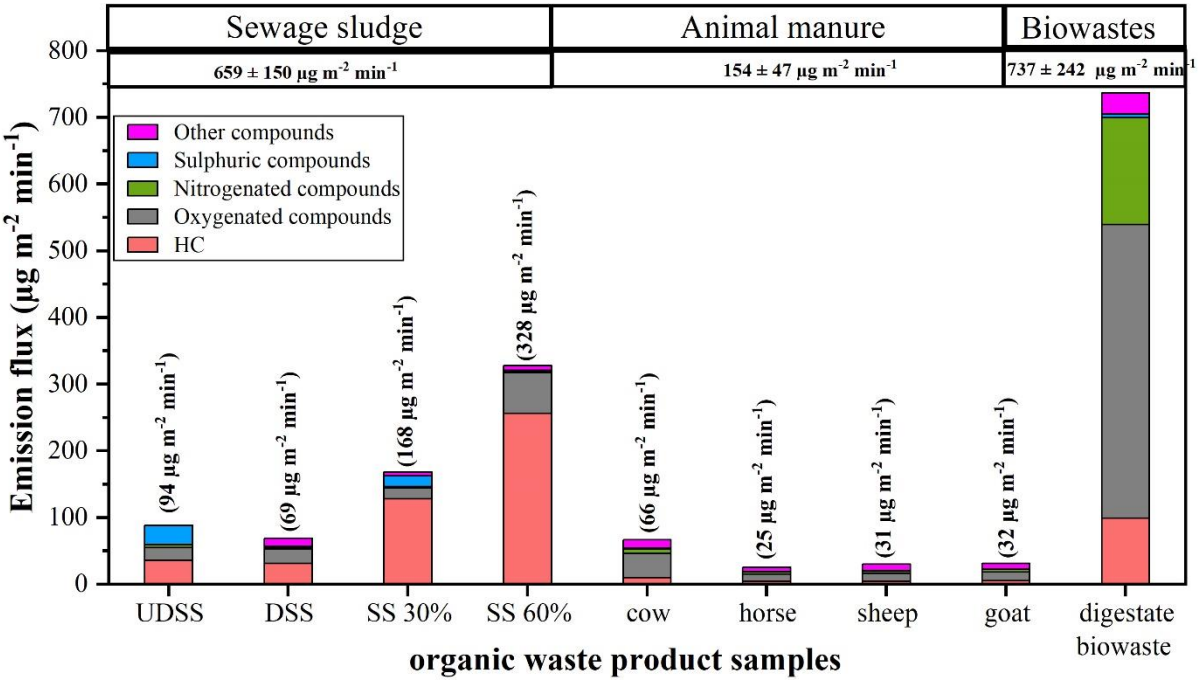

Figure 6.1 *Average emission fluxes of VOC chemical classes detected in each OWP sample. The number given in parentheses is the total emission flux of all assigned VOCs in each sample.*

The difference between the VOC distributions and fluxes among the samples is explained by their chemical composition. This is related to the source of the sample as animal-based organic wastes (e.g., manure) and urban wastes (e.g., SS and food biowaste) described in Section 1.4.1. A significant difference between the anaerobically digested samples (DSS vs.

digestate biowastes) in terms of the number of assigned VOCs (193 for DSS and 221 for digestate biowastes) and the total emission flux of VOCs with 69 ± 25 and 737 ± 242 µg m^{-2} min^{-1}, respectively, was observed. Thus, the chemical composition of gas emission from different OWP samples varied considerably depending on the sample nature. A similar aspect was observed by Rincón et al., (2019) when performing the chemical characterisation of gas emissions released during the composting of solid wastes and digestate. The samples analyzed in that work were: agricultural wastes, biowastes, green wastes, SS and municipal solid, and the main outcomes were illustrated in **Figure 1.6**. In general, terpenes and oxygenated compounds (alcohols, esters and ketones) contributed considerably to the total emission flux of samples that contain food stock such as digestate biowaste. A similar aspect was found in food waste samples analyzed at a full-scale food waste treatment plant in China (Ni et al., 2015). The authors showed that oxygenated VOCs, particularly ethanol, were the most abundant compounds in food wastes. The authors also showed significant contribution of terpenes to total VOC amount (Ni et al., 2015). This is consistent with our results where the digestate biowastes showed the highest emission of oxygenated compounds (such as aldehyde, ketones, etc.). In contrast, emissions from SS samples were mainly composed from HC and sulphur compounds. Animal manure samples were characterized by very low emissions of VOCs compared to other types of OWPs. In those samples, the most emitted VOCs were OVOCs (e.g., ethanol, acetone, cresol, acetic acid, acetaldehyde, phenol, hexanoic acid, isobutyric acid, isovaleric acid, etc.) followed by other compounds with distinct heteroatoms, nitrogenated compounds (dimethylamine, trimethylamine, etc.). In addition, several aromatic compounds (phenol, indoles and skatole), terpenes (isoprene, D-limonene, 3-carene, sesquiterpenes, etc.), and halogenated compounds were found in this work.

To the best of our knowledge, this is the first study where the DBE method is applied to PTR mass spectra. We have demonstrated the efficiency of this method to simplify the analysis of a complex mixture through classification. The large family of HC is classified into different classes of compounds, e.g., aliphatic (linear alkenes or alkynes), alicyclic (cycloalkanes, cycloalkenes, or cycloalkynes), aromatic (benzene and its derivatives) and terpenes. The emission fluxes of the HCs detected using PTR-QiTOF-MS and assigned to classes through DBE analysis were therefore estimated, as illustrated in **Figure 6.2**.

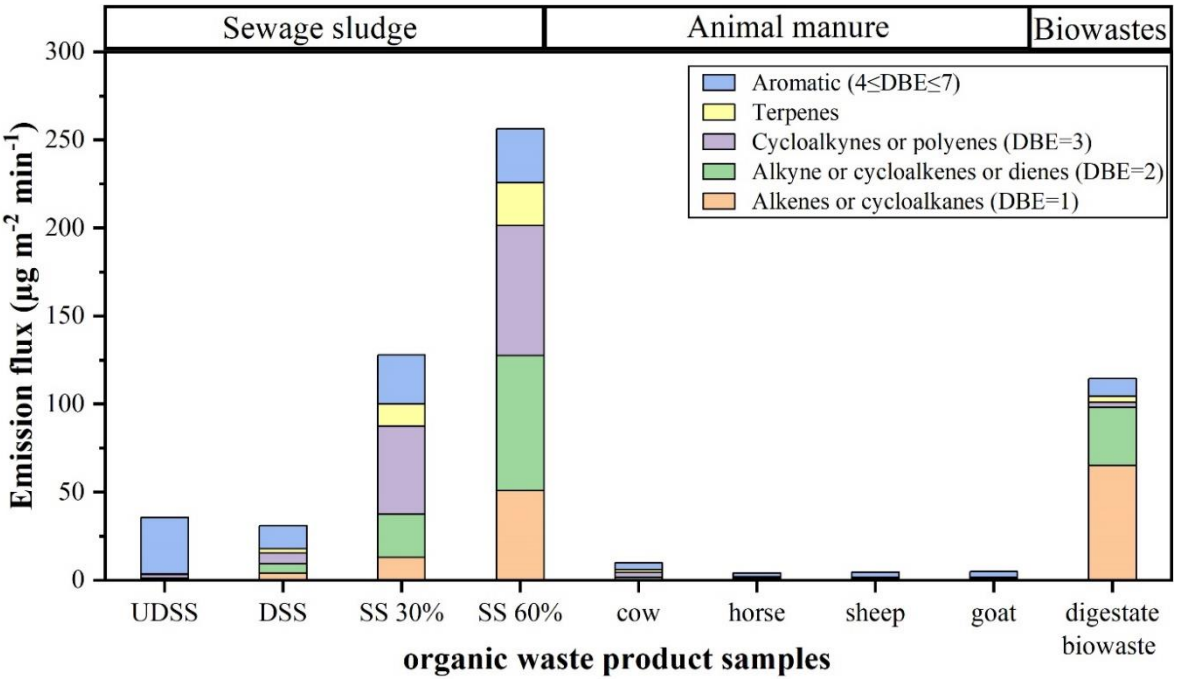

Figure 6.2 *Total emission fluxes of HC classes assigned by DBE for the studied OWP samples.*

UDSS showed the highest emission flux of aromatic compounds such as benzene, toluene, ethylbenzene, etc. Alkenes or cycloalkanes were highly emitted from digestate biowastes followed by SS 60% dryness. Terpenes were highly emitted from dewatered sludge (SS 30% and SS 60%) followed by digestate biowastes while their emissions from UDSS, DSS and animal manure samples were very low. Rincón et al., (2019) showed elevated emissions of terpenes (21-90%) from samples with lignocellulosic content such as biowastes and green wastes, while they varied from 0.07% - 21% of the total mass concentration from samples characterized by a reduced content of vegetal materials, such as pig slurry, turkey manure and solid fraction of anaerobically digested pig slurry and SS. Our results obtained for SS and the anaerobically digested biowastes are consistent with those obtained by Rincón et al., (2019).

We also addressed in this work the impact of the treatment stage of SS samples on their VOC emissions. The total number of VOCs decreased after anaerobic digestion and dewatering had little impact. This impact was also observed on the number of emission tracers, where UDSS showed the maximum number (93) compared with the anaerobically digested and dewatered samples. Our results showed that anaerobic digestion decreased the VOSC emissions (e.g., DMS, DMDS and methanethiol). Similarly, these emissions decreased after dewatering to higher degrees of dryness (e.g., 60%). Thus, anaerobic digestion and dewatering to higher degrees of dryness showed a positive impact in decreasing the potential emissions of VOSC. In addition, the total VOC emissions were reduced with the decrease in dry matter and

organic matter content of the sample. Anaerobic digestion processes break down the chemical compounds to produce HC (Du & Parker, 2012), this might explain the increased number of assigned HC and emission fluxes from dewatered sludge compared to other SS samples. The comparability of SS emissions at different treatment stages helps identify the impact of sludge treatment at WWTPs on VOC emissions.

6.1.2. C-VOCs fluxes calculation

The assigned VOCs in each sample (**Table 6.2**) were taken into account for the C-VOCs emission flux calculations. Based on the molecular assignments of the detected masses, $F_{C\text{-}VOC}$ (µg s^{-1} m^{-2}) is calculated using the following equation (Potard et al., 2017):

$$F_{C\text{-}VOC} = \frac{Q}{A} * m_{VOC} * R * \frac{Mc}{Vm} \quad \textbf{(6.1)}$$

where m_{VOC} is the mixing ratio of the VOC (in ppbv) calculated using PTR-QiTOF-MS, Q is the flow rate of dry air into the chamber (m^3 s^{-1}), A is the sample surface area (m^2), M_C is the molecular weight of carbon (28.0101 kg $kmol^{-1}$), V_m is the molar gas volume of 23.233 m^3 $kmol^{-1}$ at 1013.25 hPa and 283 K (10 ^{0}C) and R is the number of carbon atoms associated with the VOC. As we did three experiments for each OWP sample, the average C-VOCs emission flux was calculated for each sample. The results are illustrated in **Figure 6.3**. For SS samples, the C-VOC fluxes varied from 7630 – 39000 µg of C-VOCs h^{-1} m^{-2}. The highest C-VOC fluxes were emitted from the dewatered samples with a high degree of dryness (i.e. SS 60%), followed by SS 30% (19630 µg of C-VOCs h^{-1} m^{-2}), UDSS (9417 µg of C-VOCs h^{-1} m^{-2}), and anaerobically digested sludge (DSS, 7633 µg of C-VOCs h^{-1} m^{-2}). This trend of C-VOC fluxes could be explained by the dry matter and organic carbon content of the sample. The digestate biowaste samples showed the highest C-VOC fluxes among the analyzed OWP samples of 74520 µg of C-VOCs h^{-1} m^{-2} which is almost double that of SS 60%. Animal manure samples showed low C-VOC fluxes compared to other samples, in the range 2268 – 6080 µg of C-VOCs h^{-1} m^{-2}. In this work, we calculated the C-VOC fluxes for all emitted compounds by each samples (e.g., 233 VOCs emitted by UDSS). Thus, our values are much higher than those reported by Potard et al., (2017) where the authors calculated the C-VOCs fluxes for only 10 VOCs emitted from soil amended with pig slurry and methanized pig slurry. The soil VOC emissions were monitored just before and up to 64 days following the amendment. Their results showed that C fluxes varied from 12 to 76 µg of C-VOCs h^{-1} m^{-2} from the unamended soil (that is considered as control). The amendment of soil with pig slurry and methanized pig slurry affected the soil VOC emissions. The soil amended with methanized pig slurry showed a

reduction in the C-VOCs fluxes by half compared to the control sample, while the soil amended with pig slurry showed higher C-VOCs fluxes. The latter showed a significant increase in the C-VOCs fluxes of 174 µg of C-VOCs h^{-1} m^{-2} after 3 to 36 days following the soil amendment with pig slurry and then decreased down to less than 12 µg of C-VOCs h^{-1} m^{-2} after 64 days of amendment. The authors explained this increase by the high emission fluxes of methanol (Potard et al., 2017). The values obtained in our study are much higher as the OWP samples were analyzed in a concentrated chamber that could explain the elevated emissions compared to the fluxes measured from a soil amended with OWP in a field up to 64 days after the spreading (Potard et al., 2017).

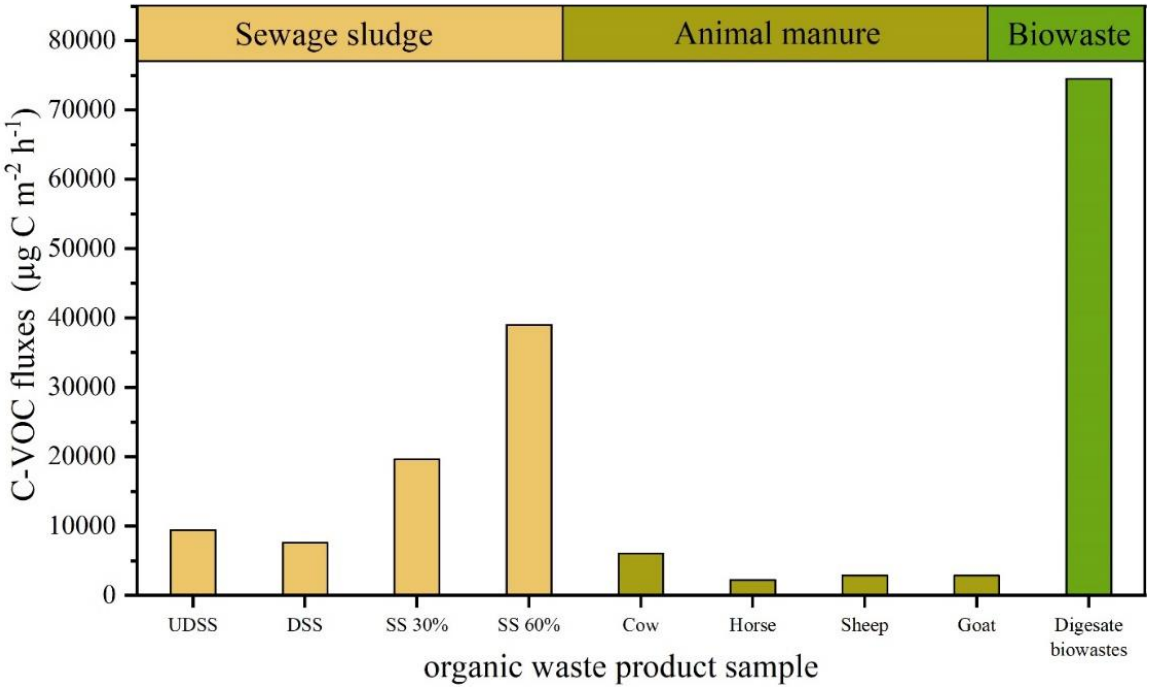

Figure 6.3 *Average carbon-VOC fluxes emitted by different OWP samples analyzed using atmospheric simulation chambers.*

6.1.3. Secondary organic aerosol formation from OWPs

The second topic of this PhD thesis focused on the NPF from OWP ozonolysis. First we performed a study to investigate atmospheric particle formation from oxidized organic molecules and SO_2, both emitted by undigested SS samples (Ciuraru et al., 2021). We extended this study to several types of OWPs. Along this PhD thesis, we presented the results of comprehensive laboratory measurements on different types of SS samples, animal manures and digestate biowastes. **Figure 6.4** summarizes the results obtained in this work. Our results showed that skatole was significantly emitted from undigested sludge, cow manure and digestate biowastes. However, only the undigested sludge and the digestate biowastes

contributed to NPF due to the significant emissions of SO_2, which is not the case of cow manure.

The ozonolysis of skatole emitted by OWP samples led to particle nucleation and growth in the presence of SO_2. We have recently published the binary reaction Criegee mechanism that involves the organics (i.e. skatole) and SO_2 via sulphuric acid formation (Ciuraru et al., 2021). This was the first study that estimated the SOA formation from OWP recycling in the agricultural sector. In this work, we identified the compound 2-acetyl phenyl formamide as the main skatole ozonolysis product and its formation pathways have been proposed (**Chapter 5**). Criegee mechanism involves skatole of agricultural origin. Also, we showed the oxidation of SO_2 by stabilized Criegee intermediates as the main source of atmospheric H_2SO_4 via SO_3 formation and hydrolysis. The fundamental role of SO_2 in the NPF process was demonstrated by experiments performed on pure skatole, in addition to the cow manure samples that showed no particle formation due to very low emissions of SO_2. The ozonolysis of OWP samples, therefore, provides observational evidence of the involvement of skatole emitted by OWP in particle formation. Finally, we also mention that high nucleation rates were observed under low ammonia concentrations. This study showed that indoles, and more specifically skatole, together with SO_2 emitted from OWP samples, are the species pertinent to initiating reactions with O_3, leading to particle nucleation and growth events.

Table 6.4 *Summary of skatole emissions and ozonolysis experiments performed on different OWP samples.*

OWP type	Name of sample	Skatole emissions	SO_2 emissions	NPF event
SS from WWTP1	Undigested SS	+++	+++	observed
SS from WWTP2	UDSS	++	+++	observed
	DSS	-	+	not observed
	SS 30%	+	+	not observed
	SS 60%	+	+	not observed
Animal manure	Cow	++	+	not observed
	Horse	+	+	not observed
	Sheep	+	+	not observed
	Goat	+	+	not observed
Food biowaste	Digestate biowastes	++++	++++	observed

-: no emissions / +: very low emissions / ++: moderate emissions / +++: high emissions / ++++: very high emissions.

To verify the emission of skatole over a long period of time, an experiment was performed over a continuous 24 hr for undigested SS. The results are displayed in **Figure 6.4**. Following the sample introduction into the chamber, a strong burst release of skatole was observed reaching a maximum of 12.3 ppb. The signal slightly decreased and then stabilized around 9 ppb for 24 hr. Our findings, therefore, showed the long-time of skatole emissions that could last for hours after OWP spreading. Skatole is shown as a significant potential contributor to the NPF under atmospheric conditions.

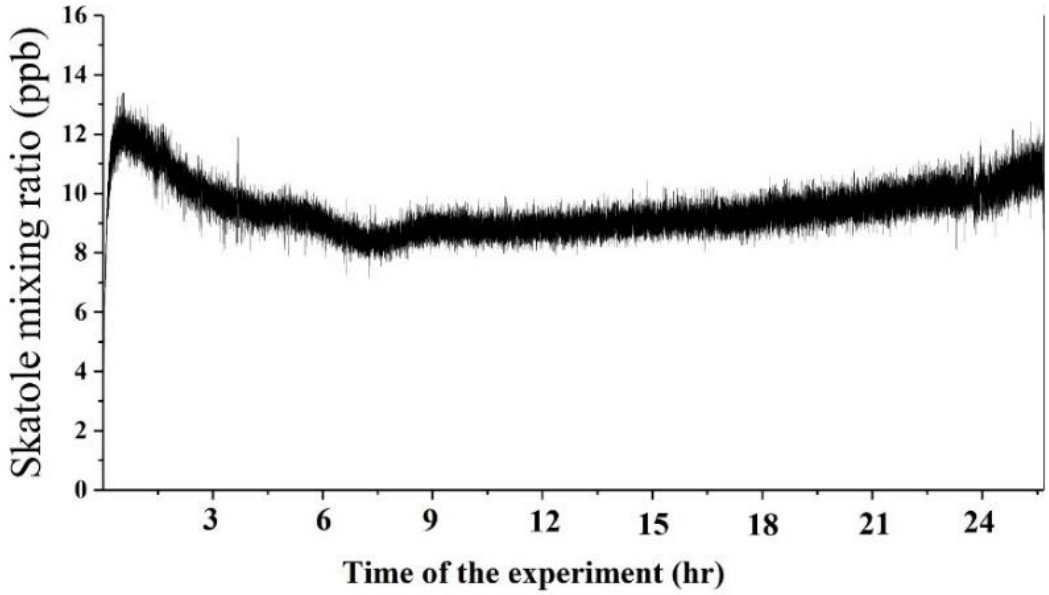

Figure 6.4 *Temporal evolution of the signal of skatole detected by PTR-QiTOF-MS. The y-axis represents the mixing ratio of skatole (calculated using PTR-QiTOF-MS) and the x-axis represents the time of the experiments lasted for ~ 24 hr.*

In this work, skatole emissions of ~ 50 and 116 µg m^{-2} min^{-1} were estimated from undigested SS and digestate biowastes, respectively. Production and release of 4.91 - 8.3 µg m^{-2} min^{-1} skatole following the land spreading of pig slurry (Liu et al., 2018) or land application of swine manure slurry (Parker et al., 2013) have been shown in literature. Based on the experiments we performed on undigested sludge (from WWTP1), we estimated the particle mass of 2.9 µg m^{-3} and number concentrations of 5 * 10^6 cm^{-3}. Our values exceed some of the field measurements conducted at various locations and the measurements in other laboratory experiments performed on agricultural samples. In addition, we estimated the particle nucleation rate up to 1.1 * 10^6 cm^{-3} s^{-1} during NPF. Joutsensaari et al., (2005) found an aerosol number concentration of 5.5 * 10^3 cm^{-3} from the ozonolysis of VOCs emitted by living white cabbage plants and a particle formation rate of ~ 3 cm^{-3} s^{-1} (over a particle diameter range of

5.5-70 nm). Our numbers are higher than the particle formation rates observed in the atmosphere (often in the range of 0.01-10 cm^{-3} s^{-1}) in the boundary layer for 3 nm articles. In urban, coastal areas and industrial plumes, the formation rates are higher with 100 cm^{-3} s^{-1} and 10^4-10^5 cm^{-3} s^{-1}, respectively (Kulmala et al., 2004).

In our experiments, the emissions were limited by the volume of the chamber, while in real atmosphere, they would be more diluted that leads to a lower concentration of precursors. In addition, the ozonolysis reaction time was limited to the residence time of O_3 in the chamber, however, in real atmosphere, skatole ozonolysis will not be limited and would occur all along the emission plume. The longer oxidation would lead to more oxidized compounds contributing to NPF. Our work evidences the potential role of OWP recycling in SOA formation, despite the difficulty in the comparison with real atmospheric processes.

As the application of OWPs is expected to increase with continuously growing agricultural activities (Aneja et al., 2009), this additional VOC source may have a significant influence on atmospheric NPF and O_3 reactivity during the spreading period. In this work, the experiments performed were designed to match the real atmospheric conditions as closely as possible and could be applicable to NPF events and growth in the atmosphere. The processes suggested in this work would serve as qualitative approach for the particle number concentration, as a high nucleation rate can induce the formation of a significant annual source of particles. Also, we suggested that skatole emissions can change the chemistry and oxidative capacity of the atmosphere via their contribution to local concentrations.

6.2. Perspectives and future work

This PhD thesis is a part of the ANR project SOFORA, which aims to investigate SOA formation and fate in real atmospheric and controlled simulation chamber conditions by two different OWPs: urban waste and livestock manure. This thesis aimed to prove the importance of the OWPs as a VOC source and their role in SOA formation. We were able to identify and quantify a large number of VOCs emitted from different OWP: urban waste (SS and food biowastes) and livestock manure. This comprehensive qualitative and quantitative study can therefore serve as an accurate inventory reference for future OWP VOC emission studies. In addition, the work done in this PhD thesis is the first step to provide new insights into fundamental processes involved in the formation and fate of SOA formed as a result of the ozone reactivity of VOCs emitted by OWPs. The presented work and conclusions give the motivation of more advanced steps of this research, such as performing in situ observations

during field campaigns where the VOC concentrations, fluxes and potential SOA formation can be studied.

Moreover, the laboratory studies using atmospheric simulation chambers combined with various mass spectrometric techniques can provide reference information to support field measurements (scheduled in the SOFORA project, for instance). Our results help to assess different abatement technologies and recommendations for potential VOCs and odorants emitted following land application of OWPs. Moreover, the dataset provided in this thesis can help to evaluate the fate and impacts on the environment of these OWPs compared to mineral fertilizers and provide guidelines for their use and application. The laboratory setup designed in the current work could be used for future studies, such as:

1. Study the effect of manure treatment (by anaerobic or aerobic digestion) on VOC emissions or the impact of manure storage on VOC emission fluxes.
2. Investigate the ozone reactivity and NPF from OWP samples in homogeneous and heterogeneous conditions by performing laboratory experiments using simulation chambers. Those experiments can be performed in two sequences: first, ozone is introduced into the chamber containing OWP sample to determine the heterogeneous ozone reactivity at the soil interface, and second, the gas phase from the first chamber is transferred into a second chamber (no OWP sample) to study the gas phase reactivity toward ozone.

In addition, detailed molecular analysis of the SOA chemical composition can be performed by using mass spectrometric techniques and advanced statistical tools (i.e. multivariate analysis). We performed here preliminary investigations on the chemical composition of the newly formed particles by a laser-based mass spectrometric technique (L2MS) and SIMS. The results showed several organic compounds that include oxygen and nitrogen atoms and contributed to the growth in particle size (Ciuraru et al., 2021). However, the low loading of filters collected upon NPF prevented a more comprehensive analysis. Future work is scheduled to design a sampling system for improved SOA collection and define appropriate sampling and offline analysis parameters. Increasing the sampling time would result in improved filter coverage, however it may also result in sampling very different particles as they continue to age in the chamber. A double-filter sampling system (Ngo et al., 2020) may allow separate collection of particle and gas phases. Both filters can be analyzed

off-line using the L2MS and SIMS techniques, which would further allow comparing the sampled gas composition with the PTR-QiTOF-MS results.

Finally, recent advances on the PTR-MS technique combined with the novel CHARON (Chemical Analysis of aeRosol ON-line) particle inlet system can be employed for collection and real-time analysis of the chemical composition of submicron particulate organic matter (Eichler et al., 2015, 2017; Gkatzelis et al., 2018). This approach, used to characterize the gas-to-particle partitioning of SOA formation and oxidation (Gkatzelis et al., 2018), would further allow the comparison with other complementary studies such as L2MS and SIMS measurements. We note however that the current particle lower size limit of CHARON (150 nm) makes it more appropriate for field measurements or particle growth and aging processes, rather than for new particle formation (nucleation) ones.

This page is intentionally left blank

Bibliography

Abdi, H., & Williams, L. J. (2010). Principal component analysis. *Wiley Interdisciplinary Reviews: Computational Statistics*, *2*(4), 433–459. https://doi.org/10.1002/wics.101

Abis, L., Loubet, B., Ciuraru, R., Lafouge, F., Dequiedt, S., Houot, S., Maron, P. A., & Bourgeteau-Sadet, S. (2018). Profiles of volatile organic compound emissions from soils amended with organic waste products. *Science of the Total Environment*, *636*, 1333–1343. https://doi.org/10.1016/j.scitotenv.2018.04.232

Abubaker, J., Risberg, K., & Pell, M. (2012). Biogas residues as fertilisers – Effects on wheat growth and soil microbial activities. *Applied Energy*, *99*, 126–134. https://doi.org/10.1016/j.apenergy.2012.04.050

Adam, T., Baker, R. R., & Zimmermann, R. (2007). Characterization of puff-by-puff resolved cigarette mainstream smoke by single photon ionization-time-of-flight mass spectrometry and principal component analysis. *Journal of Agricultural and Food Chemistry*, *55*(6), 2055–2061. https://doi.org/10.1021/jf062360x

ADEME (Miscellaneous INIS-FR-11-0189; p. 56 p. pages). (2011). Agence de l'Environnement et de la Maitrise de l'Energie, ADEME, 75 - Paris (France).

Air quality in Europe – EEA report (No. 13). (2017).

Allen, M. R., Braithwaite, A., & Hills, C. C. (1997). Trace Organic Compounds in Landfill Gas at Seven U.K. Waste Disposal Sites. *Environmental Science & Technology*, *31*(4), 1054–1061. https://doi.org/10.1021/es9605634

Almeida, F. N., Htoo, J. K., Thomson, J., & Stein, H. H. (2013). Amino acid digestibility in camelina products fed to growing pigs. *Canadian Journal of Animal Science*, *93*(3), 335–343. https://doi.org/10.4141/cjas2012-134

Al-Rubaye, A. F., Hameed, I. H., & Kadhim, M. J. (2017). A Review: Uses of Gas Chromatography-Mass Spectrometry (GC-MS) Technique for Analysis of Bioactive

Natural Compounds of Some Plants. *INTERNATIONAL JOURNAL OF TOXICOLOGICAL AND PHARMACOLOGICAL RESEARCH*, *9*(01). https://doi.org/10.25258/ijtpr.v9i01.9042

Alvarenga, P., Mourinha, C., Farto, M., Santos, T., Palma, P., Sengo, J., Morais, M., & Cunha-Queda, C. (2015). Sewage sludge, compost and other representative organic wastes as agricultural soil amendments: Benefits versus limiting factors. *Waste Management*, *40*, 44–52.

Amador-Muñoz, O., Misztal, P. K., Weber, R., Worton, D. R., Zhang, H., Drozd, G., & Goldstein, A. H. (2016). Sensitive detection of n-alkanes using a mixed ionization mode proton-transfer-reaction mass spectrometer. *Atmospheric Measurement Techniques*, *9*(11), 5315–5329. https://doi.org/10.5194/amt-9-5315-2016

Anand, S. S., Philip, B. K., & Mehendale, H. M. (2014). Volatile Organic Compounds. In P. Wexler (Ed.), *Encyclopedia of Toxicology (Third Edition)* (Third Edition, pp. 967–970). Academic Press. https://doi.org/10.1016/B978-0-12-386454-3.00358-4

Anderson, N. J., Dixon, D. R., Harbour, P. J., & Scales, P. J. (2002). Complete characterisation of thermally treated sludges. *Water Science and Technology*, *46*(10), 51–54. https://doi.org/10.2166/wst.2002.0287

Andreae, M. O., & Crutzen, P. J. (1997). Atmospheric Aerosols: Biogeochemical Sources and Role in Atmospheric Chemistry. *Science*, *276*(5315), 1052–1058.

Aneja, V. P., Schlesinger, W. H., & Erisman, J. W. (2009). Effects of agriculture upon the air quality and climate: Research, policy, and regulations. *Environmental Science and Technology*, *43*(12), 4234–4240. https://doi.org/10.1021/es8024403

Annabi, M., Le Bissonnais, Y., Le Villio-Poitrenaud, M., & Houot, S. (2011). Improvement of soil aggregate stability by repeated applications of organic amendments to a cultivated

silty loam soil. *Agriculture, Ecosystems & Environment*, *144*(1), 382–389. https://doi.org/10.1016/j.agee.2011.07.005

Appels, L., Lauwers, J., Degrève, J., Helsen, L., Lievens, B., Willems, K., Impe, J. V., & Dewil, R. (2011). Anaerobic digestion in global bio-energy production: Potential and research challenges. *Renewable and Sustainable Energy Reviews*, *15*(9), 4295–4301. https://doi.org/10.1016/j.rser.2011.07.121

Aprea, E., Biasioli, F., Sani, G., Cantini, C., Märk, T. D., & Gasperi, F. (2006). Proton Transfer Reaction−Mass Spectrometry (PTR-MS) Headspace Analysis for Rapid Detection of Oxidative Alteration of Olive Oil. *Journal of Agricultural and Food Chemistry*, *54*(20), 7635–7640. https://doi.org/10.1021/jf060970r

Arthurson, V. (2009). Closing the Global Energy and Nutrient Cycles through Application of Biogas Residue to Agricultural Land – Potential Benefits and Drawback. *Energies*, *2*(2), 226–242. https://doi.org/10.3390/en20200226

Atalia, K. R., Buha, D. M., Bhavsar, K., & Shah, N. K. (2015). *A Review on Composting of Municipal Solid Waste*.

Atkinson, R. (2000). Atmospheric chemistry of VOCs and NOx. *Atmospheric Environment*, *34*(12–14), 2063–2101. https://doi.org/10.1016/S1352-2310(99)00460-4

Atkinson, R., & Arey, J. (2003). Atmospheric Degradation of Volatile Organic Compounds. *Chemical Reviews*, *103*(12), 4605–4638. https://doi.org/10.1021/cr0206420

Atkinson, R., & Arey, J. (2007). Mechanisms of the gas-phase reactions of aromatic hydrocarbons and PAHs with OH and NO3 radicals. *Polycyclic Aromatic Compounds*, *27*(1), 15–40. https://doi.org/10.1080/10406630601134243

Atkinson, R., Baulch, D. L., Cox, R. A., Crowley, J. N., Hampson, R. F., Hynes, R. G., Jenkin, M. E., & Rossi, M. J. (2004). Evaluated kinetic and photochemical data for atmospheric

chemistry: Volume I – gas phase reactions of O x , HO x , NO x and SO x species. *Atmospheric Chemistry and Physics*, *I*, 1461–1738.

Bauer, S. E., Tsigaridis, K., & Miller, R. (2016). Significant atmospheric aerosol pollution caused by world food cultivation. *Geophysical Research Letters*, *43*(10), 5394–5400. https://doi.org/10.1002/2016GL068354

Beck, J. P., Heutelbeck, A., & Dunkelberg, H. (2007). Volatile organic compounds in dwelling houses and stables of dairy and cattle farms in Northern Germany. *Science of the Total Environment*, *372*(2–3), 440–454. https://doi.org/10.1016/j.scitotenv.2006.10.009

Bergman, T., Laaksonen, A., Korhonen, H., Malila, J., Dunne, E., Mielonen, T., Lehtinen, K., Kühn, T., Arola, A., & Kokkola, H. (2015). Geographical and Diurnal Features of Amine-Enhanced Boundary Layer Nucleation. *Journal of Geophysical Research: Atmospheres*, *120*, n/a-n/a. https://doi.org/10.1002/2015JD023181

Bernal, M. P., Alburquerque, J. A., & Moral, R. (2009). Composting of animal manures and chemical criteria for compost maturity assessment. A review. *Bioresource Technology*, *100*(22), 5444–5453. https://doi.org/10.1016/j.biortech.2008.11.027

Bianchi, F., Kurtén, T., Riva, M., Mohr, C., Rissanen, M. P., Roldin, P., Berndt, T., Crounse, J. D., Wennberg, P. O., Mentel, T. F., Wildt, J., Junninen, H., Jokinen, T., Kulmala, M., Worsnop, D. R., Thornton, J. A., Donahue, N. M., Kjaergaard, H. G., & Ehn, M. (2019). Highly Oxygenated Organic Molecules (HOM) from Gas-Phase Autoxidation Involving Peroxy Radicals: A Key Contributor to Atmospheric Aerosol. *Chemical Reviews*, *119*, 3472–3509.

Bianchini, A., Bonfiglioli, L., Pellegrini, M., & Saccani, C. (2016). Sewage sludge management in Europe: A critical analysis of data quality. *International Journal of Environment and Waste Management*, *18*(3), 226–238. https://doi.org/10.1504/IJEWM.2016.080795

Boy, M., Taipale, D., Smolander, S., Zhou, L., Nieminen, T., Paasonen, P., Plass-Dülmer, C., Sipilä, M., Petäjä, T., Mauldin, R., Berresheim, H., & Kulmala, M. (2012). Oxidation of SO2 by stabilized Criegee Intermediate (sCI) radicals as a crucial source for atmospheric sulphuric acid concentrations. *Atmospheric Chemistry & Physics Discussions*, *12*, 27693–27736. https://doi.org/10.5194/acpd-12-27693-2012

Bradley, J. V. (1982). The insidious L-shaped distribution. *Bulletin of the Psychonomic Society*, *20*(2), 85–88. https://doi.org/10.3758/BF03330089

Büyüksönmez, F., & Evans, J. J. (2007). Biogenic Emissions from Green Waste and Comparison to the Emissions Resulting from Composting Part II: Volatile Organic Compounds (VOCs). *Compost Science & Utilization*, *15*, 191–199.

Byliński, H., Barczak, R. J., Gębicki, J., & Namieśnik, J. (2019). Monitoring of odors emitted from stabilized dewatered sludge subjected to aging using proton transfer reaction–mass spectrometry. *Environmental Science and Pollution Research*, *26*(6), 5500–5513. https://doi.org/10.1007/s11356-018-4041-4

Bzdek, B. R., & Johnston, M. V. (2010). New particle formation and growth in the troposphere. *Analytical Chemistry*, *82*(19), 7871–7878. https://doi.org/10.1021/ac100856j

C. Gross, T. S. (1993). Thermal Drying of Sewage Sludge. *Water and Environment Journal*, *7*(3), 255–261. https://doi.org/10.1111/j.1747-6593.1993.tb00843.x

Cappa, C. (2016). Atmospheric science: Unexpected player in particle formation. *Nature*, *533*, 478–479.

Cappellin, L. (2018). *What is Proton Transfer Reaction Mass Spectrometry (PTR-MS)?* ptr@tofwerk.com

Cappellin, L., Biasioli, F., Granitto, P. M., Schuhfried, E., Soukoulis, C., Costa, F., Märk, T. D., & Gasperi, F. (2011). On data analysis in PTR-TOF-MS: From raw spectra to data

mining. *Sensors and Actuators B: Chemical*, *155*(1), 183–190. https://doi.org/10.1016/j.snb.2010.11.044

Carvalho, T. C., Peters, J. I., & Williams, R. O. (2011). Influence of particle size on regional lung deposition – What evidence is there? *International Journal of Pharmaceutics*, *406*(1), 1–10. https://doi.org/10.1016/j.ijpharm.2010.12.040

Chemiluminescence Ammonia and nitrogen oxides analyzer. (n.d.). https://www.envea.global/design/medias/AC32e_CNH3_ammonia-monitoring-air-pollution-ENVEA-EN.pdf

Chen, W.-H., Deng, M.-J., Luo, H., Zhang, J.-Y., Ding, W.-J., Liu, J.-X., & Liu, J.-X. (2014). Characteristics of odors and VOCs from sludge direct drying process. *Huan Jing Ke Xue= Huanjing Kexue*, *35*(8), 2897—2902.

Chen, X., Millet, D. B., Singh, H. B., Wisthaler, A., Apel, E. C., Atlas, E. L., Blake, D. R., Bourgeois, I., Brown, S. S., Crounse, J. D., de Gouw, J. A., Flocke, F. M., Fried, A., Heikes, B. G., Hornbrook, R. S., Mikoviny, T., Min, K.-E., Müller, M., Neuman, J. A., … Yuan, B. (2019). On the sources and sinks of atmospheric VOCs: An integrated analysis of recent aircraft campaigns over North America. *Atmospheric Chemistry and Physics*, *19*(14), 9097–9123. https://doi.org/10.5194/acp-19-9097-2019

Chen, Y.-C., Higgins, M., Murthy, S., Maas, N., Covert, K., Weaver, J., Toffey, W., Rupke, M., & Ross, D. (2004). Mechanism forthe production of odorous volatile aromatic compounds in wastewater biosolisds. *Proceedings of the Water Environment Federation*, *2004*(1), 540–553. https://doi.org/10.2175/193864704784342811

Chiriac, R., De Araujos Morais, J., Carre, J., Bayard, R., Chovelon, J. M., & Gourdon, R. (2011). Study of the VOC emissions from a municipal solid waste storage pilot-scale cell: Comparison with biogases from municipal waste landfill site. *Waste Management*, *31*(11), 2294–2301. https://doi.org/10.1016/j.wasman.2011.06.009

Chojnacka, K., Moustakas, K., & Witek-Krowiak, A. (2020). Bio-based fertilizers: A practical approach towards circular economy. *Bioresource Technology*, *295*, 122223. https://doi.org/10.1016/j.biortech.2019.122223

Christodoulou, A., & Stamatelatou, K. (2016a). Overview of legislation on sewage sludge management in developed countries worldwide. *Water Science and Technology: A Journal of the International Association on Water Pollution Research*, *73*(3), 453–462. https://doi.org/10.2166/wst.2015.521

Christodoulou, A., & Stamatelatou, K. (2016b). Overview of legislation on sewage sludge management in developed countries worldwide. *Water Science and Technology*, *73*(3), 453–462. https://doi.org/10.2166/wst.2015.521

Chrit, M., Sartelet, K., Sciare, J., Pey, J., Marchand, N., Couvidat, F., Sellegri, K., & Beekmann, M. (2017). Modelling organic aerosol concentrations and properties during ChArMEx summer campaigns of 2012 and 2013 in the western Mediterranean region. *Atmospheric Chemistry and Physics*, *17*(20), 12509–12531. https://doi.org/10.5194/acp-17-12509-2017

Cicolella, A. (2008). [Volatile Organic Compounds (VOC): Definition, classification and properties]. *Revue des maladies respiratoires*, *25*(2), 155–163. https://doi.org/10.1016/s0761-8425(08)71513-4

Ciganek, M., & Neca, J. (2008). Chemical characterization of volatile organic compounds on animal farms. *Veterinarni Medicina*, *53*(12), 641–651. https://doi.org/10.17221/1969-VETMED

Ciuraru, R., Kammer, J., Decuq, C., Vojkovic, M., Haider, K., Carpentier, Y., Lafouge, F., Berger, C., Bourdat-Deschamps, M., Ortega, I. K., Levavasseur, F., Houot, S., Loubet, B., Petitprez, D., & Focsa, C. (2021). New particle formation from agricultural

recycling of organic waste products. *Npj Climate and Atmospheric Science*, *4*(1), 5. https://doi.org/10.1038/s41612-021-00160-3

Clarke, B. O., & Smith, S. R. (2011). Review of "emerging" organic contaminants in biosolids and assessment of international research priorities for the agricultural use of biosolids. *Environment International*, *37*(1), 226–247. https://doi.org/10.1016/j.envint.2010.06.004

Collivignarelli, M., Abbà, A., Frattarola, A., Carnevale Miino, M., Padovani, S., Katsoyiannis, I., & Torretta, V. (2019). Legislation for the Reuse of Biosolids on Agricultural Land in Europe: Overview. *Sustainability*, *11*(21), 6015. https://doi.org/10.3390/su11216015

Colón, J., Alarcón, M., Healy, M., Namli, A., Ponsá, S., Sanin, F. D., & Taya, C. (2014). Producing sludge for agricultural applications. *Innovative Wastewater Treatment and Resource Recovery Technologies*, 292–314.

Colón, J., Cadena, E., Pognani, M., Barrena, R., Sánchez, A., Font, X., & Artola, A. (2012). Determination of the energy and environmental burdens associated with the biological treatment of source-separated Municipal Solid Wastes. *Energy and Environmental Science*, *5*, 5731–5741.

Covey, T. R., Thomson, B. A., & Schneider, B. B. (2009). Atmospheric pressure ion sources. *Mass Spectrometry Reviews*, *28*(6), 870–897. https://doi.org/10.1002/mas.20246

Daumont, D., Brion, J., Charbonnier, J., & Malicet, J. (1992). Ozone UV spectroscopy I: Absorption cross-sections at room temperature. *Journal of Atmospheric Chemistry*, *15*(2), 145–155. https://doi.org/10.1007/BF00053756

David Sparkman, O., E. Penton, Z., & G. Kitson, F. (2011). *Gas Chromatography and Mass Spectrometry A Practical Guide* (Second edition).

Davoli, E., Gangai, M. L., Morselli, L., & Tonelli, D. (2003). Characterisation of odorants emissions from landfills by SPME and GC/MS. *Chemosphere*, *51*(5), 357–368. https://doi.org/10.1016/S0045-6535(02)00845-7

de Gouw, J., & Warneke, C. (2007). Measurements of volatile organic compounds in the earth's atmosphere using proton-transfer-reaction mass spectrometry. *Mass Spectrometry Reviews*, *26*(2), 223–257. https://doi.org/10.1002/mas.20119

de Gouw, J., Warneke, C., Karl, T., Eerdekens, G., van der Veen, C., & Fall, R. (2003). Sensitivity and specificity of atmospheric trace gas detection by proton-transfer-reaction mass spectrometry. *International Journal of Mass Spectrometry*, *223–224*, 365–382. https://doi.org/10.1016/S1387-3806(02)00926-0

DEIMOS UZA TOTAL - Ultra Zero Air Total Gas generator | F-DGSi. *FDGSI*. Retrieved April 16, 2022, from https://www.f-dgs.com/produit/deimos-uza-total-ultra-zero-total-air-gas-generator/

Deng, W.-Y., Yan, J.-H., Li, X.-D., Wang, F., Zhu, X.-W., Lu, S.-Y., & Cen, K.-F. (2009). Emission characteristics of volatile compounds during sludges drying process. *Journal of Hazardous Materials*, *162*(1), 186–192. https://doi.org/10.1016/j.jhazmat.2008.05.022

Dhamodharan, K., Varma, V. S., Veluchamy, C., Pugazhendhi, A., & Rajendran, K. (2019). Emission of volatile organic compounds from composting: A review on assessment, treatment and perspectives. *Science of The Total Environment*, *695*, 133725. https://doi.org/10.1016/j.scitotenv.2019.133725

Di Capua, F., Spasiano, D., Giordano, A., Adani, F., Fratino, U., Pirozzi, F., & Esposito, G. (2020). High-solid anaerobic digestion of sewage sludge: Challenges and opportunities. *Applied Energy*, *278*, 115608. https://doi.org/10.1016/j.apenergy.2020.115608

Diacono, M., & Montemurro, F. (2010). Long-term effects of organic amendments on soil fertility. A review. *Agronomy for Sustainable Development*, *30*(2), 401–422. https://doi.org/10.1051/agro/2009040

Ding, W., Li, L., & Liu, J. (2015). Investigation of the effects of temperature and sludge characteristics on odors and VOC emissions during the drying process of sewage sludge. *Water Science and Technology*, *72*(4), 543–552. https://doi.org/10.2166/wst.2015.246

Dittmar, H., Drach, M., Vosskamp, R., Trenkel, M. E., Gutser, R., & Steffens, G. (2009). Fertilizers, 2. Types. In Wiley-VCH Verlag GmbH & Co. KGaA (Ed.), *Ullmann's Encyclopedia of Industrial Chemistry* (p. n10_n01). Wiley-VCH Verlag GmbH & Co. KGaA. https://doi.org/10.1002/14356007.n10_n01

Dobbins, R. A., Fletcher, R. A., & Chang, H.-C. (1998). The evolution of soot precursor particles in a diffusion flame. *Combustion and Flame*, *115*(3), 285–298. https://doi.org/10.1016/S0010-2180(98)00010-8

Donahue, N. M., Drozd, G. T., Epstein, S. A., Presto, A. A., & Kroll, J. H. (2011). Adventures in ozoneland: Down the rabbit-hole. *Physical Chemistry Chemical Physics : PCCP*, *13 23*, 10848–10857.

Dorno, N., Feilberg, A., Balsari, P., & Nyord, T. (2013). Nitrous oxide losses from untreated and digested slurry as influenced by soil moisture and application method. *Biosystems Engineering*, *115*(4), 423–433. https://doi.org/10.1016/j.biosystemseng.2013.04.004

Du, W., & Parker, W. (2012). Modeling volatile organic sulfur compounds in mesophilic and thermophilic anaerobic digestion of methionine. *Water Research*, *46*(2), 539–546. https://doi.org/10.1016/j.watres.2011.11.043

Duan, Z., Lu, W., Li, D., & Wang, H. (2014). Temporal variation of trace compound emission on the working surface of a landfill in Beijing, China. *Atmospheric Environment*, *88*, 230–238. https://doi.org/10.1016/j.atmosenv.2014.01.051

Duca, D., Irimiea, C., Faccinetto, A., Noble, J. A., Vojkovic, M., Carpentier, Y., Ortega, I. K., Pirim, C., & Focsa, C. (2019). On the benefits of using multivariate analysis in mass spectrometric studies of combustion-generated aerosols. *Faraday Discussions*, *218*, 115–137. https://doi.org/10.1039/c8fd00238j

Edelenbos, M., Larsen, E., & Feilberg, A. (2012). *Investigation of Volatiles Emitted from Freshly Cut Onions (*. 16060–16076. https://doi.org/10.3390/s121216060

Eden, M., Gerke, H. H., & Houot, S. (2017). Organic waste recycling in agriculture and related effects on soil water retention and plant available water: A review. *Agronomy for Sustainable Development*, *37*(2), 11. https://doi.org/10.1007/s13593-017-0419-9

Ehn, M., Thornton, J. A., Kleist, E., Sipilä, M., Junninen, H., Pullinen, I., Springer, M., Rubach, F., Tillmann, R., Lee, B., Lopez-Hilfiker, F., Andres, S., Acir, I.-H., Rissanen, M., Jokinen, T., Schobesberger, S., Kangasluoma, J., Kontkanen, J., Nieminen, T., … Mentel, T. F. (2014). A large source of low-volatility secondary organic aerosol. *Nature*, *506*(7489), 476–479. https://doi.org/10.1038/nature13032

Eichler, P., Müller, M., D'Anna, B., & Wisthaler, A. (2015). A novel inlet system for online chemical analysis of semi-volatile submicron particulate matter. *Atmospheric Measurement Techniques*, *8*(3), 1353–1360. https://doi.org/10.5194/amt-8-1353-2015

Eichler, P., Müller, M., Rohmann, C., Stengel, B., Orasche, J., Zimmermann, R., & Wisthaler, A. (2017). Lubricating Oil as a Major Constituent of Ship Exhaust Particles. *Environmental Science & Technology Letters*, *4*(2), 54–58. https://doi.org/10.1021/acs.estlett.6b00488

Eitzer, B. D. (1995). Emissions of Volatile Organic Chemicals from Municipal Solid Waste Composting Facilities. *Environmental Science & Technology*, *29*(4), 896–902. https://doi.org/10.1021/es00004a009

European Environment Agency (EEA). (2008). [Annual European Community LRTAP Convention emission inventory report 1990–2006].

Eurostat. Sewage sludge production and disposal. (2020). https://ec.europa.eu/ eurostat/

Faburé, J., Rogier, S., & Loubet, B. (2011). Bibliography review of the agricultural contribution in atmospheric particles emissions: Identification of emission factors. *INRA Paris:164 Pp*.

Faccinetto, A., Desgroux, P., Ziskind, M., Therssen, E., & Focsa, C. (2011). High-sensitivity detection of polycyclic aromatic hydrocarbons adsorbed onto soot particles using laser desorption/laser ionization/time-of-flight mass spectrometry: An approach to studying the soot inception process in low-pressure flames. *Combustion and Flame*, *158*(2), 227–239. https://doi.org/10.1016/j.combustflame.2010.08.012

Faccinetto, A., Focsa, C., Desgroux, P., & Ziskind, M. (2015). Progress toward the Quantitative Analysis of PAHs Adsorbed on Soot by Laser Desorption/Laser Ionization/Time-of-Flight Mass Spectrometry. *Environmental Science and Technology*, *49*(17), 10510–10520. https://doi.org/10.1021/acs.est.5b02703

FAO Statistical Yearbook. FAOSTAT. (2013). *Food and Agricultural Organization (FAO)*.

Feilberg, A., Bildsoe, P., & Nyord, T. (2015). Application of PTR-MS for measuring odorant emissions from soil application of manure slurry. *Sensors (Switzerland)*, *15*(1), 1148–1167. https://doi.org/10.3390/s150101148

Feilberg, A., Hansen, M. J., Liu, D., & Nyord, T. (2017). Contribution of livestock H2S to total sulfur emissions in a region with intensive animal production. *Nature Communications*, *8*(1), 1–7. https://doi.org/10.1038/s41467-017-01016-2

Feilberg, A., Hansen, M. N., & Lindholst, S. (2011). Chemical Evaluation of Odor Reduction by Soil Injection of Animal Manure. *Journal of Environmental Quality*, *40*(5), 1674–1682. https://doi.org/10.2134/jeq2010.0499

Feilberg, A., Liu, D., Adamsen, A. P. S., Hansen, M. J., & Jonassen, K. E. N. (2010). Odorant emissions from intensive pig production measured by online proton-transfer-reaction mass spectrometry. *Environmental Science and Technology*, *44*(15), 5894–5900. https://doi.org/10.1021/es100483s

Filipy, J., Rumburg, B., Mount, G., Westberg, H., & Lamb, B. (2006). Identification and quantification of volatile organic compounds from a dairy. *Atmospheric Environment*, *40*(8), 1480–1494. https://doi.org/10.1016/j.atmosenv.2005.10.048

Fisher, R. M., Barczak, R. J., Alvarez Gaitan, J. P., Le-Minh, N., & Stuetz, R. M. (2017). Odorous volatile organic compound (VOC) emissions from ageing anaerobically stabilised biosolids. *Water Science and Technology*, *75*(7), 1617–1624. https://doi.org/10.2166/wst.2017.030

François Vermeulen, A. (2020). *Industrial Machine Learning: Using Artificial Intelligence as a Transformational Disruptor*.

Franke-Whittle, I. H., Walter, A., Ebner, C., & Insam, H. (2014). Investigation into the effect of high concentrations of volatile fatty acids in anaerobic digestion on methanogenic communities. *Waste Management*, *34*(11), 2080–2089. https://doi.org/10.1016/j.wasman.2014.07.020

Gallego, E., Roca, F. J., Perales, J. F., & Guardino, X. (2010). Comparative study of the adsorption performance of a multi-sorbent bed (Carbotrap, Carbopack X, Carboxen 569) and a Tenax TA adsorbent tube for the analysis of volatile organic compounds (VOCs). *Talanta*, *81*(3), 916–924. https://doi.org/10.1016/j.talanta.2010.01.037

Gebicki, J., Byliński, H., & Namieśnik, J. (2016). Measurement techniques for assessing the olfactory impact of municipal sewage treatment plants. *Environmental Monitoring and Assessment*, *188*(1), 1–15. https://doi.org/10.1007/s10661-015-5024-2

Gentner, D. R., Ormeño, E., Fares, S., Ford, T. B., Weber, R. J., Park, J.-H., Brioude, J., Angevine, W. M., Karlik, J. F., & Goldstein, A. H. (2013). Emissions of terpenoids, benzenoids, and other biogenic gas-phase organic compounds from agricultural crops and their potential implications for air quality. *Atmospheric Chemistry and Physics*, *14*, 5393–5413.

Gkatzelis, G. I., Hohaus, T., Tillmann, R., Gensch, I., Müller, M., Eichler, P., Xu, K.-M., Schlag, P., Schmitt, S. H., Yu, Z., Wegener, R., Kaminski, M., Holzinger, R., Wisthaler, A., & Kiendler-Scharr, A. (2018). Gas-to-particle partitioning of major biogenic oxidation products: A study on freshly formed and aged biogenic SOA. *Atmospheric Chemistry and Physics*, *18*(17), 12969–12989. https://doi.org/10.5194/acp-18-12969-2018

Gomez-Rico, M. F., Fullana, A., & Font, R. (2008). Volatile organic compounds released from thermal drying of sewage sludge. *WIT Transactions on Ecology and the Environment*, *111*, 425–433. https://doi.org/10.2495/WP080411

Gontard, N., Sonesson, U., Birkved, M., Majone, M., Bolzonella, D., Celli, A., Angellier-Coussy, H., Jang, G. W., Verniquet, A., Broeze, J., Schaer, B., Batista, A. P., & Sebok, A. (2018). A research challenge vision regarding management of agricultural waste in a circular bio-based economy. *Critical Reviews in Environmental Science and Technology*, *48*(6), 614–654. https://doi.org/10.1080/10643389.2018.1471957

Gross JH. (2004). *Mass Spectrometry A Textbook.*

Guenther, A., Hewitt, C. N., Erickson, D., Fall, R., Geron, C., Graedel, T., Harley, P., Klinger, L., Lerdau, M., Mckay, W. A., Pierce, T., Scholes, B., Steinbrecher, R., Tallamraju, R.,

Taylor, J., & Zimmerman, P. (1995). A global model of natural volatile organic compound emissions. *Journal of Geophysical Research*, *100*(D5), 8873. https://doi.org/10.1029/94JD02950

Guenther, A., Karl, T., Harley, P., Wiedinmyer, C., Palmer, P. I., & Geron, C. (2006). Estimates of global terrestrial isoprene emissions using MEGAN (Model of Emissions of Gases and Aerosols from Nature). *Atmospheric Chemistry and Physics*, *6*(11), 3181–3210. https://doi.org/10.5194/acp-6-3181-2006

Guo, H., Lee, S. C., Chan, L. Y., & Li, W. M. (2004). Risk assessment of exposure to volatile organic compounds in different indoor environments. *Environmental Research*, *94*(1), 57–66. https://doi.org/10.1016/s0013-9351(03)00035-5

Guo, S., Hu, M., Zamora, M. L., Peng, J., Shang, D., Zheng, J., Du, Z., Wu, Z., Shao, M., Zeng, L., Molina, M. J., & Zhang, R. (2014). Elucidating severe urban haze formation in China. *Proceedings of the National Academy of Sciences*, *111*(49), 17373–17378. https://doi.org/10.1073/pnas.1419604111

Gutser, R., Ebertseder, T., Weber, A., Schraml, M., & Schmidhalter, U. (2005). Short-term and residual availability of nitrogen after long-term application of organic fertilizers on arable land. *Journal of Plant Nutrition and Soil Science*, *168*(4), 439–446. https://doi.org/10.1002/jpln.200520510

Haider, K. M., Lafouge, F., Carpentier, Y., Houot, S., Petitprez, D., Loubet, B., Focsa, C., & Ciuraru, R. (2022). Chemical identification and quantification of volatile organic compounds emitted by sewage sludge. *Science of The Total Environment*, *838*, 155948. https://doi.org/10.1016/j.scitotenv.2022.155948

Hall, J. E. (1995). Sewage Sludge Production, Treatment and Disposal in the European Union. *Water and Environment Journal*, *9*(4), 335–343. https://doi.org/10.1111/j.1747-6593.1995.tb00950.x

Hansel, A., Jordan, A., Holzinger, R., Prazeller, P., Vogel, W., & Lindinger, W. (1995). Proton transfer reaction mass spectrometry: On-line trace gas analysis at the ppb level. *International Journal of Mass Spectrometry and Ion Processes*, *149–150*, 609–619. https://doi.org/10.1016/0168-1176(95)04294-U

Hansen, M. J., Liu, D., Guldberg, L. B., & Feilberg, A. (2012). Application of proton-transfer-reaction mass spectrometry to the assessment of odorant removal in a biological air cleaner for pig production. *Journal of Agricultural and Food Chemistry*, *60*(10), 2599–2606. https://doi.org/10.1021/jf300182c

Harrison, E. Z., Oakes, S. R., Hysell, M., & Hay, A. (2006). Organic chemicals in sewage sludges. *Science of the Total Environment*, *367*(2–3), 481–497. https://doi.org/10.1016/j.scitotenv.2006.04.002

Hempel, S., Saha, C. K., Fiedler, M., Berg, W., Hansen, C., Amon, B., & Amon, T. (2016). Non-linear temperature dependency of ammonia and methane emissions from a naturally ventilated dairy barn. *Biosystems Engineering*, *145*, 10–21. https://doi.org/10.1016/j.biosystemseng.2016.02.006

Herbig, J., Müller, M., Schallhart, S., Titzmann, T., Graus, M., & Hansel, A. (2009). On-line breath analysis with PTR-TOF. *Journal of Breath Research*, *3*(2). https://doi.org/10.1088/1752-7155/3/2/027004

Hewitt, C. N., Hayward, S., & Tani, A. (2003). The application of proton transfer reaction-mass spectrometry (PTR-MS) to the monitoring and analysis of volatile organic compounds in the atmosphere. *Journal of Environmental Monitoring*, *5*(1), 1–7. https://doi.org/10.1039/b204712h

Higgins, M. J., Chen, Y.-C., Yarosz, D. P., Murthy, S. N., Maas, N. A., Glindemann, D., & Novak, J. T. (2006). Cycling of Volatile Organic Sulfur Compounds in Anaerobically

Digested Biosolids and its Implications for Odors. *Water Environment Research*, *78*(3), 243–252. https://doi.org/10.2175/106143005X90065

Higgins, M. J., Yarosz, B. D. P., Caldwell, Chen, Y.-C., & Mass, N. A. (2003). Mechanisms of Volatile Sulfur Compound and Odor Production in Digested Biosolids. *Residuals and Biosolids*.

Hinds, W. C. (1999). *Aerosol technology: Properties, behavior, and measurement of airborne particles*. John Wiley & Sons.

Holm-Nielsen, J. B., Seadi, T. A., & Oleskowicz-Popiel, P. (2009). The future of anaerobic digestion and biogas utilization. *Bioresource Technology*, *100*(22), 5478–5484. https://doi.org/10.1016/j.biortech.2008.12.046

Houot, S., Clergeot, D., Michelin, J., Francou, C., Bourgeois, S., Caria, G., & Ciesielski, H. (2002). Agronomic Value and Environmental Impacts of Urban Composts Used in Agriculture. In H. Insam, N. Riddech, & S. Klammer (Eds.), *Microbiology of Composting* (pp. 457–472). Springer Berlin Heidelberg.

Houot, S., Pons, M. N., & Pradel, M. (2014). Valorisation des matières fertilisantes d'origine résiduaire sur les sols à usage agricole ou forestier (Valorisation of fertilising materials from waste on agricultural and forest soils). *Expertise Scientifique Collective INRA-CNRS-Irstea*, 1–108.

Iacovidou, E., Ohandja, D.-G., & Voulvoulis, N. (2012). Food waste co-digestion with sewage sludge – Realising its potential in the UK. *Journal of Environmental Management*, *112*, 267–274. https://doi.org/10.1016/j.jenvman.2012.07.029

Insam, H., Gómez-Brandón, M., & Ascher, J. (2015). Manure-based biogas fermentation residues – Friend or foe of soil fertility? *Soil Biology and Biochemistry*, *84*, 1–14. https://doi.org/10.1016/j.soilbio.2015.02.006

Irimiea, C., Faccinetto, A., Carpentier, Y., Ortega, I. K., Nuns, N., Therssen, E., Desgroux, P., & Focsa, C. (2018). A comprehensive protocol for chemical analysis of flame combustion emissions by secondary ion mass spectrometry. *Rapid Communications in Mass Spectrometry*, *32*(13), 1015–1025. https://doi.org/10.1002/rcm.8133

Irimiea, C., Faccinetto, A., Mercier, X., Ortega, I.-K., Nuns, N., Therssen, E., Desgroux, P., & Focsa, C. (2019). Unveiling trends in soot nucleation and growth: When secondary ion mass spectrometry meets statistical analysis. *Carbon*, *144*, 815–830. https://doi.org/10.1016/j.carbon.2018.12.015

Iticescu, C., Georgescu, L. P., Murariu, G., Circiumaru, A., & Timofti, M. (2018). The characteristics of sewage sludge used on agricultural lands. *AIP Conference Proceedings*, *2022*(November). https://doi.org/10.1063/1.5060681

Jamil Khan, M., Qasim, M., & Umar, M. (2006). Utilization of sewage sludge as organic fertiliser in sustainable agriculture. *Journal of Applied Sciences*, *6*(3), 531–535. https://doi.org/10.3923/jas.2006.531.535

Jones, A. P. (1999). Indoor air quality and health. *Atmospheric Environment*, *33*(28), 4535–4564. https://doi.org/10.1016/S1352-2310(99)00272-1

Jordan, A., Haidacher, S., Hanel, G., Hartungen, E., Märk, L., Seehauser, H., Schottkowsky, R., Sulzer, P., & Märk, T. D. (2009). A high resolution and high sensitivity proton-transfer-reaction time-of-flight mass spectrometer (PTR-TOF-MS). *International Journal of Mass Spectrometry*, *286*(2–3), 122–128. https://doi.org/10.1016/j.ijms.2009.07.005

Joutsensaari, J., Loivamäki, M., Vuorinen, T., Miettinen, P., Nerg, A.-M., Holopainen, J. K., & Laaksonen, A. (2005). Nanoparticle formation by ozonolysis of inducible plant volatiles. *Atmospheric Chemistry and Physics*, *5*(6), 1489–1495. https://doi.org/10.5194/acp-5-1489-2005

Kammer, J., Décuq, C., Baisnée, D., Ciuraru, R., Lafouge, F., Buysse, P., Bsaibes, S., Henderson, B., Cristescu, S. M., Benabdallah, R., Chandra, V., Durand, B., Fanucci, O., Petit, J. E., Truong, F., Bonnaire, N., Sarda-Estève, R., Gros, V., & Loubet, B. (2020). Characterization of particulate and gaseous pollutants from a French dairy and sheep farm. *Science of the Total Environment*, *712*, 135598. https://doi.org/10.1016/j.scitotenv.2019.135598

Karl, M., Guenther, A., Köble, R., Leip, A., & Seufert, G. (2009). A new European plant-specific emission inventory of biogenic volatile organic compounds for use in atmospheric transport models. *Biogeosciences*, *6*(6), 1059–1087. https://doi.org/10.5194/bg-6-1059-2009

Kesselmeier, J., & Staudt, M. (1999). Biogenic Volatile Organic Compounds (VOC): An Overview on Emission, Physiology and Ecology. *Journal of Atmospheric Chemistry*, *33*(1), 23–88. https://doi.org/10.1023/A:1006127516791

Khan, Z. I., Ahmad, K., Batool, F., Wajid, K., Mehmood, N., Ashfaq, A., Bashir, H., Nadeem, M., & Ullah, S. (2019). Evaluation of toxic potential of metals in wheat crop grown in wastewater-contaminated soil in Punjab, Pakistan. *Environmental Science and Pollution Research International*, *26*(24), 24958—24966. https://doi.org/10.1007/s11356-019-05715-9

Kirkby, J., Duplissy, J., Sengupta, K., Frege, C., Gordon, H., Williamson, C., Heinritzi, M., Simon, M., Yan, C., Almeida, J., Tröstl, J., Nieminen, T., Ortega, I. K., Wagner, R., Adamov, A., Amorim, A., Bernhammer, A.-K., Bianchi, F., Breitenlechner, M., … Curtius, J. (2016). Ion-induced nucleation of pure biogenic particles. *Nature*, *533*(7604), 521–526. https://doi.org/10.1038/nature17953

Kotowska, U., & Isidorov, V. A. (2012). HS-SPME/GC–MS analysis of volatile and semi-volatile organic compounds emitted from municipal sewage sludge. *Environ Monit Assess*, 15.

Kroll, J. H., & Seinfeld, J. H. (2008). Chemistry of secondary organic aerosol: Formation and evolution of low-volatility organics in the atmosphere. *Atmospheric Environment*, *42*(16), 3593–3624. https://doi.org/10.1016/j.atmosenv.2008.01.003

Kühl, M., & Jørgensen, B. B. (1992). Microsensor Measurements of Sulfate Reduction and Sulfide Oxidation in Compact Microbial Communities of Aerobic Biofilms. *Applied and Environmental Microbiology*, *58*(4), 1164–1174. https://doi.org/10.1128/aem.58.4.1164-1174.1992

Kulmala, M., Vehkamäki, H., Petäjä, T., Maso, M. D., Lauri, A., Kerminen, V.-M., Birmili, W., & McMurry, P. H. (2004). Formation and growth rates of ultrafine atmospheric particles: A review of observations. *Journal of Aerosol Science*, *35*(2), 143–176. https://doi.org/10.1016/j.jaerosci.2003.10.003

Kumar, A., Alaimo, C. P., Horowitz, R., Mitloehner, F. M., Kleeman, M. J., & Green, P. G. (2011). Volatile organic compound emissions from green waste composting: Characterization and ozone formation. *Atmospheric Environment*, *45*(10), 1841–1848. https://doi.org/10.1016/j.atmosenv.2011.01.014

Kumar, S. (2012). *Biogas*. BoD – Books on Demand.

Kürten, A., Bergen, A., Heinritzi, M., Leiminger, M., Lorenz, V., Piel, F., Simon, M., Sitals, R., Wagner, A. C., & Curtius, J. (2016). Observation of new particle formation and measurement of sulfuric acid,ammonia, amines and highly oxidized organic molecules at a rural site incentral Germany. *Atmospheric Chemistry and Physics*, *16*(19), 12793–12813. https://doi.org/10.5194/acp-16-12793-2016

Lamastra, L., Suciu, N. A., & Trevisan, M. (2018). Sewage sludge for sustainable agriculture: Contaminants' contents and potential use as fertilizer. *Chemical and Biological Technologies in Agriculture*, *5*(1), 10. https://doi.org/10.1186/s40538-018-0122-3

Lee, A., Goldstein, A. H., Kroll, J. H., Ng, N. L., Varutbangkul, V., Flagan, R. C., & Seinfeld, J. H. (2006). Gas-phase products and secondary aerosol yields from the photooxidation of 16 different terpenes. *Journal of Geophysical Research*, *111*(D17), D17305. https://doi.org/10.1029/2006JD007050

Lee, S.-H., Gordon, H., Yu, H., Lehtipalo, K., Haley, R., Li, Y., & Zhang, R. (2019). New Particle Formation in the Atmosphere: From Molecular Clusters to Global Climate. *Journal of Geophysical Research: Atmospheres*, *124*(13), 7098–7146. https://doi.org/10.1029/2018JD029356

Leff, J. W., & Fierer, N. (2008). Volatile organic compound (VOC) emissions from soil and litter samples. *Soil Biology and Biochemistry*, *40*(7), 1629–1636. https://doi.org/10.1016/j.soilbio.2008.01.018

Lelieveld, J., Evans, J. S., Fnais, M., Giannadaki, D., & Pozzer, A. (2015). The contribution of outdoor air pollution sources to premature mortality on a global scale. *Nature*, *525*(7569), 367–371. https://doi.org/10.1038/nature15371

LI-840A CO2/H2O Analyzer. (2016, June). https://www.licor.com/documents/y10gor2jal2p3t8ev4hm

Lim, J.-H., Cha, J.-S., Kong, B.-J., & Baek, S.-H. (2018). Characterization of odorous gases at landfill site and in surrounding areas. *Journal of Environmental Management*, *206*, 291–303. https://doi.org/10.1016/j.jenvman.2017.10.045

Lim, S. S., Vos, T., Flaxman, A. D., Danaei, G., Shibuya, K., Adair-Rohani, H., AlMazroa, M. A., Amann, M., Anderson, H. R., Andrews, K. G., Aryee, M., Atkinson, C., Bacchus, L. J., Bahalim, A. N., Balakrishnan, K., Balmes, J., Barker-Collo, S., Baxter, A., Bell,

M. L., … Ezzati, M. (2012). A comparative risk assessment of burden of disease and injury attributable to 67 risk factors and risk factor clusters in 21 regions, 1990–2010: A systematic analysis for the Global Burden of Disease Study 2010. *The Lancet*, *380*(9859), 2224–2260. https://doi.org/10.1016/S0140-6736(12)61766-8

Lindinger, W., Hansel, A., & Jordan, A. (1998). Proton-transfer-reaction mass spectrometry (PTR-MS): On-line monitoring of volatile organic compounds at pptv levels. *Chemical Society Reviews*, *27*(5), 347–354. https://doi.org/10.1039/a827347z

Liu, D., Nyord, T., Rong, L., & Feilberg, A. (2018). Real-time quantification of emissions of volatile organic compounds from land spreading of pig slurry measured by PTR-MS and wind tunnels. *Science of the Total Environment*, *639*, 1079–1087. https://doi.org/10.1016/j.scitotenv.2018.05.149

Liu, Q., Li, M., Chen, R., Li, Z., Qian, G., An, T., Fu, J., & Sheng, G. (2009). Biofiltration treatment of odors from municipal solid waste treatment plants. *Waste Management*, *29*(7), 2051–2058. https://doi.org/10.1016/j.wasman.2009.02.002

Liu, Y., Li, L., An, J., Huang, L., Yan, R., Huang, C., Wang, H., Wang, Q., Wang, M., & Zhang, W. (2018). Estimation of biogenic VOC emissions and its impact on ozone formation over the Yangtze River Delta region, China. *Atmospheric Environment*, *186*, 113–128. https://doi.org/10.1016/j.atmosenv.2018.05.027

Liu, Y.-H., Lai, W.-S., Tsay, H.-J., Wang, T.-W., & Yu, J.-Y. (2013). Effects of maternal immune activation on adult neurogenesis in the subventricular zone–olfactory bulb pathway and olfactory discrimination. *Schizophrenia Research*, *151*(1), 1–11. https://doi.org/10.1016/j.schres.2013.09.007

Mackie, R. I., Stroot, P. G., & Varel, V. H. (1998). The online version of this article , along with updated information and services , is located on the World Wide Web at:

Biochemical Identification and Biological Origin of Key Odor Components in Livestock Waste 1 ABSTRACT : *Journal of Animal Science*, *76*, 1331–1342.

Materić, D., Bruhn, D., Turner, C., Morgan, G., Mason, N., & Gauci, V. (2015). Methods in Plant Foliar Volatile Organic Compounds Research. *Applications in Plant Sciences*, *3*(12), 1500044. https://doi.org/10.3732/apps.1500044

Mauldin, R. L. 3rd, Berndt, T., Sipilä, M., Paasonen, P., Petäjä, T., Kim, S., Kurtén, T., Stratmann, F., Kerminen, V.-M., & Kulmala, M. (2012). A new atmospherically relevant oxidant of sulphur dioxide. *Nature*, *488*(7410), 193–196. https://doi.org/10.1038/nature11278

McNeill, V. F. (2015). Aqueous organic chemistry in the atmosphere: Sources and chemical processing of organic aerosols. *Environmental Science & Technology*, *49*(3), 1237–1244. https://doi.org/10.1021/es5043707

McNeill, V. F. (2017). Atmospheric Aerosols: Clouds, Chemistry, and Climate. *Annual Review of Chemical and Biomolecular Engineering*, *8*(1), 427–444. https://doi.org/10.1146/annurev-chembioeng-060816-101538

Menta, C., & Remelli, S. (2020). Soil Health and Arthropods: From Complex System to Worthwhile Investigation. *Insects*, *11*.

Mihesan, C., Ziskind, M., Therssen, E., Desgroux, P., & Focsa, C. (2006). IR laser resonant desorption of polycyclic aromatic hydrocarbons. *Chemical Physics Letters*, *423*(4–6), 407–412. https://doi.org/10.1016/j.cplett.2006.04.032

Milieu, L., WRc, & and RPA. (2010). *Environmental economic and social impacts of the use of sewage sludge on land.* (Project Interim Reports Final Report; Part III).

Moreno, A. I., Arnáiz, N., Font, R., & Carratalá, A. (2014). Chemical characterization of emissions from a municipal solid waste treatment plant. *Waste Management*, *34*(11), 2393–2399. https://doi.org/10.1016/j.wasman.2014.07.008

Mrowiec, B., Suschka, J., & Keener, T. C. (2005). Formation and Biodegradation of Toluene in the Anaerobic Sludge Digestion Process. *Water Environment Research*, *77*(3), 274–278. https://doi.org/10.2175/106143005X41852

Muller, P. (1994). Glossary of Terms Used in Physical Organic Chemistry. *Pure and Applied Chemistry*, *66*(5), 1077–1184. https://doi.org/10.1351/pac199466051077

Munson, M. S. B., & Field, F. H. (1966). Chemical Ionization Mass Spectrometry. II. Esters. *Journal of the American Chemical Society*, *88*(19), 4337–4345. https://doi.org/10.1021/ja00971a007

Murphy, S. M., Sorooshian, A., Kroll, J. H., Ng, N. L., Chhabra, P. S., Tong, C., Surratt, J. D., Knipping, E. M., Flagan, R. C., & Seinfeld, J. H. (2007). Secondary aerosol formation from atmospheric reactions of aliphatic amines. *Atmospheric Chemistry and Physics*, *7*, 2313–2337.

Mustafa, M. F., Liu, Y., Duan, Z., Guo, H., Xu, S., Wang, H., & Lu, W. (2017). Volatile compounds emission and health risk assessment during composting of organic fraction of municipal solid waste. *Journal of Hazardous Materials*, *327*, 35–43. https://doi.org/10.1016/j.jhazmat.2016.11.046

Ngo, L. D., Duca, D., Carpentier, Y., Noble, J. A., Ikhenazene, R., Vojkovic, M., Irimiea, C., Ortega, I. K., Lefevre, G., Yon, J., Faccinetto, A., Therssen, E., Ziskind, M., Chazallon, B., Pirim, C., & Focsa, C. (2020). Chemical discrimination of the particulate and gas phases of miniCAST exhausts using a two-filter collection method. *Atmospheric Measurement Techniques*, *13*(2), 951–967. https://doi.org/10.5194/amt-13-951-2020

Ngoc, U. N., & Schnitzer, H. (2009). Sustainable solutions for solid waste management in Southeast Asian countries. *Waste Management (New York, N.Y.)*, *29*(6), 1982–1995. https://doi.org/10.1016/j.wasman.2008.08.031

Ngwabie, N. M., Schade, G. W., Custer, T. G., Linke, S., & Hinz, T. (2007). Volatile organic compound emission and other trace gases from selected animal buildings. *Landbauforschung Volkenrode*, *57*(3), 273–284.

Ngwabie, N. M., Schade, G. W., Custer, T., Linke, S., & Hinz, T. (2008). Abundances and flux estimates of volatile organic compounds from a dairy cowshed in Germany. *Journal of Environmental Quality*, *37 2*, 565–573.

Ni, J. Q., Robarge, W. P., Xiao, C., & Heber, A. J. (2012). Volatile organic compounds at swine facilities: A critical review. *Chemosphere*, *89*(7), 769–788. https://doi.org/10.1016/j.chemosphere.2012.04.061

Ni, Z., Liu, J., Song, M., Wang, X., Ren, L., & Kong, X. (2015). Characterization of odorous charge and photochemical reactivity of VOC emissions from a full-scale food waste treatment plant in China. *Journal of Environmental Sciences*, *29*, 34–44. https://doi.org/10.1016/j.jes.2014.07.031

Nie, E., Zheng, G., Gao, D., Chen, T., Yang, J., Wang, Y., & Wang, X. (2019). Emission characteristics of VOCs and potential ozone formation from a full-scale sewage sludge composting plant. *Science of the Total Environment*, *659*, 664–672. https://doi.org/10.1016/j.scitotenv.2018.12.404

Nie, E., Zheng, G., Shao, Z., Yang, J., & Chen, T. (2018). Emission characteristics and health risk assessment of volatile organic compounds produced during municipal solid waste composting. *Waste Management*, *79*. https://doi.org/10.1016/j.wasman.2018.07.024

Nkoa, R. (2014). Agricultural benefits and environmental risks of soil fertilization with anaerobic digestates: A review. *Agronomy for Sustainable Development*, *34*(2), 473–492. https://doi.org/10.1007/s13593-013-0196-z

Norman, M., Hansel, A., & Wisthaler, A. (2007). O2+ as reagent ion in the PTR-MS instrument: Detection of gas-phase ammonia. *International Journal of Mass Spectrometry*, *265*(2), 382–387. https://doi.org/10.1016/j.ijms.2007.06.010

Norman, M., Spirig, C., Wolff, V., Trebs, I., Flechard, C., Wisthaler, A., Schnitzhofer, R., Hansel, A., & Neftel, A. (2009). Intercomparison of ammonia measurement techniques at an intensively managed grassland site (Oensingen, Switzerland). *Atmospheric Chemistry and Physics*, *9*(8), 2635–2645. https://doi.org/10.5194/acp-9-2635-2009

Orzi, V., Riva, C., Scaglia, B., D'Imporzano, G., Tambone, F., & Adani, F. (2018). Anaerobic digestion coupled with digestate injection reduced odour emissions from soil during manure distribution. *Science of the Total Environment*, *621*, 168–176. https://doi.org/10.1016/j.scitotenv.2017.11.249

Pagliano, G., Ventorino, V., Panico, A., & Pepe, O. (2017). Integrated systems for biopolymers and bioenergy production from organic waste and by-products: A review of microbial processes. *Biotechnology for Biofuels*, *10*.

Parker, D. B., Gilley, J., Woodbury, B., Kim, K. H., Galvin, G., Bartelt-Hunt, S. L., Li, X., & Snow, D. D. (2013). Odorous VOC emission following land application of swine manure slurry. *Atmospheric Environment*, *66*, 91–100. https://doi.org/10.1016/j.atmosenv.2012.01.001

Particulate Matter in the United Kingdom. (n.d.).

Peltre, C., Christensen, B. T., Dragon, S., Icard, C., Kätterer, T., & Houot, S. (2012). RothC simulation of carbon accumulation in soil after repeated application of widely different organic amendments. *Soil Biology and Biochemistry*, *52*, 49–60. https://doi.org/10.1016/j.soilbio.2012.03.023

Peñuelas, J., ASENSIO, D., THOLL, D., WENKE, K., ROSENKRANZ, M., PIECHULLA, B., & SCHNITZLER, J. P. (2014). Biogenic volatile emissions from the soil. *Plant, Cell & Environment*, *37*(8), 1866–1891. https://doi.org/10.1111/pce.12340

Peres-Neto, P. R., Jackson, D. A., & Somers, K. M. (2005). How many principal components? Stopping rules for determining the number of non-trivial axes revisited. *Computational Statistics and Data Analysis*, *49*(4), 974–997. https://doi.org/10.1016/j.csda.2004.06.015

PICARRO G2103 Ammonia Analyzer, Ambient. (2012). www.picarro.com

Pidgeon, N., Parkhill, K., Corner, A., & Vaughan, N. (2013). Deliberating stratospheric aerosols for climate geoengineering and the SPICE project. *Nature Climate Change*, *3*(5), 451–457. https://doi.org/10.1038/nclimate1807

Placet, M., Mann, C. O., Gilbert, R. O., & Niefer, M. J. (2000). Emissions of ozone precursors from stationary sources: A critical review. *Atmospheric Environment*, *34*(12), 2183–2204. https://doi.org/10.1016/S1352-2310(99)00464-1

Potard, K., Monard, C., Le Garrec, J. L., Caudal, J. P., Le Bris, N., & Binet, F. (2017). Organic amendment practices as possible drivers of biogenic Volatile Organic Compounds emitted by soils in agrosystems. *Agriculture, Ecosystems and Environment*, *250*(September), 25–36. https://doi.org/10.1016/j.agee.2017.09.007

Rabaud, N. E., Ebeler, S. E., Ashbaugh, L. L., & Flocchini, R. G. (2003b). Characterization and quantification of odorous and non-odorous volatile organic compounds near a commercial dairy in California. *Atmospheric Environment*, *37*(7), 933–940. https://doi.org/10.1016/S1352-2310(02)00970-6

Radola, B., Picaud, S., Ortega, I. K., & Ciuraru, R. (2021). Formation of atmospheric molecular clusters from organic waste products and sulfuric acid molecules: A DFT study.

Environmental Science: Atmospheres, *1*(5), 267–275. https://doi.org/10.1039/D1EA00023C

Ras, M. R., Borrull, F., & Marcé, R. M. (2009). Sampling and preconcentration techniques for determination of volatile organic compounds in air samples. *Trends in Analytical Chemistry*, *28*, 347–361.

Restek™ Super-Clean™ Gas Filters.

Riccobono, F., Rondo, L., Sipilä, M., Barmet, P., Curtius, J., Dommen, J., Ehn, M., Ehrhart, S., Kulmala, M., Kürten, A., Mikkilä, J., Paasonen, P., Petäjä, T., Weingartner, E., & Baltensperger, U. (2012). Contribution of sulfuric acid and oxidized organic compounds to particle formation and growth. *Atmospheric Chemistry and Physics*, *12*(20), 9427–9439. https://doi.org/10.5194/acp-12-9427-2012

Rincón, C. A., De Guardia, A., Couvert, A., Le Roux, S., Soutrel, I., Daumoin, M., & Benoist, J. C. (2019). Chemical and odor characterization of gas emissions released during composting of solid wastes and digestates. *Journal of Environmental Management*, *233*(November 2018), 39–53. https://doi.org/10.1016/j.jenvman.2018.12.009

Rockwood, A. L., Kushnir, M. M., & Clarke, N. J. (2018). 2—Mass Spectrometry. In N. Rifai, A. R. Horvath, & C. T. Wittwer (Eds.), *Principles and Applications of Clinical Mass Spectrometry* (pp. 33–65). Elsevier. https://doi.org/10.1016/B978-0-12-816063-3.00002-5

Rosenfeld, P. E., Clark, J. J. J., Hensley, A. R., & Suffet, I. H. (2007). The use of an odour wheel classification for the evaluation of human health risk criteria for compost facilities. *Water Science and Technology*, *55*(5), 345–357. https://doi.org/10.2166/wst.2007.197

Rosenfeld, P. E., Henry, C. L., Dills, R. L., & Harrison, R. B. (2001). Comparison of odor emissions from three different biosolids applied to forest soil. *Water, Air, and Soil Pollution*, *127*(1–4), 173–191. https://doi.org/10.1023/A:1005286429528

Rotstayn, L. D. (1999). Indirect forcing by anthropogenic aerosols: A global climate model calculation of the effective-radius and cloud-lifetime effects. *Journal of Geophysical Research: Atmospheres*, *104*(D8), 9369–9380. https://doi.org/10.1029/1998JD900009

S. F. Higgins, S. A. Shearer, M. S. Coyne, & J. P. Fulton. (2004). Relationship of total nitrogen and total phosphorus concentration to solids content in animal waste slurries. *Applied Engineering in Agriculture*, *20*(3), 355–364. https://doi.org/10.13031/2013.16066

Sabbah, H., Bonnamy, A., Papanastasiou, D., Cernicharo, J., Martín-Gago, J.-A., & Joblin, C. (2017). Identification of PAH Isomeric Structure in Cosmic Dust Analogs: The AROMA Setup. *The Astrophysical Journal*, *843*(1), 34. https://doi.org/10.3847/1538-4357/aa73dd

Sabbah, H., Commodo, M., Picca, F., De Falco, G., Minutolo, P., D'Anna, A., & Joblin, C. (2021). Molecular content of nascent soot: Family characterization using two-step laser desorption laser ionization mass spectrometry. *Proceedings of the Combustion Institute*, *38*(1), 1241–1248. https://doi.org/10.1016/j.proci.2020.09.022

Safley, L. M., Westerman, P. W., & Barker, J. C. (1986). Fresh dairy manure characteristics and barnlot nutrient losses. *Agricultural Wastes*, *17*(3), 203–215. https://doi.org/10.1016/0141-4607(86)90094-6

Sánchez-Monedero, M. A., Fernández-Hernández, A., Higashikawa, F. S., & Cayuela, M. L. (2018). Relationships between emitted volatile organic compounds and their concentration in the pile during municipal solid waste composting. *Waste Management*, *79*, 179–187. https://doi.org/10.1016/j.wasman.2018.07.041

Sankhe, K., Khan, T., Bhavsar, C., Momin, M., & Omri, A. (2019). Selective drug deposition in lungs through pulmonary drug delivery system for effective management of drug-resistant TB. *Expert Opinion on Drug Delivery*, *16*(5), 525–538. https://doi.org/10.1080/17425247.2019.1609937

Scaglia, B., Orzi, V., Artola, A., Font, X., Davoli, E., Sanchez, A., & Adani, F. (2011). Odours and volatile organic compounds emitted from municipal solid waste at different stage of decomposition and relationship with biological stability. *Bioresource Technology*, *102*(7), 4638–4645. https://doi.org/10.1016/j.biortech.2011.01.016

Scheutz, C., Bogner, J., Chanton, J. P., Blake, D., Morcet, M., Aran, C., & Kjeldsen, P. (2008). Atmospheric emissions and attenuation of non-methane organic compounds in cover soils at a French landfill. *Waste Management*, *28*(10), 1892–1908. https://doi.org/10.1016/j.wasman.2007.09.010

Schiavon, M., Martini, L. M., Corrà, C., Scapinello, M., Coller, G., Tosi, P., & Ragazzi, M. (2017). Characterisation of volatile organic compounds (VOCs) released by the composting of different waste matrices. *Environmental Pollution*, *231*, 845–853. https://doi.org/10.1016/j.envpol.2017.08.096

Schiffman, S. S., Bennett, J. L., & Raymer, J. H. (2001). Quantification of odors and odorants from swine operations in North Carolina. *Agricultural and Forest Meteorology*, *108*(3), 213–240. https://doi.org/10.1016/S0168-1923(01)00239-8

Schmithausen, A., Schiefler, I., Trimborn, M., Gerlach, K., Südekum, K.-H., Pries, M., & Büscher, W. (2018). Quantification of Methane and Ammonia Emissions in a Naturally Ventilated Barn by Using Defined Criteria to Calculate Emission Rates. *Animals*, *8*(5), 75. https://doi.org/10.3390/ani8050075

Schobesberger, S., Junninen, H., Bianchi, F., Lönn, G., Ehn, M., Lehtipalo, K., Dommen, J., Ehrhart, S., Ortega, I. K., Franchin, A., Nieminen, T., Riccobono, F., Hutterli, M.,

Duplissy, J., Almeida, J., Amorim, A., Breitenlechner, M., Downard, A. J., Dunne, E. M., … Worsnop, D. R. (2013). Molecular understanding of atmospheric particle formation from sulfuric acid and large oxidized organic molecules. *Proceedings of the National Academy of Sciences*, *110*(43), 17223–17228. https://doi.org/10.1073/pnas.1306973110

Schulz, R., & Römheld, V. (1997). Recycling of municipal and industrial organic wastes in agriculture: Benefits, limitations, and means of improvement. *Soil Science and Plant Nutrition*, *43*(SPEC. ISS.), 1051–1056. https://doi.org/10.1080/00380768.1997.11863716

Seinfeld, J. H., & Pankow, J. F. (2003). Organic Atmospheric Particulate Material. *Annual Review of Physical Chemistry*, *54*(1), 121–140. https://doi.org/10.1146/annurev.physchem.54.011002.103756

Sharma, B., Sarkar, A., Singh, P., & Singh, R. P. (2017). Agricultural utilization of biosolids: A review on potential effects on soil and plant grown. *Waste Management*, *64*, 117–132. https://doi.org/10.1016/j.wasman.2017.03.002

Sharma, B., Vaish, B., Monika, Singh, U. K., Singh, P., & Singh, R. P. (2019). Recycling of Organic Wastes in Agriculture: An Environmental Perspective. *International Journal of Environmental Research*, *13*(2), 409–429. https://doi.org/10.1007/s41742-019-00175-y

Shaw, S. L., Mitloehner, F. M., Jackson, W., DePeters, E. J., Fadel, J. G., Robinson, P. H., Holzinger, R., & Goldstein, A. H. (2007). Volatile Organic Compound Emissions from Dairy Cows and Their Waste as Measured by Proton-Transfer-Reaction Mass Spectrometry. *Environmental Science & Technology*, *41*(4), 1310–1316. https://doi.org/10.1021/es061475e

Shen, Y., Chen, T.-B., Gao, D., Zheng, G., Liu, H., & Yang, Q. (2012). Online monitoring of volatile organic compound production and emission during sewage sludge composting. *Bioresource Technology*, *123*, 463–470. https://doi.org/10.1016/j.biortech.2012.05.006

Shon, Z., Kim, K., Jeon, E., Kim, M., Kim, Y., & Song, S. (2005). Photochemistry of reduced sulfur compounds in a landfill environment. *Atmospheric Environment*, *39*(26), 4803–4814. https://doi.org/10.1016/j.atmosenv.2005.06.024

Siebert, S., Gilbert, J., & Ricci-Jürgensen, M. (2019). *Compost production in EUROPE*. 3.

Silvern, R. F., Jacob, D. J., Kim, P. S., Marais, E. A., & Turner, J. R. (2016). *Incomplete Sulfate Aerosol Neutralization Despite Excess Ammonia in the Eastern US: A Possible Role of Organic Aerosol*.

Sindelarova, K., Granier, C., Bouarar, I., Guenther, A., Tilmes, S., Stavrakou, T., Müller, J. F., Kuhn, U., Stefani, P., & Knorr, W. (2014). Global data set of biogenic VOC emissions calculated by the MEGAN model over the last 30 years. *Atmospheric Chemistry and Physics*, *14*(17), 9317–9341. https://doi.org/10.5194/acp-14-9317-2014

Singh, A. P., Singh, R., Mina, U., Singh, M. P., & Varshney, C. K. (2011). Emissions of monoterpene from tropical Indian plant species and assessment of VOC emission from the forest of Haryana state. *Atmospheric Pollution Research*, *2*(1), 72–79. https://doi.org/10.5094/APR.2011.009

Sintermann, J., Schallhart, S., Kajos, M., Jocher, M., Bracher, A., Münger, A., Johnson, D., Neftel, A., & Ruuskanen, T. (2014). Trimethylamine emissions in animal husbandry. *Biogeosciences*, *11*(18), 5073–5085. https://doi.org/10.5194/bg-11-5073-2014

Smith, E. A., & Macfarlane, G. T. (1996). Enumeration of human colonie bacteria producing phenolic and indolic compounds: Effects of pH, carbohydrate availability and retention time on dissimilatory aromatic amino acid metabolism. *Journal of Applied Bacteriology*, *81*(3), 288–302. https://doi.org/10.1111/j.1365-2672.1996.tb04331.x

Spaulding, R. S., Schade, G. W., Goldstein, A. H., & Charles, M. J. (2003). Characterization of secondary atmospheric photooxidation products: Evidence for biogenic and anthropogenic sources. *Journal of Geophysical Research: Atmospheres*, *108*(D8). https://doi.org/10.1029/2002JD002478

Stinner, W., Möller, K., & Leithold, G. (2008). Effects of biogas digestion of clover/grass-leys, cover crops and crop residues on nitrogen cycle and crop yield in organic stockless farming systems. *European Journal of Agronomy*, *29*(2), 125–134. https://doi.org/10.1016/j.eja.2008.04.006

Strohalm, M., Kavan, D., Novák, P., Volný, M., & Havlíček, V. (2010). MMass 3: A cross-platform software environment for precise analysis of mass spectrometric data. *Anal Chem 82, 11,* 4648–4651. https://doi.org/10.1021/ac100818g

Sulfur Dioxide Monitor Instrument Handbook (DOE/SC-ARM-TR-180; SR Springston, p. 30). (2016).

Sulzer, P., Hartungen, E., Hanel, G., Feil, S., Winkler, K., Mutschlechner, P., Haidacher, S., Schottkowsky, R., Gunsch, D., Seehauser, H., Striednig, M., Jürschik, S., Breiev, K., Lanza, M., Herbig, J., Märk, L., Märk, T. D., & Jordan, A. (2014). A Proton Transfer Reaction-Quadrupole interface Time-Of-Flight Mass Spectrometer (PTR-QiTOF): High speed due to extreme sensitivity. *International Journal of Mass Spectrometry*, *368*, 1–5. https://doi.org/10.1016/j.ijms.2014.05.004

Sun, H., Trabue, S. L., Scoggin, K., Jackson, W. A., Pan, Y., Zhao, Y., Malkina, I. L., Koziel, J. A., & Mitloehner, F. M. (2008). Alcohol, Volatile Fatty Acid, Phenol, and Methane Emissions from Dairy Cows and Fresh Manure. *Journal of Environmental Quality*, *37*(2), 615–622. https://doi.org/10.2134/jeq2007.0357

Sundberg, R. (1970). *The Chemistry of Indoles* (1st ed.). Academic Press.

Tanaka, Y. (1988). Sensitivity analysis in principal component analysis: Influence on the subspace spanned by principal components. *Communications in Statistics - Theory and Methods*, *17*(9), 3157–3175. https://doi.org/10.1080/03610928808829796

Tay, J. H., Chen, X. G., Jeyaseelan, S., & Graham, N. (2001). A comparative study of anaerobically digested and undigested sewage sludges in preparation of activated carbons. *Chemosphere*, *44*(1), 53–57. https://doi.org/10.1016/S0045-6535(00)00384-2

Tester, C. F. (1990). Organic Amendment Effects on Physical and Chemical Properties of a Sandy Soil. *Soil Science Society of America Journal*, *54*(3), 827–831. https://doi.org/10.2136/sssaj1990.03615995005400030035x

Trost, B., & Fremgen, D. (2016). *Standard Operating Procedures Ozone (O3) Monitoring in Ambient Air by Ultraviolet Absorption Spectrophotometry* (DEC Air Monitoring & Quality Assurance Program, p. 45). www.state.ak.us/dec/

Tsai, C.-J., Chen, M.-L., Ye, A.-D., Chou, M.-S., Shen, S.-H., & Mao, I.-F. (2008). The relationship of odor concentration and the critical components emitted from food waste composting plants. *Atmospheric Environment*, *42*(35), 8246–8251. https://doi.org/10.1016/j.atmosenv.2008.07.055

Vaish, B., Sharma, B., Srivastava, V., Singh, P., Ibrahim, M. H., & Singh, R. P. (2019). Energy recovery potential and environmental impact of gasification for municipal solid waste. *Biofuels*, *10*(1), 87–100. https://doi.org/10.1080/17597269.2017.1368061

Vuolo, R. M., Loubet, B., Mascher, N., Gueudet, J.-C., Durand, B., Laville, P., Zurfluh, O., Ciuraru, R., Stella, P., & Trebs, I. (2017). Nitrogen oxides and ozone fluxes from an oilseed-rape management cycle: The influence of cattle slurry application. *Biogeosciences*, *14*(8), 2225–2244. https://doi.org/10.5194/bg-14-2225-2017

Waldron, K. (2007). 1—Waste minimization, management and co-product recovery in food processing: An introduction. In K. Waldron (Ed.), *Handbook of Waste Management*

and Co-Product Recovery in Food Processing (pp. 3–20). Woodhead Publishing. https://doi.org/10.1533/9781845692520.1.3

Wang, R., Wu, T., Dai, W., Liu, H., Zhao, J., Wang, X., Huang, F., Wang, Z., & Shi, C. (2015). Effects of straw return on C2–C5 non-methane hydrocarbon (NMHC) emissions from agricultural soils. *Atmospheric Environment*, *100*, 210–217. https://doi.org/10.1016/j.atmosenv.2014.10.051

Weiland, P. (2010). Biogas production: Current state and perspectives. *Applied Microbiology and Biotechnology*, *85*(4), 849–860. https://doi.org/10.1007/s00253-009-2246-7

Widiana, D. R., Wang, Y. F., You, S. J., Yang, H. H., Wang, L. C., Tsai, J. H., & Chen, H. M. (2019). Air pollution profiles and health risk assessment of ambient volatile organic compounds above a municipal wastewater treatment plant, Taiwan. *Aerosol and Air Quality Research*, *19*(2), 375–382. https://doi.org/10.4209/aaqr.2018.11.0408

Wiedensohler, A., Birmili, W., Nowak, A., Sonntag, A., Weinhold, K., Merkel, M., Wehner, B., Tuch, T., Pfeifer, S., Fiebig, M., Fjäraa, A. M., Asmi, E., Sellegri, K., Depuy, R., Venzac, H., Villani, P., Laj, P., Aalto, P., Ogren, J. A., … de Leeuw, G. (2010). Particle mobility size spectrometers: Harmonization of technical standards and data structure to facilitate high quality long-term observations of atmospheric particle number size distributions. *Atmospheric Measurement Techniques Discussions*, *3*(6), 5521–5587. https://doi.org/10.5194/amtd-3-5521-2010

Williams, P. E. V. (1995). Animal production and European pollution problems. *Animal Feed Science and Technology*, *53*(2), 135–144. https://doi.org/10.1016/0377-8401(95)02017-T

Wilson, S. C., Burnett, V., Waterhouse, K. S., & Jones, K. C. (1994). Volatile Organic Compounds in Digested United Kingdom Sewage Sludges. *Environmental Science and Technology*, *28*(2), 259–266. https://doi.org/10.1021/es00051a012

Woodbury, B. L., Gilley, J. E., Parker, D. B., & Marx, D. B. (2022). *Emission of Volatile Organic Compounds from Land-Applied Beef Cattle Manure as Affected by Application Method, Diet, and Soil Water Condition*. *65*(1), 123–133. https://doi.org/doi.org/10.13031/ja.14587

Woodbury, B. L., Gilley, J. E., Parker, D. B., Marx, D. B., Miller, D. N., & Eigenberg, R. A. (2014). Emission of volatile organic compounds after land application of cattle manure. *Journal of Environmental Quality*, *43*(4), 1207–1218. https://doi.org/10.2134/jeq2013.05.0185

World Bank, U.S., 2019. World Development Report, Population Growth. (2019). https://data.worldbank.org/indicator/SP. POP.GROW.

World Health Organization, Burden of disease from the joint effects of household and ambient air pollution for 2011. (2014). http://www.who.int/phe/ health_topics/outdoorair/databases/AP_jointeffect_BoD_results_ March2014.pdf?ua=1

Wu, J. J., & Masten, S. J. (2002). *Oxidation kinetics of phenolic and indolic compounds by ozone: Applications to synthetic and real swine manure slurry*. *36*, 1513–1526.

Xue, S., Ding, W., Lin Li, Ma, J., Chai, F., & Liu, J. (2021). Emission, dispersion, and potential risk of volatile organic and odorous compounds in the exhaust gas from two sludge thermal drying processes. *Waste Management*, *138*, 116–124. https://doi.org/doi.org/10.1016/j.wasman.2021.11.040

Yadav, A., & Garg, V. K. (2011). Recycling of organic wastes by employing Eisenia fetida. *Bioresource Technology*, *102*(3), 2874–2880. https://doi.org/10.1016/j.biortech.2010.10.083

Yáñez-Serrano, A. M., Filella, I., LLusià, J., Gargallo-Garriga, A., Granda, V., Bourtsoukidis, E., Williams, J., Seco, R., Cappellin, L., Werner, C., de Gouw, J., & Peñuelas, J. (2021).

GLOVOCS - Master compound assignment guide for proton transfer reaction mass spectrometry users. *Atmospheric Environment*, *244*, 117929. https://doi.org/10.1016/j.atmosenv.2020.117929

Yao, L., Garmash, O., Bianchi, F., Zheng, J., Yan, C., Kontkanen, J., Junninen, H., Mazon, S. B., Ehn, M., Paasonen, P., Sipilä, M., Wang, M., Wang, X., Xiao, S., Chen, H., Lu, Y., Zhang, B., Wang, D., Fu, Q., … Wang, L. (2018). Atmospheric new particle formation from sulfuric acid and amines in a Chinese megacity. *Science*, *361*(6399), 278–281. https://doi.org/10.1126/science.aao4839

Yao, X., Ma, R., Li, H., Wang, C., Zhang, C., Yin, S., Wu, D., He, X., Wang, J., Zhan, L., & He, R. (2019). *Assessment of the major odor contributors and health risks of volatile compounds in three disposal technologies for municipal solid waste*. *91*, 128–138. https://doi.org/10.1016/j.wasman.2019.05.009

Yu, H., McGraw, R., & Lee, S.-H. (2012). Effects of amines on formation of sub-3 nm particles and their subsequent growth: MULTICOMPONENT NUCLEATION WITH AMINES. *Geophysical Research Letters*, *39*(2), n/a-n/a. https://doi.org/10.1029/2011GL050099

Yuan, B., Coggon, M. M., Koss, A. R., Warneke, C., Eilerman, S., Peischl, J., Aikin, K. C., Ryerson, T. B., & Gouw, J. A. D. (2017). *Emissions of volatile organic compounds (VOCs) from concentrated animal feeding operations (CAFOs): Chemical compositions and separation of sources*. 4945–4956. https://doi.org/10.5194/acp-17-4945-2017

Zhang, B., Tian, H., Lu, C., Dangal, S. R. S., Yang, J., & Pan, S. (2017). *Global manure nitrogen production and application in cropland during 1860 – 2014: A 5 arcmin gridded global dataset for Earth system modeling*. 667–678.

Zhang, H., Schuchardt, F., Li, G., Yang, J., & Yang, Q. (2013). Emission of volatile sulfur compounds during composting of municipal solid waste (MSW). *Waste Management*, *33*(4), 957–963. https://doi.org/10.1016/j.wasman.2012.11.008

Zhang, Y., Zhu, Z., Zheng, Y., Chen, Y., & Yin, F. (2019). *Characterization of Volatile Organic Compound (VOC) Emissions from Swine Manure Biogas Digestate Storage*.

Zheng, J., Hu, M., Du, Z., Shang, D., Gong, Z., Qin, Y., Fang, J., Gu, F., Li, M., Peng, J., Li, J., Zhang, Y., Huang, X., He, L., Wu, Y., & Guo, S. (2017). Influence of biomass burning from South Asia at a high-altitude mountain receptor site in China. *Atmospheric Chemistry and Physics*, *17*(11), 6853–6864. https://doi.org/10.5194/acp-17-6853-2017

Zhu, Y., Zheng, G., Gao, D., Chen, T., & Wu, F. (2016). Odor composition analysis and odor indicator selection during sewage sludge composting. *Journal of the Air & Waste Management Association*, *66*(9), 930–940. https://doi.org/10.1080/10962247.2016.1188865

Zieba-Palus, J., & Borusiewicz, R. (2006). Examination of multilayer paint coats by the use of infrared, Raman and XRF spectroscopy for forensic purposes. *Journal of Molecular Structure*, *792*, 286–292.

This page is intentionally left blank

Annexes

Annex 1

Blank experiments were done for the 0.03 m^3 and a 0.18 m^3 chambers without any sample inside. The blank experiments were performed in the same protocol for the other experiments. The chamber was flushed with a high purity dry air with the same flow rates used for other experiments (**Table A.1**). After that, a known concentration of O_3 was introduced into the chamber using the dry air as a carrier gas. The residence time of air inside the chamber was calculated as follows:

Residence time (min) = Volume of the chamber (L) / Flow rate of dry air (L min^{-1}) **(A 1.1)**

Table A.1 *Atmospheric simulation chambers description.*

Chamber	**Volume (m^3)**	**Dry Air flow rate (L min^{-1})**	**Dry air residence time**
1	0.03	6	5
2	0.18	8.6 - 10	~18 - 20

Figure A.1 shows the particle number concentration and size distribution measured by SMPS (Top), SO_2 inside the chamber and O_3 mixing ratio injected into the chamber (Middle), and the mixing ratios of skatole and other oxidation products verified to be emitted from our samples (Bottom). The blue colour means that the particle number concentration was less than 10 particles/cm^3 and the red colour means it was greater than 10^5 particle/cm^3. More examples of some VOCs emitted from our samples and followed in blank chambers were illustrated in **Figure A.2**. The observed VOC emissions were relatively null or low.

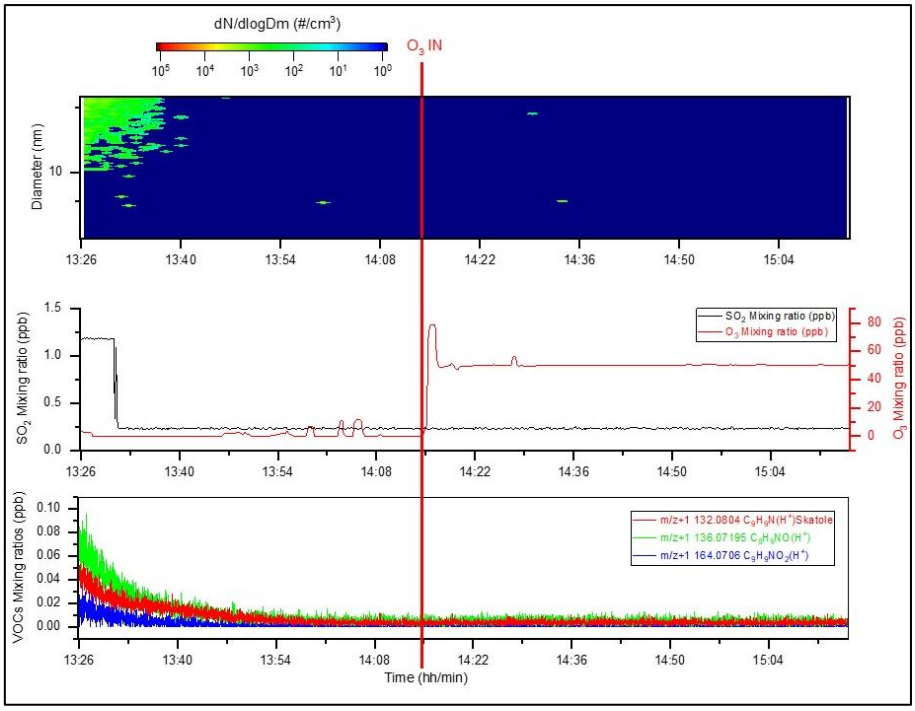

Figure A.1 *(Up) Temporal variation of the particle number concentration and size distribution in the chamber measured using SMPS. (Middle) Mixing ratio of SO_2 inside the chamber and O_3 introduced into the chamber as a function of time. (Bottom) Temporal variation of some VOCs selected as examples. The red line indicates the moment of O_3 addition into the chamber.*

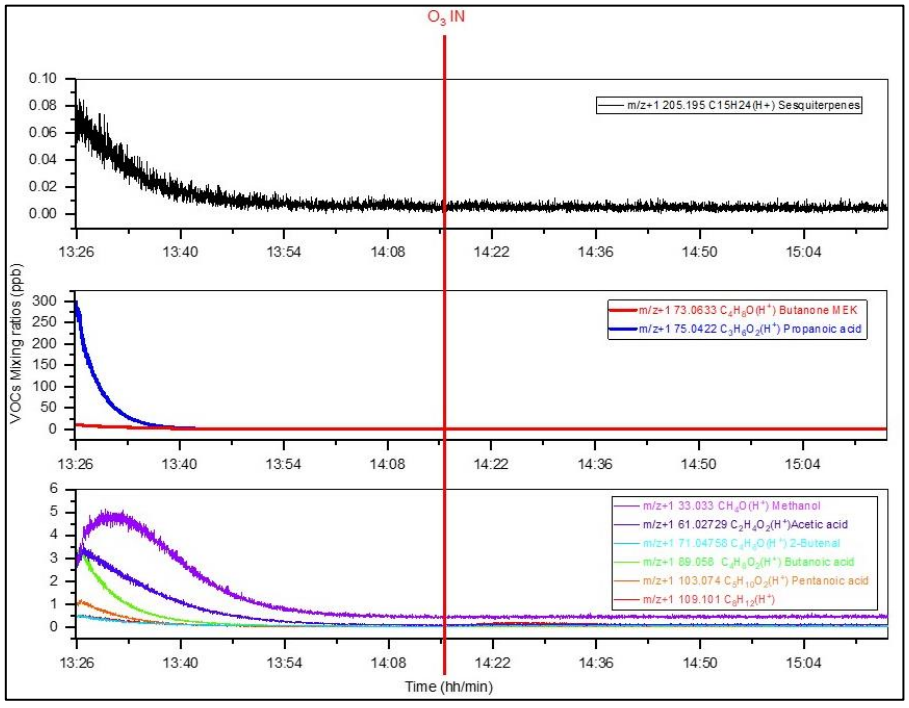

Figure A.2 *Temporal variation of some selected VOCs. The red line indicates the moment of O_3 addition into the chamber.*

Annex 2

Mixing ratio (ppbv) $=1.6575799*10^{-11} * \frac{\text{Udrift [V]Tdrift}^2\text{[K]}}{\text{k pdrift}^2\text{[mbar]}} * \frac{\text{Raw signal of VOCH}^+}{\text{Raw signal of H3O}^+} * \frac{\text{TR(H3O}^+)}{\text{TR(VOCH}^+)}$

Calculation of constant

Concentration in 1 cm^{-3}

$$C_{1/cm^3} = \frac{1}{kt} \cdot \frac{C^+}{H_3O^+} \cdot \frac{TR_{H_3O^+}}{TR_{C^+}}$$

Concentration in ppbv

$$C_{ppbV} = 10^9 \frac{C_{1/cm^3}}{air_{1/cm^3}}$$

reaction time t:

with $\frac{l}{t} = \mu \cdot E = \mu \cdot \frac{U}{l} \Rightarrow t = \frac{l^2}{\mu \cdot U}$ and the ion mobility $\mu = \mu_0 \cdot \frac{p_0}{p_{drift}} \cdot \frac{T_{drift}}{T_0}$

$$t = \frac{l^2}{\mu_0 U_{drift}} \cdot \frac{T_0[K]}{T_{drift}[K]} \cdot \frac{p_{drift}[mbar]}{p_0[mbar]}$$

number of air molecules per cm:

$$air_{1/cm^3} = \frac{N_A}{22400} \cdot \frac{T_0[K]}{T_{act}[K]} \cdot \frac{p_{drift}[mbar]}{p_0[mbar]}$$

we get for C (ppbv)

$$C_{ppbV} = \frac{10^9}{k} \cdot \frac{22400\,\mu_0}{N_A l^2} U_{drift} \cdot \frac{T^2_{drift}[K]}{T^2_0[K]} \cdot \frac{p^2_0[mbar]}{p^2_{drift}[mbar]} \cdot \frac{C^+}{H_3O^+} \cdot \frac{TR_{H_3O^+}}{TR_{C^+}}$$

$\mu_0 = 2.8 \frac{cm^2}{Vs}$	reduced mobility
$p_0 = 1013.25\,mbar$	Air pressure at standard conditions
p_{drift}	Drift-tube pressure
$T_0 = 273.15\,K$	Temperature at standard conditions
$T_{drift}[K] = T_0[K] + t_{drift}[C]$	Drift-tube temperature in Kelvin
$t_{drift}[C]$	Drift-tube temperature in Celcius
$N_A = 6.022e23$	Avogadro Number
$l = 9.3cm$	length of the reaction chamber

Substituting the values of the constants in red boxes give the constant value exist in the equation of mixing ratio (ppbv)

$$\textit{Mixing ratio (ppbv)} = 1.6575799.10^{-11} \times \frac{U_{drift}[V]T_{drift}^2[K]}{k\,p_{drift}^2[mbar]} \cdot \frac{Raw\ signal\ of\ VOCH^+}{Raw\ signal\ of\ H_3O^+} \cdot \frac{TRH_3O^+}{TRVOCH^+}$$

Figure A.3 *Derivation of the constant used in mixing ratio calculation.*

Annex 3

Table A.2 *List of compounds detected using PTR-QiTOF-MS and emitted from SS samples by decreasing order of the molecular weight of compounds assigned in each chemical family. The number of compounds assigned to each chemical family is given in parenthesis.*

Molecular formula	Molecular weight	Theoretical protonated mass	SS sample with compound detected
Hydrocarbons (95)			
C3H6	42.0470	43.0548	All samples
C3H4	40.0313	41.0391	All samples
C4H2	50.0157	51.0235	SS60%, DSS
C4H4	52.0313	53.0391	All samples
C4H6	54.0470	55.0548	All samples
C4H8	56.0626	57.0704	All samples
C5H4	64.0313	65.0391	SS60%, DSS
C5H6	66.0470	67.0548	All samples

C5H8	68.0626	69.0704	All samples
C5H10	70.0783	71.0861	All samples
C6H4	76.0313	77.0391	UDSS
C5H2	78.0106	79.0184	SS30%, UDSS
C6H6	78.0470	79.0548	All samples
C6H8	80.0621	81.0699	All samples
C6H10	82.0783	83.0861	All samples
C6H12	84.0939	85.1017	All samples
C7H6	90.0470	91.0548	All samples
C7H8	92.0626	93.0704	All samples
C7H10	94.0783	95.0861	All samples
C7H12	96.0939	97.1017	All samples
C7H14	98.1096	99.1174	All samples
C8H8	104.0626	105.0704	SS60% , SS30% , DSS
C8H10	106.0783	107.0861	All samples
C8H12	108.0939	109.1017	SS60% , SS30% , DSS
C8H14	110.1096	111.1174	All samples
C8H16	112.1252	113.1330	All samples
C9H10	118.0783	119.0861	SS60% , SS30% , DSS
C9H12	120.0939	121.1017	All samples
C9H14	122.1096	123.1174	All samples
C9H16	124.1252	125.1330	All samples
C9H18	126.1409	127.1487	SS60% , SS30% , DSS
C10H10	130.0783	131.0861	SS30%, DSS
C10H12	132.0939	133.1017	SS60% , SS30% , DSS
C10H14	134.1096	135.1174	All samples
C10H16	136.1252	137.1330	All samples
C10H18	138.1409	139.1487	All samples
C10H20	140.1565	141.1643	SS60% , SS30%
C11H14	146.1096	147.1174	All samples
C11H16	148.1252	149.1330	All samples
C11H18	150.1409	151.1487	All samples
C11H20	152.1565	153.1643	SS60% , SS30%
C11H22	154.1722	155.1800	SS60% , SS30%
C12H12	156.0939	157.1017	SS60% , SS30% , DSS

C12H14	158.1096	159.1174	SS60% , SS30% , DSS
C12H16	160.1252	161.1330	All samples
C12H18	162.1409	163.1487	All samples
C12H20	164.1565	165.1643	All samples
C12H22	166.1722	167.1800	SS60% , SS30% , DSS
C12H24	168.1878	169.1956	SS60% , SS30% , DSS
C13H14	170.1096	171.1174	All samples
C13H18	174.1409	175.1487	All samples
C13H20	176.1565	177.1643	All samples
C13H22	178.1722	179.1800	All samples
C13H24	180.1878	181.1956	SS60% , SS30% , DSS
C13H26	182.2035	183.2113	SS60%
C14H16	184.1252	185.1330	DSS, UDSS
C14H18	186.1409	187.1487	All samples
C14H20	188.1565	189.1643	All samples
C14H22	190.1722	191.1800	All samples
C14H24	192.1878	193.1956	All samples
C14H26	194.2035	195.2113	SS60% , SS30% , DSS
C14H28	196.1252	197.1330	SS60% , SS30% , DSS
C15H16	196.1252	197.1330	SS30%
C15H18	198.1409	199.1487	SS30%
C15H20	200.1565	201.1643	All samples
C15H22	202.1722	203.1800	All samples
C15H24	204.1878	205.1956	All samples
C15H26	206.2035	207.2113	All samples
C15H28	208.2191	209.2269	SS60% , SS30% , DSS
C15H30	210.2348	211.2426	SS60% , SS30% , DSS
C16H20	212.1565	213.1643	SS30%, UDSS
C16H22	214.1722	215.1800	All samples
C16H24	216.1878	217.1956	All samples
C16H26	218.2035	219.2113	All samples
C16H28	220.2191	221.2269	SS60% , SS30% , DSS
C16H30	222.2348	223.2426	SS60% , SS30% , DSS
C16H32	224.2504	225.2582	SS60% , SS30% , DSS
C17H24	228.1878	229.1956	SS60%

C17H26	230.2035	231.2113	All samples
C17H28	232.2191	233.2269	All samples
C17H30	234.2348	235.2426	SS60%
C17H32	236.2504	237.2582	SS60%
C17H34	238.2661	239.2739	SS60% , SS30%
C18H26	242.2035	243.2113	SS60% , SS30%
C18H28	244.2191	245.2269	SS60% , SS30% , DSS
C18H30	246.2348	247.2426	SS60% , SS30% , DSS
C18H32	248.2504	249.2582	SS60% , SS30%
C18H34	250.2661	251.2739	SS60%
C18H36	252.2817	253.2895	SS60% , SS30%
C19H30	258.2348	259.2426	SS60%
C19H32	260.2504	261.2582	SS60% , SS30% ,UDSS
C19H34	262.2661	263.2739	SS60% , SS30%
C20H32	272.2504	273.2582	All samples
C20H34	274.2661	275.2739	All samples
C21H34	286.2661	287.2739	SS60% , SS30% ,UDSS
Oxygenated compounds (103)			
CH2O	30.0106	31.0184	SS60% , SS30% ,UDSS
CH4O	32.0262	33.0340	SS60%, DSS, UDSS
C2H2O	42.0106	43.0184	SS60% , UDSS
C2H4O	44.0262	45.0340	All samples
CH2O2	46.0055	47.0133	SS60%, DSS
C2H6O	46.0419	47.0497	SS60%, DSS
C3H4O	56.0262	57.0340	DSS, UDSS
C3H5O	57.0340	58.0418	SS60% , UDSS
C3H6O	58.0419	59.0497	All samples
C2H4O2	60.0211	61.0289	All samples
C4H2O	66.0106	67.0184	UDSS
C4H6O	70.0419	71.0497	SS30%, DSS, UDSS
C3H4O2	72.0211	73.0289	UDSS
C4H8O	72.0575	73.0653	All samples
C3H6O2	74.0368	75.0446	All samples
C3H8O2	76.0524	77.0602	SS60% , SS30% , DSS
C5H4O	80.0262	81.0340	UDSS

C5H6O	82.0419	83.0497	UDSS
C4H4O2	84.0211	85.0289	UDSS
C5H8O	84.0575	85.0653	All samples
C4H6O2	86.0368	87.0446	All samples
C5H10O	86.0732	87.0810	All samples
C4H8O2	88.0524	89.0602	SS60%, DSS, UDSS
C6H4O	92.0262	93.0340	SS60%
C6H6O	94.0419	95.0497	UDSS
C5H4O2	96.0211	97.0289	SS60%
C6H10O	98.0732	99.0810	SS30%, DSS, UDSS
C5H8O2	100.0524	101.0602	All samples
C6H12O	100.0888	101.0966	All samples
C5H10O2	102.0681	103.0759	All samples
C7H4O	104.0262	105.0340	SS60% , UDSS
C7H6O	106.0419	107.0497	SS60% , UDSS
C7H8O	108.0575	109.0653	UDSS
C6H6O2	110.0368	111.0446	DSS
C5H4O3	112.0160	113.0238	UDSS
C7H12O	112.0888	113.0966	SS30%, DSS
C6H10O2	114.0681	115.0759	SS60% , UDSS
C7H14O	114.1045	115.1123	All samples
C5H8O3	116.0473	117.0551	UDSS
C6H12O2	116.0837	117.0915	All samples
C8H8O	120.0575	121.0653	UDSS
C8H10O	122.0732	123.0810	UDSS
C7H8O2	124.0524	125.0602	UDSS
C7H10O2	126.0681	127.0759	UDSS
C8H14O	126.1045	127.1123	All samples
C8H16O	128.1201	129.1279	All samples
C7H14O2	130.0994	131.1072	SS60%
C5H10O4	134.0579	135.0657	UDSS
C9H14O	138.1045	139.1123	DSS, UDSS
C9H16O	140.1201	141.1279	SS30%, DSS, UDSS
C8H14O2	142.0994	143.1072	SS60%
C9H18O	142.1358	143.1436	All samples

C10H10O	146.0732	147.0810	UDSS
C8H4O3	148.0160	149.0238	UDSS
C9H8O2	148.0524	149.0602	DSS
C10H16O	152.1201	153.1279	SS30%, DSS, UDSS
C10H18O	154.1358	155.1436	SS30%, DSS, UDSS
C10H20O	156.1514	157.1592	All samples
C9H18O2	158.1307	159.1385	UDSS
C10H10O2	162.0681	163.0759	UDSS
C9H10O3	166.0630	167.0708	SS30%
C11H18O	166.1358	167.1436	UDSS
C8H8O4	168.0423	169.0501	SS60%
C10H16O2	168.1150	169.1228	UDSS
C11H20O	168.1514	169.1592	UDSS
C11H22O	170.1671	171.1749	All samples
C10H20O2	172.1463	173.1541	SS30%, DSS
C12H22O	182.1671	183.1749	UDSS
C12H8O2	184.0524	185.0602	SS60%
C12H24O	184.1827	185.1905	All samples
C13H22O	194.1671	195.1749	UDSS
C12H20O2	196.1463	197.1541	UDSS
C13H24O	196.1827	197.1905	UDSS
C13H26O	198.1984	199.2062	SS60% , SS30% , DSS
C14H24O	208.1827	209.1905	UDSS
C14H26O	210.1984	211.2062	UDSS
C14H28O	212.2140	213.2218	SS60% , SS30% , DSS
C15H10O2	222.0681	223.0759	DSS
C15H26O	222.1984	223.2062	UDSS
C14H8O3	224.0475	225.0553	DSS
C15H28O	224.2140	225.2218	UDSS
C15H30O	226.2297	227.2375	SS60% , SS30% , DSS
C14H28O2	228.2089	229.2167	SS30%
C16H26O	234.1984	235.2062	SS30%, DSS, UDSS
C16H28O	236.2140	237.2218	SS30%, DSS
C16H14O2	238.0994	239.1072	DSS
C16H30O	238.2297	239.2375	UDSS

C15H12O3	240.0786	241.0864	SS30%, DSS
C16H32O	240.2453	241.2531	SS60% , SS30% , DSS
C14H10O4	242.0579	243.0657	DSS
C15H30O2	242.2246	243.2324	SS30%, DSS
C16H24O2	248.1776	249.1854	UDSS
C16H26O2	250.1933	251.2011	DSS, UDSS
C16H28O2	252.2089	253.2167	UDSS
C16H30O2	254.2246	255.2324	UDSS
C16H32O2	256.2402	257.2480	SS30%
C18H26O	258.1984	259.2062	UDSS
C15H30O3	258.2195	259.2273	SS30%, DSS
C18H36O	268.2766	269.2844	DSS
C17H34O2	270.2559	271.2637	SS60% , SS30% ,UDSS
C19H32O	276.2453	277.2531	SS30%
C16H22O4	278.1518	279.1596	All samples
C17H12O4	280.0736	281.0814	SS60%
Sulphuric compounds (25)			
CH4S	48.0034	49.0112	All samples
C2H6S	62.0190	63.0268	SS30%, DSS, UDSS
C3H6S	74.0190	75.0268	SS60% , SS30%
C3H8S	76.0347	77.0425	SS30%
CH2S2	77.9598	78.9676	SS30%, UDSS
C4H8S	88.0347	89.0425	SS30%, UDSS
C2H6S2	93.9911	94.9989	SS30%, UDSS
C5H10S	102.0503	103.0581	SS30%
C6H8S	112.0347	113.0425	SS30%, DSS
C6H10S	114.0503	115.0581	SS30%
C6H13S	117.0738	118.0816	DSS
C4H6S2	117.9911	118.9989	DSS
C2H6S3	125.9632	126.9710	SS30%, UDSS
C7H12S	128.0660	129.0738	SS60% , SS30%
C8H14S	142.0816	143.0894	SS30%
C8H16S	144.0973	145.1051	SS60% , SS30% , DSS
C6H12S2	148.0380	149.0458	SS60%
C10H12S	164.0660	165.0738	UDSS

C8H10S2	170.0224	171.0302	SS60%
C10H20S	172.1286	173.1364	SS60% , UDSS
C11H18S	182.1129	183.1207	UDSS
C9H18S3	222.0571	223.0649	SS60% , SS30%
C14H26S	226.1756	227.1834	UDSS
C14H28S	228.1912	229.1990	DSS, UDSS
C20H10S	282.0503	283.0581	SS60%
Nitrogenated compounds (37)			
C2H3N	41.0265	42.0343	UDSS
C2H5N	43.0422	44.0500	UDSS
C2H7N	45.0578	46.0656	SS30%, DSS
C3H9N	59.0735	60.0813	SS60% , SS30% , DSS
C2H8N2	60.0687	61.0765	DSS
C4H5N	67.0422	68.0500	UDSS
C4H7N	69.0578	70.0656	DSS, UDSS
C2H5N3	71.0483	72.0561	SS60% , SS30%
C5H5N	79.0422	80.0500	DSS, UDSS
C3H3N3	81.0327	82.0405	UDSS
C5H11N	85.0891	86.0969	UDSS
C7H5N	103.0422	104.0500	SS60% , UDSS
C5H3N3	105.0327	106.0405	SS60% , UDSS
C5H5N3	107.0483	108.0561	SS60% , UDSS
C7H9N	107.0735	108.0813	SS60% , SS30% , DSS
C8H7N	117.0578	118.0656	SS60% , SS30% ,UDSS
C8H8N	118.0657	119.0735	UDSS
C8H9N	119.0735	120.0813	UDSS
C8H11N	121.0891	122.0969	UDSS
C6H9N3	123.0796	124.0874	UDSS
C9H8N	130.0657	131.0735	UDSS
C9H9N	131.0735	132.0813	SS60% , SS30% ,UDSS
C9H11N	133.0891	134.0969	All samples
C9H8N2	144.0687	145.0765	UDSS
C10H15N	149.1204	150.1282	DSS, UDSS
C10H6N2	154.0531	155.0609	UDSS
C10H5N3	167.0483	168.0561	SS30%

C11H20N2	180.1626	181.1704	UDSS
C12H23N	181.1831	182.1909	UDSS
C12H23N	181.1830	182.1908	SS30%, DSS
C13H13N	183.1048	184.1126	SS30%, DSS
C13H15N	185.1204	186.1282	SS30%
C14H24N2	220.1939	221.2017	UDSS
C15H27N	221.2143	222.2221	UDSS
C16H31N	237.2456	238.2534	SS30%
C15H30N2	238.2409	239.2487	DSS
C16H26N2	246.2096	247.2174	UDSS
Other compounds (120)			
CH3NO	45.0215	46.0293	SS30%, DSS, UDSS
C2H5NO	59.0371	60.0449	DSS
CH3NO2	61.0164	62.0242	DSS
C3H5NO	71.0371	72.0449	DSS, UDSS
C2H3NO2	73.0164	74.0242	SS30%, DSS, UDSS
C3H7NO	73.0528	74.0606	SS60% , SS30% , DSS
C2H5NO2	75.0320	76.0398	SS60% , SS30% , DSS
C3H9NO	75.0684	76.0762	SS30%
CH4N2S	76.0095	77.0173	SS60%
CH3NOS	76.9935	78.0013	SS30%
C4H5NO	83.0371	84.0449	UDSS
C3H3NS	84.9986	86.0064	SS30%, UDSS
C4H7NO	85.0528	86.0606	All samples
C3H5NO2	87.0320	88.0398	SS30%, DSS, UDSS
C4H9NO	87.0684	88.0762	All samples
C2H3NO3	89.0113	90.0191	SS60%
C2H7N3O	89.0589	90.0667	SS60%
CH4O3S	95.9881	96.9959	SS30%, UDSS
C4H5NS	99.0143	100.0221	SS30%
C4H5NO2	99.0320	100.0398	SS60%, DSS, UDSS
C5H9NO	99.0684	100.0762	UDSS
C4H7NO2	101.0477	102.0555	All samples
C5H11NO	101.0841	102.0919	All samples
C4H9NO2	103.0633	104.0711	UDSS

C4H11NS	105.0612	106.0690	SS60% , SS30% , DSS
C6H7NO	109.0528	110.0606	DSS
C6H9NO	111.0684	112.0762	UDSS
C5H7NS	113.0299	114.0377	UDSS
C5H7NO2	113.0477	114.0555	SS60%
C6H11NO	113.0841	114.0919	SS30%, DSS, UDSS
C5H6OS	114.0139	115.0217	SS60%, DSS, UDSS
C5H9NS	115.0456	116.0534	SS30%, UDSS
C5H9NO2	115.0633	116.0711	SS60%
C6H13NO	115.0997	116.1075	SS60% , SS30% , DSS
C7H5NO	119.0371	120.0449	SS60% , UDSS
C5H13NS	119.0769	120.0847	SS60%
C7H17NO	121.0528	122.0606	UDSS
C6H7NS	125.0299	126.0377	UDSS
C5H6N2S	126.0252	127.0330	UDSS
C6H9NO2	127.0633	128.0711	UDSS
C7H13NO	127.0997	128.1075	UDSS
C6H8OS	128.0296	129.0374	UDSS
C5H7NOS	129.0248	130.0326	DSS
C6H11NS	129.0612	130.0690	SS60% , UDSS
C6H11NO2	129.0790	130.0868	SS30%
C7H15NO	129.1154	130.1232	SS60% , SS30% , DSS
C8H7NO	133.0528	134.0606	SS60%
C7H5NS	135.0143	136.0221	DSS
C8H9NO	135.0684	136.0762	DSS, UDSS
C7H7NO2	137.0477	138.0555	UDSS
C6H6N2O2	138.0429	139.0507	UDSS
C6H5NO3	139.0269	140.0347	UDSS
C4H4N4O2	140.0343	141.0421	UDSS
C6H7NOS	141.0248	142.0326	UDSS
C7H11NS	141.0612	142.0690	SS30%
C8H15NO	141.1154	142.1232	UDSS
C5H6N2OS	142.0201	143.0279	UDSS
C7H12NO2	142.0868	143.0946	UDSS
C7H12NO2	142.0868	143.0946	DSS

C6H9NO3	143.0582	144.0660	UDSS
C6H11N2O2	143.0821	144.0899	DSS
C7H13NO2	143.0946	144.1024	SS60%
C8H17NO	143.1310	144.1388	All samples
C6H7NOS	145.0561	146.0639	UDSS
C7H15NO2	145.1103	146.1181	SS30%
C2H5N5O3	147.0392	148.0470	SS60%
C9H9NO	147.0684	148.0762	UDSS
C8H7NO2	149.0477	150.0555	SS60% , UDSS
C9H11NO	149.0841	150.0919	DSS
C8H9NO2	151.0633	152.0711	UDSS
C7H8N2O2	152.0586	153.0664	UDSS
C8H13NO2	155.0946	156.1024	SS60%
C9H17NO	155.1310	156.1388	UDSS
C8H15NS	157.0925	158.1003	SS60%
C9H19NO	157.1467	158.1545	All samples
C8H17NS	159.1082	160.1160	SS60%
C8H17NO2	159.1259	160.1337	SS30%
C9H7NO2	161.0477	162.0555	SS30%, DSS, UDSS
C9H9NO2	163.0633	164.0711	SS60%, DSS, UDSS
C10H15NO	165.1154	166.1232	DSS
C6H6N4O2	166.0491	167.0569	SS60%
C5H5N5O2	167.0443	168.0521	SS60%
C10H19NO	169.1467	170.1545	SS30%, DSS
C9H17NS	171.1082	172.1160	SS60%
C9H17NO2	171.1259	172.1337	UDSS
C10H21NO	171.1623	172.1701	UDSS
C10H7NS	173.0299	174.0377	UDSS
C9H19NO2	173.1416	174.1494	SS60% , SS30% ,UDSS
C10H11NS	177.0612	178.0690	UDSS
C9H9NO3	179.0584	180.0662	UDSS
C8H7NS2	181.0020	182.0098	UDSS
C11H21NO	183.1623	184.1701	DSS
C9H16N2O2	184.1212	185.1290	SS30%
C11H19NS	197.1238	198.1316	DSS, UDSS

C11H22N2O	198.1732	199.1810	UDSS
C11H21NO2	199.1572	200.1650	SS30%
C11H23NO2	201.1729	202.1807	DSS, UDSS
C13H25NO	211.1936	212.2014	UDSS
C12H23NS	213.1551	214.1629	UDSS
C12H25NO2	215.1885	216.1963	DSS, UDSS
C14H6N2O	218.0480	219.0558	All samples
C14H9NO2	223.0633	224.0711	DSS
C13H8N2S	224.0408	225.0486	SS60%
C15H27NO	237.2093	238.2171	DSS
C13H10N4O	238.0855	239.0933	SS60% , SS30%
C15H13NO2	239.0946	240.1024	DSS
C15H29NO	239.2249	240.2327	DSS
C14H28N2O	240.2202	241.2280	UDSS
C14H11NO3	241.0739	242.0817	SS60% , SS30% , DSS
C14H30N2O	242.2358	243.2436	UDSS
C13H28N2O2	244.2151	245.2229	UDSS
C15H24N2O	248.1889	249.1967	DSS
C16H27NO	249.2093	250.2171	DSS
C16H29NO	251.2249	252.2327	SS30%, DSS
C15H28N2O	252.2202	253.2280	DSS
C16H31NO	253.2406	254.2484	DSS
C15H30N2O	254.2358	255.2436	SS30%, DSS
C16H27NO2	265.2042	266.2120	DSS
C18H29NO	275.2249	276.2327	UDSS
C12H15N3O6	297.0961	298.1039	All samples

Table A.3 *DBE value of each assigned HC detected in this work in the decreasing order of the DBE value.*

HC	**Molecular weight**	**DBE value**	**SS samples with compound detected**
C3H6	42.0470	1	All samples
C4H8	56.0626	1	All samples
C5H10	70.0783	1	All samples

C6H12	84.0939	1	All samples
C7H14	98.1096	1	All samples
C8H16	112.1252	1	All samples
C9H18	126.1409	1	SS60% , SS30% , DSS
C10H20	140.1565	1	SS60% , SS30%
C11H22	154.1722	1	SS60% , SS30%
C12H24	168.1878	1	SS60% , SS30% , DSS
C13H26	182.2035	1	SS60%
C14H28	196.1252	1	SS60% , SS30% , DSS
C15H30	210.2348	1	SS60% , SS30% , DSS
C16H32	224.2504	1	SS60% , SS30% , DSS
C17H34	238.2661	1	SS60% , SS30%
C18H36	252.2817	1	SS60% , SS30%
C3H4	40.0313	2	All samples
C4H6	54.0470	2	All samples
C5H8	68.0626	2	All samples
C6H10	82.0783	2	All samples
C7H12	96.0939	2	All samples
C8H14	110.1096	2	All samples
C9H16	124.1252	2	All samples
C10H18	138.1409	2	All samples
C11H20	152.1565	2	SS60% , SS30%
C12H22	166.1722	2	SS60% , SS30% , DSS
C13H24	180.1878	2	SS60% , SS30% , DSS
C14H26	194.2035	2	SS60% , SS30% , DSS
C15H28	208.2191	2	SS60% , SS30% , DSS
C16H30	222.2348	2	SS60% , SS30% , DSS
C17H32	236.2504	2	SS60%
C18H34	250.2661	2	SS60%
C4H4	52.0313	3	All samples
C5H6	66.0470	3	All samples
C6H8	80.0621	3	All samples
C7H10	94.0783	3	All samples
C8H12	108.0939	3	SS60% , SS30% , DSS
C9H14	122.1096	3	All samples

C10H16	136.1252	3	All samples
C11H18	150.1409	3	All samples
C12H20	164.1565	3	All samples
C13H22	178.1722	3	All samples
C14H24	192.1878	3	All samples
C15H26	206.2035	3	All samples
C16H28	220.2191	3	SS60% , SS30% , DSS
C17H30	234.2348	3	SS60%
C18H32	248.2504	3	SS60% , SS30%
C19H34	262.2661	3	SS60% , SS30%
C4H2	50.0157	4	SS60%, DSS
C5H4	64.0313	4	SS60%, DSS
C6H6	78.0470	4	All samples
C7H8	92.0626	4	All samples
C8H10	106.0783	4	All samples
C9H12	120.0939	4	All samples
C10H14	134.1096	4	All samples
C11H16	148.1252	4	All samples
C12H18	162.1409	4	All samples
C13H20	176.1565	4	All samples
C14H22	190.1722	4	All samples
C15H24	204.1878	4	All samples
C16H26	218.2035	4	All samples
C17H28	232.2191	4	All samples
C18H30	246.2348	4	SS60% , SS30% , DSS
C19H32	260.2504	4	SS60% , SS30% ,UDSS
C20H34	274.2661	4	All samples
C6H4	76.0313	5	UDSS
C5H2	78.0106	5	SS30%, UDSS
C7H6	90.0470	5	All samples
C8H8	104.0626	5	SS60% , SS30% , DSS
C9H10	118.0783	5	SS60% , SS30% , DSS
C10H12	132.0939	5	SS60% , SS30% , DSS
C11H14	146.1096	5	All samples
C12H16	160.1252	5	All samples

C13H18	174.1409	5	All samples
C14H20	188.1565	5	All samples
C15H22	202.1722	5	All samples
C16H24	216.1878	5	All samples
C17H26	230.2035	5	All samples
C18H28	244.2191	5	SS60% , SS30% , DSS
C19H30	258.2348	5	SS60%
C20H32	272.2504	5	All samples
C21H34	286.2661	5	SS60% , SS30% ,UDSS
C10H10	130.0783	6	SS30%, DSS
C12H14	158.1096	6	SS60% , SS30% , DSS
C14H18	186.1409	6	All samples
C15H20	200.1565	6	All samples
C16H22	214.1722	6	All samples
C17H24	228.1878	6	SS60%
C18H26	242.2035	6	SS60% , SS30%
C12H12	156.0939	7	SS60% , SS30% , DSS
C13H14	170.1096	7	All samples
C14H16	184.1252	7	DSS, UDSS
C15H18	198.1409	7	SS30%
C16H20	212.1565	7	SS30%, UDSS
C15H16	196.1252	8	SS30%

Table A.4 *Chemical assignments of protonated mass peaks that show high statistical significance and logarithm of FC > 1 or < -1.*

Chemical compound	**Logarithm of fold change**
DSS [(a)]	
C10H16O	1.4457
C10H16	1.3609
C4H7N	1.3560
C2H3N	1.2293
C6H8	1.0597
C3H5O	1.0575
C7H14	1.0191

C6H10O	1.0040
UDSS [a]	
C2H6S	-6.4355
CH4S	-5.8979
C7H8	-4.1604
C5H4	-3.5247
C4H2	-3.4212
C2H6S2	-3.2911
C7H8O	-3.1651
C9H9N	-3.0337
CH2S2	-3.0001
CH3NO2	-2.7435
C8H12	-2.6523
CH2O2	-2.6255
C7H6	-2.2149
C6H7NO	-2.0443
C2H4O2	-1.9543
C4H4	-1.9382
C5H2	-1.7687
C6H6O	-1.5409
C5H5N3	-1.4651
C7H9N	-1.3535
C3H8O2	-1.2849
C6H13S	-1.2684
C8H7N	-1.2597
C6H4	-1.2357
CH4O3S	-1.1671
C7H4O	-1.1090
C4H8O2	-1.0551
C4H8S	-1.0464
C2H6O	-1.0399
C3H6O2	-1.0217
SS 30% dryness [b]	
C2H6S	-5.256
CH2S2	-3.084

C2H6S2	-2.936
CH4S	-2.684
C8H12	-2.552
C9H14	-2.535
C7H10	-2.499
C5H4	-2.490
C13H22	-2.414
C12H20	-2.346
C5H6	-2.315
C5H8	-2.313
C7H12	-2.267
C3H4	-2.192
C6H10	-2.159
CH3NO2	-2.156
C14H24	-2.137
C6H8	-2.078
C8H14	-2.074
C5H2	-2.002
C13H20	-1.948
C14H22	-1.916
C4H8	-1.897
C3H4O	-1.890
C9H16	-1.678
C5H10	-1.627
C11H18	-1.626
C15H26	-1.603
C10H14	-1.601
C9H12	-1.573
C4H4	-1.540
C4H6O	-1.515
C6H12	-1.481
C4H6	-1.480
C10H16	-1.453
C15H24	-1.443
CH2O2	-1.424

C12H18	-1.420
C3H6	-1.360
C6H7NO	-1.350
C5H8O	-1.319
C10H18	-1.155
C7H14	-1.129
C6H6	-1.104
C2H4O2	-1.060
CH4O3S	-1.041
SS 60% dryness [(c)]	
C2H8N2	-5.256
C6H6	-3.084
C5H4O2	-2.936
C2H6O	-2.684
C7H9N	-2.552
C9H10	-2.535
C7H12	-2.499
CH3NO2	-2.490
C5H5N5O2	-2.414
C10H20O	-2.346
C2H6S	-2.315
C5H4	-2.313
C7H14	-2.267
C3H4	-2.192
C6H12	-2.159
C2H4O2	-2.156
C13H20	-2.137
C5H8O	-2.078
C6H6O2	-2.074
C5H5N	-2.002
C12H22	-1.948
C13H18	-1.916
C3H4O	-1.897
C4H6	-1.890
C7H5NO	-1.678

C4H7N	-1.627
C2H5N5O3	-1.626
C14H22	-1.603
C7H14O2	-1.601
C4H6S2	-1.573
C4H2	-1.540
C5H8	-1.515
C4H6O2	-1.481
C4H4	-1.480
C8H7NO	-1.453
C14H20	-1.443
C2H7N	-1.424
C8H13NO2	-1.420
C2H2O	-1.360
C8H12	-1.350
C4H7NO	-1.319
C10H14	-1.155
C5H8O2	-1.129
C6H8	-1.104
C2H5NO	-1.060
C6H10O	-1.041
SS 30% dryness [(d)]	
C2H6S	-4.753
CH4S	-3.778
CH2S2	-3.609
C2H6S2	-2.183
C5H4	-1.794
SS 60% dryness [(d)]	
C4H8O	2.526
C2H4O	1.976
C5H10O	1.788
C2H6O	1.725
C2H2O	1.696
C2H7N	1.694
C5H10	1.679

C4H6O	1.675
C3H6	1.673
C6H12	1.670
C4H6O2	1.659
C5H8O	1.645
C9H18	1.619
C7H6O	1.592
C2H4O2	1.579
C8H16	1.572
C8H14O	1.528
C4H8	1.526
C3H6O2	1.473
C3H6S	1.436
C14H28	1.419
C3H6O	1.390
C7H12O	1.372
C3H4	1.364
C9H16	1.315
C3H7NO	1.256
C10H18	1.255
C8H10	1.213
C15H30	1.186
C2H5N3	1.163
C8H14	1.159
CH4O	1.143
C14H26	1.140
C5H8	1.088
C7H14	1.056
C3H9N	1.051
C4H9NO	1.048
C3H5O	1.043
C10H20	1.034

[(a)]: chemical compounds observed in volcano plot in **Figure 3.10 (a)**.

[(b)]: chemical compounds observed in volcano plot in **Figure 3.10 (b)**.

[(c)]: chemical compounds observed in volcano plot in **Figure 3.10 (c)**.

[(d)]: chemical compounds observed in volcano plot in **Figure 3.10 (d)**.

Annex 4

Table A.5 *List of compounds detected using PTR-QiTOF-MS and emitted from animal manure samples by decreasing order of the molecular weight of compounds assigned in each chemical family. The number of compounds assigned to each chemical family is given in parenthesis.*

Molecular formula	Molecular weight	Theoretical protonated mass	Manure sample with compound detected
Hydrocarbons (56)			
C3H4	40.0296	41.0376	All samples
C3H6	42.0453	43.0533	All samples
C4H2	50.0147	51.0227	cow, sheep, goat
C4H4	52.0295	53.0375	All samples
C4H6	54.0427	55.0507	cow
C4H8	56.0608	57.0688	All samples
C5H4	64.0303	65.0383	cow
C5H6	66.0456	67.0536	All samples
C5H8	68.0616	69.0696	All samples
C5H10	70.0768	71.0848	All samples
C6H6	78.0438	79.0518	All samples
C6H6	78.0443	79.0523	cow, horse, goat
C6H8	80.0597	81.0677	All samples
C6H10	82.0762	83.0842	All samples
C6H12	84.0921	85.1001	horse, sheep, goat
C7H6	90.0465	91.0545	horse, sheep, goat
C7H8	92.0598	93.0678	All samples
C7H10	94.0756	95.0836	All samples
C7H12	96.0929	97.1009	All samples
C7H12	98.1087	99.1167	horse, sheep, goat
C8H8	104.0613	105.0693	All samples
C8H10	106.0766	107.0846	All samples
C8H12	108.0922	109.1002	All samples
C8H14	110.1056	111.1136	All samples
C8H16	112.1273	113.1353	horse, goat
C9H10	118.0773	119.0853	horse, sheep, goat
C9H12	120.0923	121.1003	horse, sheep, goat
C9H14	122.1073	123.1153	All samples
C9H16	124.1243	125.1323	sheep
C10H12	132.0913	133.0993	horse, sheep, goat
C10H14	134.1082	135.1162	All samples
C10H16	136.1223	137.1303	All samples
C11H14	146.1103	147.1183	cow, sheep, goat

C11H16	148.1233	149.1313	All samples
C11H18	150.1403	151.1483	cow, horse
C12H16	160.1243	161.1323	All samples
C12H18	162.1351	163.1431	cow
C12H20	164.1533	165.1613	cow, sheep
C13H18	174.1414	175.1494	All samples
C13H20	176.1549	177.1629	All samples
C13H22	178.1683	179.1763	horse
C14H18	186.1432	187.1512	cow, horse, goat
C14H20	188.1556	189.1636	All samples
C14H22	190.1702	191.1782	cow, horse, goat
C14H24	192.1833	193.1913	horse
C15H20	200.1553	201.1633	All samples
C15H22	202.1723	203.1803	cow, sheep, goat
C15H24	204.1873	205.1953	All samples
C15H26	206.1943	207.2023	horse
C16H22	214.1783	215.1863	cow
C17H28	232.2133	233.2213	sheep, goat
C17H34	238.2643	239.2723	horse
C18H30	246.2229	247.2309	horse, sheep, goat
C19H32	260.2493	261.2573	sheep, goat
C20H32	272.2493	273.2573	All samples
Oxygenated compounds (119)			
CH2O	30.0106	31.0186	cow, sheep, goat
CH4O	32.0263	33.0343	horse, sheep, goat
C2H2O	42.0101	43.0181	All samples
C2H4O	44.0248	45.0328	All samples
CH2O2	46.0052	47.0132	All samples
C2H6O	46.0413	47.0493	All samples
C3H4O	56.0271	57.0351	cow, sheep, goat
C3H5O	57.0320	58.0400	All samples
C3H6O	58.0413	59.0493	All samples
C2H4O2	60.0211	61.0291	All samples
C4H4O	68.0255	69.0335	cow, goat
C4H6O	70.0404	71.0484	All samples
C3H4O2	72.0207	73.0287	horse, sheep, goat
C4H8O	72.0563	73.0643	All samples
C3H6O2	74.0358	75.0438	All samples
C3H8O2	76.0500	77.0580	All samples
C5H2O	78.0123	79.0203	goat
C5H6O	82.0403	83.0483	All samples
C4H4O2	84.0195	85.0275	horse, sheep, goat
C5H8O	84.0564	85.0644	All samples
C4H6O2	86.0355	87.0435	horse, sheep, goat

C5H10O	86.0717	87.0797	All samples
C4H8O2	88.0494	89.0574	All samples
C4H10O2	90.0637	91.0717	cow
C6H4O	92.0268	93.0348	horse, sheep, goat
C6H6O	94.0406	95.0486	All samples
C5H4O2	96.0201	97.0281	horse, sheep, goat
C6H8O	96.0562	97.0642	All samples
C4H2O3	97.9980	99.0060	sheep
C5H6O2	98.0359	99.0439	horse, sheep, goat
C6H10O	98.0716	99.0796	All samples
C4H4O3	100.0153	101.0233	horse, sheep
C5H8O2	100.0513	101.0593	horse, sheep, goat
C6H12O	100.0873	101.0953	All samples
C4H6O3	102.0323	103.0403	horse, sheep, goat
C5H10O2	102.0669	103.0749	All samples
C7H4O	104.0253	105.0333	cow, horse, goat
C7H8O	108.0582	109.0662	cow, horse, goat
C6H6O2	110.0353	111.0433	horse, goat
C7H10O	110.0713	111.0793	All samples
C6H8O2	112.0493	113.0573	horse, sheep, goat
C7H12O	112.0878	113.0958	All samples
C6H10O2	114.0643	115.0723	All samples
C7H14O	114.1026	115.1106	All samples
C5H8O3	116.0453	117.0533	cow
C6H12O2	116.0823	117.0903	horse, sheep, goat
C8H6O	118.0453	119.0533	goat
C8H8O	120.0579	121.0659	cow, goat
C7H6O2	122.0364	123.0444	horse, sheep, goat
C8H10O	122.0723	123.0803	cow, sheep
C8H12O	124.0870	125.0950	All samples
C8H14O	126.1035	127.1115	All samples
C7H12O2	128.0763	129.0843	cow, horse
C8H16O	128.1173	129.1253	All samples
C6H10O3	130.0671	131.0751	cow
C7H14O2	130.0945	131.1025	horse, sheep, goat
C8H8O2	136.0533	137.0613	goat
C9H12O	136.0913	137.0993	cow
C9H14O	138.1035	139.1115	All samples
C9H16O	140.1183	141.1263	All samples
C8H14O2	142.0993	143.1073	horse, sheep, goat
C9H18O	142.1346	143.1426	cow, sheep, goat
C8H16O2	144.1139	145.1219	All samples
C8H4O3	148.0151	149.0231	All samples
C10H14O	150.1043	151.1123	All samples

C10H16O	152.1193	153.1273	All samples
C9H14O2	154.0993	155.1073	horse, sheep
C10H18O	154.1323	155.1403	All samples
C9H16O2	156.1143	157.1223	goat
C10H20O	156.1463	157.1543	All samples
C9H18O2	158.1293	159.1373	All samples
C8H18O3	162.1285	163.1365	horse
C8H18O3	162.1373	163.1453	sheep
C11H16O	164.1211	165.1291	horse
C10H14O2	166.1013	167.1093	horse
C11H18O	166.1278	167.1358	cow
C10H16O2	168.1133	169.1213	horse, sheep, goat
C10H18O2	170.1293	171.1373	All samples
C11H8O2	172.0513	173.0593	horse
C10H20O2	172.1453	173.1533	All samples
C12H18O	178.1363	179.1443	sheep
C11H18O2	182.1283	183.1363	horse, sheep, goat
C11H20O2	184.1443	185.1523	horse, sheep, goat
C11H22O2	186.1613	187.1693	sheep
C13H20O	192.1637	193.1717	cow, sheep, goat
C13H22O	194.1653	195.1733	cow, horse, sheep
C12H20O2	196.1423	197.1503	sheep, goat
C13H24O	196.1847	197.1927	cow
C12H22O2	198.1523	199.1603	sheep
C13H26O	198.1988	199.2068	cow
C12H8O3	200.0413	201.0493	sheep, goat
C14H22O	206.1671	207.1751	sheep, goat
C13H22O2	210.1653	211.1733	cow, sheep, goat
C14H26O	210.1983	211.2063	horse
C14H28O	212.1783	213.1863	cow
C13H24O2	212.1903	213.1983	goat
C14H28O	212.2091	213.2171	horse, sheep
C15H22O	218.1703	219.1783	cow, sheep, goat
C14H20O2	220.1543	221.1623	goat
C15H24O	220.1787	221.1867	cow, horse, sheep
C12H14O4	222.0923	223.1003	sheep
C14H22O2	222.1653	223.1733	goat
C15H26O	222.1973	223.2053	cow, sheep
C15H28O	224.2125	225.2205	cow
C15H30O	226.2242	227.2322	cow, sheep, goat
C14H28O2	228.2053	229.2133	horse, sheep, goat
C15H20O2	232.1483	233.1563	cow, horse
C11H26O	234.1853	235.1933	sheep
C16H26O	234.1943	235.2023	cow, horse, goat

C15H24O2	236.1763	237.1843	cow, sheep, goat
C16H30O	238.2333	239.2413	cow, sheep, goat
C16H32O	240.2393	241.2473	All samples
C15H30O2	242.2273	243.2353	goat
C16H34O	242.2659	243.2739	sheep
C16H24O2	248.1784	249.1864	horse, sheep, goat
C16H32O2	256.2388	257.2468	horse, sheep, goat
C18H36O	268.2733	269.2813	horse, sheep, goat
C17H34O2	270.2533	271.2613	All samples
C16H22O4	278.1513	279.1593	All samples
Sulphuric compounds (12)			
CH4S	48.0022	49.0102	All samples
C2H6S	62.0177	63.0257	All samples
C4H4S	75.9437	85.0129	cow
C2H6S2	84.0049	94.9969	horse
C5H6S	93.9889	99.0271	cow
C5H8S	98.0191	101.0423	cow
C6H8S	100.0343	113.0463	cow
C6H12S	112.0383	117.0783	cow
C7H10S	116.0703	127.0613	cow
C8H10S2	126.0533	171.0263	horse
C8H12S2	170.0183	173.0414	sheep
CS2	172.0334	76.9517	goat
Nitrogenated compounds (64)			
C2H3N	41.0259	42.0339	All samples
C2H7N	45.0561	46.0641	cow, sheep, goat
C3H3N	53.0255	54.0335	horse, sheep, goat
C3H5N	55.0417	56.0497	All samples
C2H4N2	56.0358	57.0438	horse
C3H7N	57.0576	58.0656	All samples
C3H9N	59.0735	60.0815	All samples
C2H8N2	60.0702	61.0782	cow
C4H5N	67.0422	68.0502	All samples
C4H7N	69.0568	70.0648	cow, sheep, goat
C2H5N3	71.0471	72.0551	cow
C4H9N	71.0725	72.0805	horse, sheep, goat
C4H11N	73.0877	74.0957	cow, sheep, goat
C5H5N	79.0405	80.0485	All samples
C4H4N2	80.0365	81.0445	cow, goat
C5H7N	81.0613	82.0693	All samples
C3H5N3	83.0481	84.0561	cow
C5H9N	83.0741	84.0821	All samples
C5H11N	85.0875	86.0955	sheep, goat
C5H13N	87.1025	88.1105	All samples

C6H7N	91.0471	92.0551	horse, sheep, goat
C6H7N	93.0557	94.0637	All samples
C6H9N	95.0763	96.0843	horse, sheep, goat
C4H7N3	97.0606	98.0686	cow
C6H11N	97.0921	98.1001	All samples
C7H5N	103.0413	104.0493	goat
C7H9N	107.0726	108.0806	cow, horse
C7H9N	107.0743	108.0823	sheep, goat
C5H7N3	109.0623	110.0703	cow, horse, goat
C7H11N	109.0903	110.0983	All samples
C7H13N	111.1063	112.1143	All samples
C8H7N	117.0573	118.0653	All samples
C8H11N	121.0893	122.0973	All samples
C8H13N	123.1083	124.1163	All samples
C6H11N3	125.0934	126.1014	cow
C6H13N3	127.1057	128.1137	cow
C6H15N3	129.1230	130.1310	sheep, goat
C9H9N	131.0734	132.0814	All samples
C9H11N	133.0883	134.0963	All samples
C9H13N	135.1113	136.1193	cow
C7H13N3	139.1083	140.1163	cow
C10H9N	143.0723	144.0803	goat
C9H8N2	144.0633	145.0713	cow
C10H13N	147.1033	148.1113	goat
C10H15N	149.1203	150.1283	All samples
C11H15N	161.1203	162.1283	cow, horse, goat
C10H14N2	162.1223	163.1303	goat
C11H17N	163.1363	164.1443	sheep, goat
C10H16N2	164.1323	165.1403	goat
C9H15N3	165.1322	166.1402	cow, goat
C11H19N	165.1583	166.1663	sheep
C12H17N	175.1373	176.1453	All samples
C12H19N	177.1528	178.1608	All samples
C11H18N2	178.1403	179.1483	cow, goat
C13H19N	189.1594	190.1674	horse, goat
C12H18N2	190.1514	191.1594	sheep
C13H21N	191.1660	192.1740	horse, goat
C11H19N3	193.1590	194.1670	cow
C10H20N4	196.1780	197.1860	horse
C14H23N	205.1883	206.1963	horse
C14H20N2	216.1623	217.1703	horse, sheep, goat
C25H22N2	218.1754	219.1834	horse
C15H27N	221.2102	222.2182	cow, sheep, goat
C15H16N2	224.1463	225.1543	sheep, goat

Other compounds (133)			
CH3NO	45.0204	46.0284	All samples
C2H5NO	59.0388	60.0468	horse, goat
CH3NO2	61.0156	62.0236	All samples
C3H3NO	69.0214	70.0294	cow, sheep, goat
C3H5NO	71.0389	72.0469	horse, sheep, goat
C4H9NS	71.0713	72.0793	cow
C2H3NO2	73.0156	74.0236	horse, sheep, goat
C3H7NO	73.0535	74.0615	All samples
C2H5NO2	75.0299	76.0379	horse, sheep, goat
C3H9NO	75.0660	76.0740	cow
C4H5NO	83.0368	84.0448	sheep, goat
C3H3NS	84.9969	86.0049	cow, horse, goat
C3H3NO2	85.0161	86.0241	sheep
C4H7NO	85.0526	86.0606	All samples
C3H5NO2	87.0323	88.0403	horse, sheep, goat
C4H9NO	87.0684	88.0764	All samples
C2H4N2O2	88.0273	89.0353	sheep
C2H3NO3	89.0110	90.0190	horse, sheep, goat
C3H7NO2	89.0472	90.0552	goat
C4H11NO	89.0816	90.0896	cow
C3H9NO2	91.0628	92.0708	cow
C5H5NO	95.0385	96.0465	horse, sheep, goat
C4H3NO2	97.0161	98.0241	All samples
C5H7NO	97.0535	98.0615	horse, sheep, goat
C4H5NS	99.0179	100.0259	cow
C4H5NO2	99.0314	100.0394	horse, sheep, goat
C5H9NO	99.0673	100.0753	All samples
C4H7NO2	101.0483	102.0563	All samples
C5H11NO	101.0832	102.0912	All samples
C4H9NS	103.0463	104.0543	horse, sheep
C4H9NO2	103.0633	104.0713	cow
C4H11NS	105.0658	106.0738	All samples
C5H5NO2	111.0323	112.0403	horse, sheep, goat
C6H9NO	111.0683	112.0763	All samples
C4H3NO3	113.0153	114.0233	horse, sheep
C3H3N3O2	113.0243	114.0323	goat
C5H7NO2	113.0493	114.0573	sheep
C6H11NO	113.0833	114.0913	All samples
C3H2N2O3	114.0063	115.0143	horse
C5H6OS	114.0173	115.0253	sheep, goat
C4H5NO3	115.0272	116.0352	horse, sheep, goat
C5H9NO2	115.0553	116.0633	cow, sheep
C6H13NO	115.0993	116.1073	cow, sheep, goat

C4H8N2S	116.0413	117.0493	horse, sheep
C4H10N2O2	118.0706	119.0786	cow
C7H5NO	119.0353	120.0433	sheep, goat
C5H13NS	119.0763	120.0843	All samples
C7H7NO	121.0553	122.0633	horse, sheep, goat
C6H5NO2	123.0323	124.0403	horse, sheep
C7H9NO	123.0673	124.0753	sheep
C7H11NO	125.0853	126.0933	sheep, goat
C5H5NOS	127.0083	128.0163	horse, goat
C6H9NS	127.0553	128.0633	cow
C7H13NO	127.1033	128.1113	horse, sheep, goat
C3H3N3O3	129.0173	130.0253	horse
C6H11NS	129.0603	130.0683	cow
C7H15NO	129.1162	130.1242	cow
C4H7NO2S	133.0153	134.0233	horse, sheep, goat
C8H7NO	133.0523	134.0603	horse, sheep, goat
C8H9NO	135.0686	136.0766	All samples
C8H11NO	137.0843	138.0923	cow
C9H15NO	137.1203	138.1283	All samples
C6H5NO3	139.0273	140.0353	horse, sheep, goat
C5H5N3O2	139.0383	140.0463	cow
C8H13NO	139.0983	140.1063	horse, sheep, goat
C6H7NOS	141.0223	142.0303	horse, sheep, goat
C6H7NO3	141.0393	142.0473	cow
C8H15NO	141.1163	142.1243	All samples
C8H17NO	143.1310	144.1390	cow, horse, sheep
C6H7NOS	145.0593	146.0673	cow
C6H14N2O2	146.1053	147.1133	horse
C8H5NO2	147.0333	148.0413	goat
C9H9NO	147.0693	148.0773	cow, sheep, goat
C9H11NO	149.0833	150.0913	horse
C9H13NO	151.1013	152.1093	All samples
C9H15NO	153.1153	154.1233	All samples
C8H13NO2	155.0943	156.1023	horse, sheep
C9H17NO	155.1303	156.1383	cow, sheep, goat
C9H19NO	157.1463	158.1543	All samples
C8H17NO2	159.1283	160.1363	horse, sheep, goat
C9H9NO2	163.0640	164.0720	All samples
C9H14N2O	166.1057	167.1137	sheep, goat
C8H13N3O	167.1099	168.1179	sheep
C10H17NO	167.1273	168.1353	cow, horse, goat
C9H16N2O	168.1299	169.1379	cow
C9H15NO2	169.1180	170.1260	horse, sheep, goat
C10H19NO	169.1444	170.1524	cow

C9H18N2O	170.1573	171.1653	cow
C9H17NO2	171.1283	172.1363	horse, sheep, goat
C10H21NO	171.1598	172.1678	cow
C9H19NO2	173.1443	174.1523	sheep
C10H23NO	173.1760	174.1840	cow
C9H6N2O2	174.0423	175.0503	sheep
C9H13N3O	179.1043	180.1123	sheep
C10H16N2O	180.1263	181.1343	All samples
C11H19NO	181.1473	182.1553	cow, sheep, goat
C10H17NO2	183.1303	184.1383	horse, sheep, goat
C11H21NO	183.1572	184.1652	cow
C10H20N2O	184.1656	185.1736	cow
C10H19NO2	185.1433	186.1513	horse, sheep, goat
C10H12NO2	187.1523	188.1603	sheep, goat
C11H25NO	187.1931	188.2011	cow
C11H18N2O	194.1443	195.1523	goat
C12H21NO	195.1613	196.1693	cow, horse, sheep
C12H23NO	197.1834	198.1914	cow
C11H22N2O	198.1703	199.1783	horse, goat
C11H21NO2	199.1574	200.1654	sheep
C12H25NO	199.1919	200.1999	cow, horse
C13H21NO	207.1703	208.1783	sheep
C12H20N2O	208.1443	209.1523	horse, sheep, goat
C13H25NO	211.1814	212.1894	cow, sheep
C10H15NO2S	213.0813	214.0893	horse, sheep, goat
C13H27NO	213.2071	214.2151	cow
C11H22N2O2	214.1633	215.1713	sheep, goat
C11H21NO3	215.1533	216.1613	sheep
C9H14O2S2	218.0423	219.0503	sheep, goat
C14H21NO	219.1633	220.1713	goat
C13H22N2O	222.1733	223.1813	horse
C11H13NO4	223.0873	224.0953	sheep
C13H8N2S	224.0373	225.0453	sheep, goat
C14H11NO2	225.0773	226.0853	goat
C13H26N2O	226.2043	227.2123	horse
C14H29NO	227.2273	228.2353	cow, sheep
C12H26N2O2	230.1943	231.2023	All samples
C15H31NO	241.2393	242.2473	cow
C14H30N2O	242.2353	243.2433	horse
C13H28N2O2	244.2163	245.2243	All samples
C15H24N2O	248.1847	249.1927	cow
C15H23NO2	249.1753	250.1833	goat
C15H23NO2	249.1818	250.1898	cow
C14H30N2O2	258.2250	259.2330	cow, sheep, goat

C16H27NO2	265.2076	266.2156	cow
C16H12N2O4	296.0776	297.0856	sheep
Halogenated compounds (2)			
C7H6OCl2	175.9813	176.9893	horse, goat
C7H5OCl3	209.9433	210.9513	cow, horse, sheep

This page is intentionally left blank

Rôle de la réactivité des déchets organiques dans la formation d'aérosols organiques secondaires

Résumé

Le recyclage des produits résiduaires organiques (PRO) en tant qu'engrais agricoles se développe aujourd'hui comme une approche plus durable et plus écologique par rapport aux méthodes traditionnelles d'élimination des déchets. Cependant, l'épandage des déchets organiques pourrait libérer divers polluants tels que des composés organiques volatils (COV). Ces derniers présentent des effets néfastes sur l'écosystème et la santé humaine liés à la production d'ozone et peuvent servir comme précurseurs critiques d'aérosols organiques secondaires (AOS) dans l'atmosphère. La mesure des COV émis par les PRO est donc indispensable pour évaluer leur impact sur l'environnement et la santé humaine, ainsi que pour comprendre les mécanismes de formation des AOS associés, qui sont jusqu'à ce jour peu documentés.

Nous avons étudié les émissions de COV de divers échantillons : des boues d'épuration, du fumier animal (vache, cheval, mouton et chèvre), des digestats de biodéchets ainsi que leurs produits d'oxydation en phase gazeuse dus aux réactions d'ozonolyse. Cette étude a été faite grâce au développement d'un dispositif expérimental, composé de chambres de simulation atmosphérique combinées à des techniques de spectrométrie de masse telles que : la spectrométrie de masse à temps de vol par réaction de transfert de protons (PTR-QiTOF-MS) et de désorption thermique - chromatographie en phase gazeuse - spectrométrie de masse (TD-GC-MS) pour identifier et quantifier les émissions de COV de chaque échantillon. L'étude de la composition chimique des AOS a été effectuée en utilisant la spectrométrie de masse laser à deux étapes (L2MS).

Nos résultats ont montré que les échantillons de boues d'épuration, de fumier animal et de biodéchets digérés émettent une large gamme de COV, avec plusieurs centaines de composés détectés et quantifiés. Les COV identifiés ont été classés en différentes familles chimiques : hydrocarbures, composés oxygénés, soufrés, azotés et "autres" (contenant des hétéroatomes distincts dans la formule moléculaire). Les échantillons de boues d'épuration ont émis un flux élevé d'hydrocarbures tels que les composés aromatiques (phénol, indoles et skatole), et les terpènes (isoprène, D-limonène, sesquiterpènes, etc.). Les composés oxygénés (par exemple, l'éthanol, la butanone, le crésol, l'acide acétique, le phénol) ont été fortement émis par les digestats de biodéchets et les échantillons de fumier. Des composés azotés (ammoniac, triméthylamine, scatole, etc.) et des composés soufrés (méthanethiol, DMS, DMDS, etc.) ont également été trouvés dans ce travail.

Des émissions significatives de scatole ont été estimées à partir des boues d'épuration et de digestat. Le mécanisme de formation de nouvelles particules a été démontré. Nos résultats impliquent que pendant l'épandage des PRO, le scatole est un important contributeur potentiel à la formation de nouvelles particules dans des conditions atmosphériques pertinentes. Les résultats de ce travail contribuent à faire progresser nos connaissances sur les COV et leur rôle dans la formation des AOS. Ils pourraient également être utiles pour mieux comprendre les caractéristiques des émissions des PRO, concevoir des stratégies de contrôle de ces émissions.

Mots clés: émissions agricoles, produits résiduels organiques, composés organiques volatils, aérosols organiques secondaires, ozonolyse, précurseurs d'aérosols, spectrométrie de masse.

Role of the organic waste products reactivity in secondary organic aerosol formation

Abstract

Recycling of organic waste products (OWP) as agricultural fertilizers is nowadays expanding as a more sustainable and eco-friendly approach compared to the traditional methods of waste disposal. However, OWP spreading may release various pollutants such as volatile organic compounds (VOC), which adversely affect the ecosystem and human health through ozone production and may serve as critical precursors of atmospheric secondary organic aerosols (SOA). The measurement of VOCs emitted by OWPs is therefore essential to assess their environmental and human health impact and, furthermore, to fundamentally understand the associated SOA formation mechanisms, which remain to date poorly documented.

With this aim, we studied the VOC emissions from various sewage sludge (SS) samples, animal manure (cow, horse, sheep and goat) and digestate biowastes, along with their gas-phase oxidation products due to ozonolysis reactions. With the development of an experimental set-up consisting of atmospheric simulation chambers combined with mass spectrometric techniques, it has become possible to characterize the VOC emissions and follow the process of new particle formation (NPF) upon ozonolysis. We used proton transfer reaction quadrupole-ion-guide time-of-flight mass spectrometry (PTR-QiTOF-MS) and thermal desorption - gas chromatography - mass spectrometry (TD-GC-MS) techniques to identify and quantify the VOC emissions from each sample. In addition, we studied the chemical composition of SOA using two-step laser mass spectrometry (L2MS).

Our results showed that sewage sludge, animal manure and digestate biowaste samples emitted a large spectrum of VOCs where 380, 385 and 221 compounds were detected and quantified, respectively. The assigned VOCs were classified into different chemical families: hydrocarbons, oxygenated, sulphuric, nitrogenated, and “other” compounds (containing distinct heteroatoms in the molecular formula). Sewage sludge samples were characterized by high emission flux of hydrocarbons such as aromatic compounds (phenol, indoles and skatole), terpenes (isoprene, D-limonene, sesquiterpenes, etc.). Oxygenated compounds (e.g., ethanol, butanone, cresol, acetic acid, phenol) were highly emitted from digestate biowastes and manure samples. Nitrogenated compounds (ammonia, trimethylamine, skatole, etc.) and sulphur compounds (methanethiol, DMS, DMDS, etc.) were also found in this work.

Significant skatole emissions were estimated from undigested SS and digestate biowastes. The ozonolysis of skatole resulted in the formation of 2-acetyl phenyl formamide identified as the main skatole ozonolysis product. The NPF mechanism was demonstrated. Our findings imply that during OWPs spreading, skatole is an important potential contributor to the formation of new particles under atmospherically relevant conditions. The results of this work would advance our knowledge of VOCs and their impact on SOA formation and would be helpful in understanding the OWP emission characteristics and designing effective emission control strategies.

Keywords: agricultural emissions, organic waste products, volatile organic compounds, secondary organic aerosols, ozonolysis, aerosol precursors, mass spectrometry.